AFWAL-TM-83-214

F-15 MODEL INTERNOZZLE DYNAMIC PRESSURE ACQUISITION

Phyllis Bolds
David Banaszak
Leonard L. Shaw, Jr.

Analytical Structural Mechanics Branch (AFRL/VASM)
Structures Division
Air Vehicles Directorate
Air Force Research Laboratory, Air Force Materiel Command
Wright-Patterson Air Force Base, OH 45433-7542

MAY 1984

Final Report for 01 November 1982 – 01 August 1983

AIR VEHICLES DIRECTORATE
AIR FORCE RESEARCH LABORATORY
AIR FORCE MATERIEL COMMAND
WRIGHT-PATTERSON AIR FORCE BASE, OH 45433-7542

NOTICE

Using government drawings, specifications, or other data included in this document for any purpose other than government procurement does not in any way obligate the U.S. Government. The fact that the government formulated or supplied the drawings, specifications, or other data does not license the holder or any other person or corporation; or convey and rights or permission to manufacture, use, or sell any patented invention that may relate to them.

This report has been reviewed by the Office of Public Affairs (ASC/PA) and is releasable to the National Technical Information Service (NTIS). At NTIS, it will be available to the general public, including foreign nations.

This technical report has been reviewed and is approved for publication.

DAVID BANASZAK
Project Engineer
Analytical Structural Mechanics Branch
Structures Division

GERALD PLZAK
Technical Manager
Analytical Structural Mechanics Branch
Structures Division

JEROME PEARSON
Chief
Analytical Structural Mechanics Branch
Structures Division

Copies of this report should not be returned unless return is required by security considerations, contractual obligations, or notice on a specific document.

REPORT DOCUMENTATION PAGE

Form Approved
OMB No. 0704-0188

1. REPORT DATE *(DD-MM-YY)*	2. REPORT TYPE	3. DATES COVERED *(From - To)*
May 1984	Final	11/01/1982 – 08/01/1983

4. TITLE AND SUBTITLE
F-15 MODEL INTERNOZZLE DYNAMIC PRESSURE ACQUISITION

5a. CONTRACT NUMBER
In-house

5b. GRANT NUMBER

5c. PROGRAM ELEMENT NUMBER
61102F

6. AUTHOR(S)
Phyllis Bolds
David Banaszak
Leonard L. Shaw, Jr.

5d. PROJECT NUMBER
2307

5e. TASK NUMBER
N6

5f. WORK UNIT NUMBER
03

7. PERFORMING ORGANIZATION NAME(S) AND ADDRESS(ES)
Analytical Structural Mechanics Branch (AFRL/VASM)
Structures Division
Air Vehicles Directorate
Air Force Research Laboratory, Air Force Materiel Command
Wright-Patterson Air Force Base, OH 45433-7542

8. PERFORMING ORGANIZATION REPORT NUMBER
AFWAL-TM-83-214-FIBG

9. SPONSORING/MONITORING AGENCY NAME(S) AND ADDRESS(ES)
Air Vehicles Directorate
Air Force Research Laboratory
Air Force Materiel Command
Wright-Patterson Air Force Base, OH 45433-7542

10. SPONSORING/MONITORING AGENCY ACRONYM(S)
AFRL/VASM

11. SPONSORING/MONITORING AGENCY REPORT NUMBER(S)
AFWAL-TM-83-214

12. DISTRIBUTION/AVAILABILITY STATEMENT
Approved for public release; distribution is unlimited.

13. SUPPLEMENTARY NOTES
This version of the report is the best quality available.

14. ABSTRACT

A dynamic pressure survey of a 4.7-percent model of the F-15 aircraft was conducted during buffeting of F-15 afterbody nozzle in the NASA LaRC's 16-foot tunnel to obtain insight into the internozzle dynamic pressure phenomena germane to closely spaced engine installations. This test consisted of varying the Mach number from 0.48 to 1.2, the nozzle pressure ratio from 1 to 5, and the angle of attack from 0 to 6 degrees. These conditions were measured at six locations on the afterbody using strain gauge pressure transducers. It was determined that the measured data were broadband random, strongly stationary, and correlated.

15. SUBJECT TERMS
buffeting, internozzle, pressure transducers, acoustic fatigue, afterbody, F-15 aircraft

16. SECURITY CLASSIFICATION OF:			17. LIMITATION OF ABSTRACT:	18. NUMBER OF PAGES	19a. NAME OF RESPONSIBLE PERSON (Monitor)
a. REPORT	b. ABSTRACT	c. THIS PAGE			David Banaszak
Unclassified	Unclassified	Unclassified	SAR	184	19b. TELEPHONE NUMBER *(Include Area Code)* (937) 904-6859

HES&S 31-15093-1

Standard Form 298 (Rev. 8-98)
Prescribed by ANSI Std. Z39-18

TABLE OF CONTENTS

LIST OF ILLUSTRATIONS

LIST OF ILLUSTRATIONS (CON'T)

LIST OF ILLUSTRATIONS (CON'T)

LIST OF ILLUSTRATIONS (CON'T)

LIST OF ILLUSTRATIONS (CON'T)

LIST OF ILLUSTRATIONS (CON'T)

LIST OF ILLUSTRATIONS (CON'T)

LIST OF ILLUSTRATIONS (CON'T)

LIST OF ILLUSTRATIONS

LIST OF ILLUSTRATIONS

LIST OF TABLES

FOREWORD

This effort was performed by the combined efforts of the Structural Vibration and Structural Integrity Branches, Structures and Dynamics Division, Flight Dynamics Laboratory, Air Force Wright Aeronautical Laboratory, Wright-Patterson Air Force Base, Ohio. It was initiated under Project 2307, Computational Aerospace, Program Element 61102F, and performed in support of the F-15 SPO. The work was requested by the Aeromechanics Division, Flight Dynamics Laboratory. James Mace, AFWAL/FIMM, is the focal point for the activity.

This work was performed by David Banaszak and Phyllis G. Bolds of the Structural Vibration Branch and Leonard L. Shaw of the Structural Integrity Branch during the period of November 1982 - August 1983. The authors wish to extend their appreciation to Earl Rogers, Charles Willhite, Dansen Brown and Lowell Vaughn, who were responsible for the acquisition and the reduction of the measured data. The manuscript was released by the authors in March 1984 as a Technical Memorandum.

The Technical Memorandum has been reviewed and approved.

DAVEY L. SMITH, Chief
Structural Vibration Branch
Structures and Dynamics Division

SECTION I

INTRODUCTION

Several of the Air Force aircraft; the F-15 and the B1-A, have experienced similar structural damage in the internozzle region because of severe aeroacoustic loads. It appears that this phenomenon is germane to aircraft with closely-spaced engine installation and is not well documented or understood. The Aerodynamic and Airframe Branch of the Air Force Wright Aeronautical Laboratories has initiated this program under Work Unit 2307N603, Computational Aerodynamics to examine the internozzle dynamic pressure phenomena.

The Structures and Dynamics Division of the Air Force Wright Aeronautical Laboratories measured, recorded and reduced the pressure data to describe the dynamic environment in the internozzle region. The objective of this test was to conduct a dynamic survey on an 4.7% scale model of the F-15 aircraft, Figure 1, in the NASA LaRC 16-foot transonic wind tunnel. In order to explore the dynamics response characteristics, seven Kulite pressure transducers were installed in the internozzle region Figure 2. This test consisted of varying the Mach number from 0.48 to 1.2, the nozzle pressure ratio from 1 to 5 and angle of attack from 0 to 6 degrees for 3 wing-tail configurations. It was determined that the pressure data were broadband random, strongly stationary, and correlated.

The F-15 aircraft, as shown in Figure 3, is a high performance fighter aircraft designed for the air superiority mission. Although both subsonic and supersonic capabilities were designed into the aircraft, most emphasis was placed on performance between 0.6 and 1.0 Mach and 5,000 to 30,000 feet

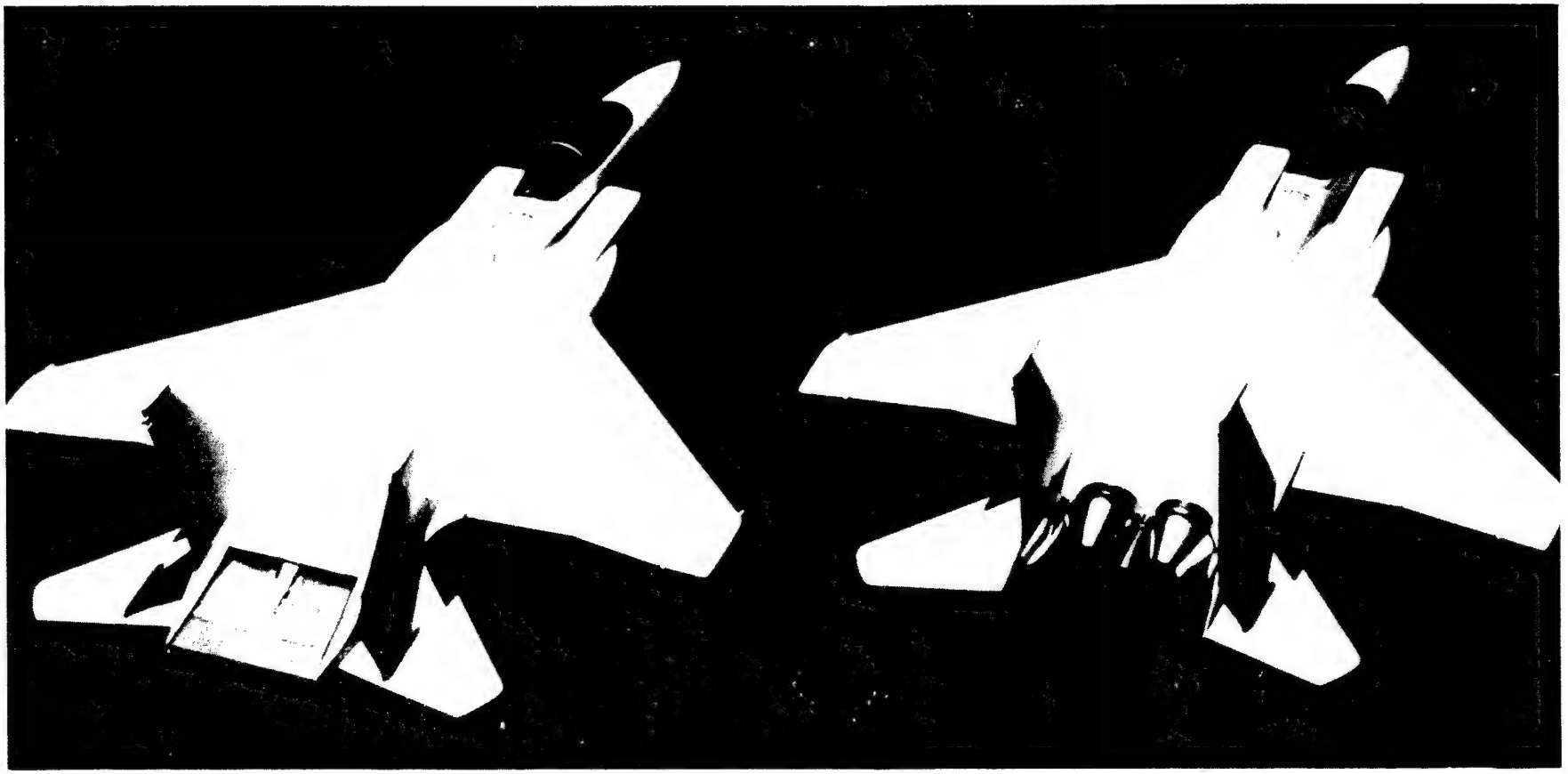

Figure 1. F-15 Model

DYNAMIC PRESSURE INSTRUMENTATION

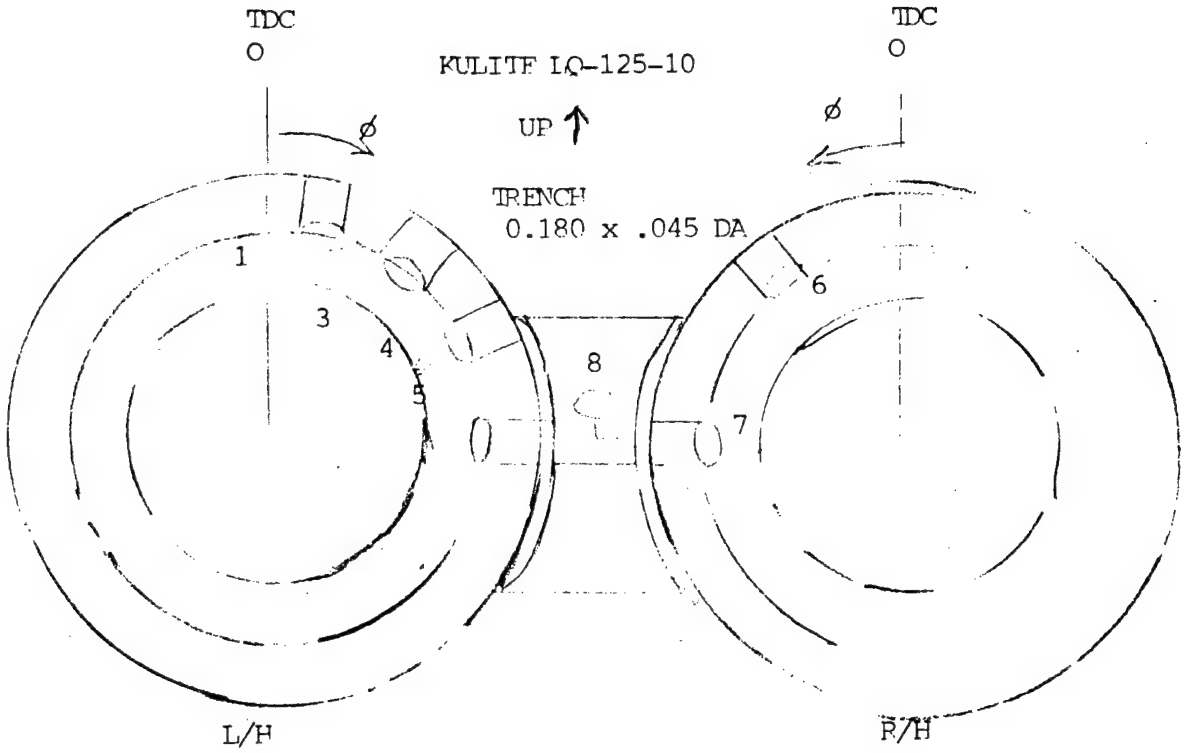

KULITE	FS	θ	Quality
1	37.8	14°	OK
2	Wall	N/A	???
3	37.8	38°	OK
4	37.8	62°	Ok
5	37.8	90°	OK
6	37.8	38°	OK
7	37.8	90°	OK
8	37.8	00	broke

Figure 2. Pressure Transducer Locations

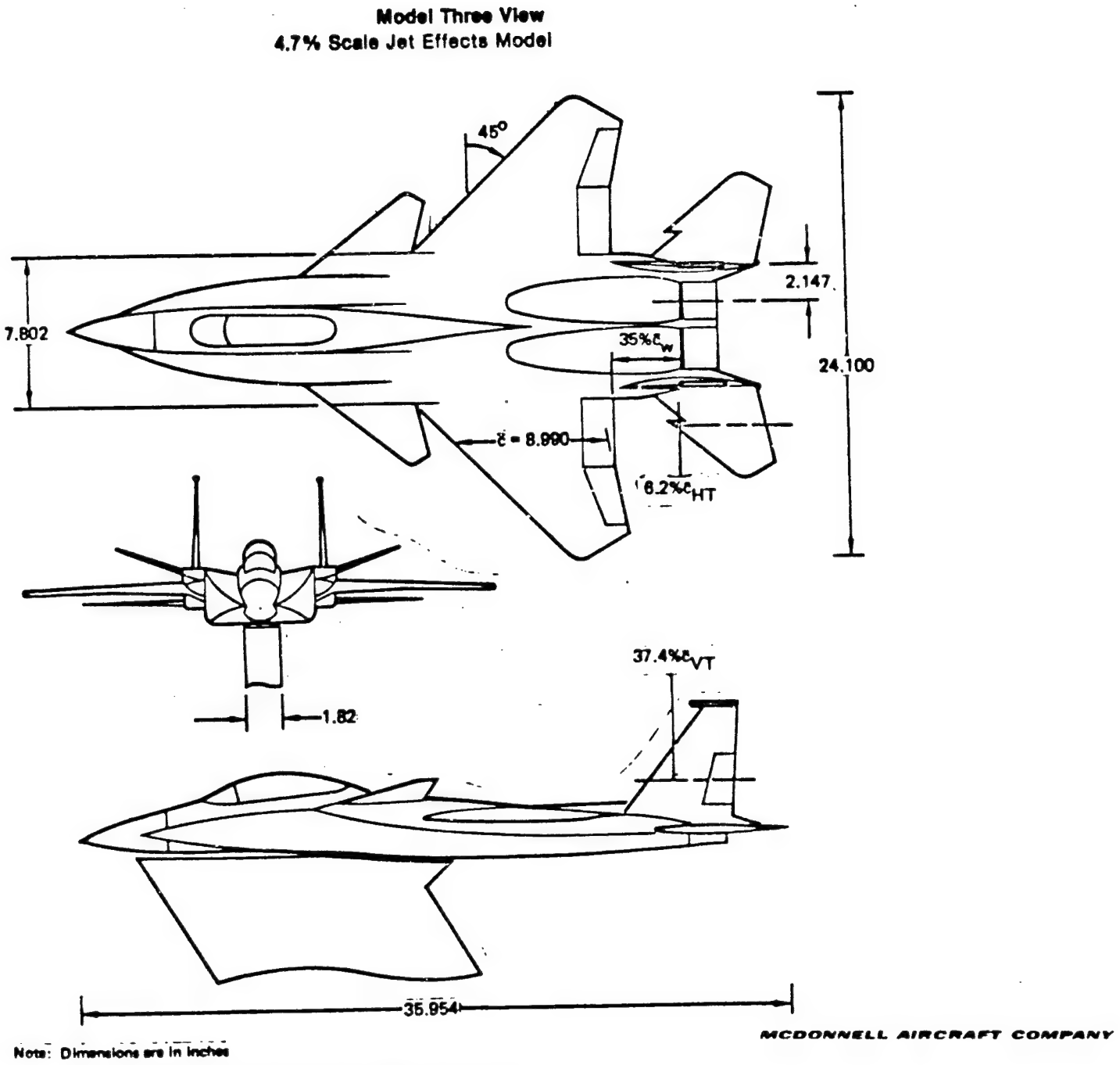

Figure 3. F-15 Aircraft Model Drawing

altitude. This includes the part of the flight envelope where most high load factor maneuvers are performed. These maneuvers such as wind-up turns and pullups are required the aircraft to perform at high angles of attack, and can cause airframe structural vibration from the aeroacoustic phenomenon associated with separated flow. This report deals with presenting the statistical characteristics of the data measured during the wind tunnel testing conducted to determine the nature of this phenomenon.

SECTION II

MEASUREMENT AND ANALYSIS

MODEL DESCRIPTION. The 4.7% scale model of the F-15 aircraft was tested with three basic structure configurations; baseline, baseline with no vertical tails, and baseline with canards. Seven pressure transducers were placed in the internozzle region to describe the dynamic environment during the tunnel conditions listed in Table 1.

INSTRUMENTATION. Seven pressure transducers (Kulite type LQ-125-10), Figures 4 & 5, were installed by McDonnell Douglas personnel onto the F-15 nozzles in the locations shown in Figure 2. An additional pressure transducer was installed in a wall probe as a tunnel reference. NASA provided wiring between the model in the 16 foot transonic wind tunnel and the control room patch-board. The unique strain gage conditioning rack packaged by the Structural Vibration Branch (containing 8 strain gage signal conditioners) was connected to NASA's patch board to provide 5VDC excitation for each pressure transducer bridge and to condition each output signal. Each pressure transducer's strain gage conditioner was used for bridge balancing, voltage excitation adjustment, and 40dB amplification of the transducer output signal before transmission to the Structural Vibration Branch's Mobile Data Acquisition Van (Figure 6) located outside of the wind tunnel building. During checkout and calibration, pressure transducer #8 was found to have a cut wire, so a dummy 350 Ohm bridge was connected to its strain gage signal conditioner. Also, the reference transducer was quite noisy and suspected of being open circuited.

The eight strain gage conditioner outputs (6 pressure transducers on the nozzle, 1 dummy and 1 tunnel reference pressure transducer) were connected

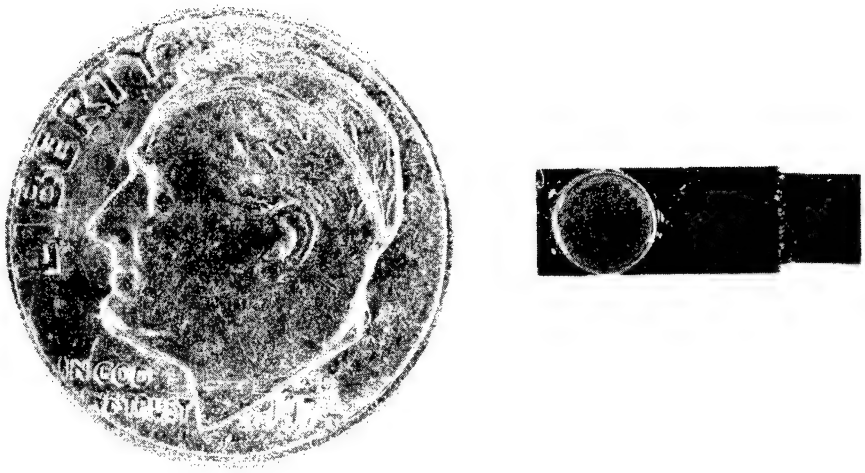

Figure 4. Kulite Type LQ-125-10

Figure 5. Internozzle Region of
The F-15 Aircraft

TABLE 1

TUNNEL CONDITIONS

RUN	POINT	MACH	EPR		CONFIGURATION	REMARKS
54	0/1	0	1.0	0	Baseline-- with Canards	(Do not heat hot zero balance)
	2	1.2	1.0			
	3		2.0			
	4		3.5			
	5		5.0			
	6		1.0			
	7	0.9	1.0	0		
	8			3		
	9			6		
	10		3.5	0		
	11			3		
	12			6		
	13		5.0	0		
	14			3		
	15			6		
	16	0.9	1.0	0		
	17		2.0			
	18		3.5			
	19		5.0			
	20		1.0			
	21	0.875	1.0	0		
	22			3		
	23			6		
	24		3.5	0		
	25			3		
	26			6		
	27		1.0	0		
	28		2.0			
	29		3.5			
	30	0.875	5.0	0		
	31		1.0			
	32	0.85	1.0	0		
	33		2.0			
	34		3.5			
	35		5.0			
	36		1.0			
	37	0.80	1.0			
	38		2.0			
	39		3.5			

TABLE 1 (CON'T)

RUN	POINT	MACH	EPR	α	CONFIGURATION	REMARKS
54	40		5.0			
	41	0.70	1.0			
	43		2.0			
	44		5.0			
	45		1.0			
	46	0.60	1.0	0		
	47			3		
	48			6		
	49		2.0	0		
	50			3		
	51			6		
	52		3.5	0		
	53			3		
	54			6		
	55		1.0	0		
	56		2.0			
	57		3.5			
	58		5.0			
	59	0.6	1.0	0		
	60/61	0.0	1.0			
55	0/1	0.0	1.0		Baseline with No	
	2	0.9	1.0		Vertical Tails	
	3		3.5			
	4		5.0			
	5		1.0			
	6		3.5			
	7		5.0			
	8		1.0			
	9	0.875	1.0			
	10		3.5			
	11		5.0			
	12		1.0			
	13		3.5			
	14		5.0			
	15		1.0			
	16	0.80	1.0			
	17		3.5			
	18		5.0			
	19		1.0			
	20		3.5			
	21		1.0			
	22	0.60	1.0			
	23		3.5			
	24		5.0			
	25		1.0			
	26		3.5			
	27		1.0	0		

TABLE 1 (CON'T)

RUN	POINT	MACH	EPR		CONFIGURATION	REMARKS
56	0/1	0	1.0	0	Baseline with	
	2	0.9	1.0	0	Canards	
	3		3.5			
	4		5.0			
	5		1.0			
	6		3.5			
	7		5.0			
	8		1.0			
	9	0.875	1.0	0		
	10		3.5			
	11		5.0			
	12		1.0			
	13		3.5			
	14		5.0			
	15/16		1.0			Point 16 bad
	17	0.80	1.0	0		
	18		3.5			
	19		5.0			
	20		1.0			
	21		3.5			
	22		1.0			
	23	0.60	1.0	0		
	24		3.5			
	25		5.0			
	26		1.0			
	27		3.5			
	28		1.0			
57	0/1	0.0	1.0	0	Baseline	Hot Zero
	2	0.90	1.0	0		Balance
	3		3.5			
	4/5		5.0			Point 5 bad
	6		3.5			
	7		5.0			
	8		1.0			
	9	0.875	1.0			
	10		3.5			
	11		5.0			
	12		1.0			
	13	0.80	1.0			
	14		3.5			
	15		5.0			
	16		1.0			
	17	0.60	1.0			
	18		3.5			
	19		5.0			
	20		1.0			
	21	0	1.0			Bad

between the strain gage conditioning rack and NASA's patch panel by ten foot long twisted shielded pair (TSP) cables. Pre-existing NASA wiring connected the control room patch to NASA's facility patch board located below the tunnel's test section. Structural Vibration personnel routed eight TSP cables with 6 pin connectors matching NASA's electrical connector board on one end and BNC connectors on the other end as input to the van. As shown in the block diagram in Figure 7, the signals into the van were routed through automatic gain changing (AGC) amplifiers operated in a fixed mode of 20dB gain before input to a Honeywell 96 wideband tape recorder where each signal was recorded at 15 ips using frequency modulation (FM) techniques. The recorder was modified so that signals were routed through an optical isolator before actual input to the recorder. This allowed isolation between the ground of the van recorder and the wind tunnel. Also, an additional amplifier was included in the optical isolator. It was used during calibration for adjusting voltage level into the recorder for a given input to the strain gage conditioner located in the tunnel's control room. Pressure data were recorded on tape tracks 1 through 8.

A hand microphone inside the van was used to record voice on the tape edge tracks during data recording. A pulse amplitude modulated (PAM) signal containing gain information for each AGC amplifier was recorded on tape track #13. A coaxial cable was routed between the van and the tunnel's control room so that a video camera and recorder located in the control room could transmit a picture of the tunnel monitors and displays to a video receiver located inside of the van. This video system was set up so that tunnel time code could be viewed to insure synchronization of the van's time code which was recorded on tape track #14 of the tape recorder. Additional voice

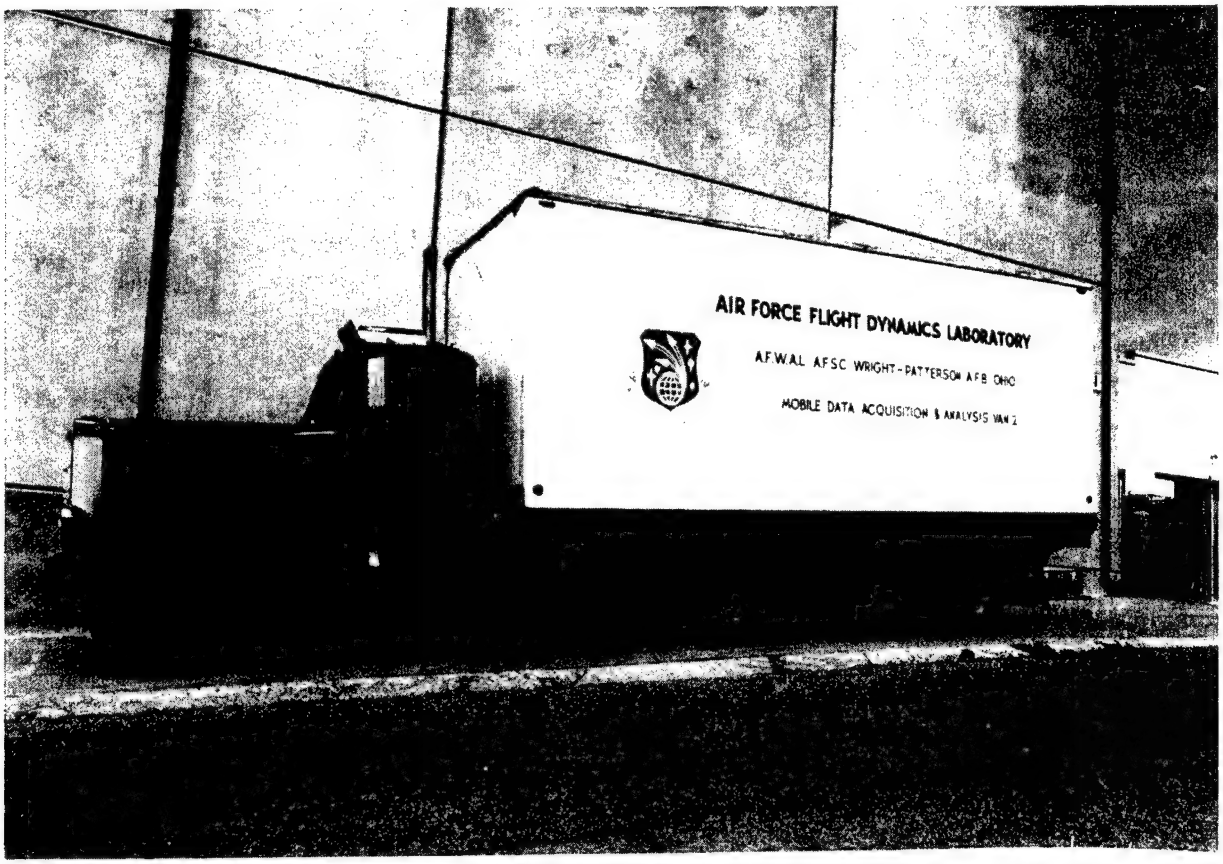

Figure 6. Instrumentation Van

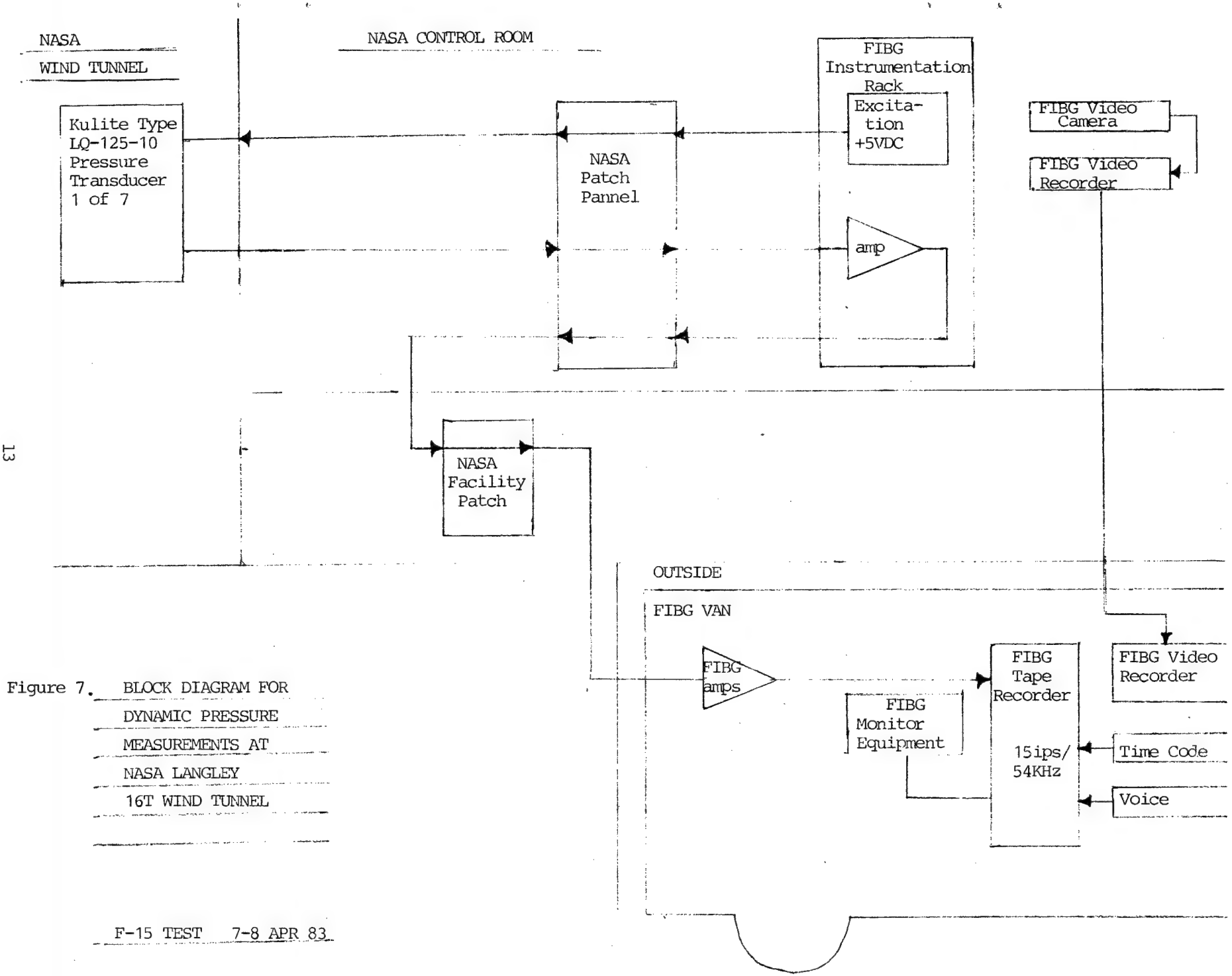

Figure 7. BLOCK DIAGRAM FOR DYNAMIC PRESSURE MEASUREMENTS AT NASA LANGLEY 16T WIND TUNNEL

F-15 TEST 7-8 APR 83

communication between the van and tunnel operator was provided by a headset to the tunnel's intercom system.

The van contained monitoring equipment for viewing pressure data as they were recorded and reproduced. Switches allowed for viewing any recorder input or reproduced signal on either oscilloscopes, voltmeters, or a dual channel spectrum analyzer. This allowed for a quick-look of the data for ascertaining quality.

CALIBRATION Each pressure channel was calibrated by inserting an electrical sine wave, with an amplitude equivalent to the pressure transducer's sensitivity, into the strain gage amplifier's input in the tunnel control room. This simulated a pressure input of 1 psi rms. In the van, the input to the recorder was adjusted for 1 volt rms by adjusting the gain of the applicable optical isolator amplifier. This calibration signal was inserted separately for each channel and a tape recording was made of the calibration signal. The sensitivities used for each pressure transducer were provided by on-site McDonnell Douglas personnel and are tabulated in Table 2. Thus the voltage recorded on tape was close to 1 Vrms per 1 psi rms. In addition to sine wave calibration signals, a random signal (DC to 25KHz) was inserted into 8 strain gage amplifiers simultaneously and recorded on tape to determine each channel's frequency response. Typical data recorded on tape at 15 ips are shown in Figure 8. The large amount of 60 Hertz was induced by the noise source. As the plots show, the system has a flat spectrum over a range of 10 to 10K Hertz.

DATA ACQUISITION A Honeywell 9600 tape recorder was used to record the pressure data. Data were recorded for 58 test points on tunnel Run #54, baseline model with canards, on 7 April 1983. On 8 April 1983, data were recorded for 22 test points on Run #55, baseline no vertical tails, and on Run

#57, baseline. Using the tunnel's intercom system, the NASA tunnel operator informed the van personnel when each tunnel test point was stabilized. A 30 second recording was made for the test point.

DATA ANALYSIS Analog tapes, recorded during the tunnel test in the Mobile Data Acquisition Van were analyzed in the Vibration and Aeroelastic Facility, located at Wright-Patterson Air Force Base, Ohio. Figure 9 shows the block diagram of the analysis system. Using the results of a quick-look digital rms program, applying the proper amplifier gain factors and matching transducer sensitivity for each data sample, an rms time history curve in engineering units of psi is produced. The rms time history indicated whether these data were reasonable and stationary. The digitized parameters used in the analysis of the Power Spectral Density, and RMS time histories of the pressure data are contained in Table 3 and Figure 10 respectively.

TABLE 2

PRESSURE TRANSDUCER SENSITIVITIES

FIBG No.	SN	McAir No.	Vexcit = 5VDC Sensitivity (MV/PSI)
1	4360-1-15	1	2.038403
2	5288-4-9	Reference	1.876988
3	4360-1-16	2	2.212809
4	4360-1-18	3	2.104024
5	4360-1-26	4	2.254806
6	4360-1-14	6	2.061306
7	004-5-13	5	1.930021
8	4360-1-30	7	2.157885 *

*8 In FIBG no. 8, a substituted dummy gage was used.

TABLE 3

DIGITIZING PARAMETERS

Cutoff Frequency	5000Hz
Data Sample Length	3.2767 Seconds
Delta Frequency	4.8828Hz
Number of Transform	16
Transform Size	4096

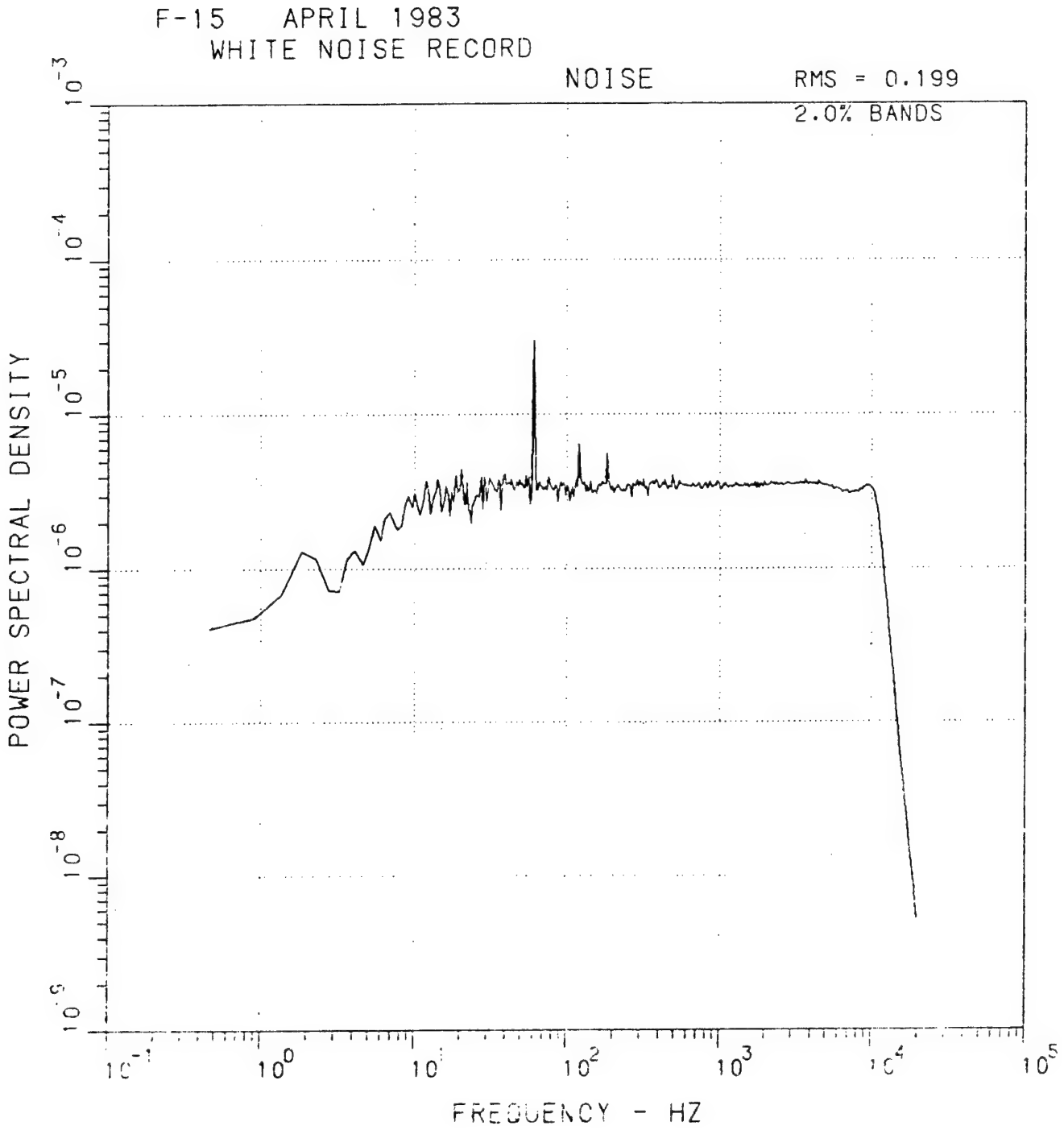

Figure 8. Frequency Response of the Measurement System

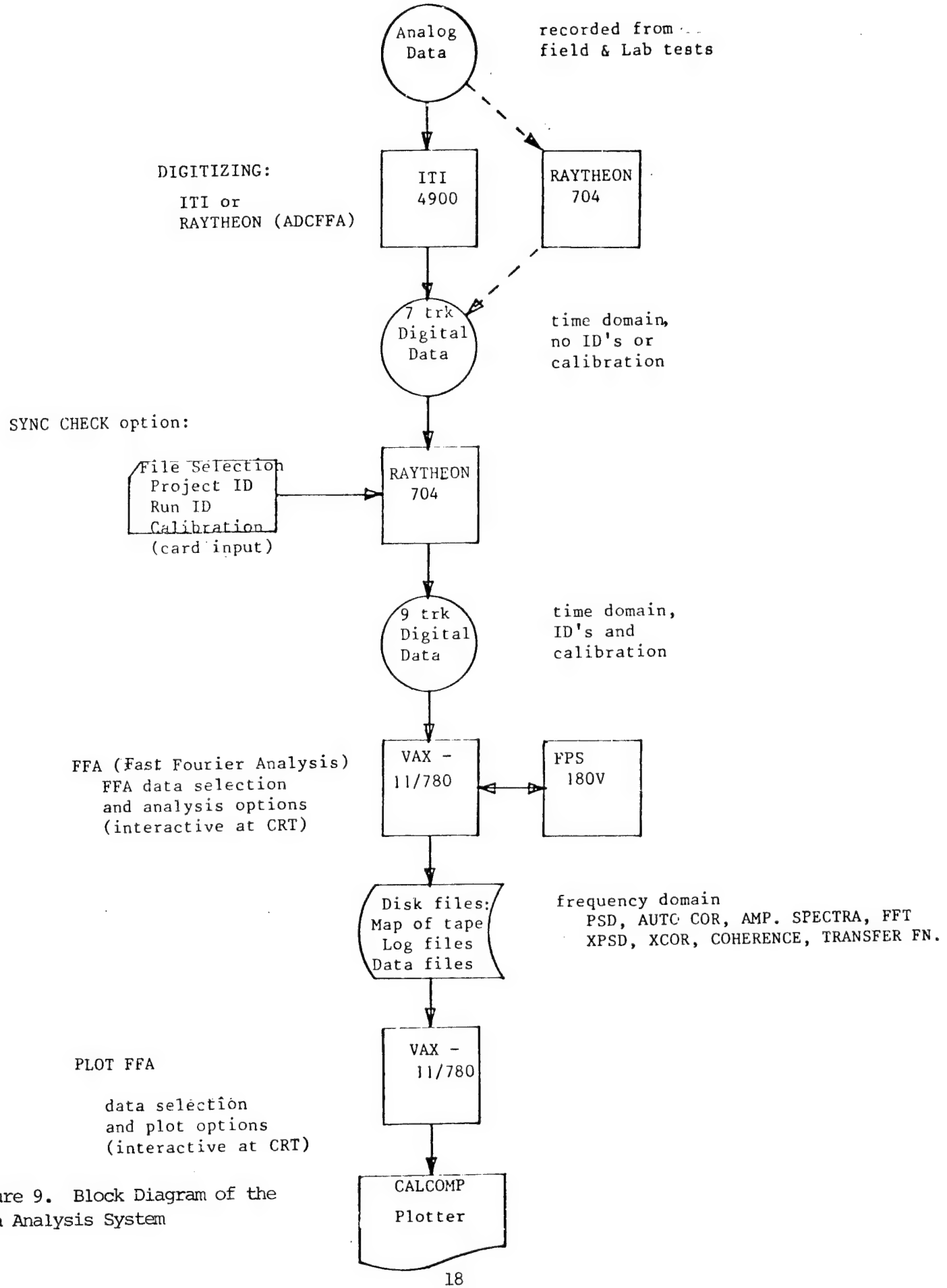

Figure 9. Block Diagram of the Data Analysis System

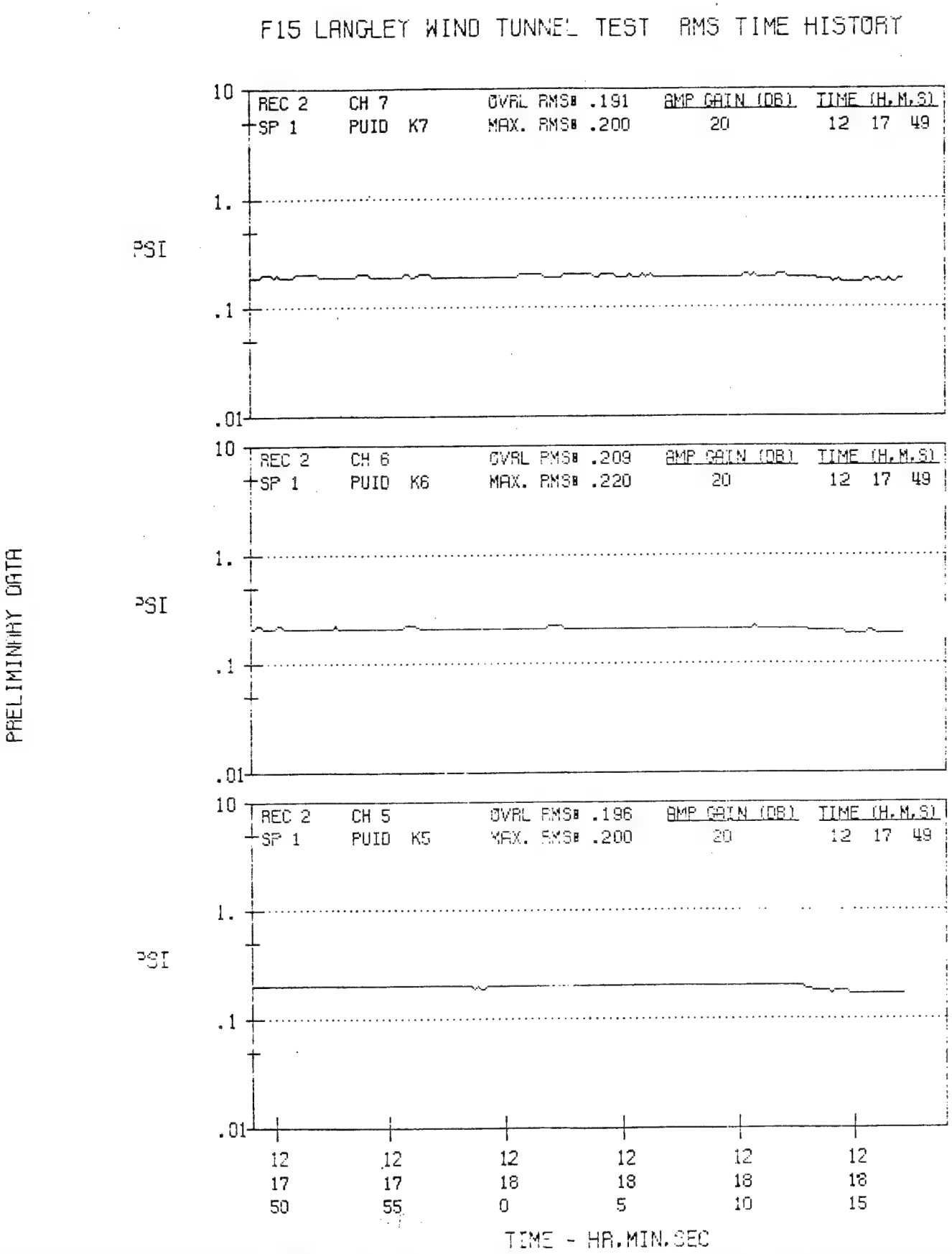

Figure 10. Typical RMS Time Histories of the F-15 Pressure Data

SECTION III

DATA PRESENTATION

The pressure data selected for presentation in this report are shown in Figures 13 to 240 and were obtained during the conditions contained in Tables 4 to 6.

TIME HISTORY PLOTS

Individual RMS time history plots were produced for each record. A typical RMS time history plot of one record is included in Figure 10. All RMS time histories were flat for each stable condition.

PROBABILITY DENSITY FUNCTION

Figure 11 is a plot of the Probability Density Function (PDF) of a 0.5 VRMS random signal. Figure 12 is a plot of the PDF of 1.0 VRMS 200Hz sine wave. A comparison was made of these figures using the same software, with the PDF's presented in Figure 13 to 30 of the actual pressure data. During 0.9 Mach, EPR of 1.0 for the baseline configuration (Run 57), a PDF plot was made of the relatively flat spectrum contained in Figures 13 through 24. Also presented are plots of PDFs of the actual data recorded during 1.2 Mach, EPR of 1.0 for the configuration (Run 54) showing a broad peek in the spectrum from approximately 125 to 200Hz, are included in Figures 25 through 30. The plot of the PDF, assuming the data are stationary is given by:

$$\rho(F/\sigma) = (1/\sqrt{2\pi})e^{-\frac{1}{2}(\bar{F}/\sigma)^2} \qquad (1)$$

TABLE 4

F-15 BASELINE WITH CANARDS

RUN 54

TUNNEL CONDITIONS			TRANSDUCERS - KULITES RMS (PSI)					
Mach #	EPR	α	K1	K3	K4	K5	K6	K7
1.20	2.0	0	.058	.101	.232	.148	.073	.172
	3.5		.056	.102	.218	.140	.074	.153
	5.0		.049	.096	.200	.130	.066	.140
	1.0		.041	.061	.080	.120	.064	.140
0.90	1.0	0	.068	.144	.184	.161	.170*	.163
		3	.083	.172	.188	.166	.160	.173
		6	.091	.187	.200	.170	.174	.176
	3.5	0	.069	.164	.189	.145	.149	.154
		3	.080	.198	.204	.150	.100	.162
		6	.081	.213	.220	.153	.083	.162
	5.0	0	.067	.152	.179	.141	.098	.150
		3	.075	.168	.185	.145	.097	.159
		6	.078	.176	.192	.143	.084	.159
	2.0	0	.069	.170	.193	.149	.104	.155
	3.5		.071	.169	.188	.144	.098	.154
	5.0		.068	.151	.177	.141	.096	.150
0.90	1.0	0	.069	.142	.182	.159	.108*	.160

TABLE 5

F-15 BASELINE

RUN 57

			TRANSDUCERS - KULITES RMS PSI					
Mach #	EPR	α	K1	K3	K4	K5	K6	K7
0.90	3.5	0	.202	.273	.242	.144	.187	.185
	5.0		.180	.257	.231	.139	.179	.181
	1.0		.205	.272	.255	.165	.209	.195
0.88	1.0		.181	.254	.251	.188	1.93	.186
	3.5		.163	.258	.236	.169	.174	.180
	5.0		.154	.245	.223	.162	.168	.179
0.80	3.5		.094	.193	.224	.156	.134	.166
	5.0		.089	.178	.213	.151	.134	.162
	1.0		.100	.175	.218	.174	.143	.170
0.60	1.0		.061	.091	.172	.126	.083	.124
0.60	3.5		.060	.109	.173	.119	.090	.123
	5.0		.050	.105	.171	.116	.091	.121

TABLE 6

F-15 BASELINE

NO VERTICAL TAILS

RUN 55

TUNNEL CONDITION			TRANSDUCERS - KULITES - RMS (PSI)					
MACH	EPR	α	K1	K3	K4	K5	K6	K7
.90	3.5	0	.107	.202	.220	.156	.158	.158
	5.0		.093	.187	.219	.148	.155	.158
	1.0		.110	1.85	.226	.169	.158	.170

Where σ is the standard deviation or RMS magnitude of the variable (f) and $-\infty < F < +\infty$. The normal probability distribution has been found to describe suitably the statistical distribution of the instantaneous magnitude of the pressure data. The Statistical Properties of the PDF in Fig. 13-30 are contained in Table 7.

AUTOCORRELATION FUNCTION

The PDF plot is a sensitive indicator of the presence of random components, but it is a relatively insensitive indicator of sinusoidal components; therefore, the authors are also including the Auto Correlation Function of the same data to determine if a sinusoidal component is buried in these data. The baseline data (Run 57) are shown in Figures 31 through 42 and the baseline data with Canards (Run 54) are shown in Figures 43 through 48. The Auto Correlation Function $R_x(\tau,T)$ associated with a single analytic record X (t) of fixed finite length T will be defined by:

$$R_x(\tau,T) = \frac{1}{(t-\tau)} \int_0^{T-\tau} x(t)\ x(t+\tau)\ dt \quad 0 \leq \tau \leq T \tag{2}$$

$$\frac{1}{t} + \int_0^T x(t)\ x(t+\tau)dt \quad \text{if } \tau << T$$

for fixed τ, as T approaches infinity, the Autocorrelation Function, $R_x(\tau)$ is defined by:

$$R_x(\tau) = \lim_{T\to\infty} (1/T) \int_0^T x(t)\ x(t+\tau)dt \tag{3}$$

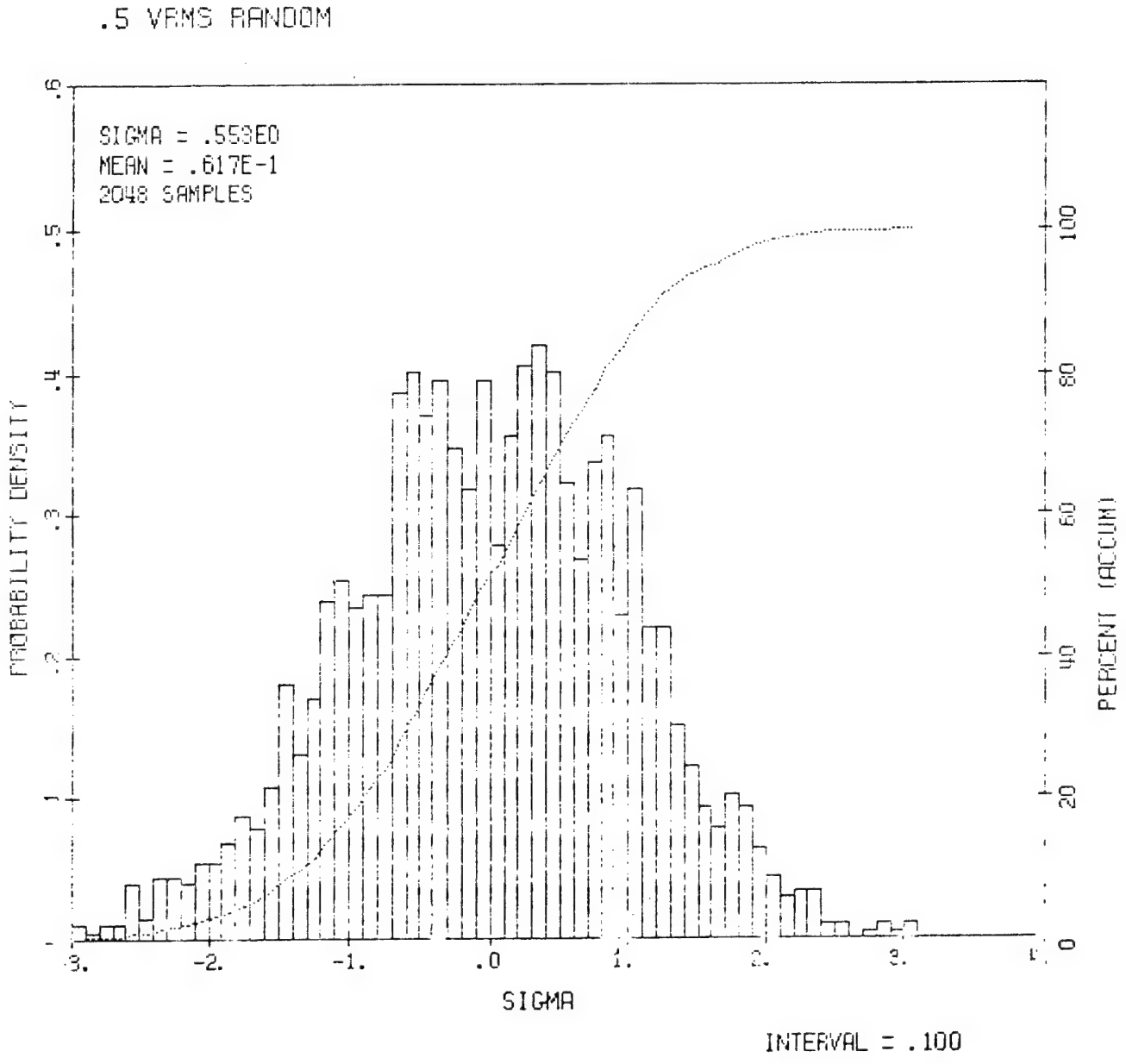

Figure 11. Probability Density Function of a Random Signal

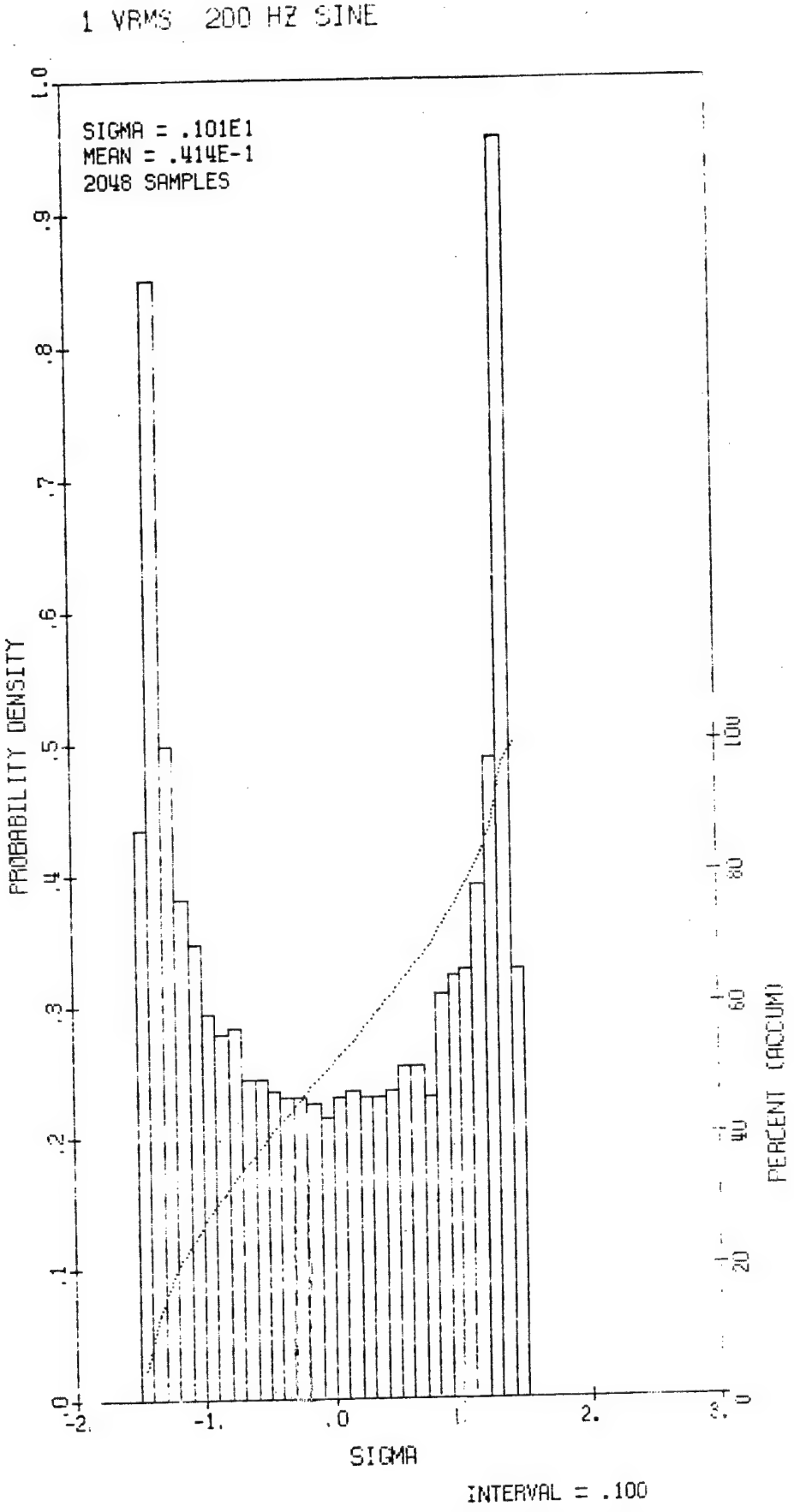

Figure 12. Probability Function of a Sine Wave

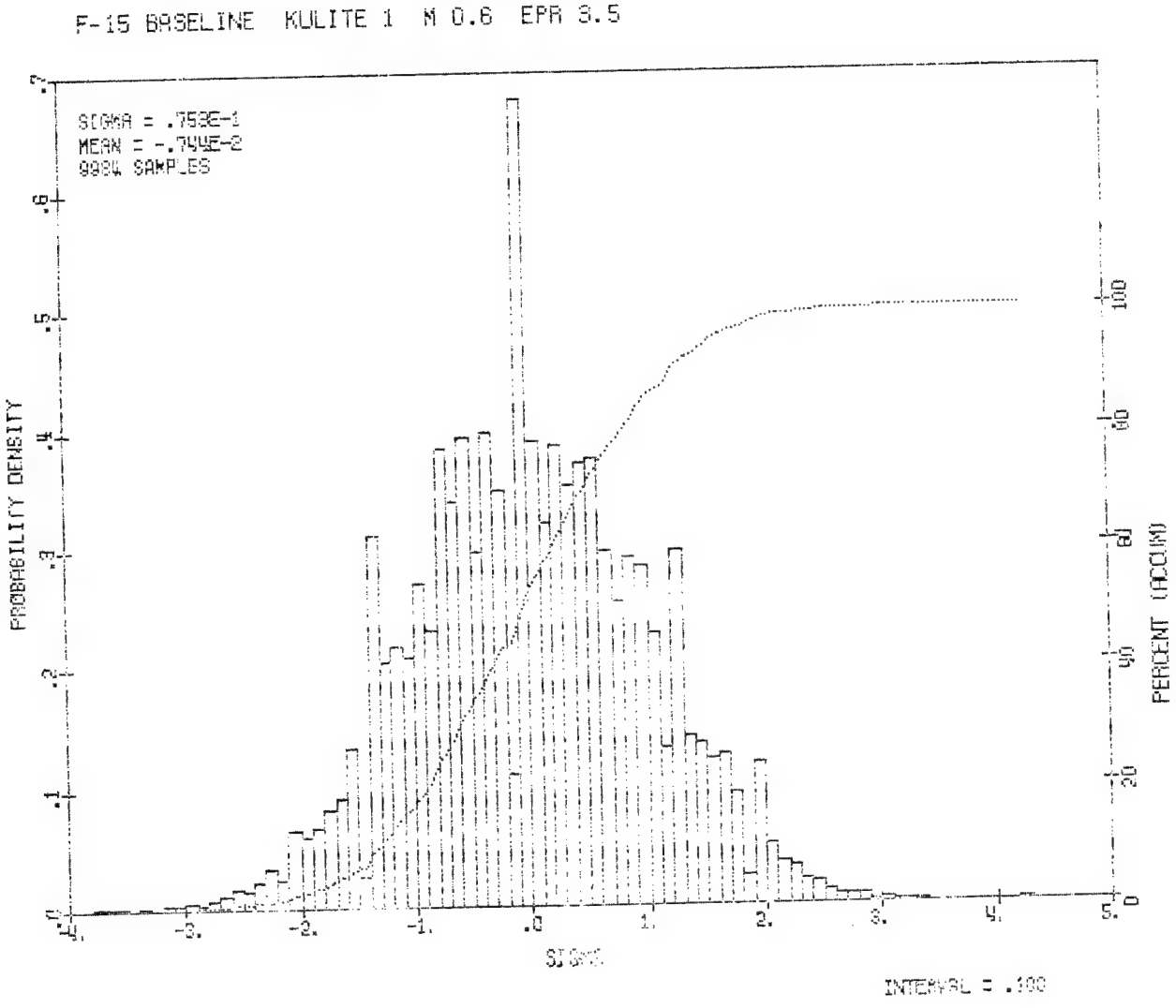

Figure 13. Probability Density Function-
Base Line Kulite 1 MACH 0.6 EPR 3.5

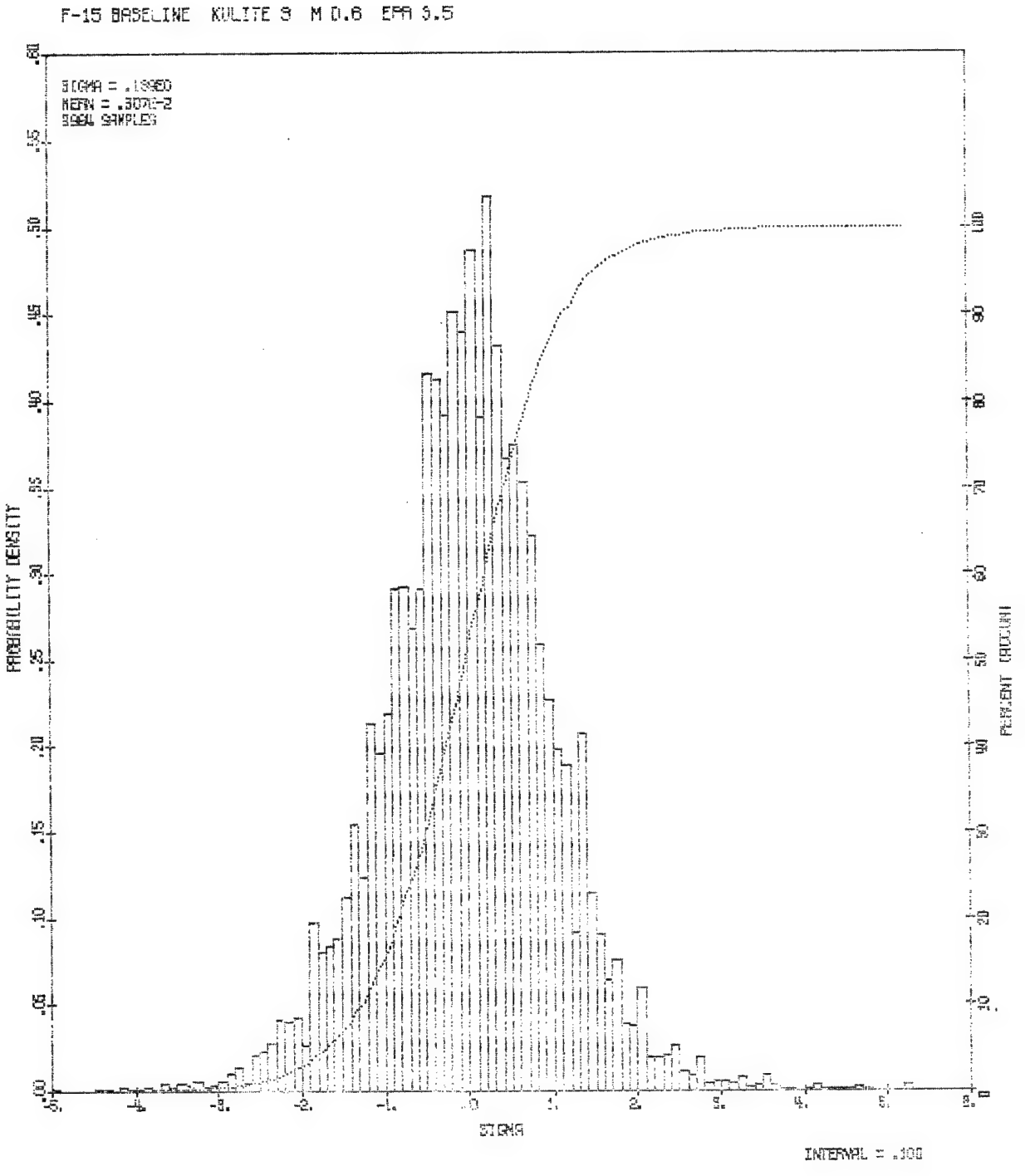

Figure 14. Probability Density Function-
Baseline Kulite 3 MACH 0.6 EPR 3.5

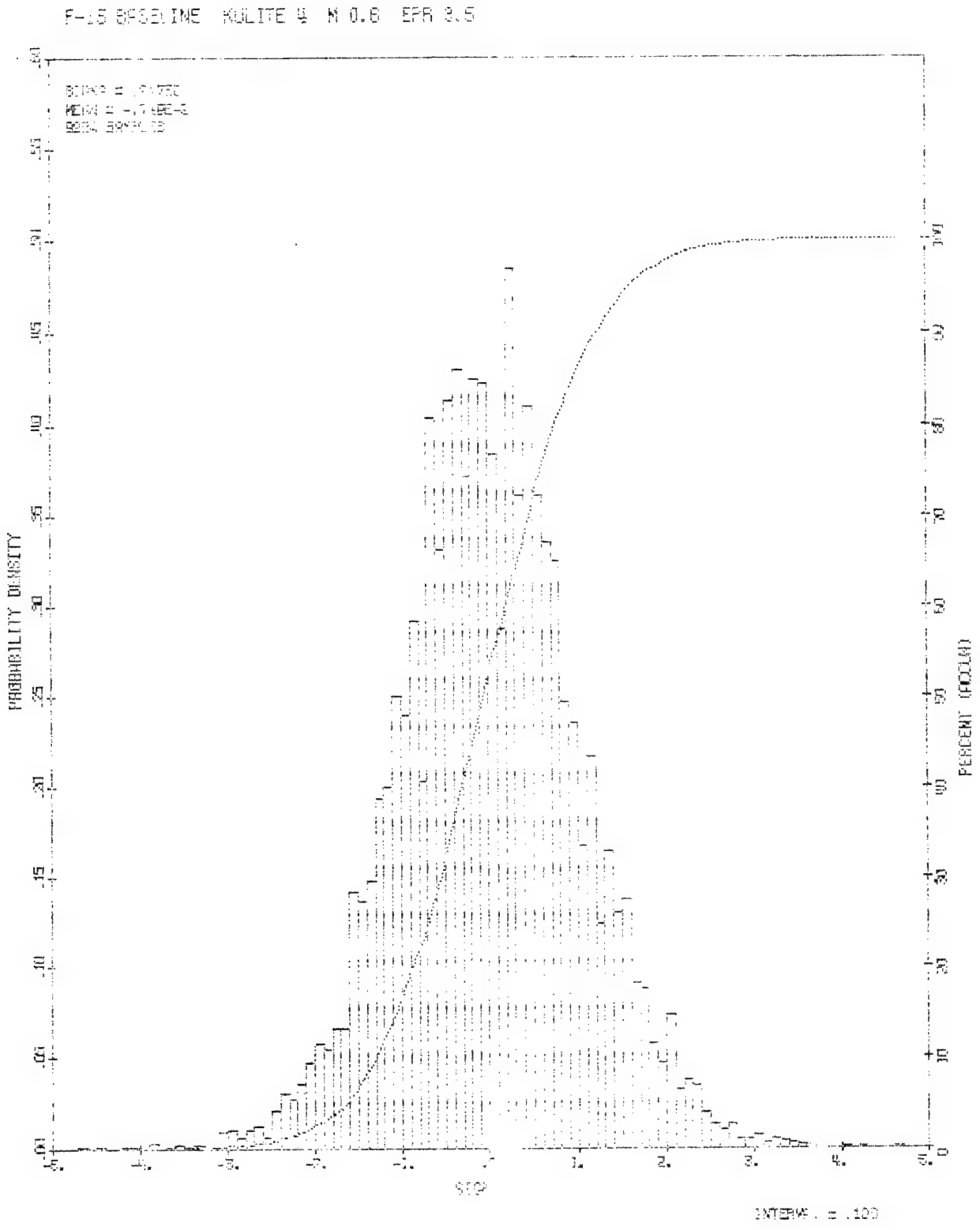

Figure 15. Probability Density Function
-Baseline Kulite 4 MACH 0.6 EPR 3.5

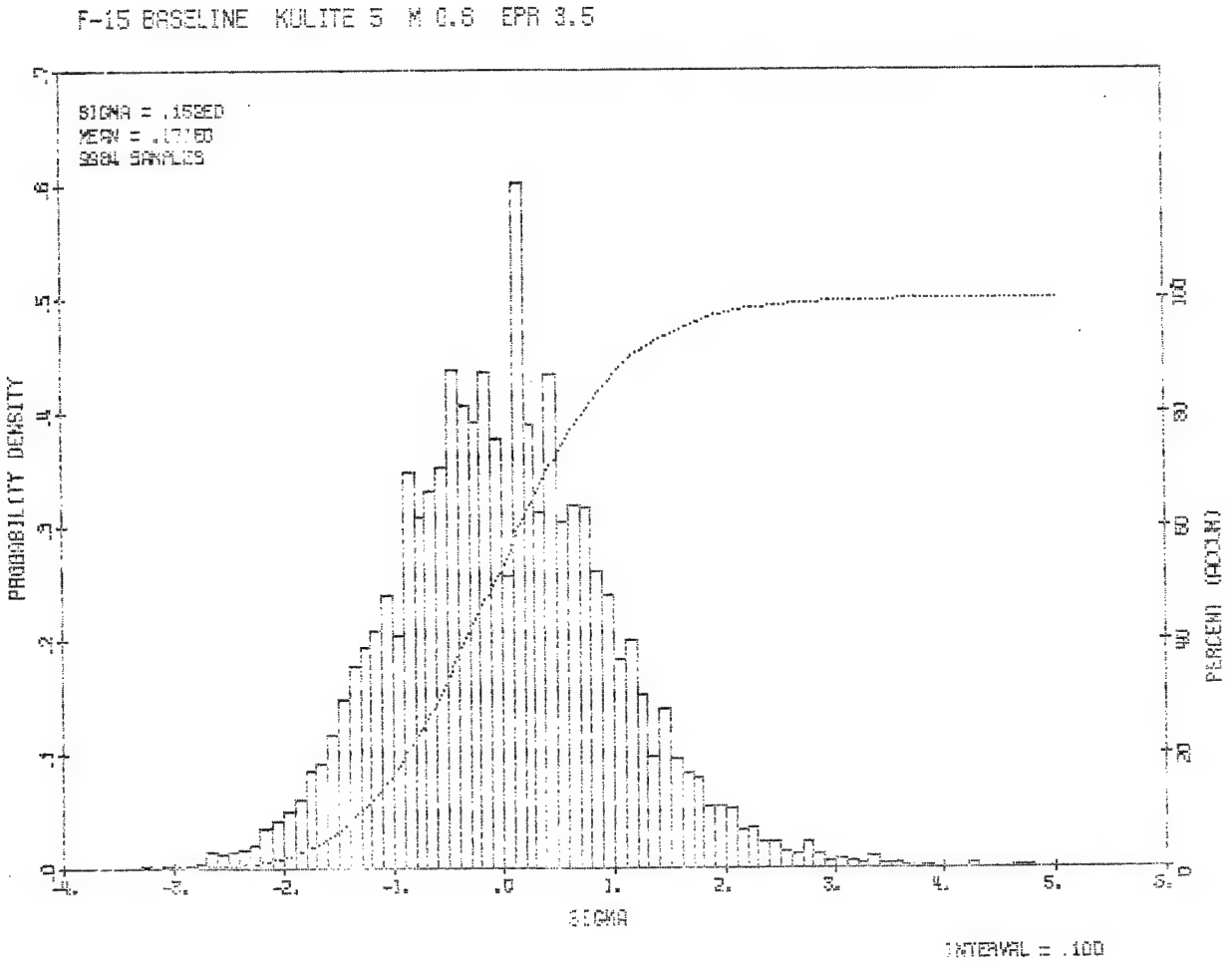

Figure 16. Probability Density Function-
Baseline Kulite 5 MACH 0.6 EPR 3.5

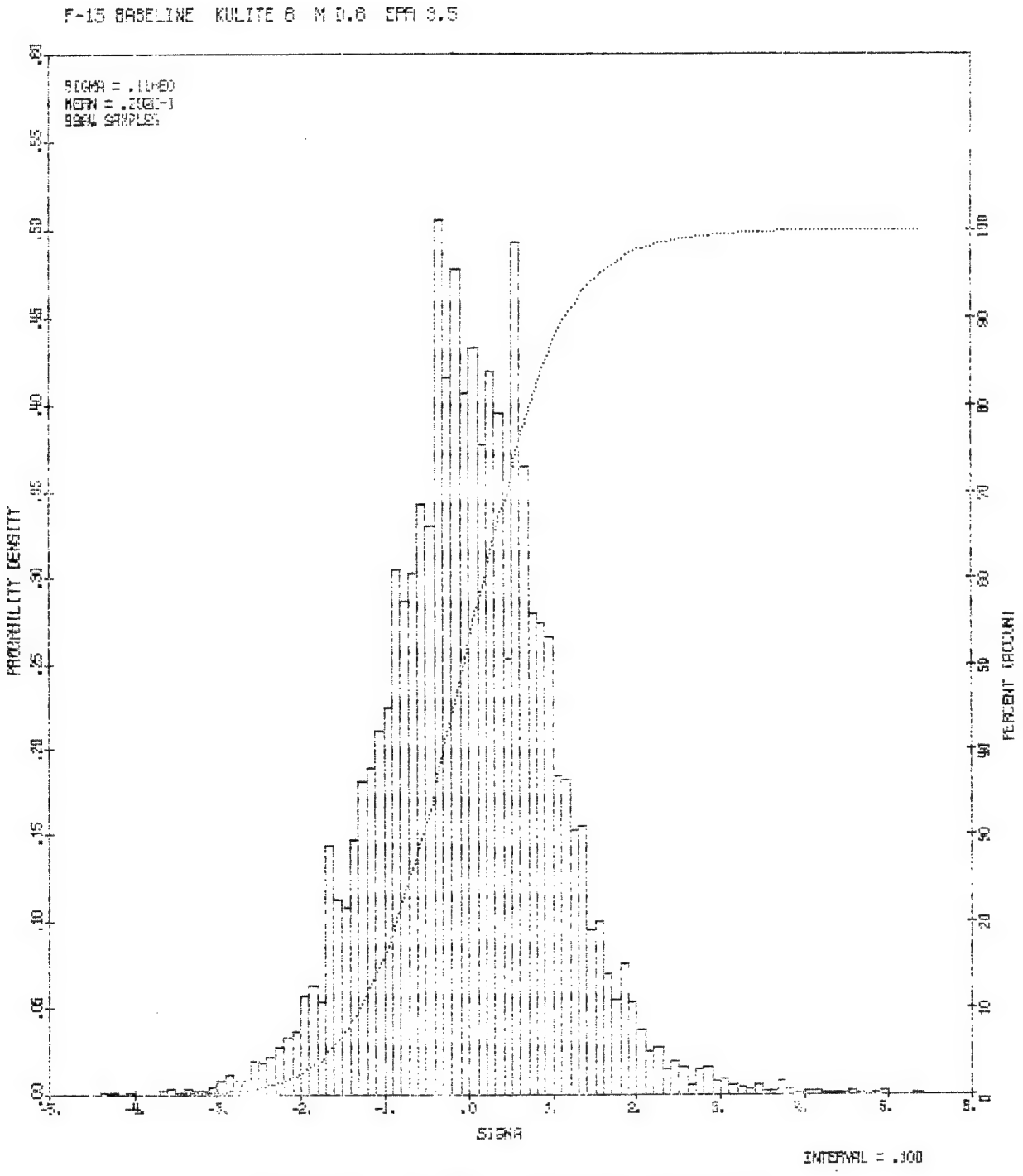

Figure 17. Probability Density Function
-Baseline Kulite 6 MACH 0.6 EPR 3.5

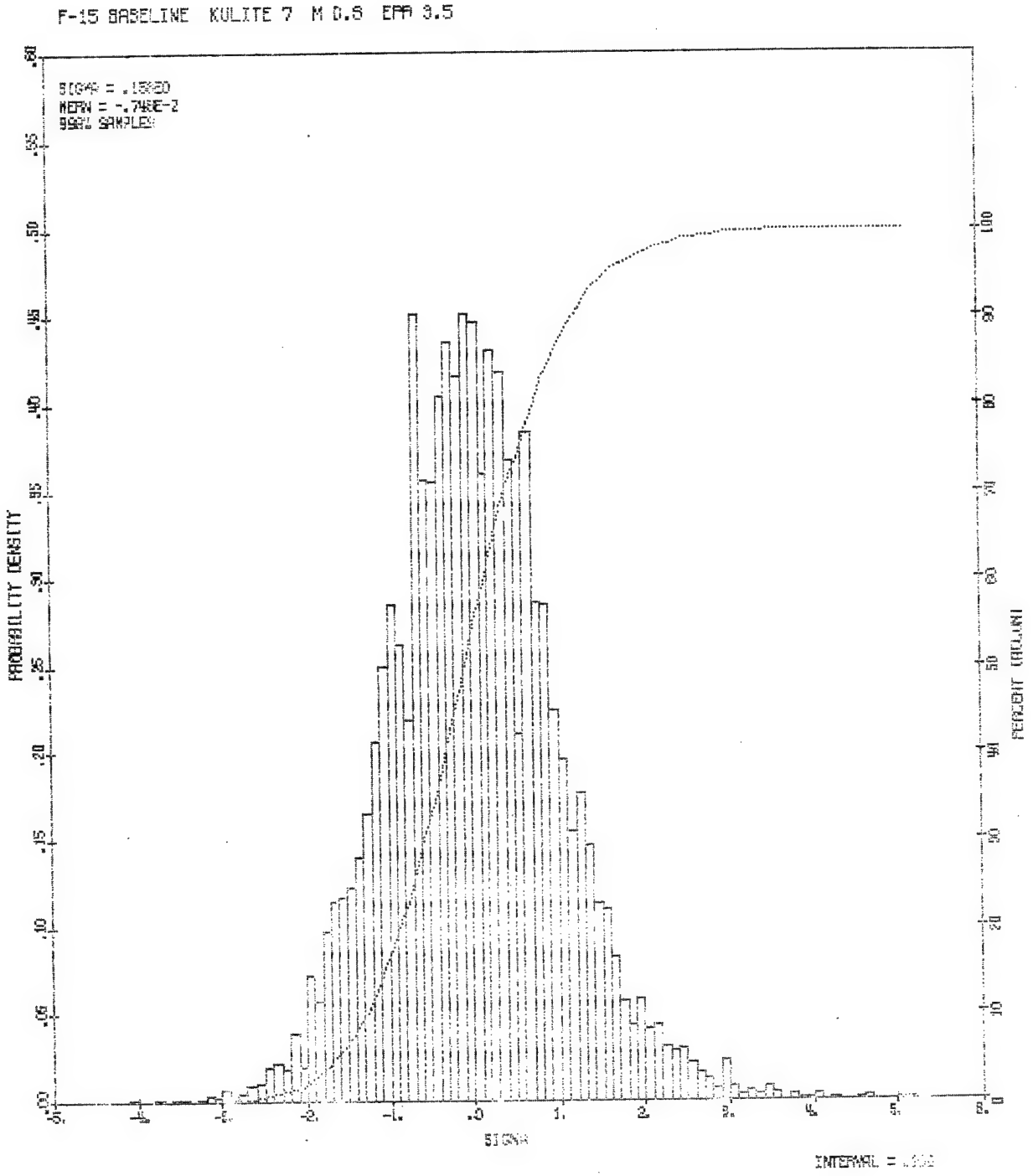

Figure 18. Probability Density Function
-Baseline Kulite 7 MACH 0.9 EPR 3.5

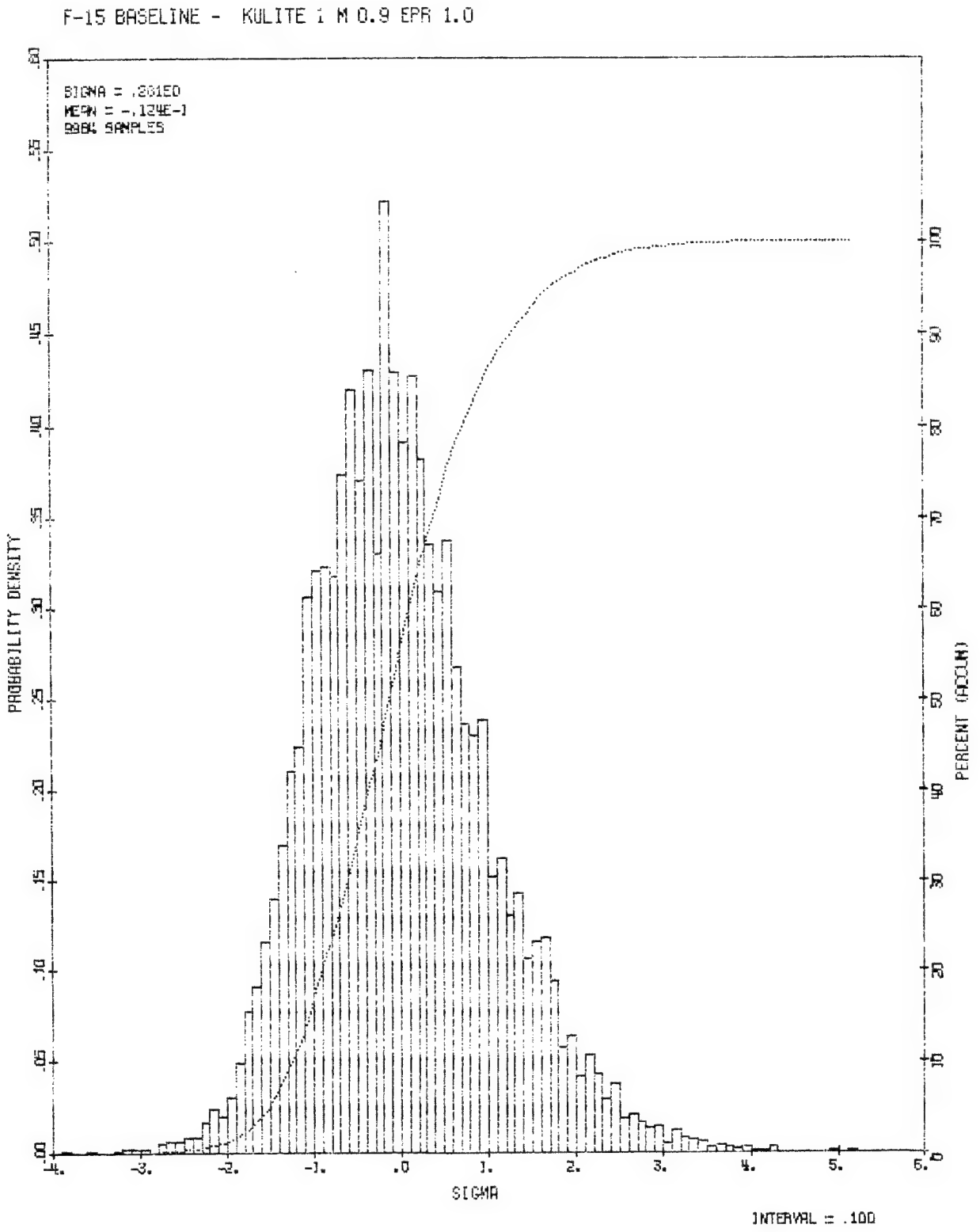

Figure 19. Probability Density Function
-Baseline Kulite 1 MACH 0.9 EPR 1.0

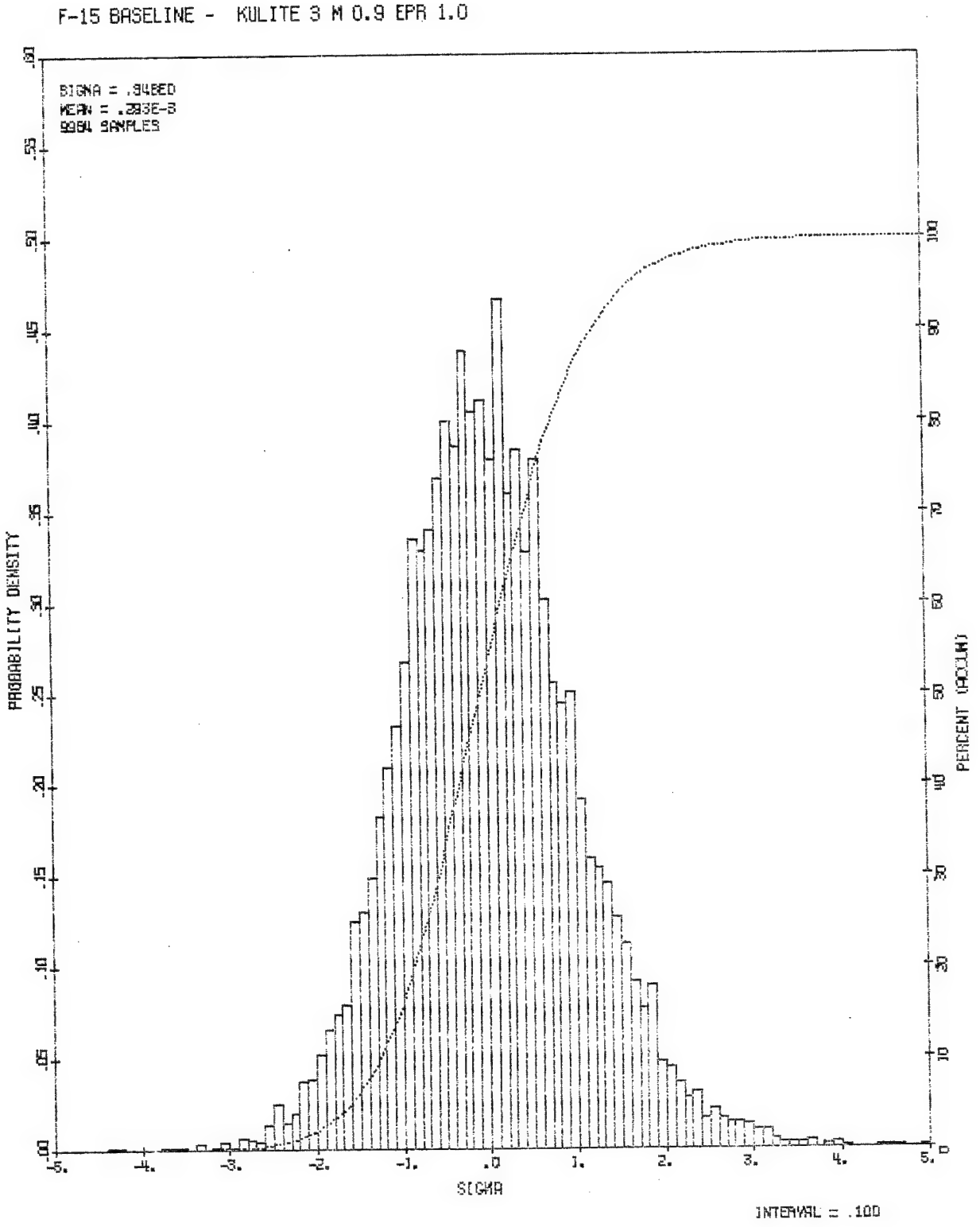

Figure 20. Probability Density Function
-Baseline Kulite 3 MACH 0.9 EPR 1.0

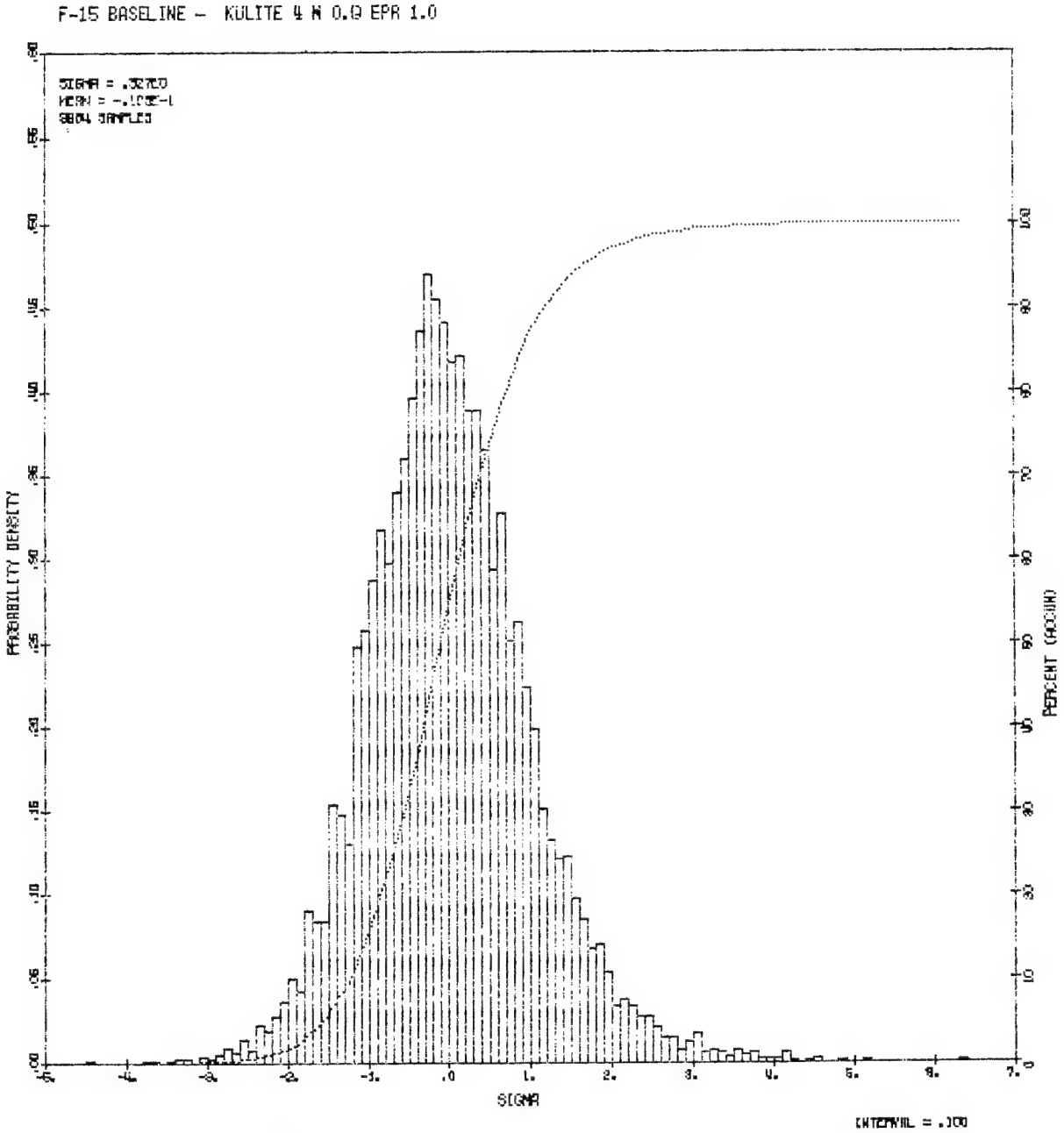

Figure 21. Probability Density Function
-Baseline Kulite 4 MACH 0.9 EPR 1.0

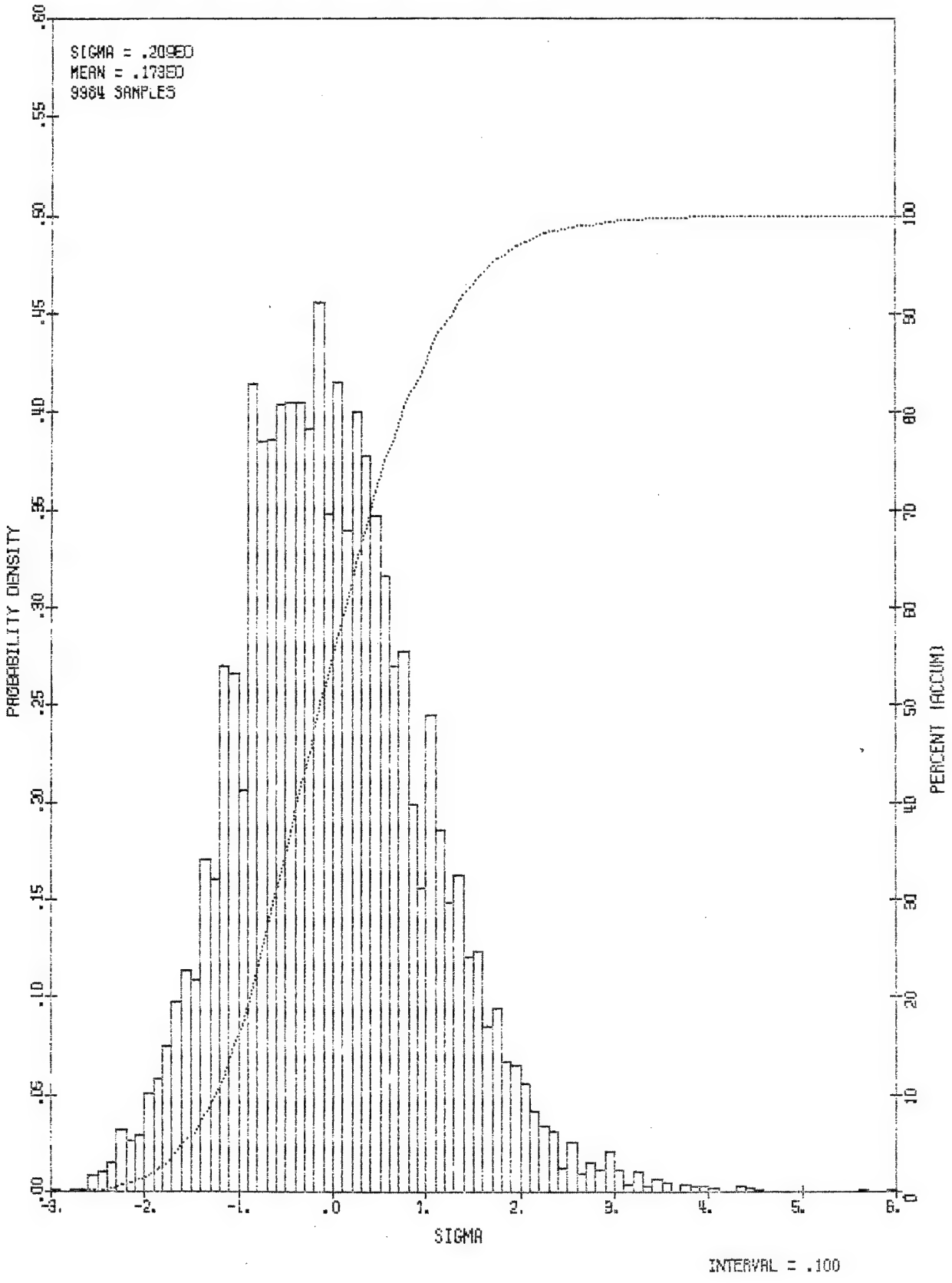

Figure 22. Probability Density Function
-Baseline 5 MACH 0.9 EPR 1.0

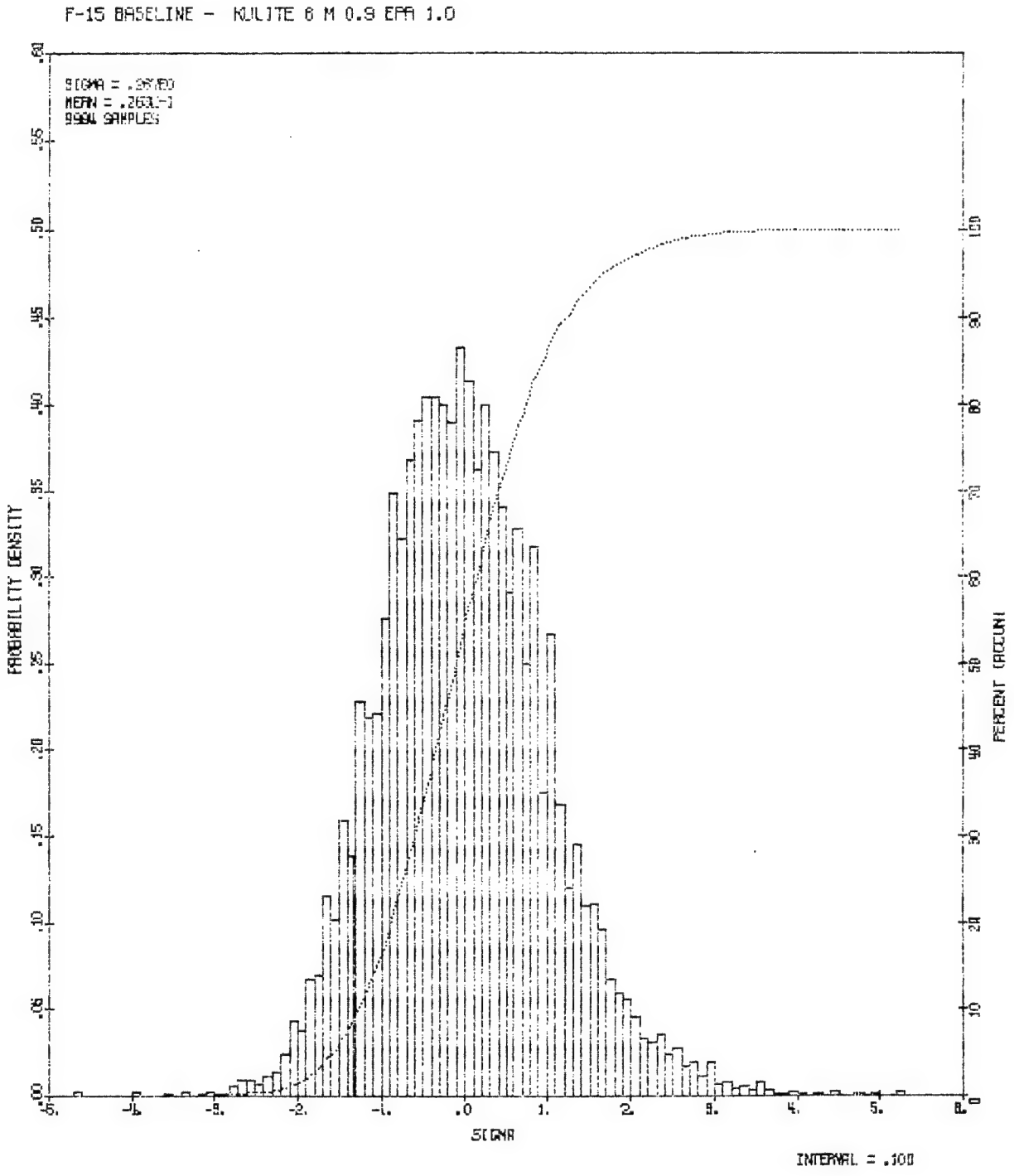

Figure 23. Probability Density Function
-Baseline Kulite 6 MACH 0.9 EPR 1.0

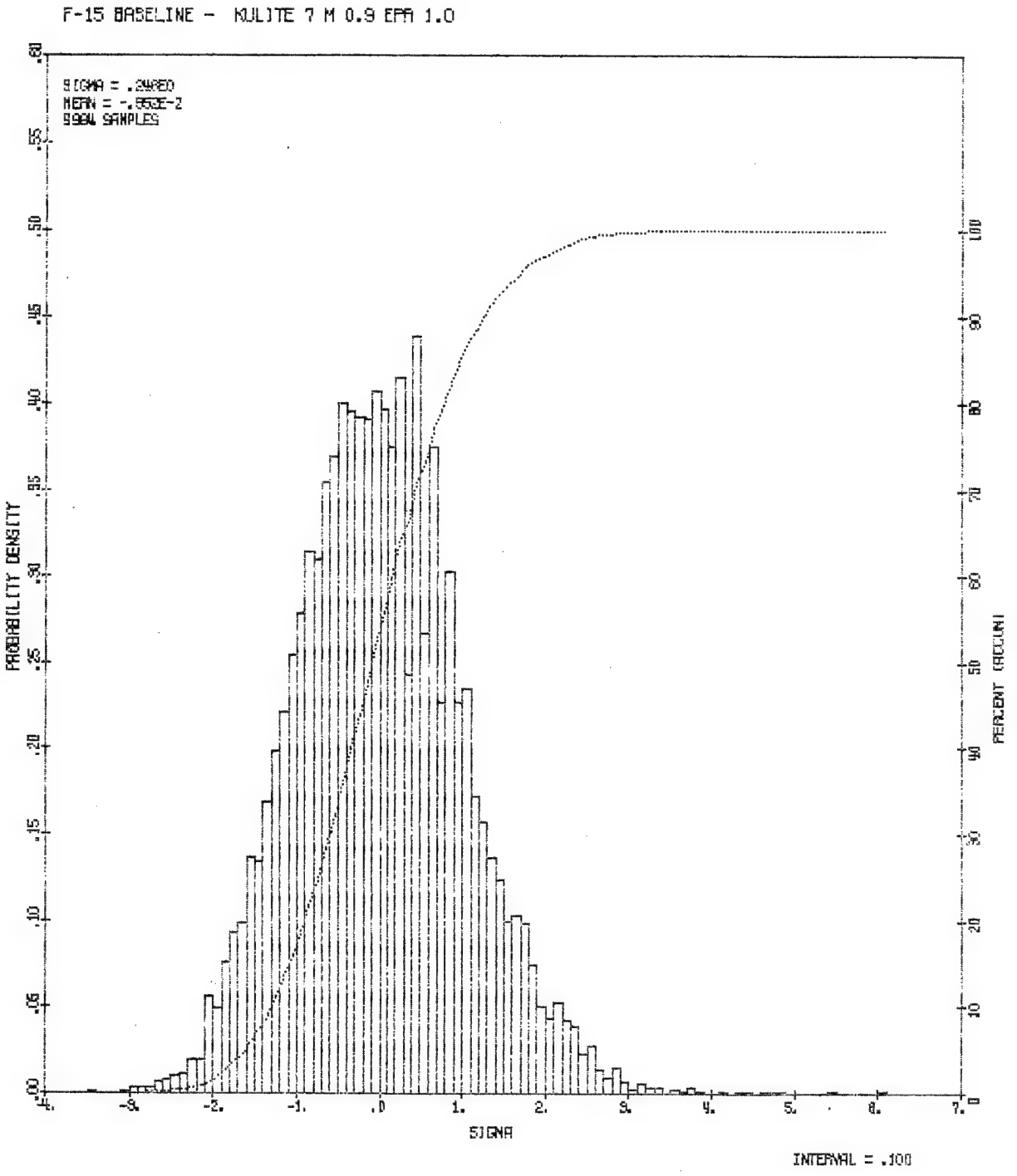

Figure 24. Probability Density Function
-Baseline Kulite 7 MACH 0.9 EPR. 1.0

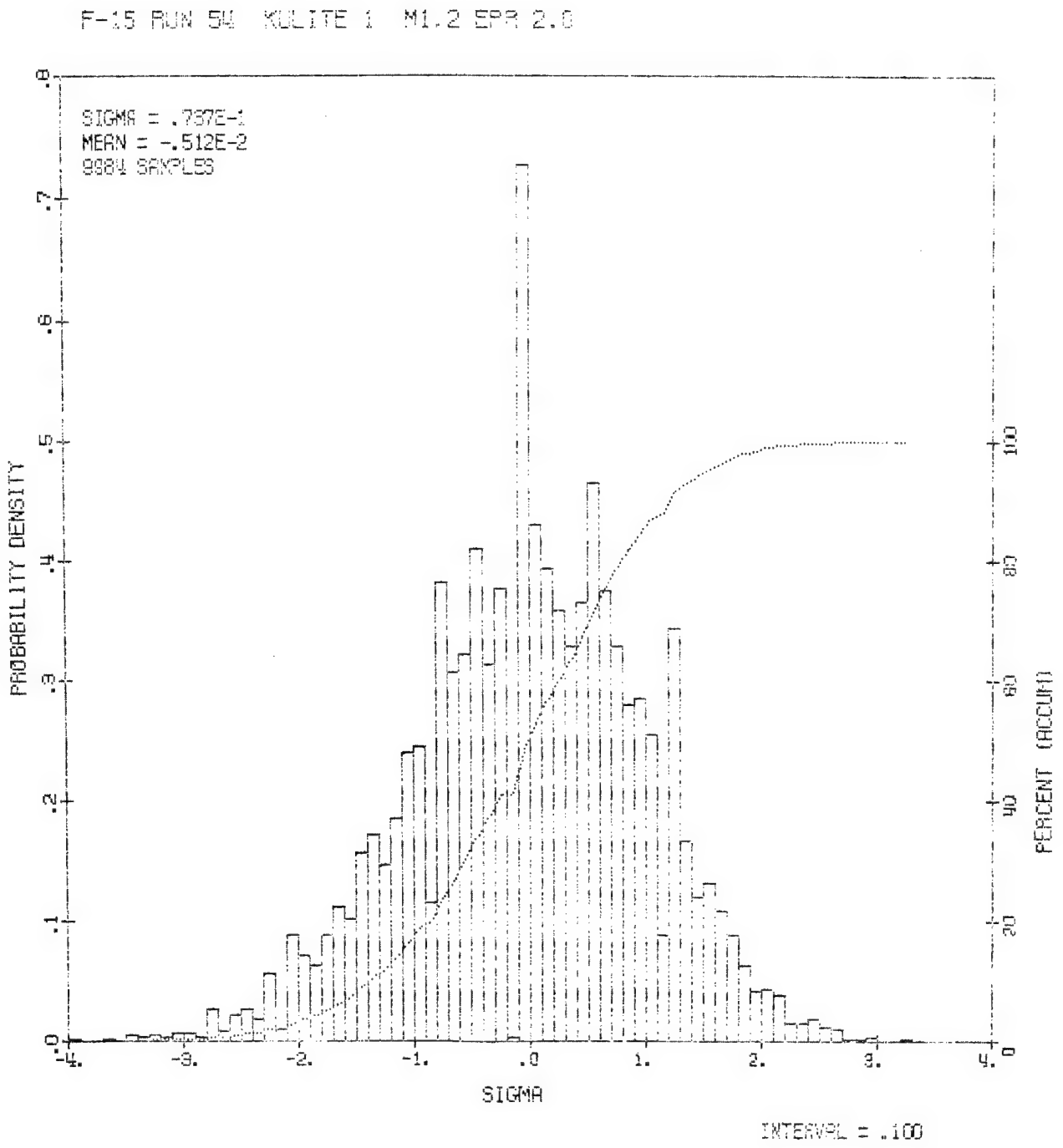

Figure 25. Probability Density Function-Baseline
Kulite 1 MACH 1.2 EPR 2.0

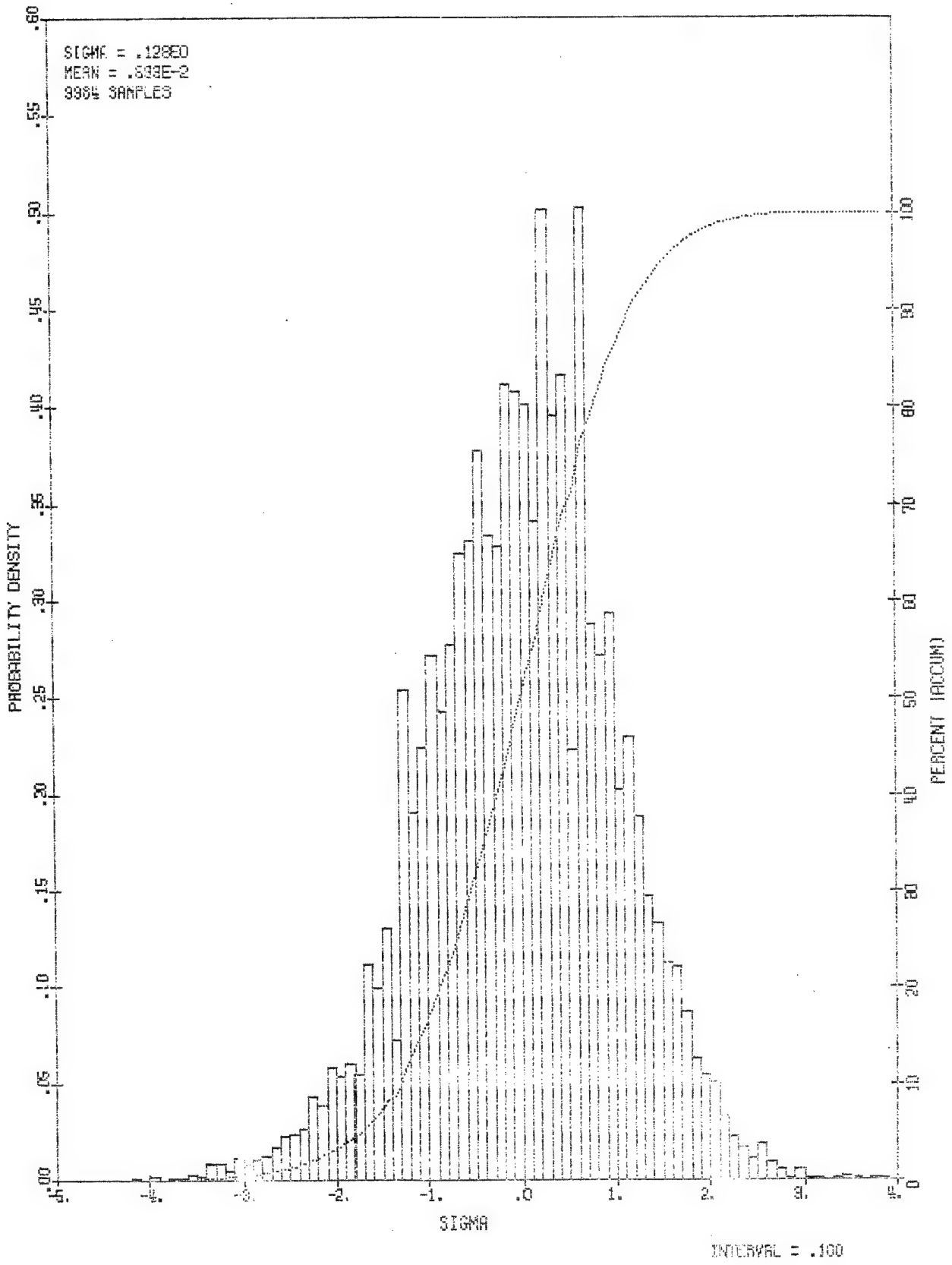

Figure 26. Probability Density Function-
with Canards Kulite 3 MACH 1.2 EPR 2.0

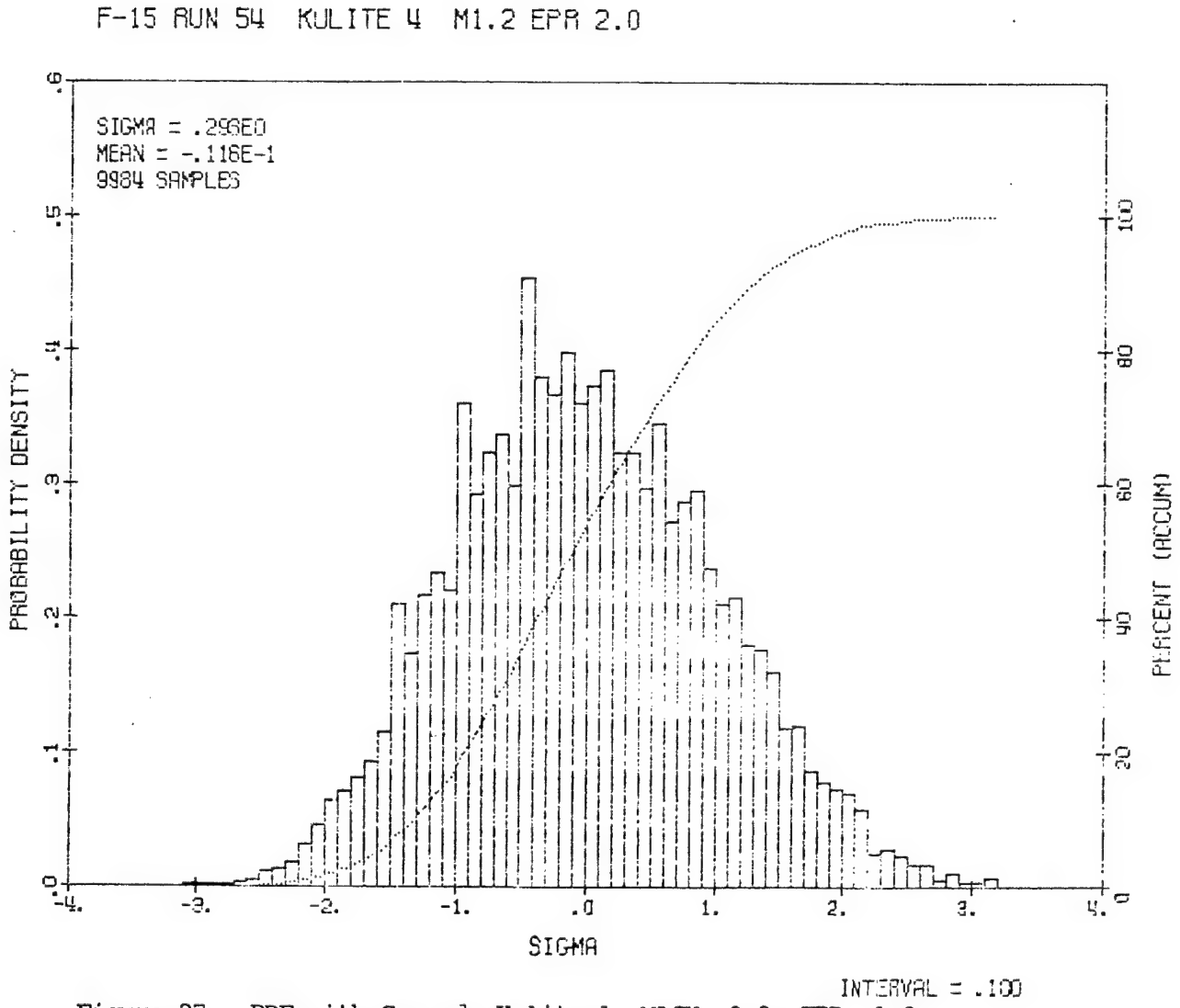

Figure 27. PDF-with Canards Kulite 1 MACH 0.9 EPR 1.0

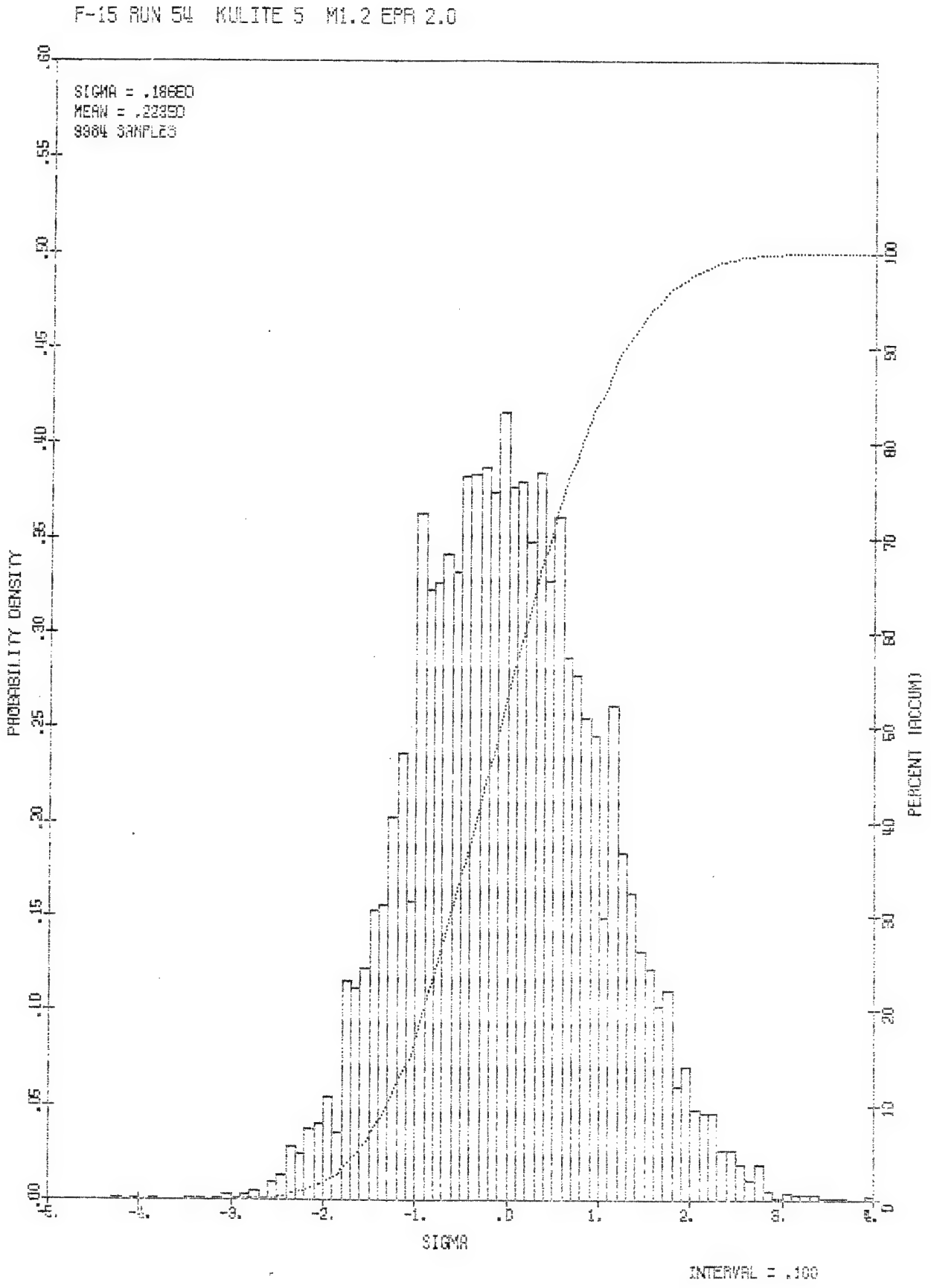

Figure 28. Probability Density Function-
With Canards Kulite 5 MACH 1.2 EPR 2.0

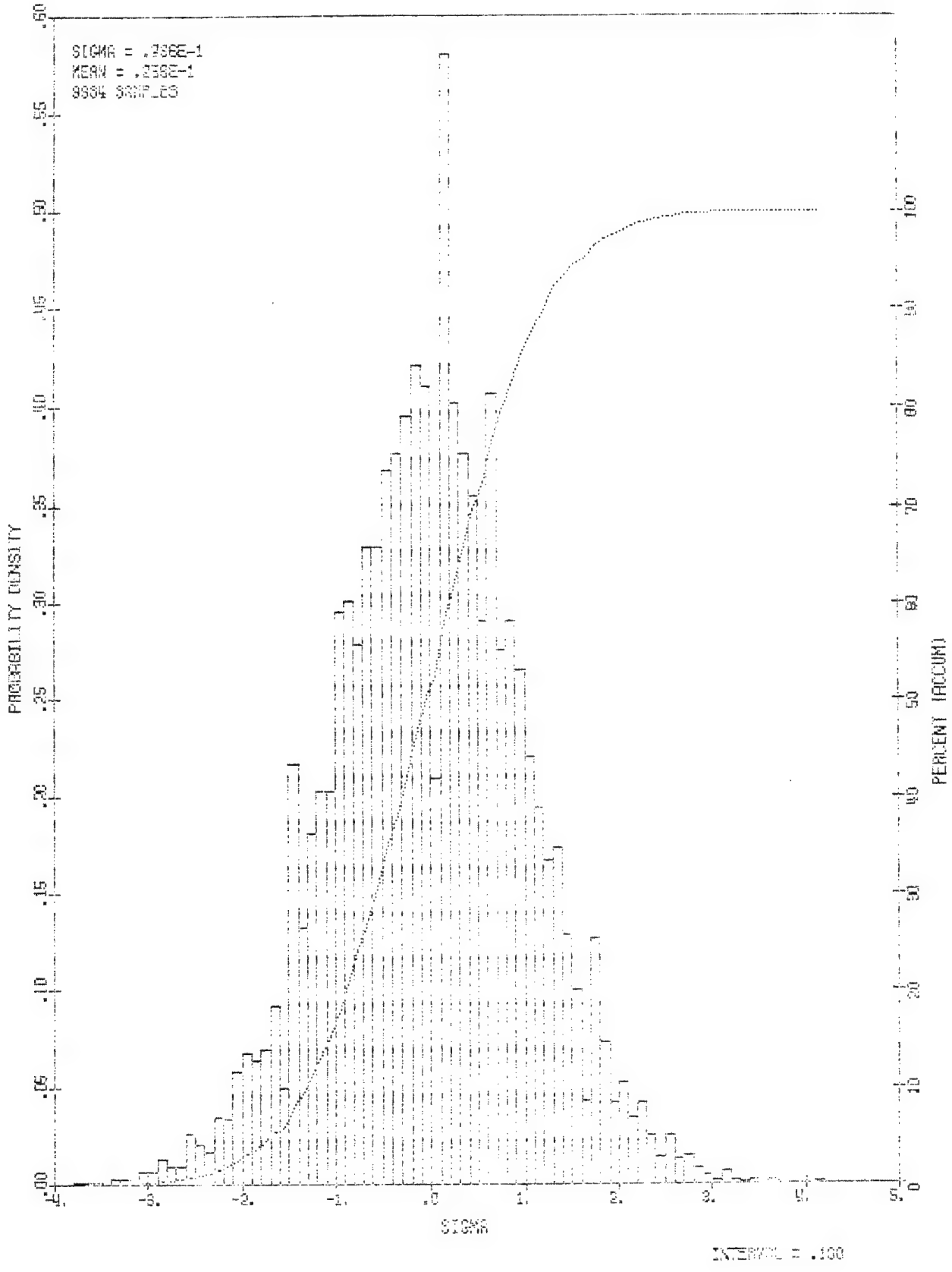

Figure 29. Probability Density Function-
with Canards Kulite 6 MACH 1.2 EPR 2.0

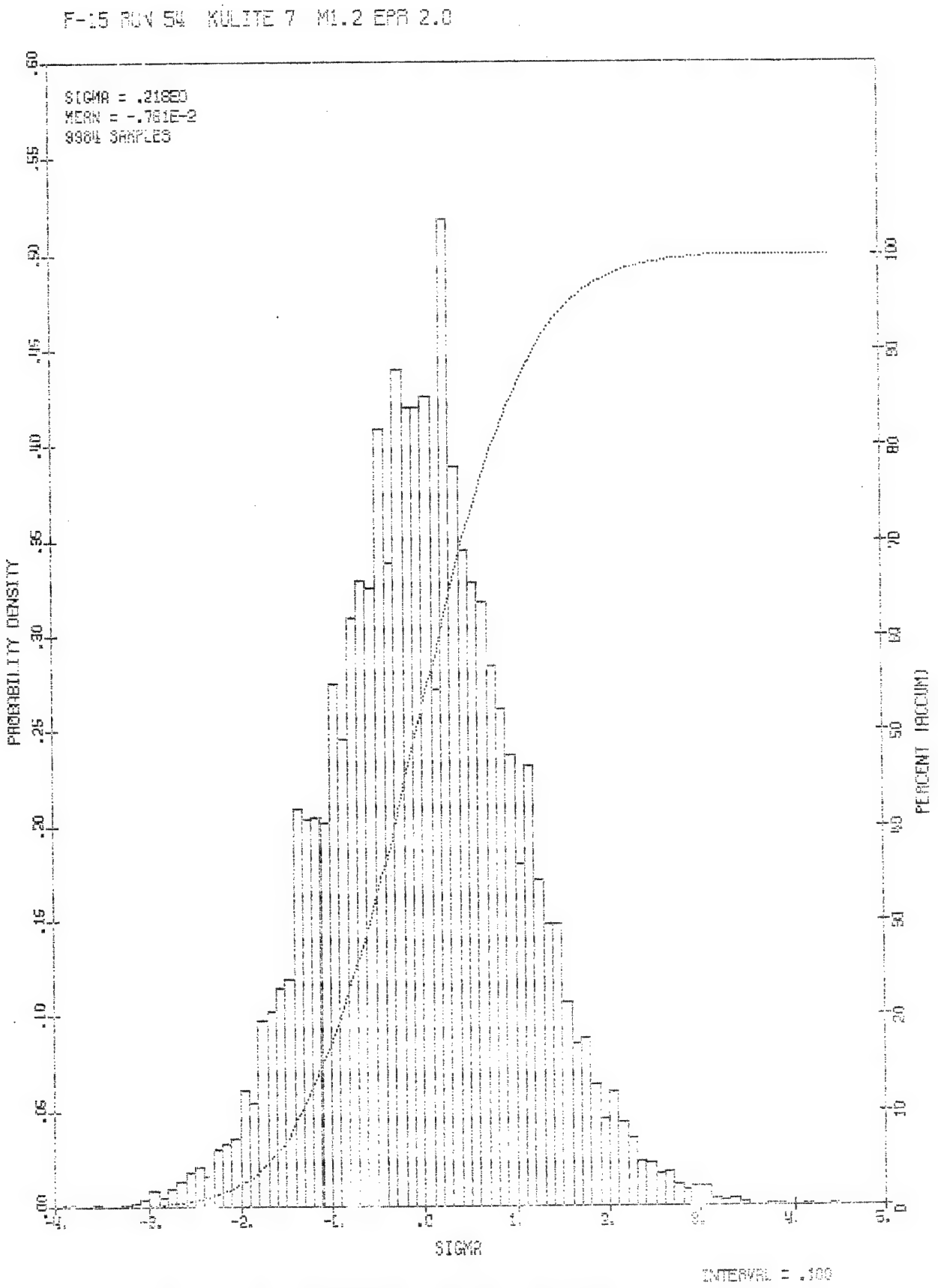

Figure 30 Probability Density Function-
with Canards Kulite 7 MACH 1.2 EPR 2.0

TABLE 7

STATISTICAL PROPERTIES OF THE PROBABILITY DENSITY FUNCTION

SOURCE	MACH	TRANSDUCER	SAMPLES/ INTERVAL	MEAN	RMS	ST DEV	SKEWNESS	KURTOSIS	NUMBER OF INTERVALS
Normal Distribution			2048/0.100	0.0617	0.0617	.553	0.0	3.0	60
Sine Wave			2048/0.100	0.0414	.0414	1.01	0.0	1.5	30
Run 57/Pt 19	0.60	1	9984/0.100	-.00744	.0757	.0053	.0002	2.835	81
		3		.00307	.1394	.1394	.0385	4.282	103
		4		-.0075	.2176	.2174	.0354	3.432	94
		5		.1706	.2288	.1524	.3547	3.775	84
		6		.0292	.1194	.1158	.2033	4.092	98
		7		-.0075	.1564	.1562	.2936	3.712	93
Run 54/Pt 3	1.20	1		-.0051	.0739	.0737	-.2309	2.968	73
		3		.0069	.1286	.1285	-.2014	3.253	81
		4		-.0116	.2937	.2935	.1807	2.659	63
		5		.2226	.2900	.1858	.1481	2.946	83
		6		.0258	.0971	.0936	.0090	3.153	80
		7		-.0076	.2183	.2181	.1106	3.171	84
Run 57/Pt 8	0.90	1		-.0124	.2612	.2609	.5047	3.610	91
		3		.003	.3483	.3483	.2694	3.560	94
		4		-.0105	.3276	.3274	.4375	4.159	109
		5		.1733	.2717	.2092	.4972	3.672	90
		6		-.0263	.2679	.2666	.3855	3.739	100
		7		-.0095	.2461	.2459	.3211	3.404	96

17
1

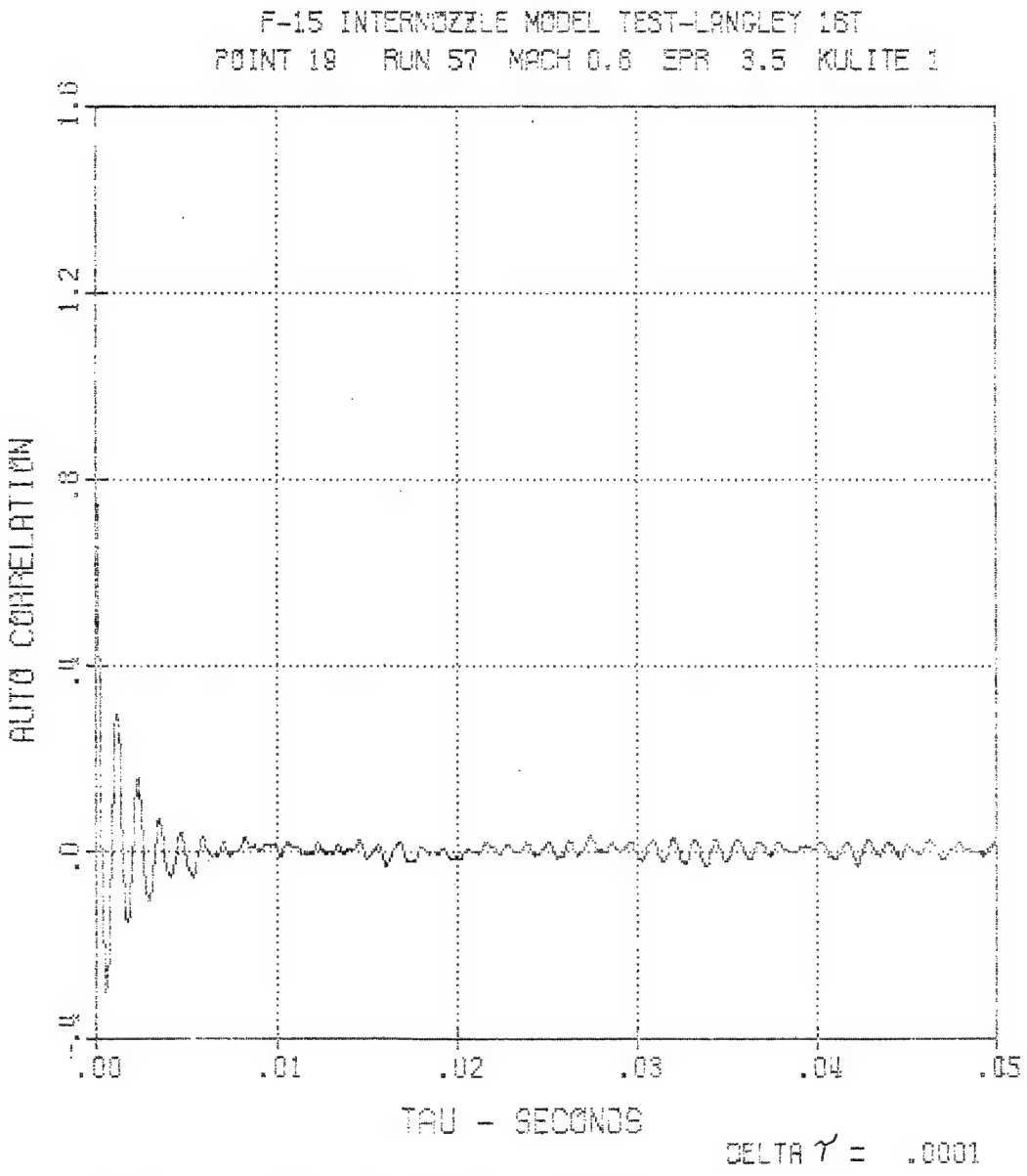

Figure 31. Auto Correlation Function-
Baseline Kulite 1 MACH 0.6 EPR 3.5

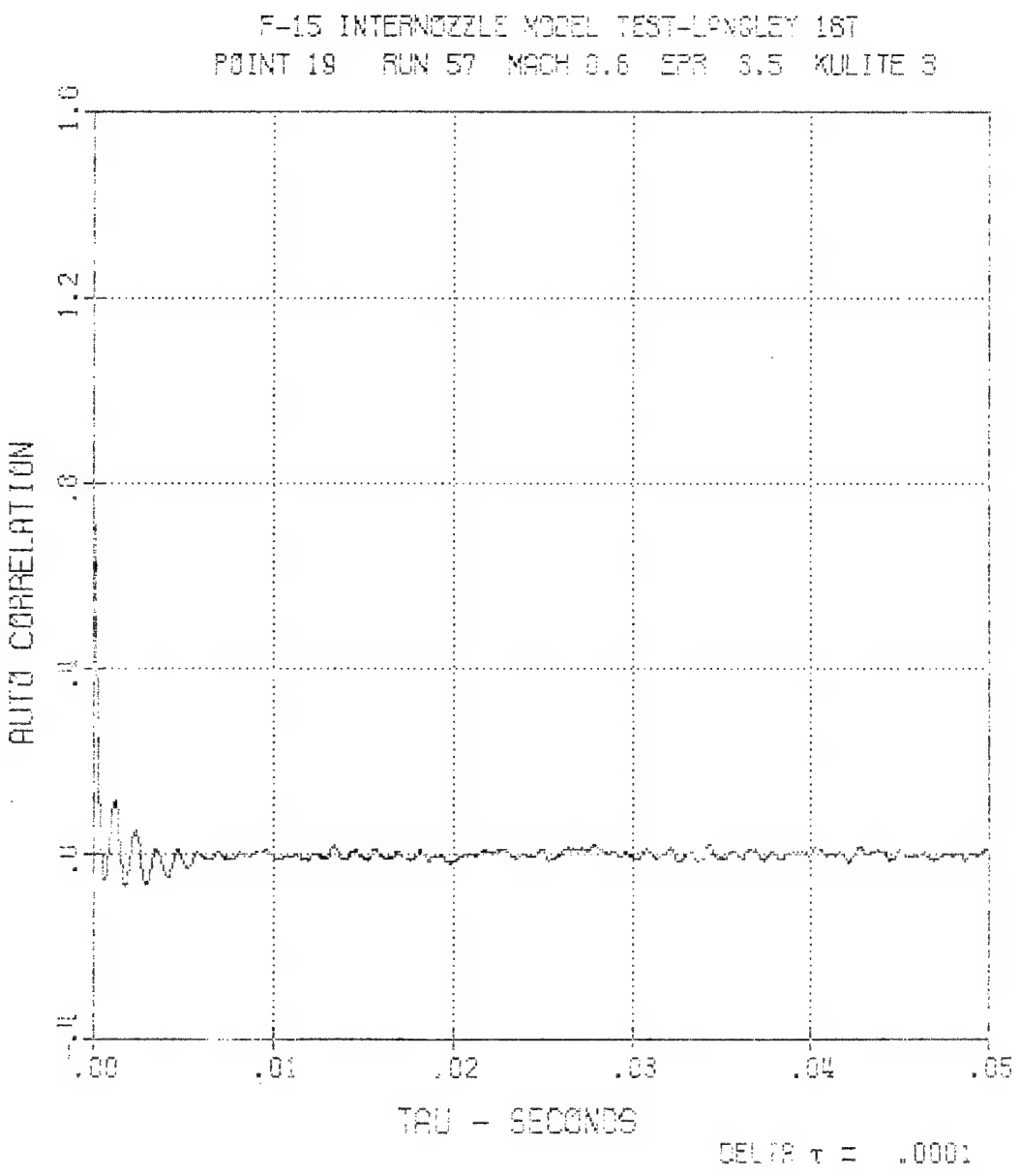

Figure 32. Auto Correlation Function-
Baseline Kulite 3 MACH 0.6 EPR 3.5

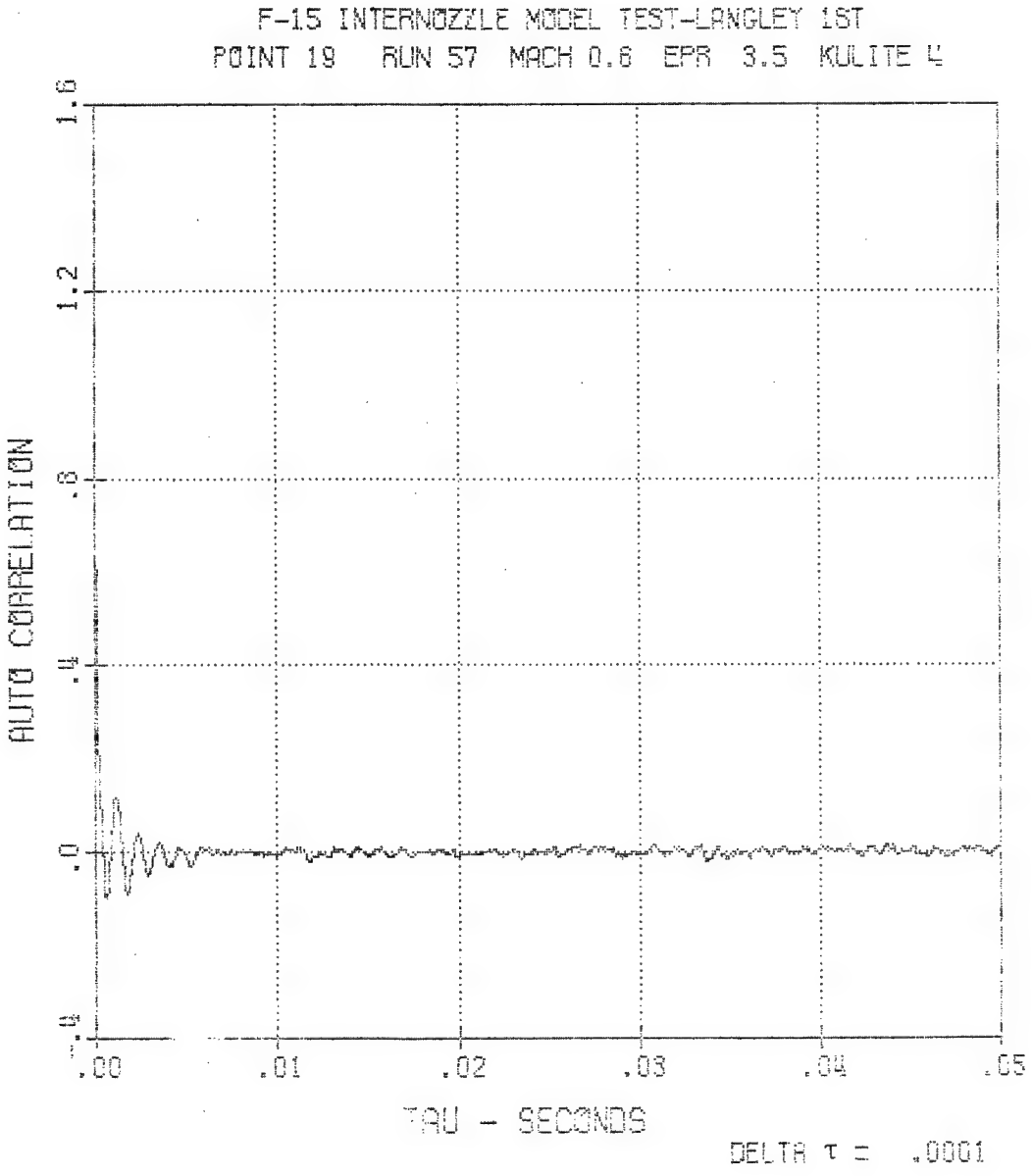

Figure 33. Auto Correlation Function-Baseline
Kulite 4 MACH 0.6 EPR 3.5

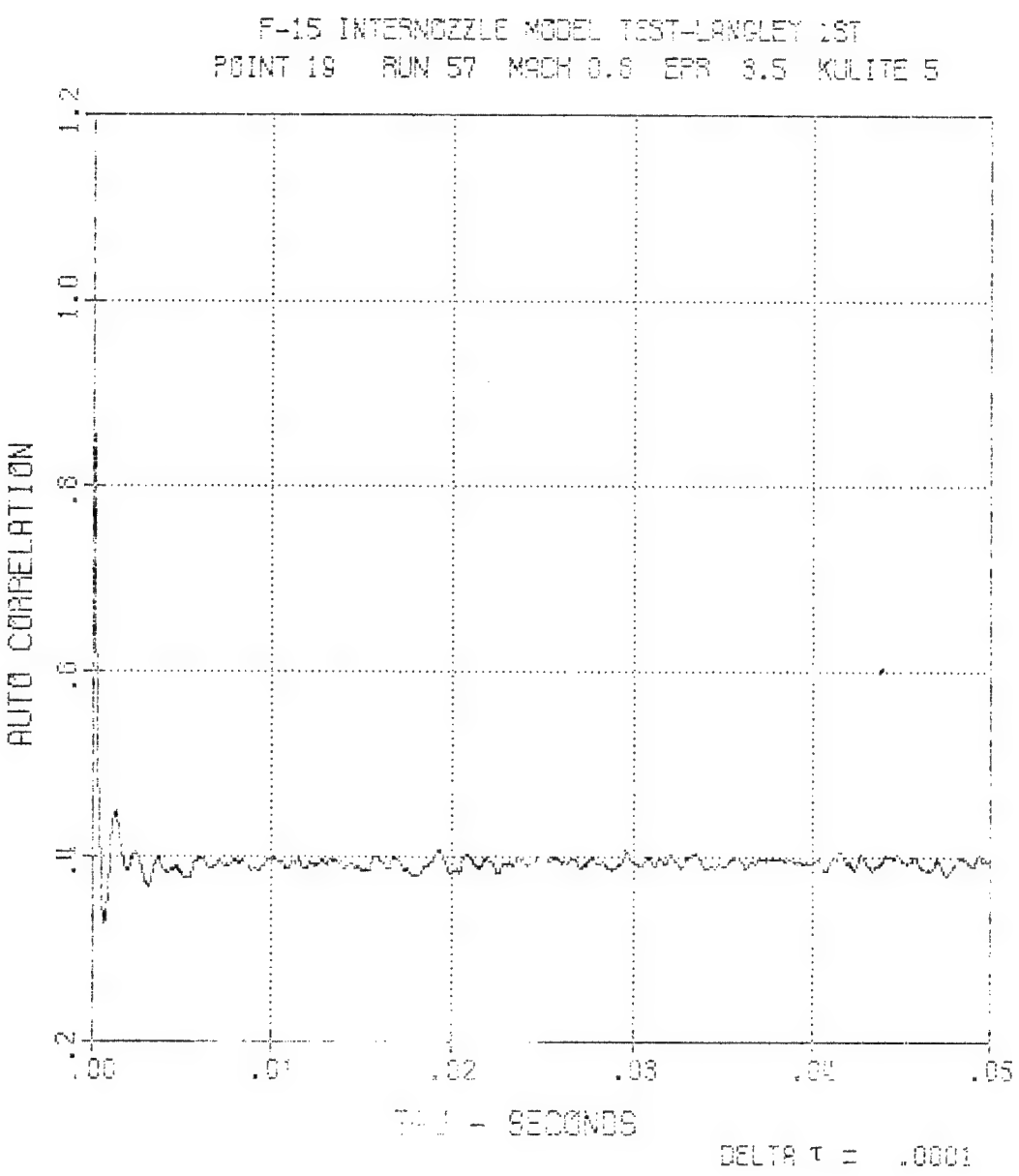

Figure 34. Auto Correlation Function-Baseline
Kulite 5 MACH 0.6 EPR 3.5

19
6

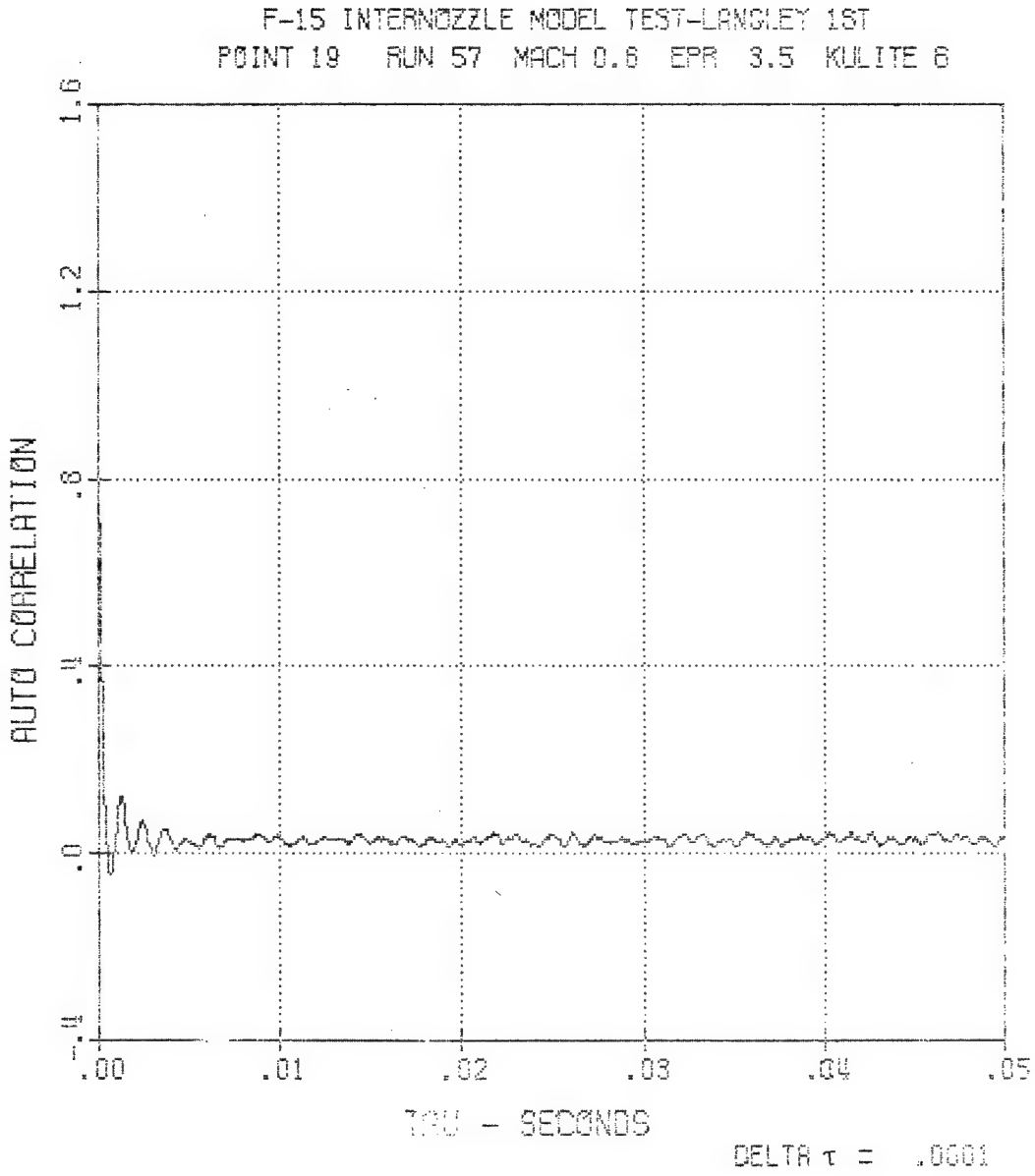

Figure 35. Auto Correlation Function-Baseline
Kulite 6 MACH 0.6 EPR 3.5

19
7

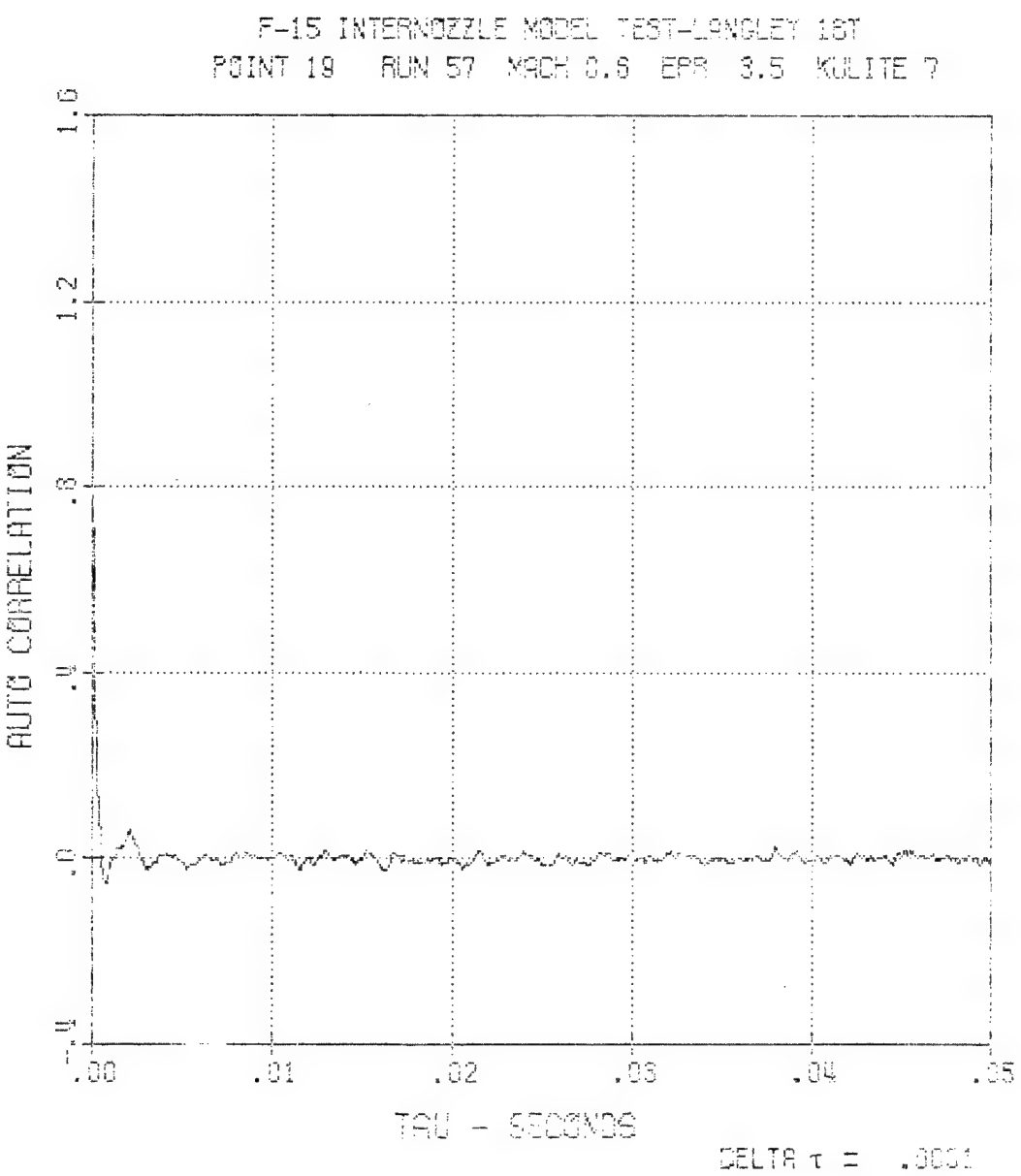

Figure 36. Auto Correlation Function-Baseline
Kulite 7 MACH 0.6 EPR 3.5

16
1

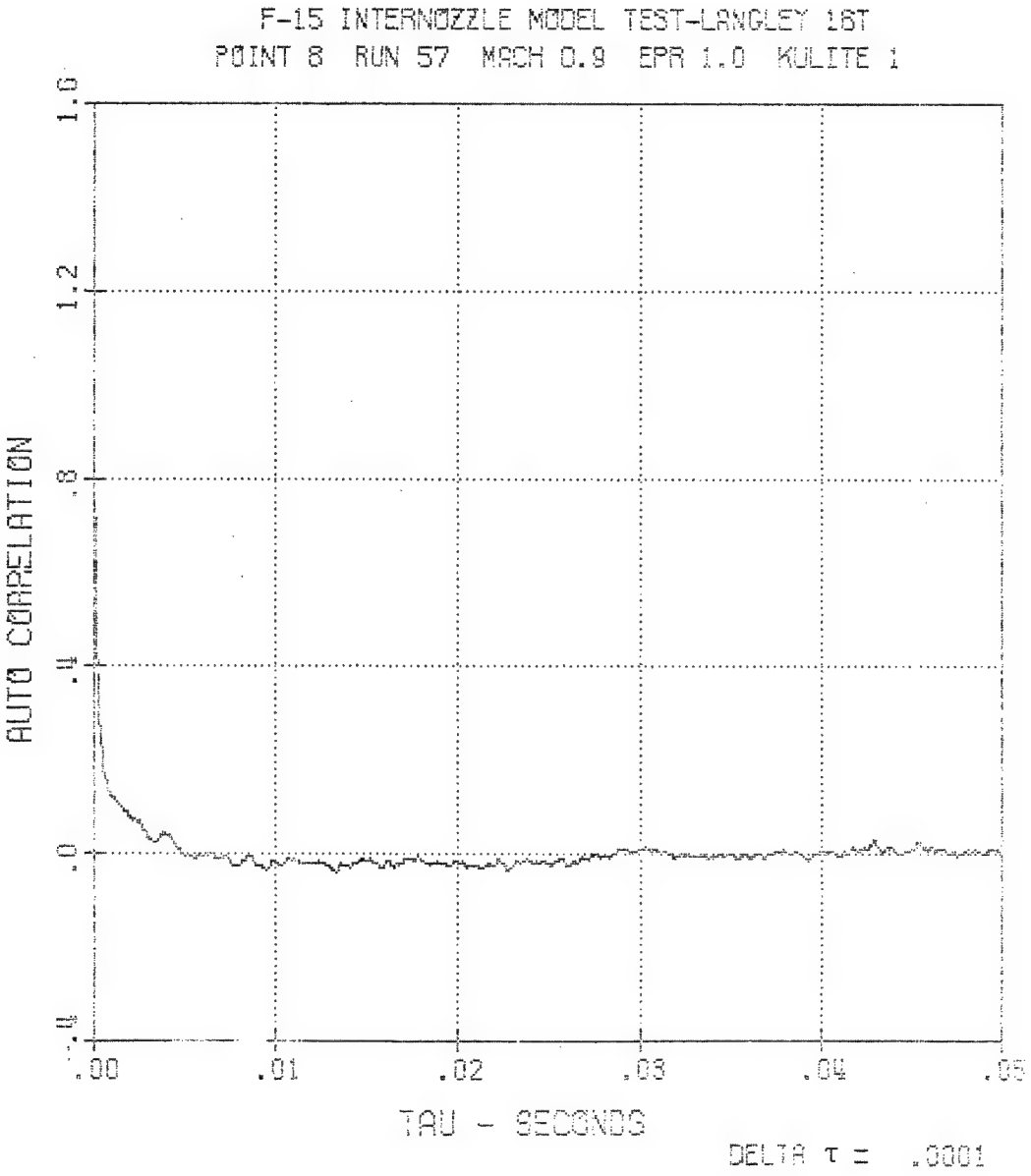

Figure 37. Auto Correlation Function-Baseline
Kulite 1 MACH 0.9 EPR 1.0

16
3

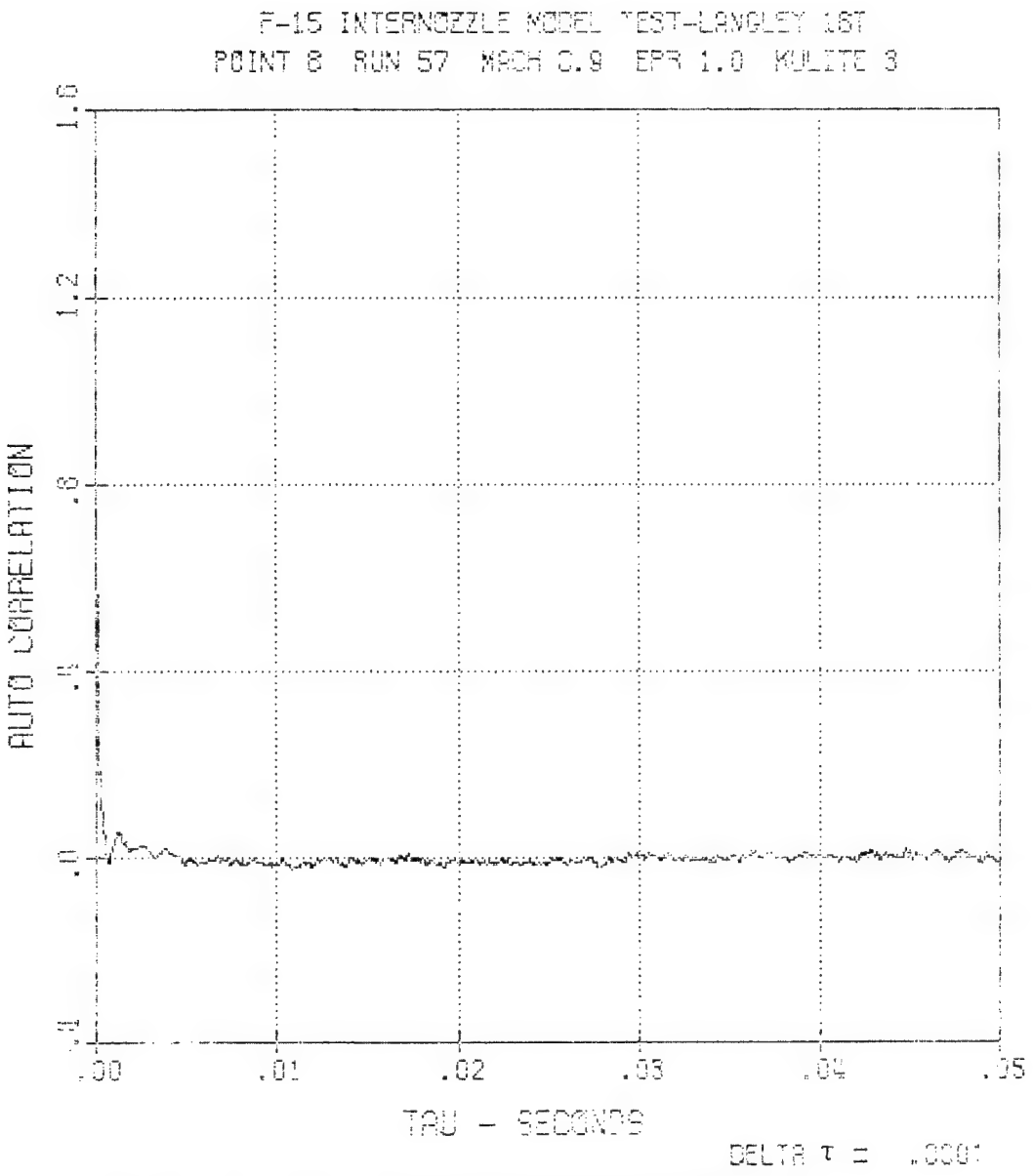

Figure 38. Auto Correlation Function-Baseline
Kulite 3 MACH 0.9 EPR 1.0

17
4

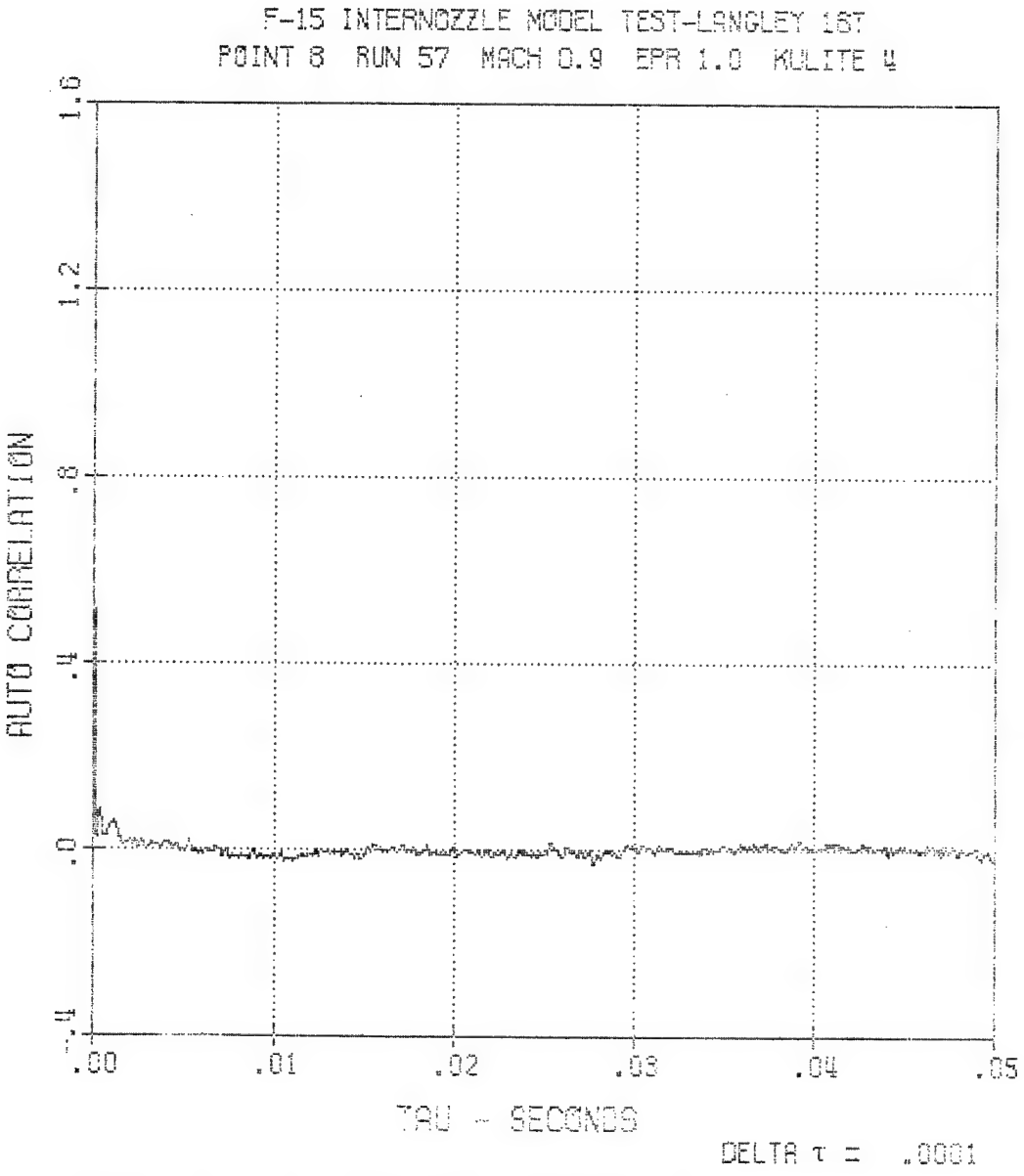

Figure 39. Auto Correlation Function-Baseline
Kulite 4 MACH 0.9 EPR 1.0

17
5

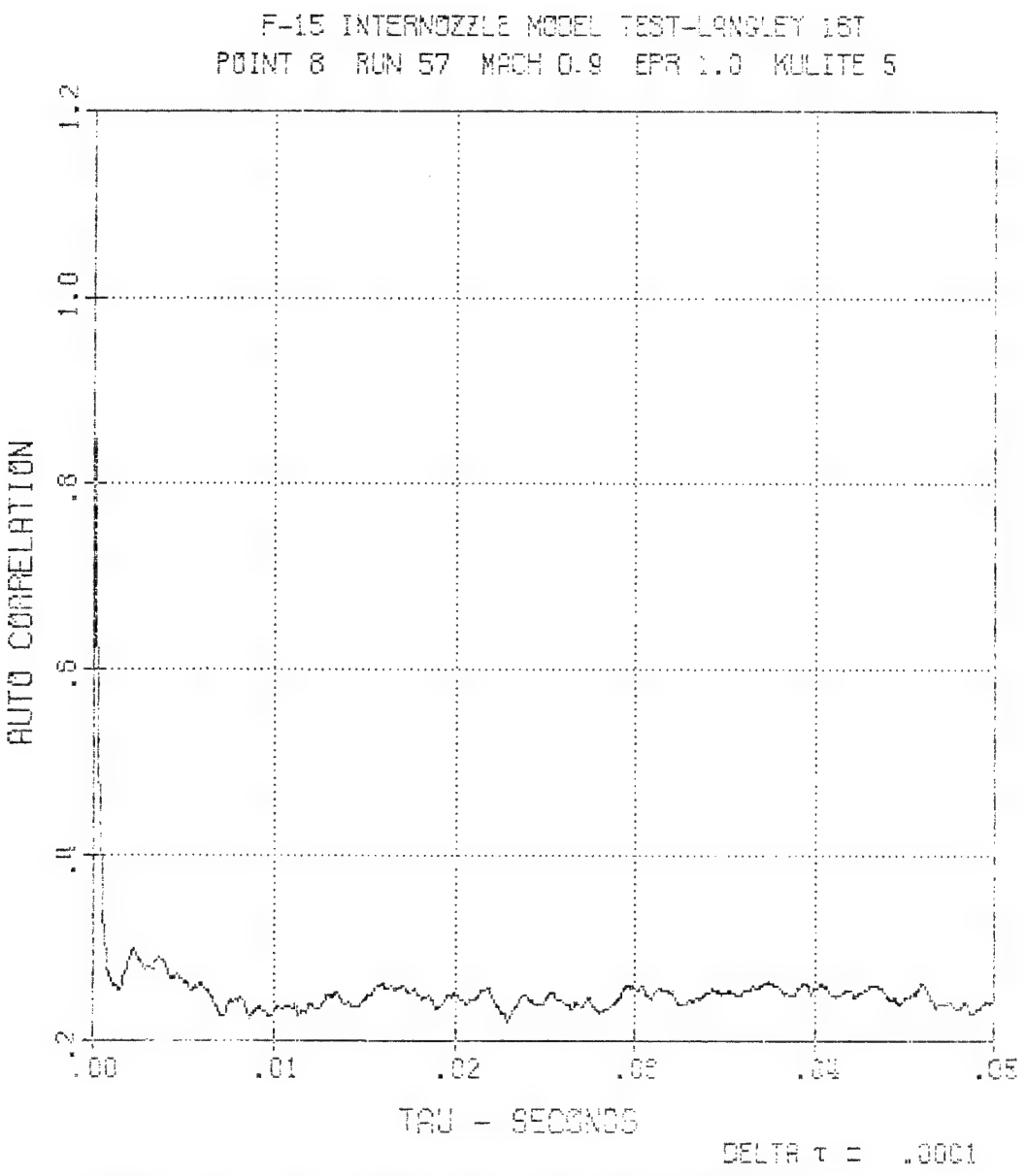

Figure 40. Auto Correlation Function-Baseline
Kulite 5 MACH 0.9 EPR 1.0

18
6

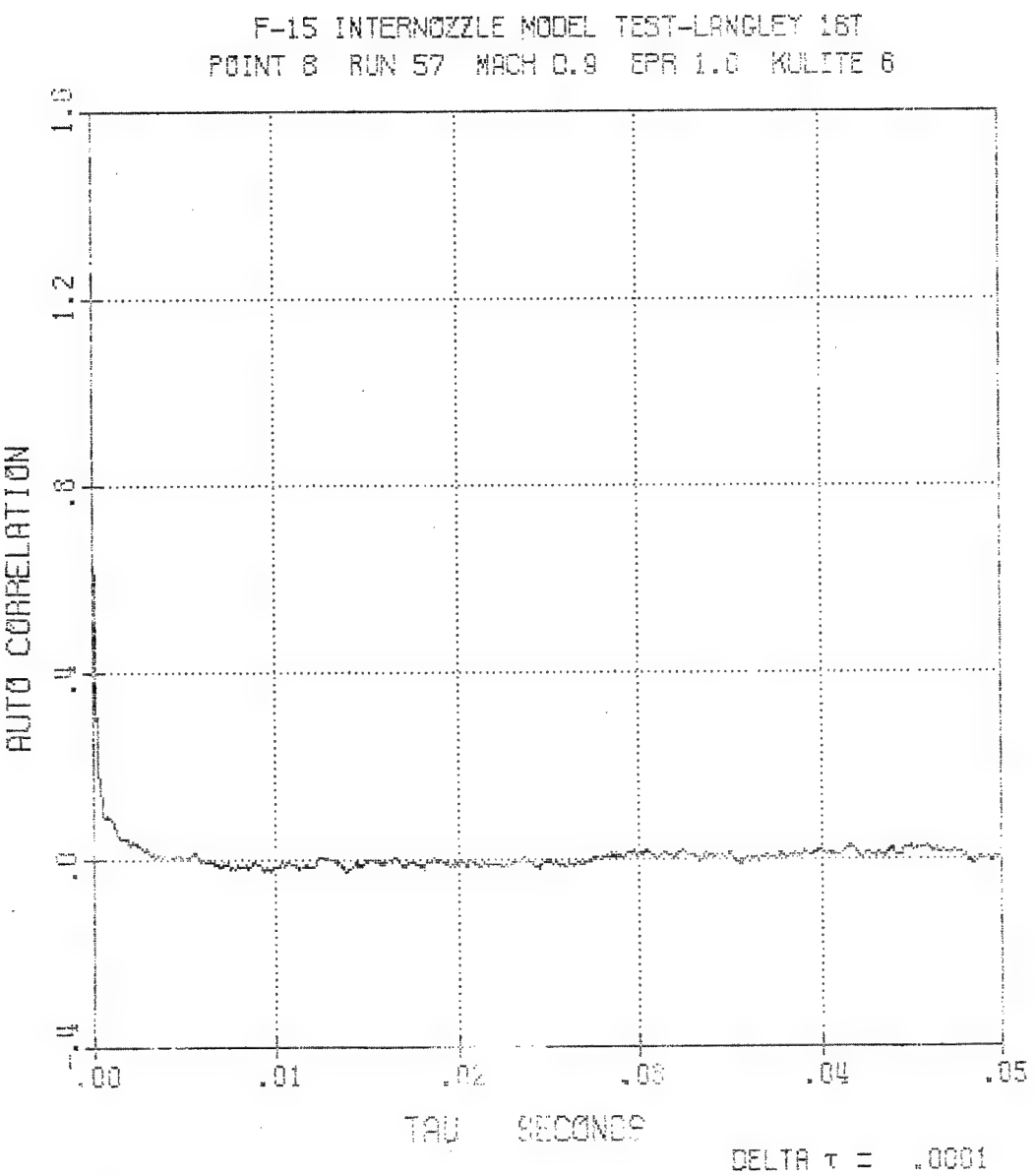

Figure 41. Auto Correlation Function-Baseline
Kulite 6 MACH 0.9 EPR 1.0

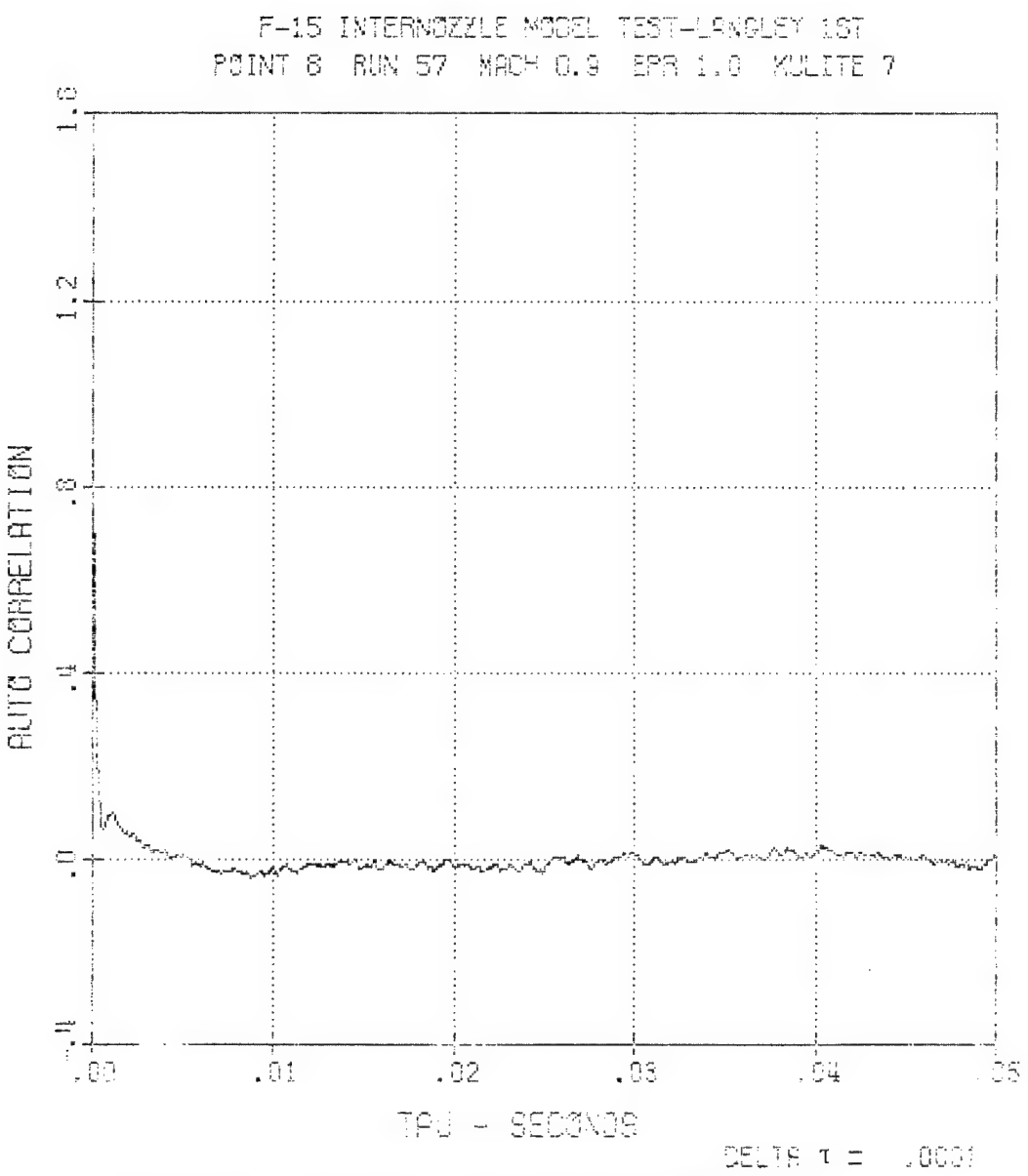

Figure 42. Auto Correlation Function-Baseline
Kulite 7 MACH 0.9 EPR 1.0

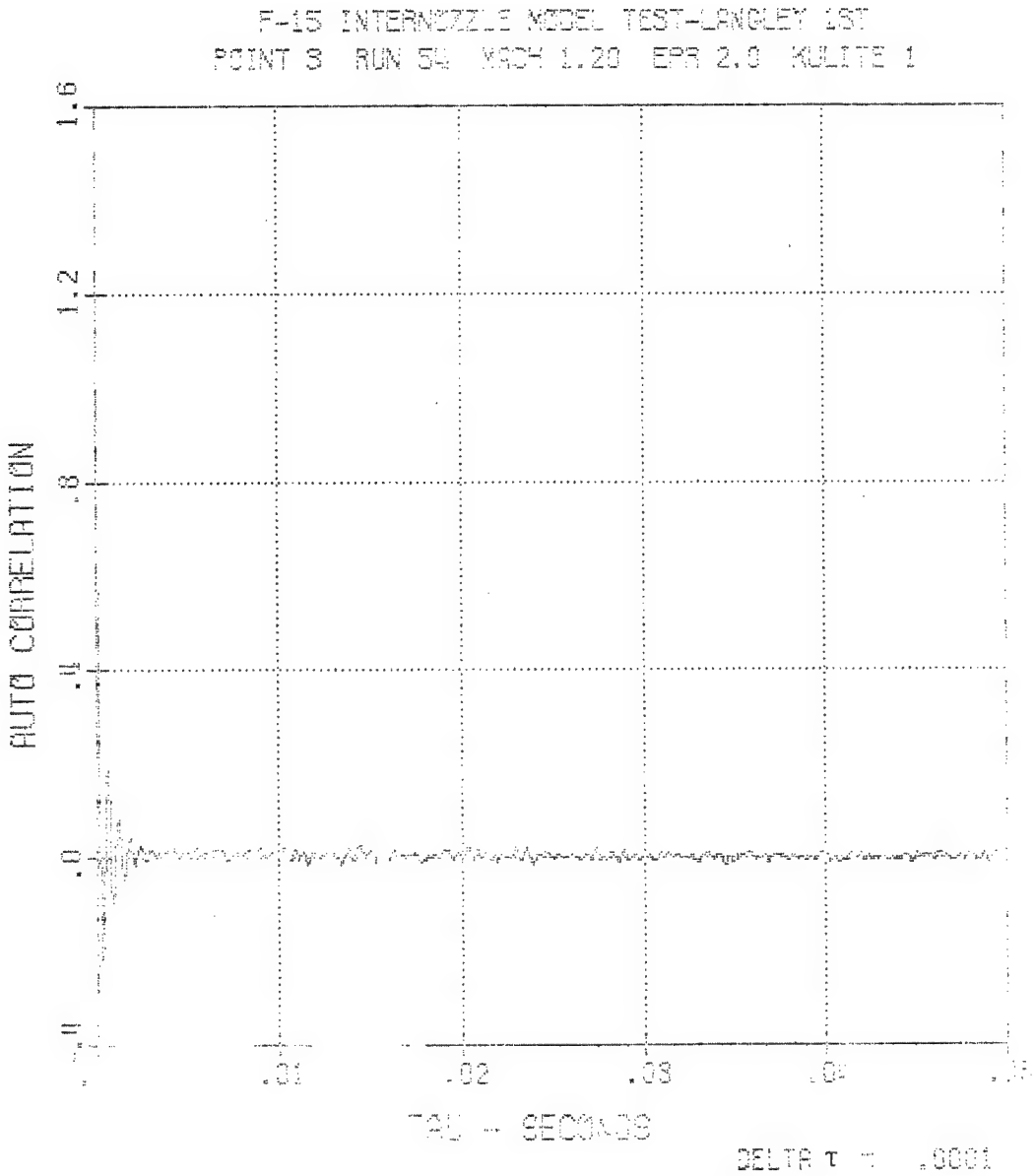

Figure 43. Auto Correlation Function-
with Canards Kulite 1 MACH 1.2 EPR 2.0

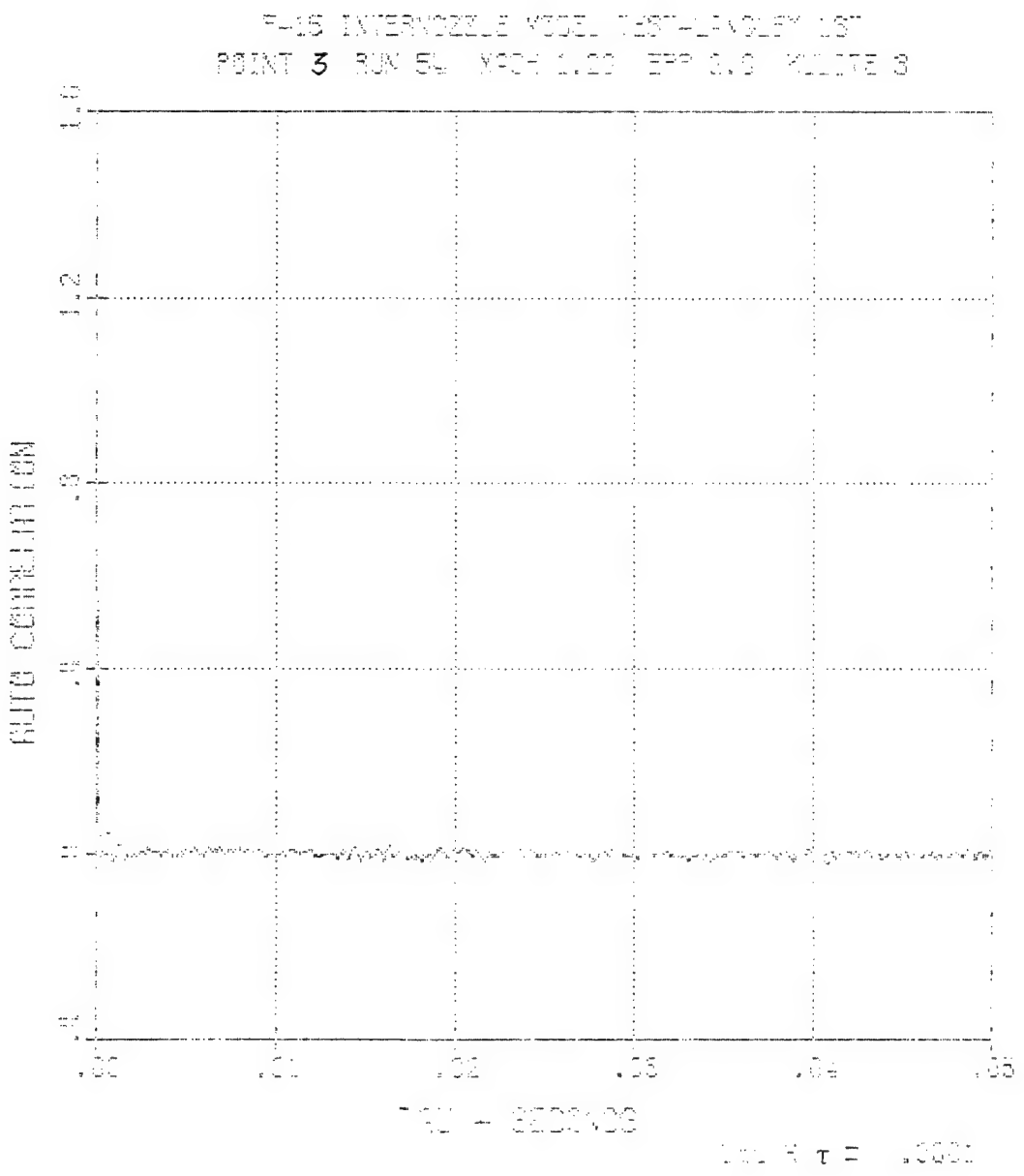

Figure 44. Auto Correlation Function-with Canards Kulite 3 MACH 1.2 EPR 2.0

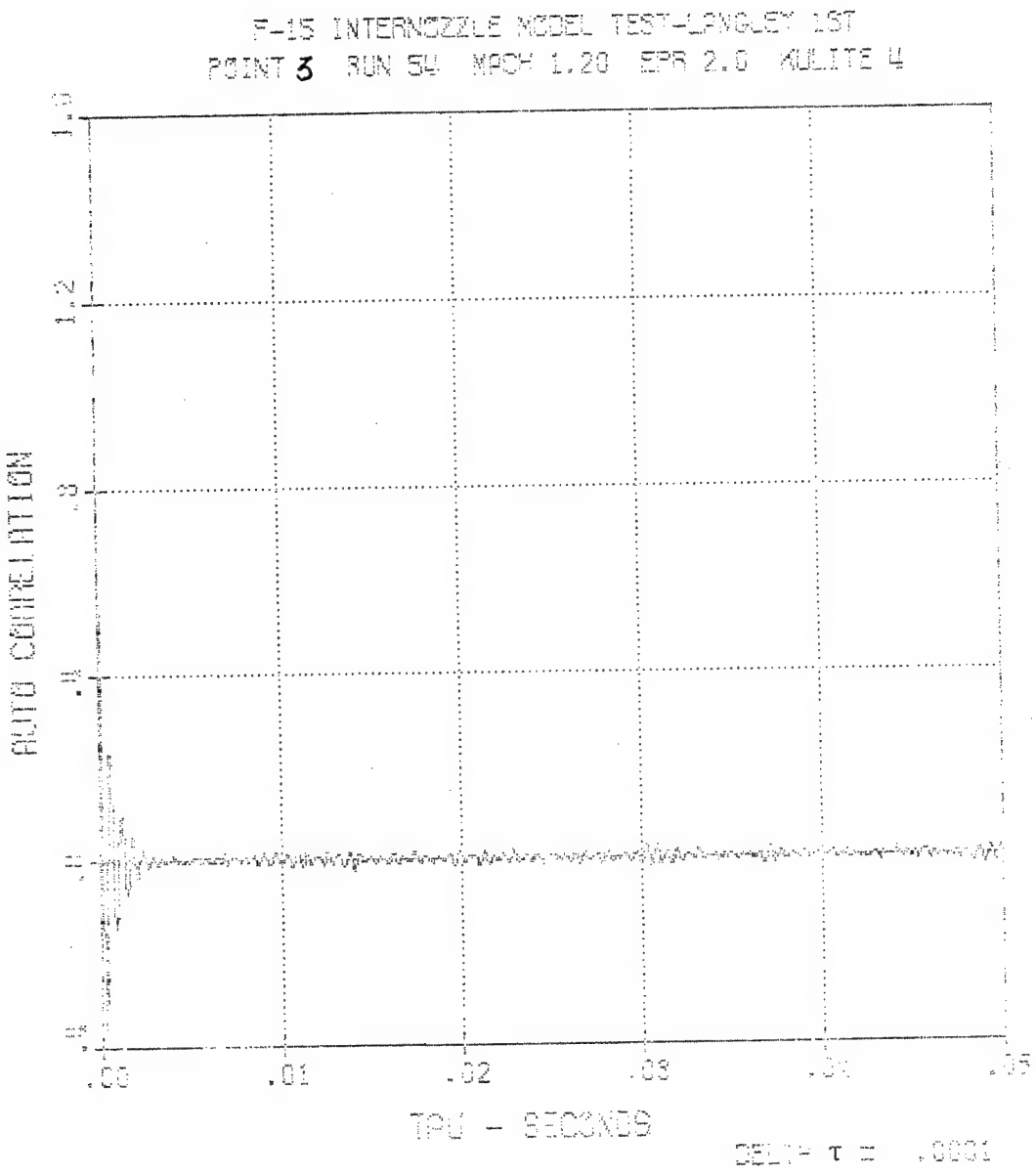

Figure 45 Auto Correlation Function-with Canards Kulite 4 MACH 1.2 EPR 2.0

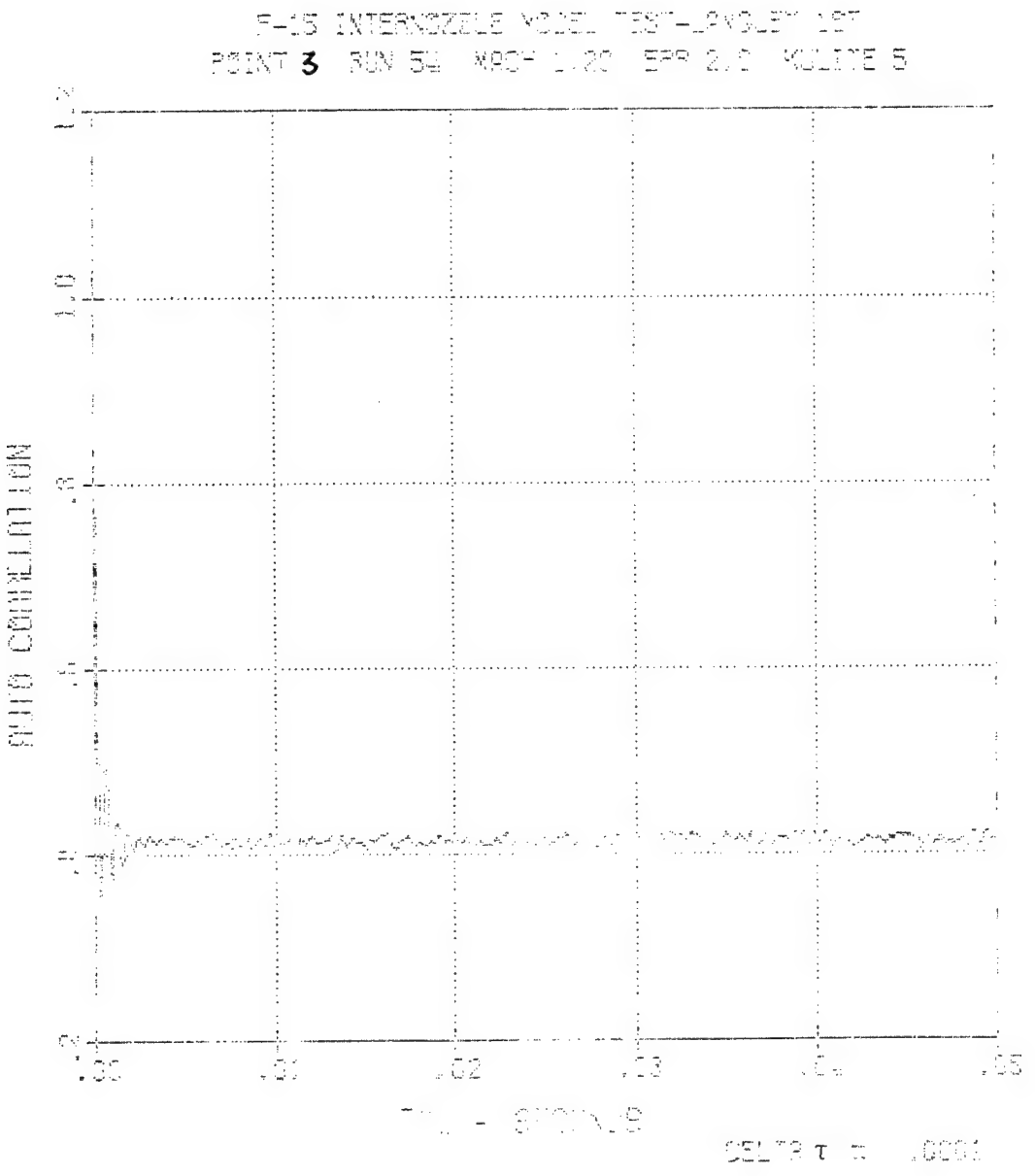

Figure 46. Auto Correlation Function-with Canards Kulite 5 MACH 1.2 EPR 2.0

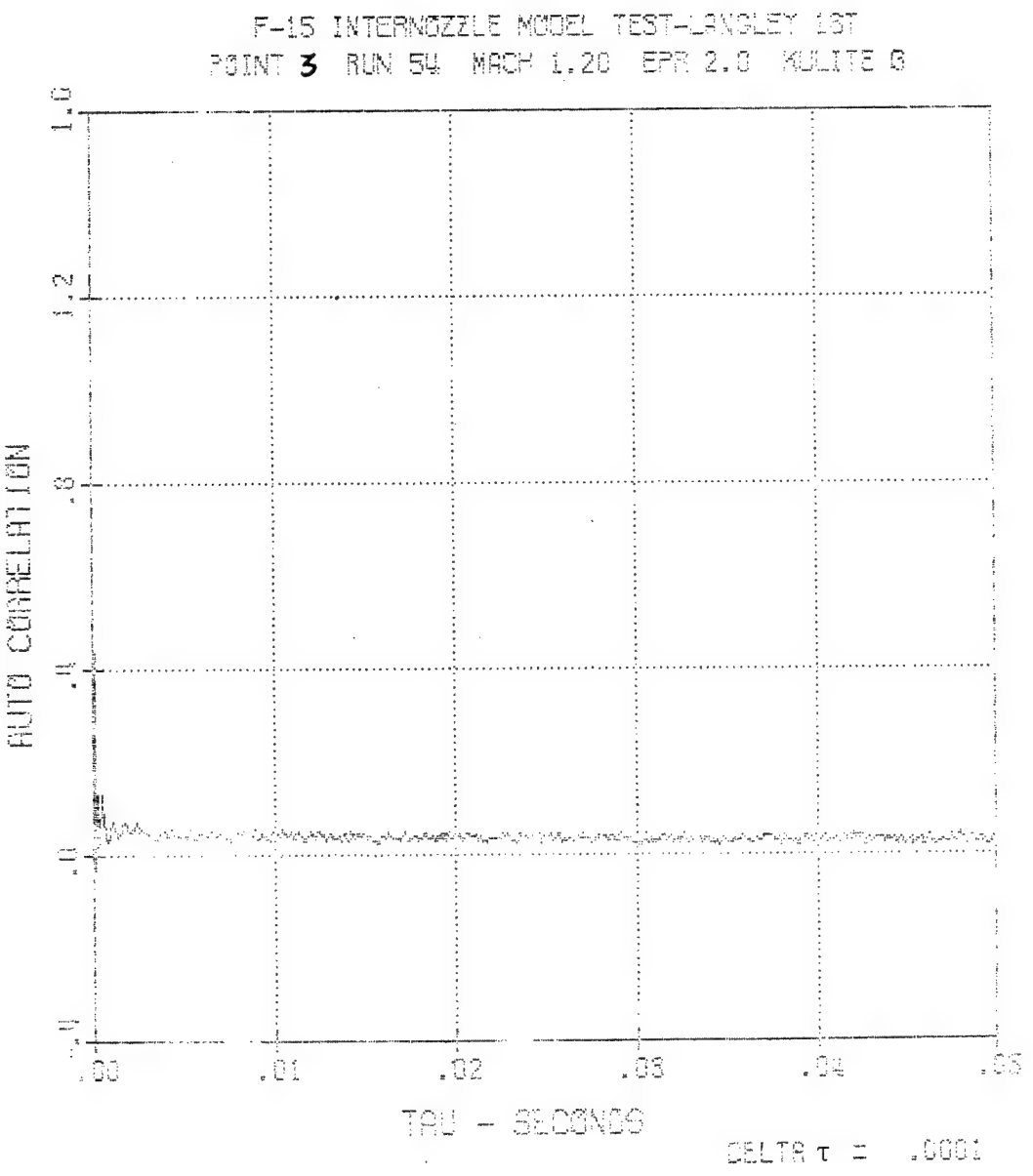

Figure 47. Auto Correlation Function-with Canards Kulite 6 MACH 1.20 EPR 2.0

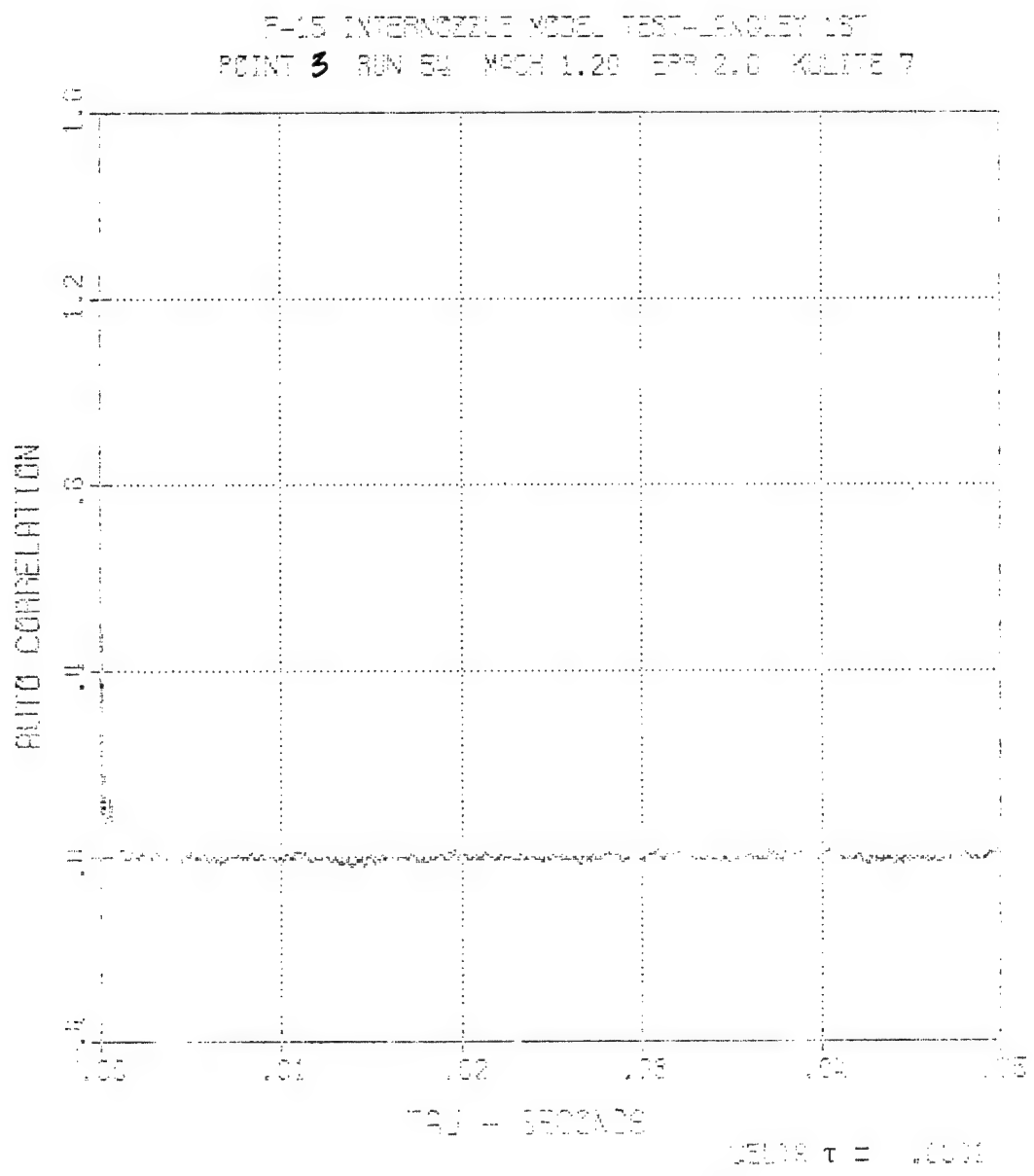

Figure 48. Auto Correlation Function-with Canards Kulite 7 MACH 1.2 EPR 2.0

ROOT MEAN SQUARE (RMS) VALUES

The RMS data in RMS PSI along with the corresponding tunnel conditions are shown in Tables 4, 5 and 6; for all the pressure data presented in this report.

POWER SPECTRAL DENSITY FUNCTION (PSD)

The frequency content of the tabulated RMS values are presented as Power Spectral Density plots, in Figure 49 to 240 over the frequency range of 0.0 to 5KHz. The PSD is compiled using standard Fast Fourier Transform (FFT) techniques. These figures are included to allow for a more detailed look at the frequency content of the selected pressure data. The PSD Function was selected for two reasons; (1) the data were predominately broadband random in nature, and (2) the data in the PSD log/log format are easier to compare with existing dynamic specifications.

SECTION IV

DISCUSSION OF RESULTS

GENERAL

The results of this study consist of discussion of the figures and tables contained in Section II of this report. Compared with the statistical properties of the random signal and the sinewave; the use of the time history, PDF, skewness, kurtosis, RMS, Auto Correlation and PSD values showed that the measured data were broadband random, strongly stationary and correlated with the tunnel conditions. As a result of these analysis, the data measured from pressure transducer number six appears to be questionable.

TIME HISTORY PLOTS

The individual RMS time history plots produced for each record were relatively flat over the portion of the length of the record selected for digitizing. As a result of this, standard analysis techniques for stationary data were used i.e., PDF, PSD and Auto Correlation. Figure 10 shows a typical RMS time history record for the Kulite pressure transducers 5, 6 and 7 for Run 57/Point 2.

PROBABILITY DENSITY FUNCTION

Knowledge of the relative levels of sinusoidal and random components of the tunnel-pressure environment is necessary to determine what statistical techniques are to be used in further analysis of these data as well as the development of appropriate vibration testing criteria. Figures 17 through 30 show the PDF plots for three records. These plots were compared with Figures 15 and 16, the PDF plot of white noise and sinewave respectively and it was determined that the data were predominately random in nature. Additional

statistical information was obtained by the calculation of the skewness and kurtosis of the PDF, Table 7. The skewness and kurtosis values compared to the measured data further substantiate the randomness of these data. A more detailed description of the skewness, the third moment and the kurtosis, the fourth moment is contained in Reference 1.

AUTOCORRELATION FUNCTION

To further determine the randomness of these data, a plot of the autocorrelation function of the selected data was obtained in Figures 31 through 48. With a few exceptions from transducer five, the autocorrelation function showed a random response, that is, its rapid decline to 0.0 value. Transducer number five in Figures 34, 40 and 46 showed a DC component and did not reach 0.0. The pressure data measured from transducer number five are random in nature.

ROOT MEAN SQUARE (RMS) VALUES

The RMS pressure data contained in Tables 4, 5 and 6 are correlated with the tunnel condition measured for each configuration. The values for identical tunnel conditions in Table 4 distinguished by the asterisk were not repeatable for Kulite 6. This observation gives rise to the questionableness of this transducer. The highest RMS values, Table 5, were obtained during Mach 0.90, EPR 1.0 and = 0 tunnel conditions. Overall the baseline data are higher than either Baseline with Canards or Baseline without the vertical tails.

SECTION V

CONCLUSIONS

1. The authors conclude that the pressure data presented in this report are representative of the pressure environment on the 4.7% model in the F-15 internozzle region.

2. The dynamic pressure statistically is strongly stationary and broadband random.

3. The highest root-mean-square pressure data values were obtained during MACH 0.90, EPR 1.0 and Angle of Attack 0.0 condition.

SECTION VI

RECOMMENDATIONS

1. A pressure survey using a larger model of the F-15 (15% or more) should be conducted to support a sufficient number of transducers (a minimum of 22) to radially and transversely measure the flow characteristics of the closely-spaced engine installation.

2. These pressure data should be compared with similar internozzle dynamic pressure data acquired from the B1 aircraft, AFWAL TM-83-212-FIBG.

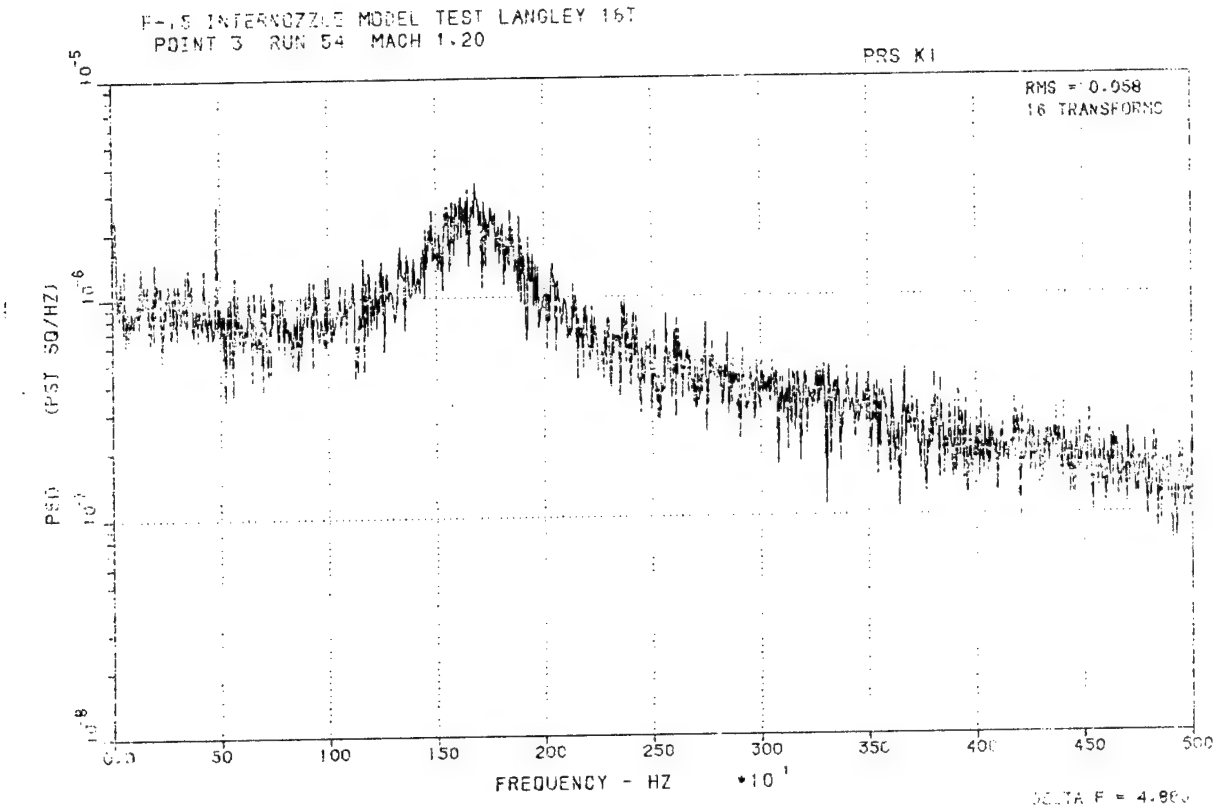

Figure 49. Power Spectral Density Function-with Canards Kulite 1
MACH 1.20 EPR 2.0

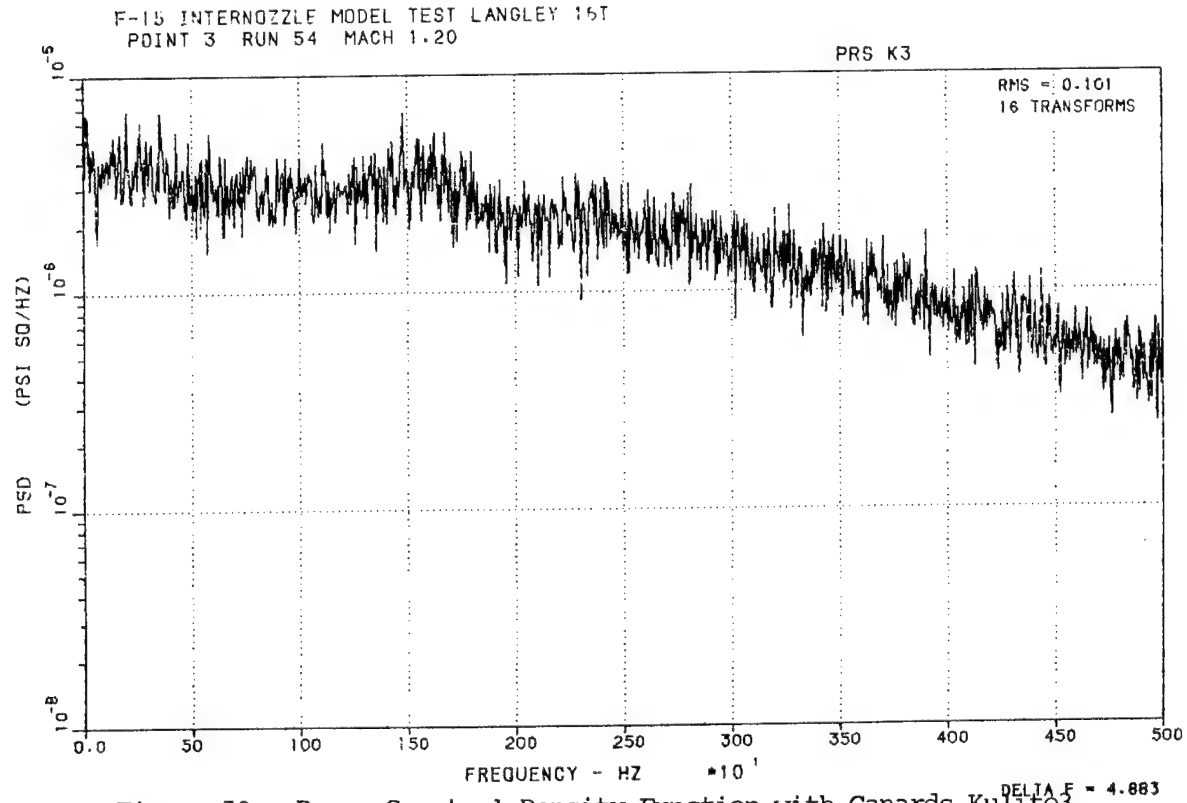

Figure 50. Power Spectral Density Function-with Canards Kulite3
MACH 1.20 EPR 2.0

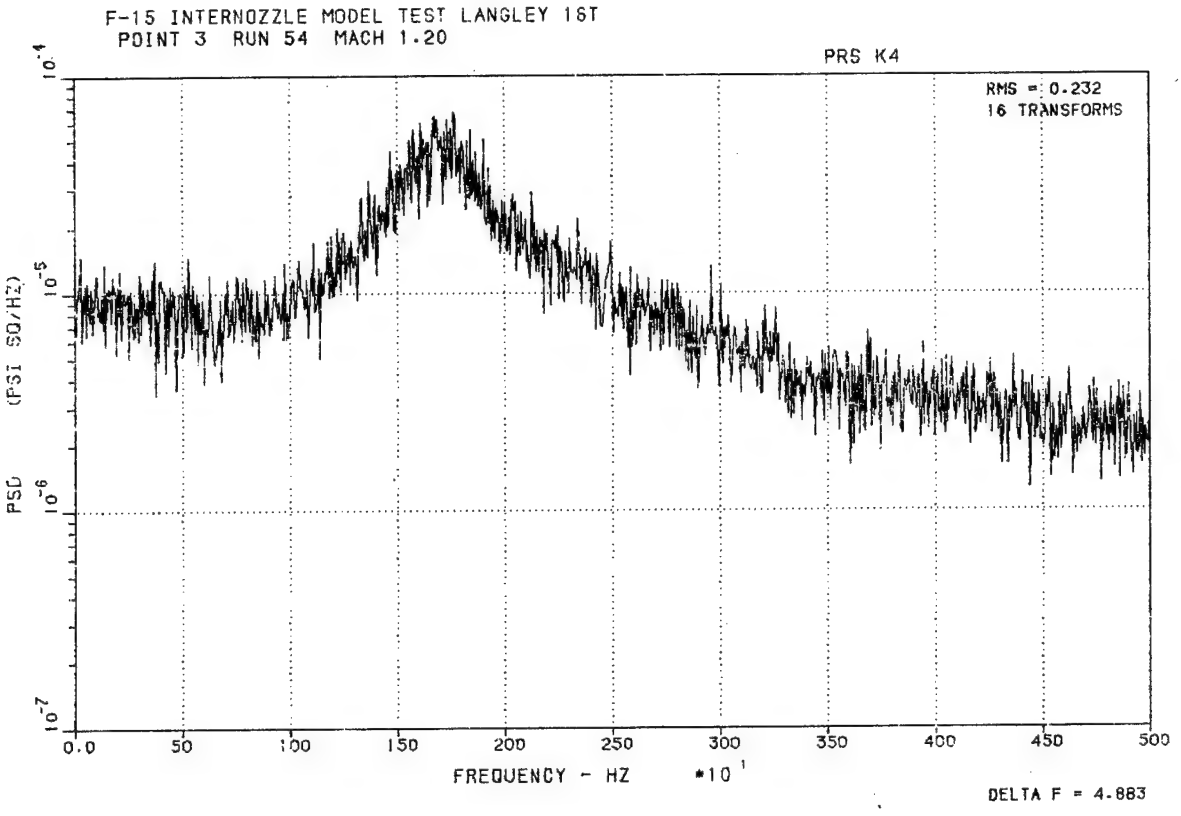

Figure 51. Power Spectral Density Function-with Canards Kulite 4
MACH 1.2 EPR 2.0

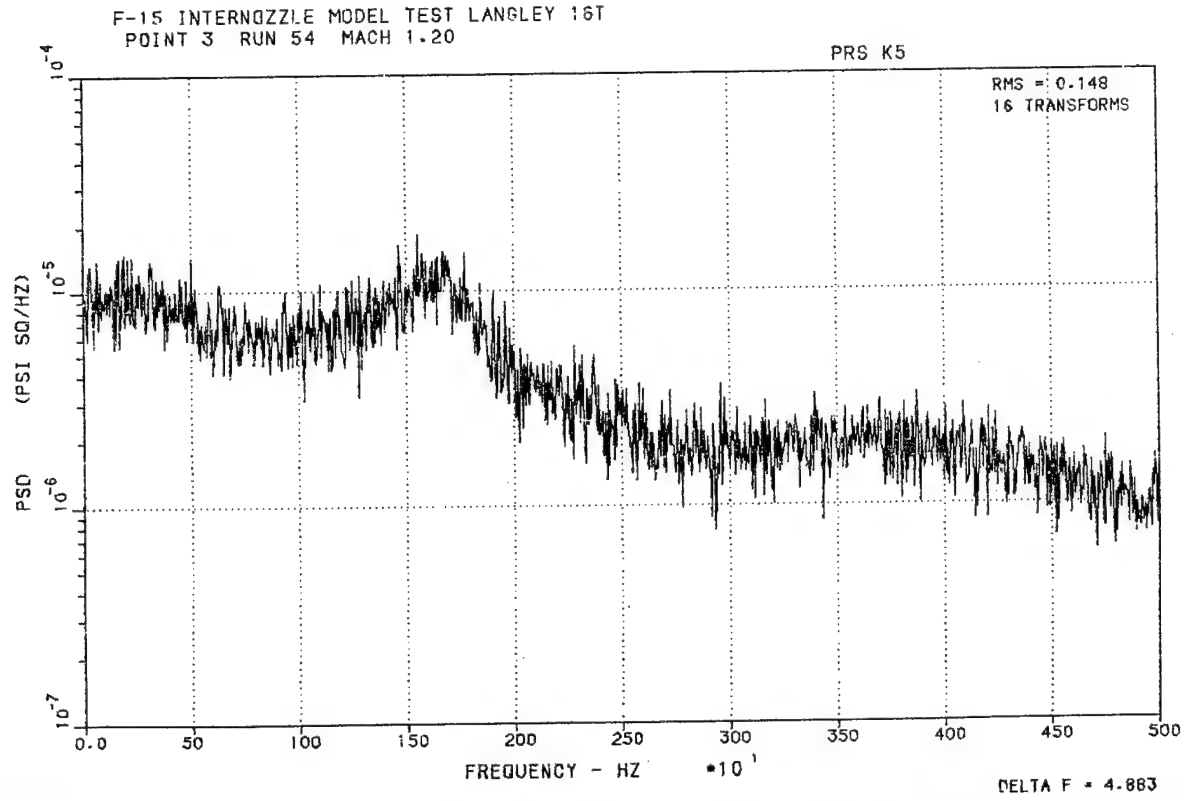

Figure 52. Power Spectral Density Function-with Canards
Kulite 4 MACH 1.2 EPR 2.0

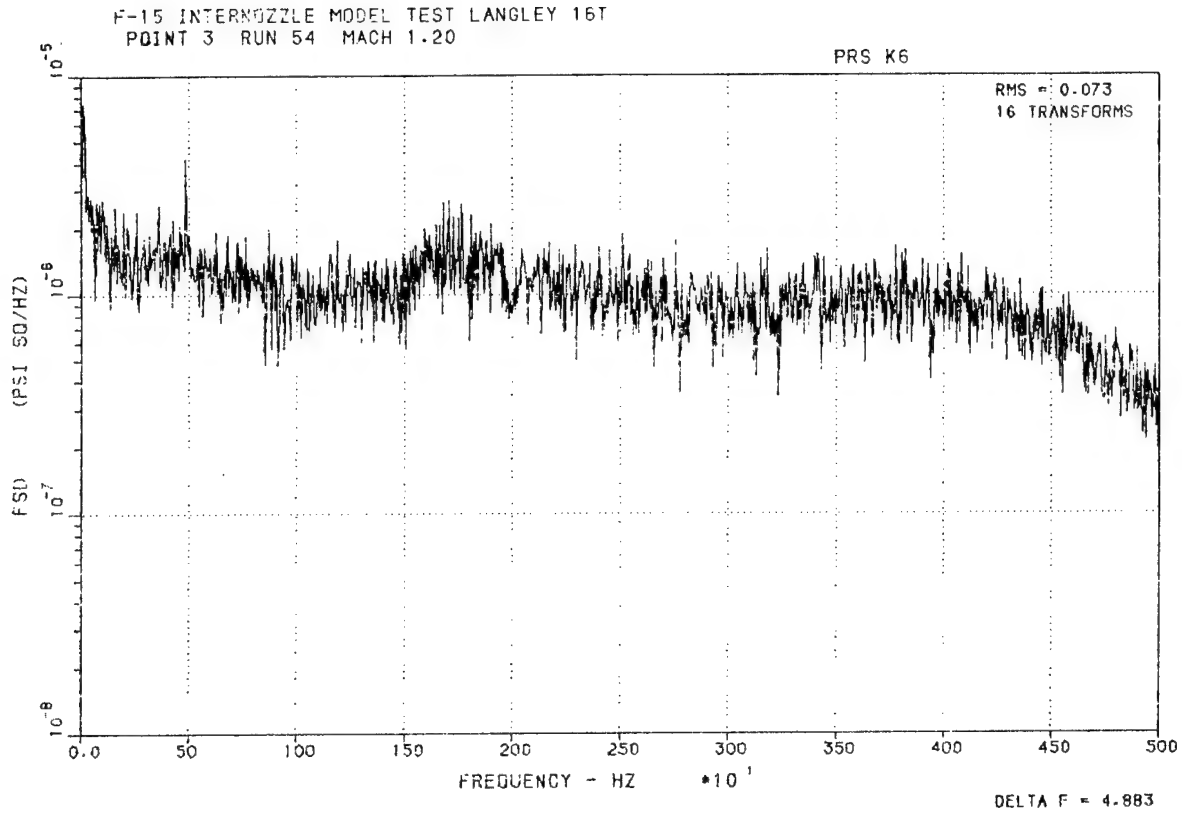

Figure 53. Power Spectral Density Function-with Canards Kulite 6
MACH 1.2 EPR 2.0

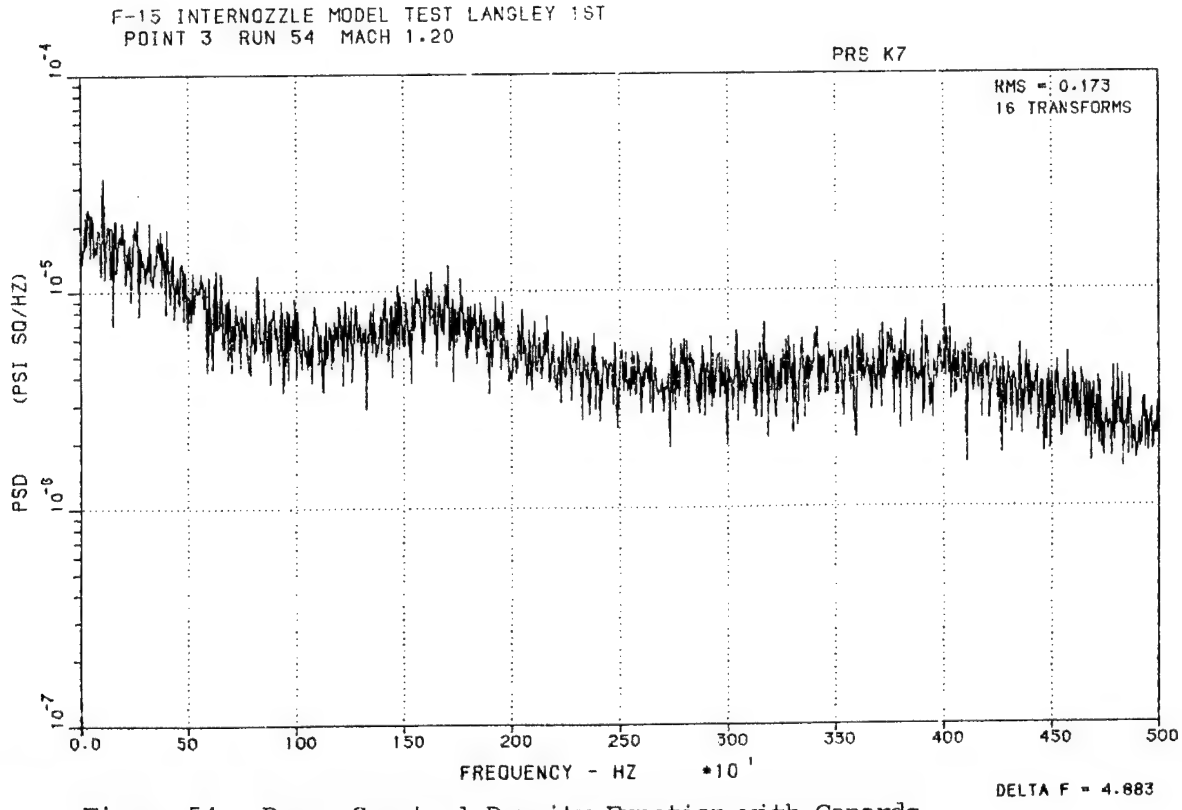

Figure 54. Power Spectral Density Function-with Canards
Kulite 7 MACH 1.2 EPR 2.0

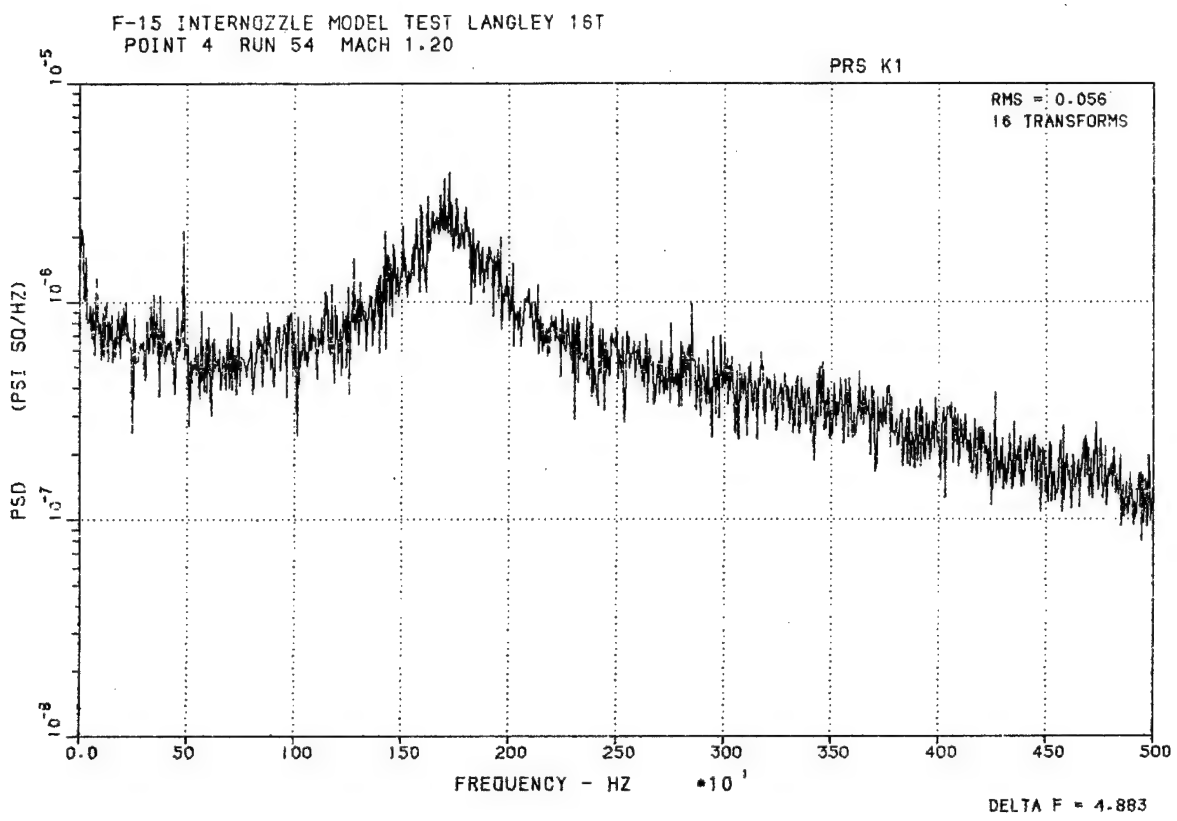

Figure 55. Power Spectral Density Function-with Canards Kulite 1 MACH 1.2 EPR 3.5

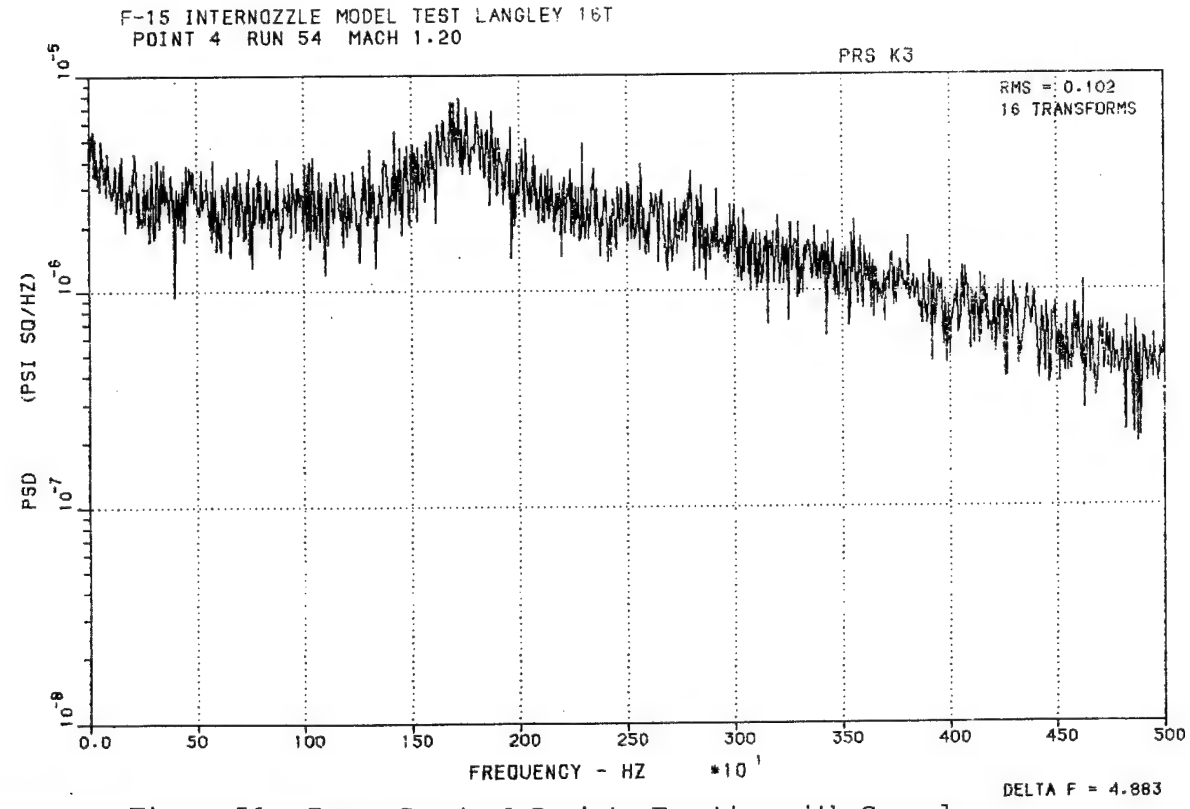

Figure 56. Power Spectral Denisty Function-with Canards Kulite 3 MACH 1.2 EPR 3.5

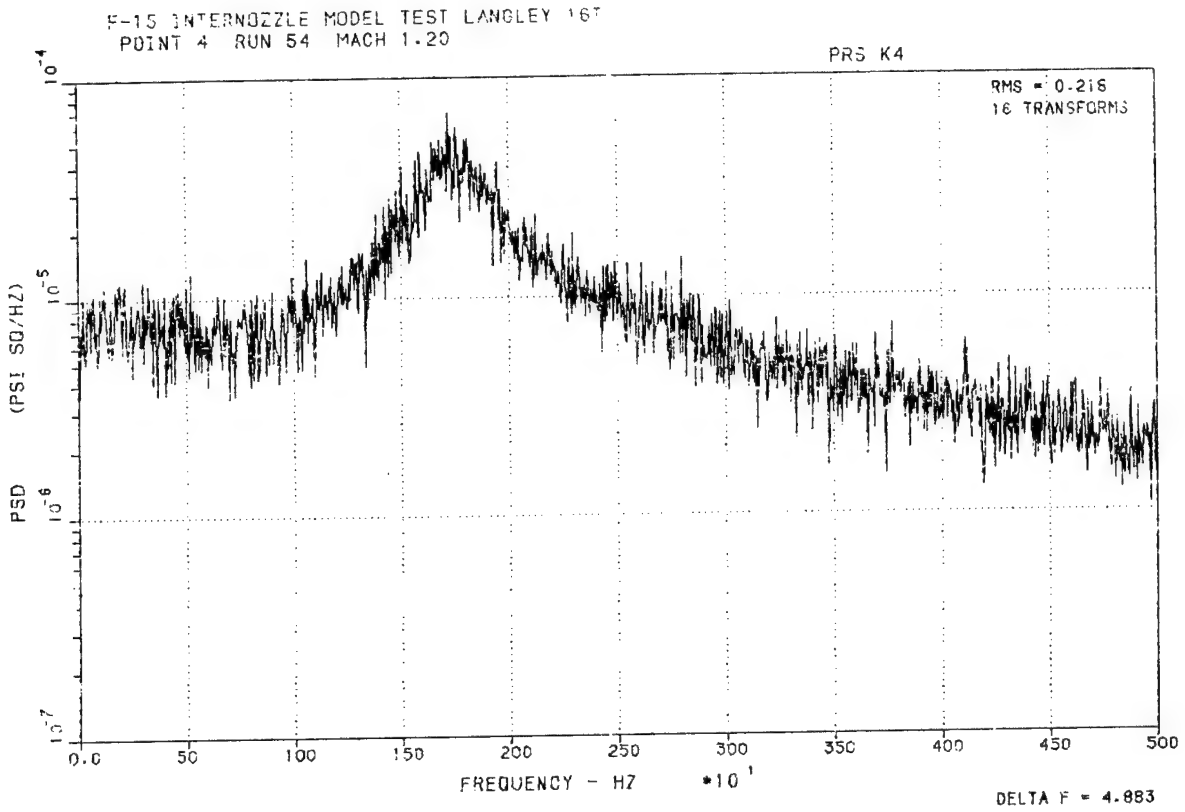

Figure 57. Power Spectral Density Function-with Canards Kulite 4 MACH 1.2 EPR 3.5

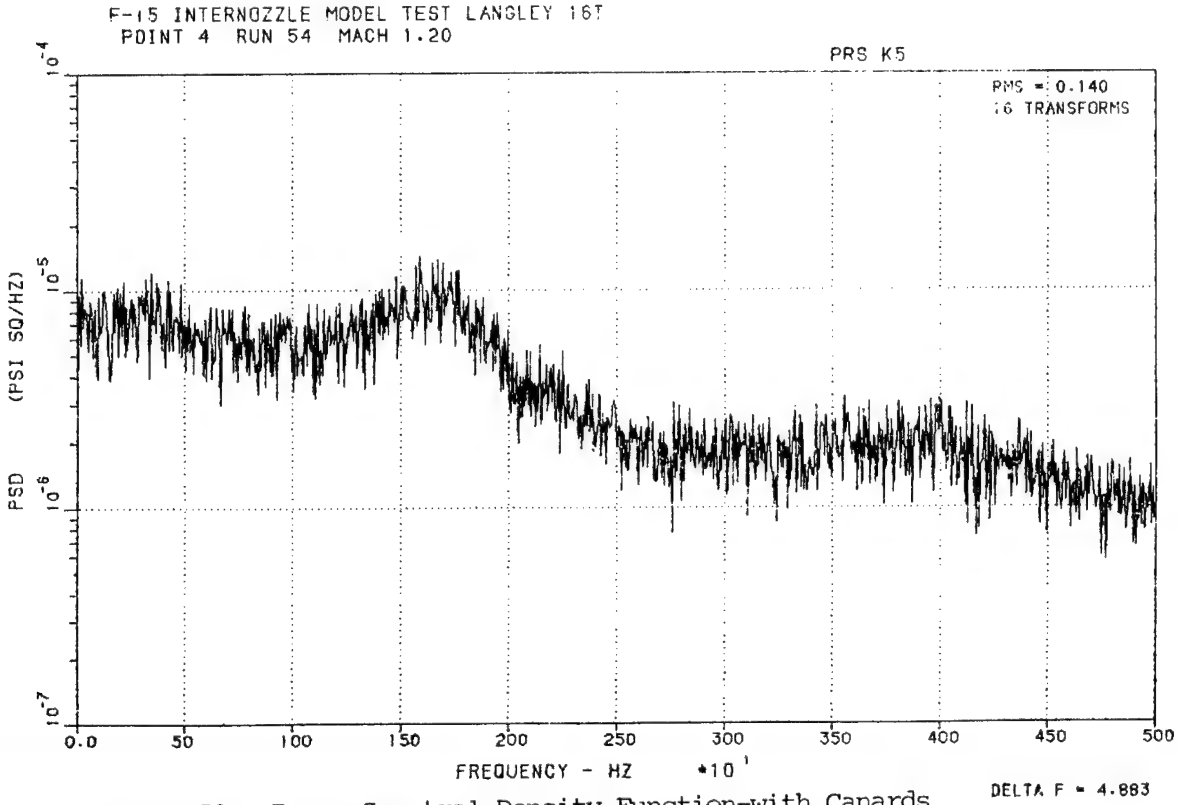

Figure 58. Power Spectral Density Function-with Canards Kulite 5 MACH 1.2 EPR 3.5

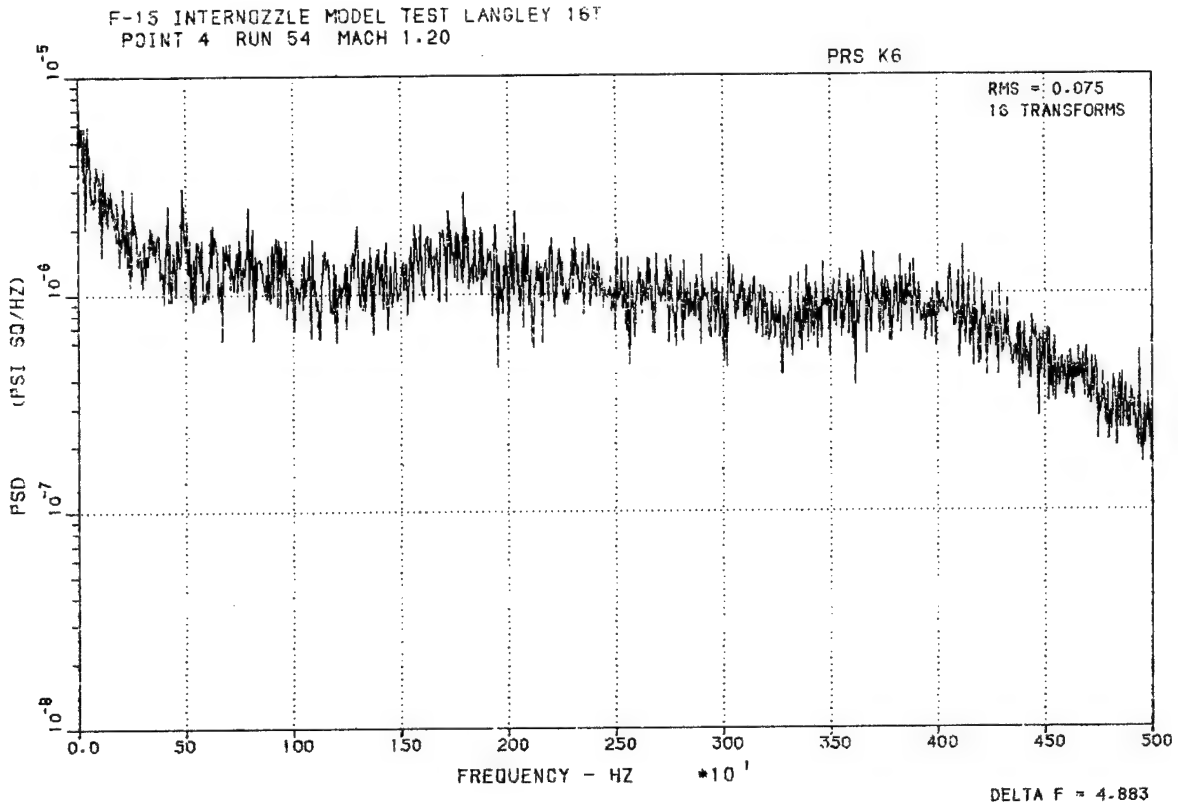

Figure 59. Power Spectral Density Function-with Canards Kulite 6 MACH 1.2 EPR 3.5

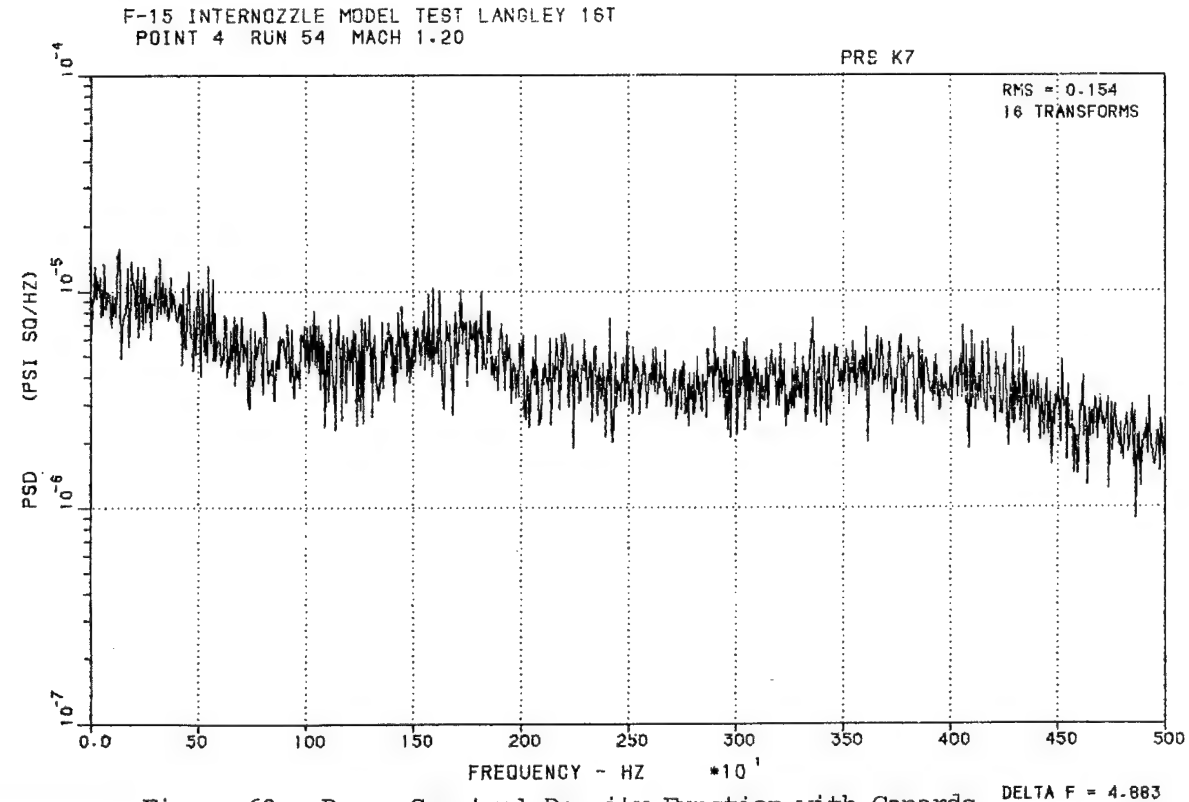

Figure 60. Power Spectral Density Function-with Canards Kulite 6 MACH 1.2 EPR 3.5

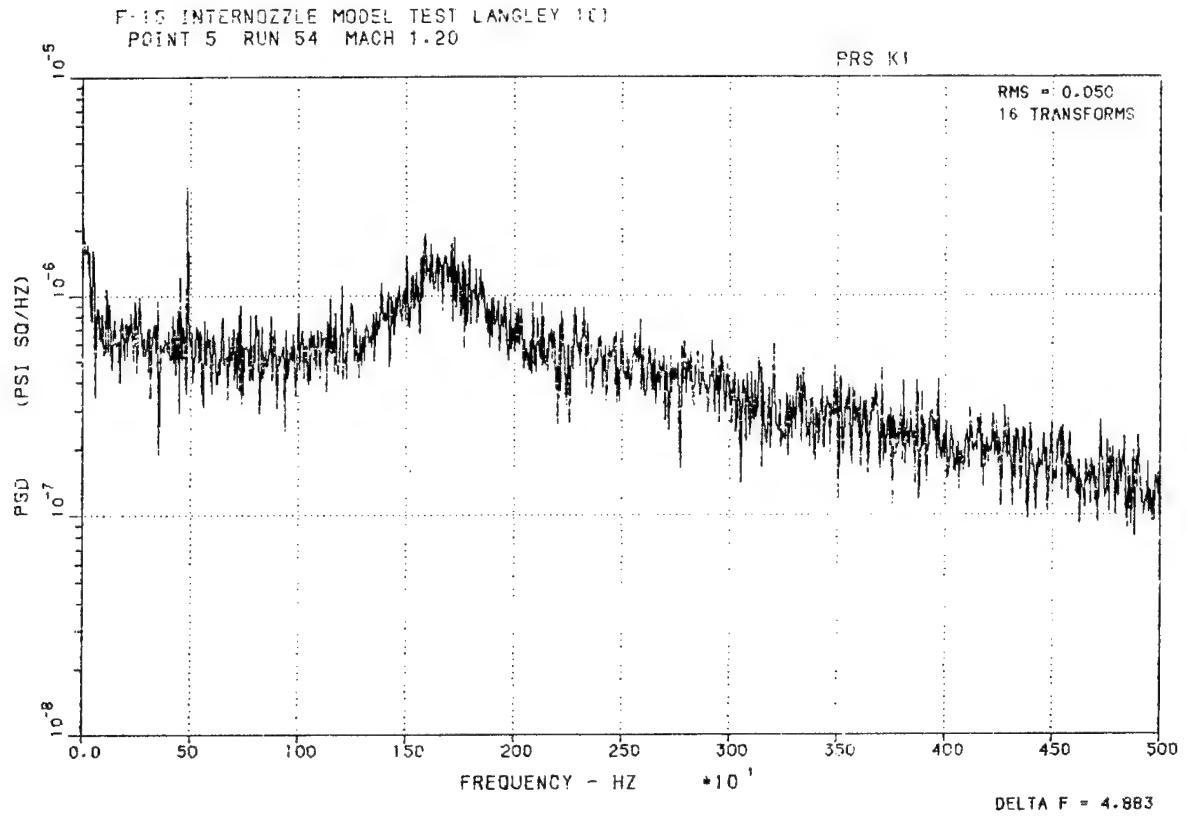

Figure 61. Power Spectral Density Function-with Canards Kulite 1
MACH 1.2 EPR 5.0

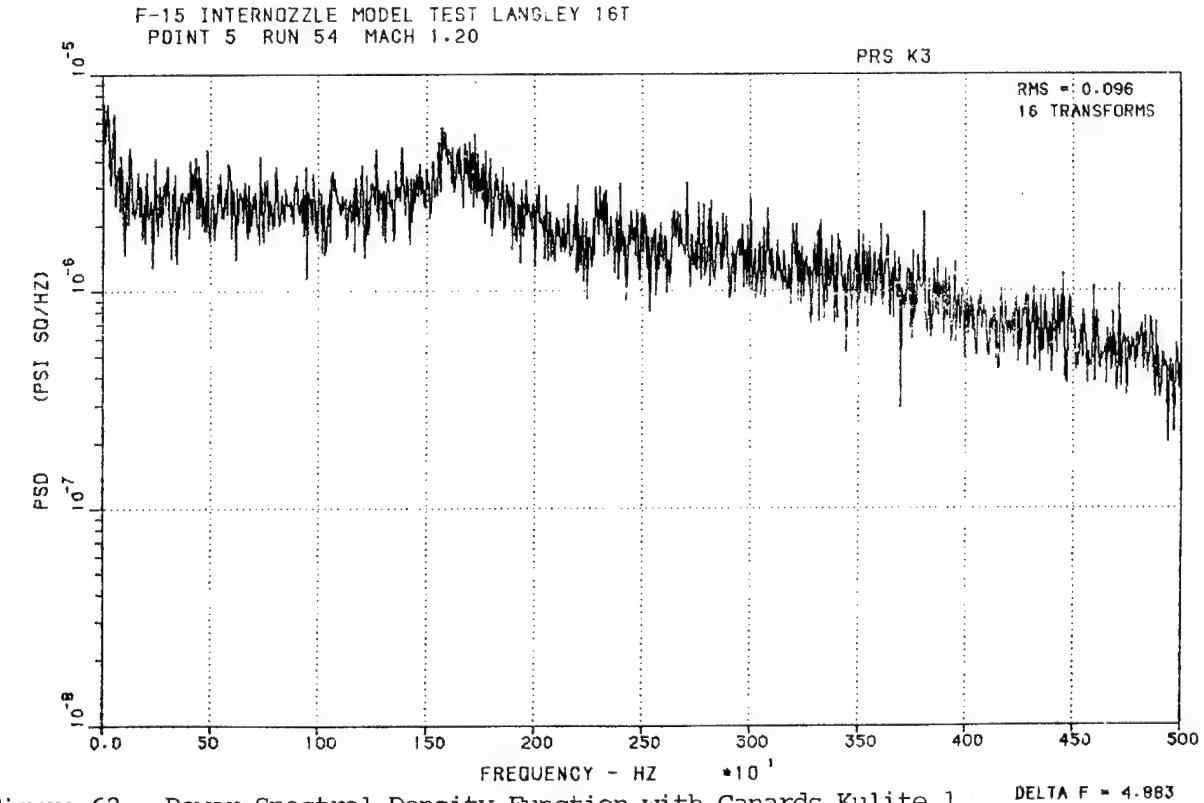

Figure 62. Power Spectral Density Function-with Canards Kulite 1
MACH 1.2 EPR 5.0

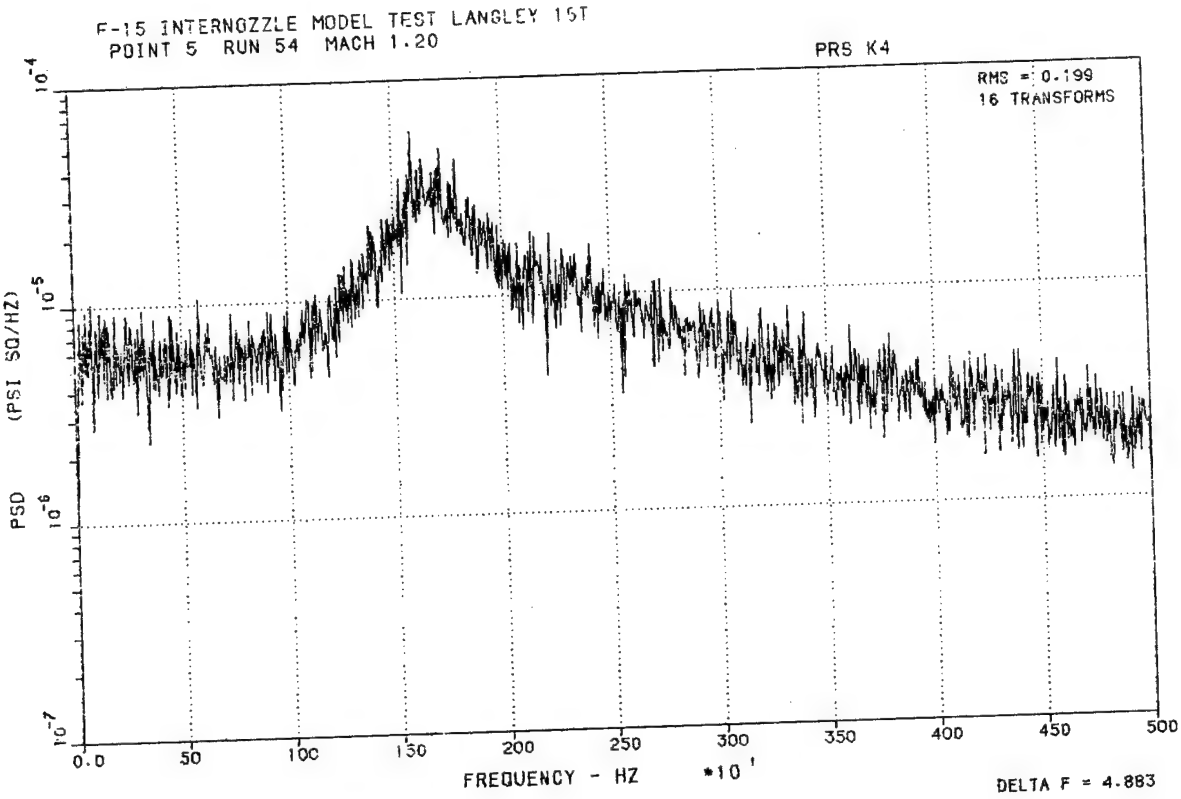

Figure 63. Power Spectral Density Function-with Canards Kulite 4 MACH 1.2 EPR 5.0

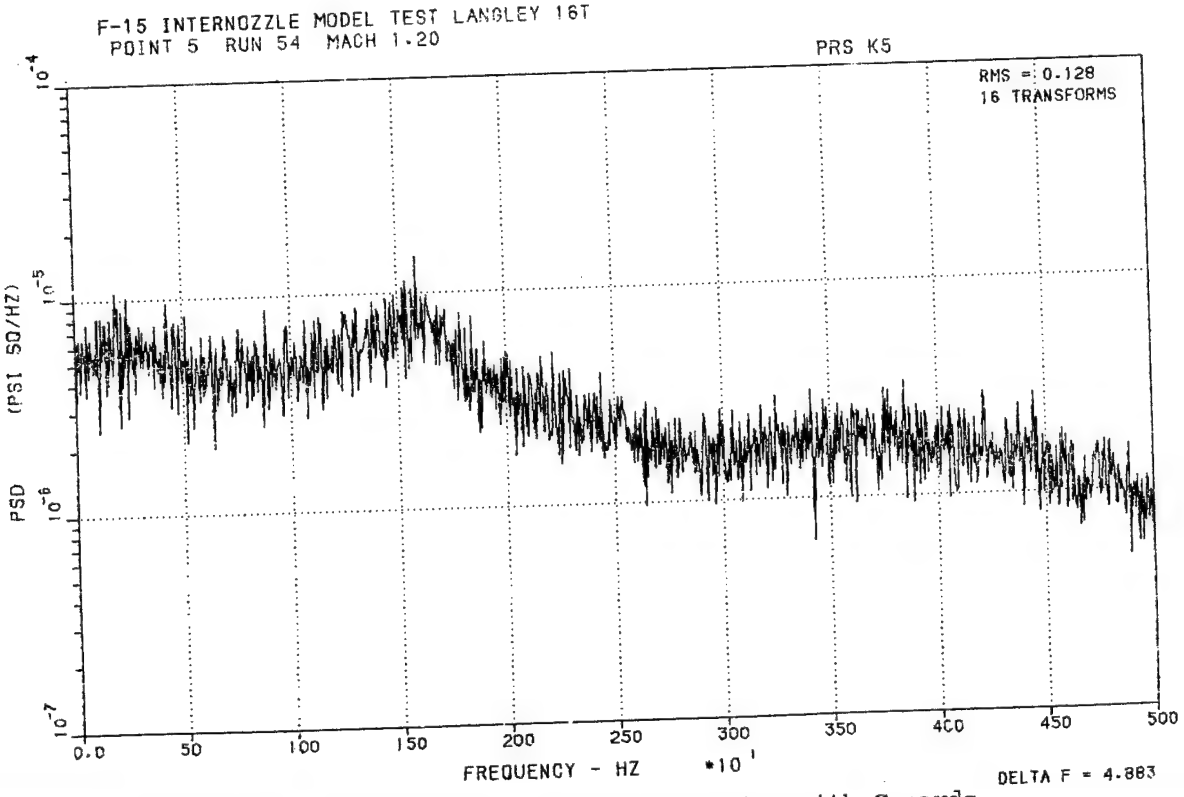

Figure 64. Power Spectral Density Function-with Canards Kulite 5 MACH 1.2 EPR 5.0

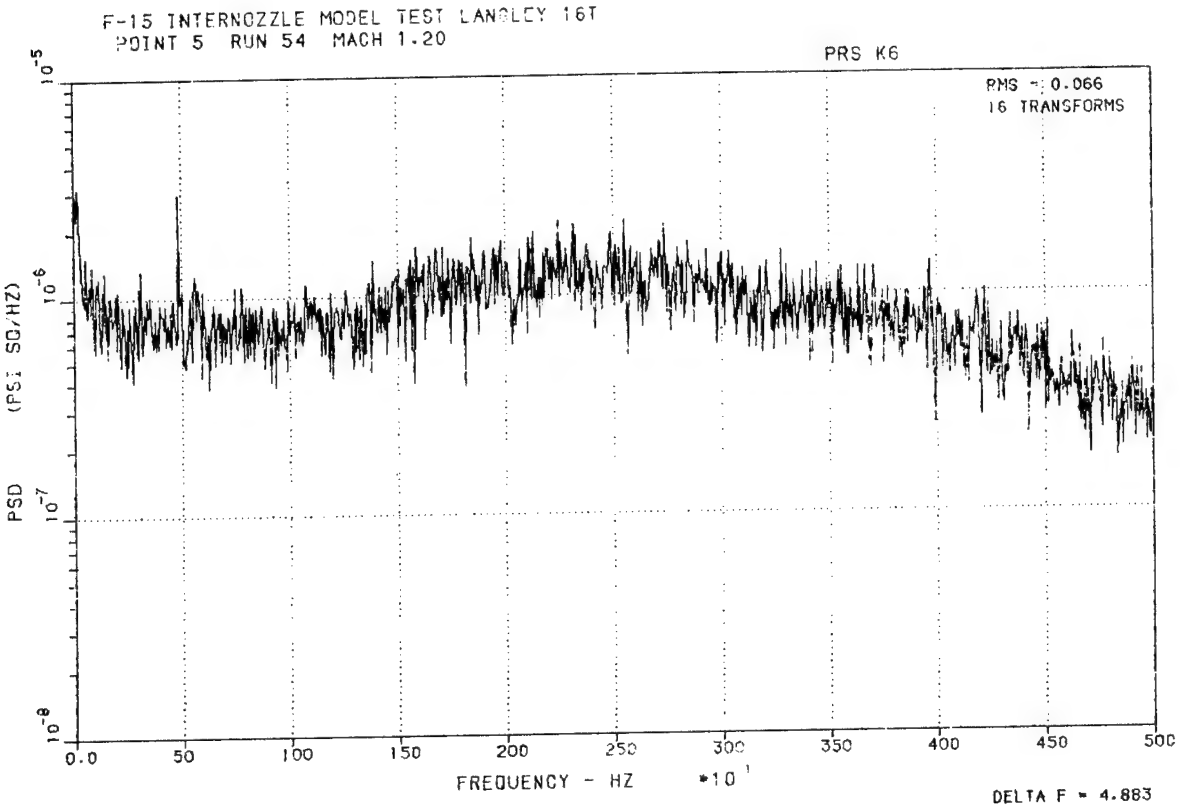

Figure 65. Power Spectral Density Function -with Canards Kulite 6
MACH 1.2 EPR 5.0

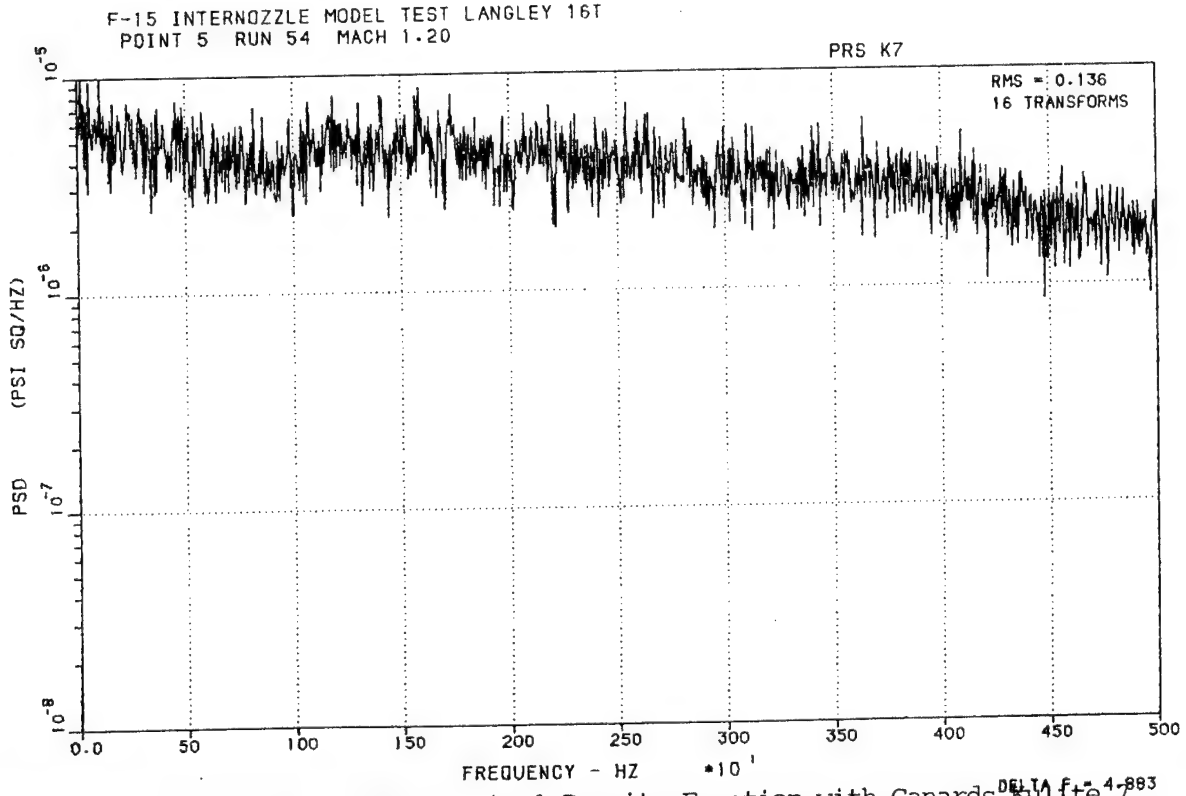

Figures 66. Power Spectral Density Function-with Canards Kulite 7
MACH 1.2 EPR 5.0

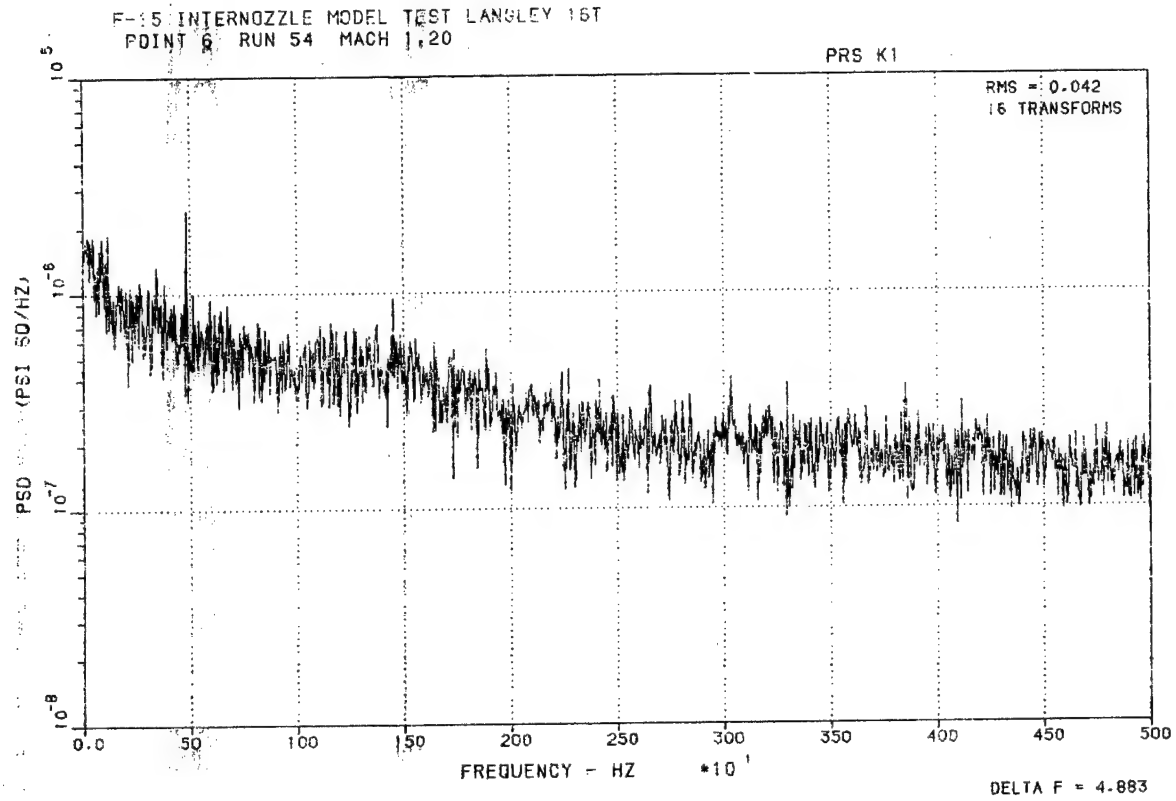

Figure 67. Power Spectral Density Function-with Canards Kulite 1 MACH 1.2 EPR 1.0

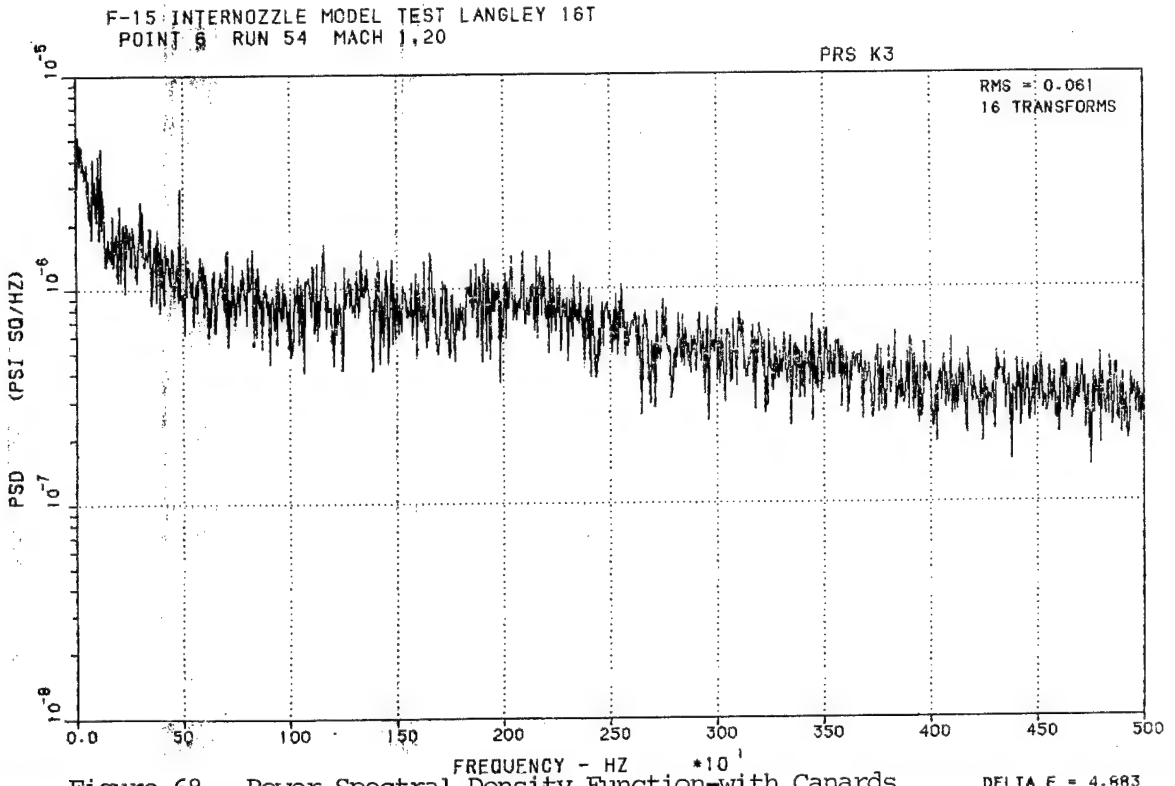

Figure 68. Power Spectral Density Function-with Canards Kulite 3 MACH 1.2 EPR 1.0

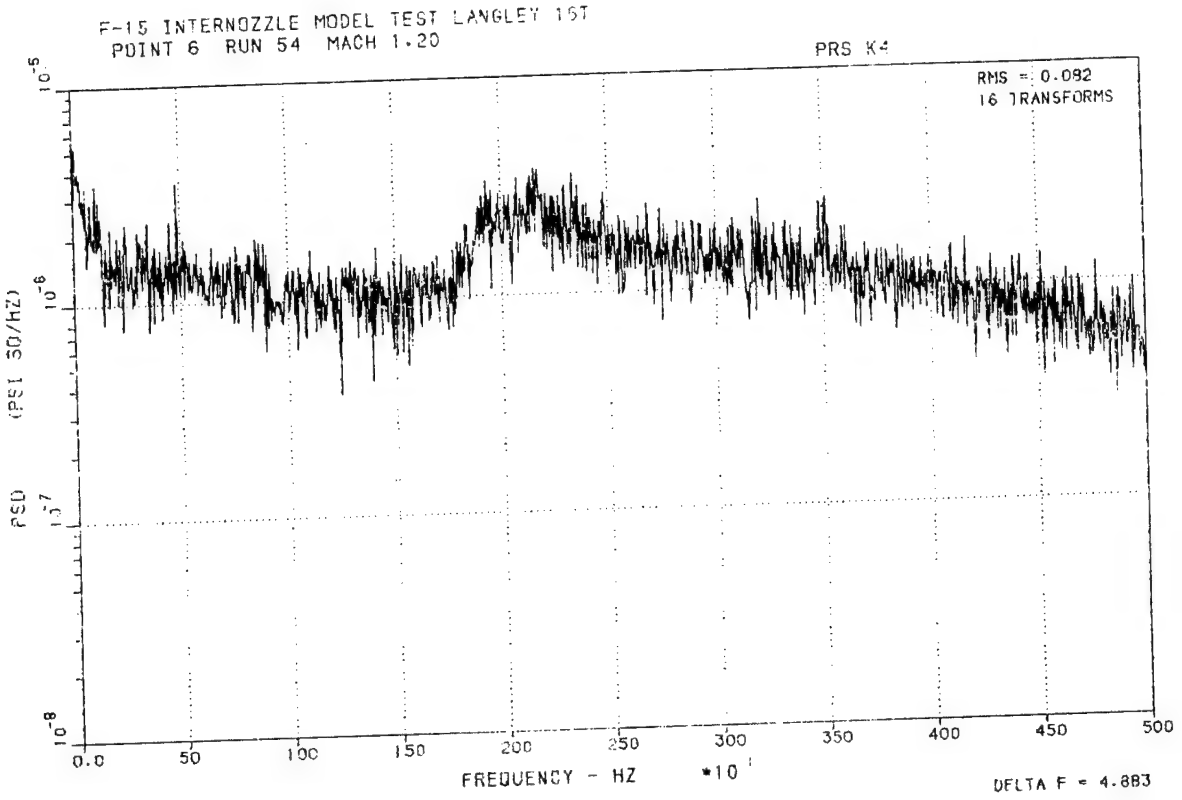

Figure 69. Power Spectral Density Function-with Canards Kulite 4 MACH 1.2 EPR 1.0

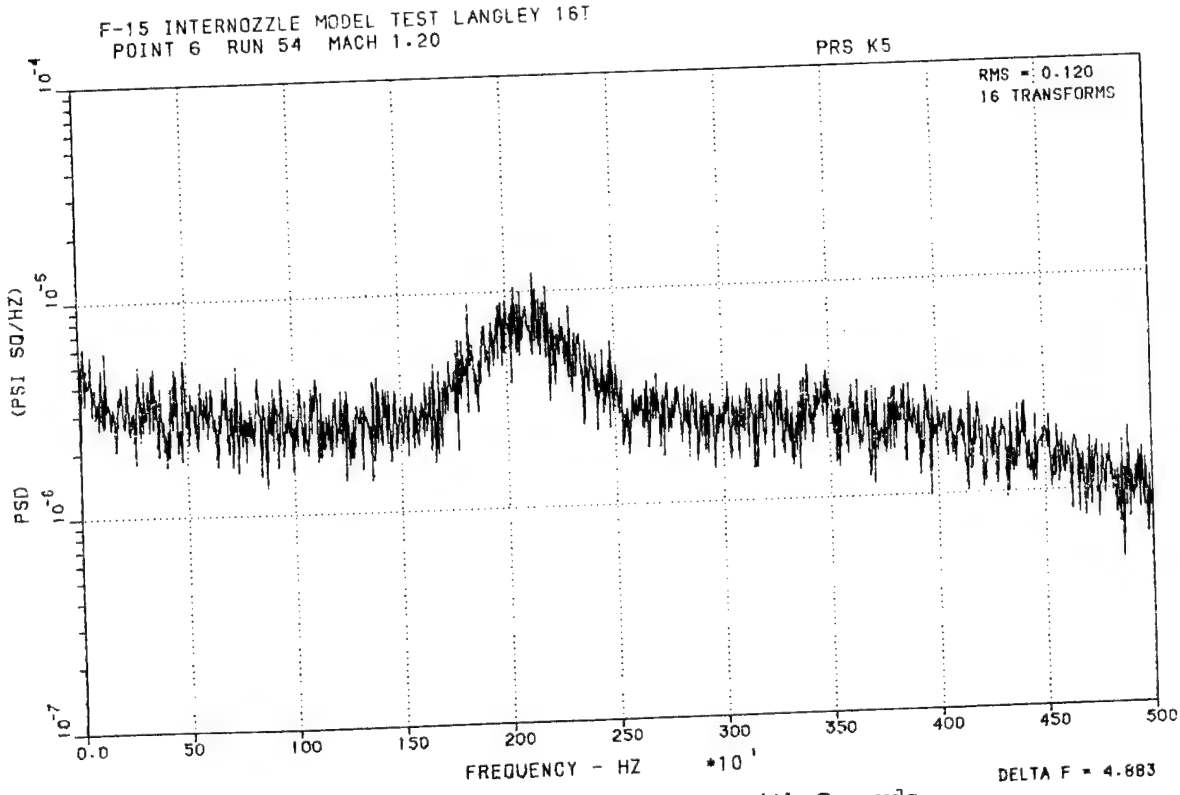

Figure 70. Power Spectral Density Function-with Canards Kulite 4 MACH 1.2 EPR 1.0

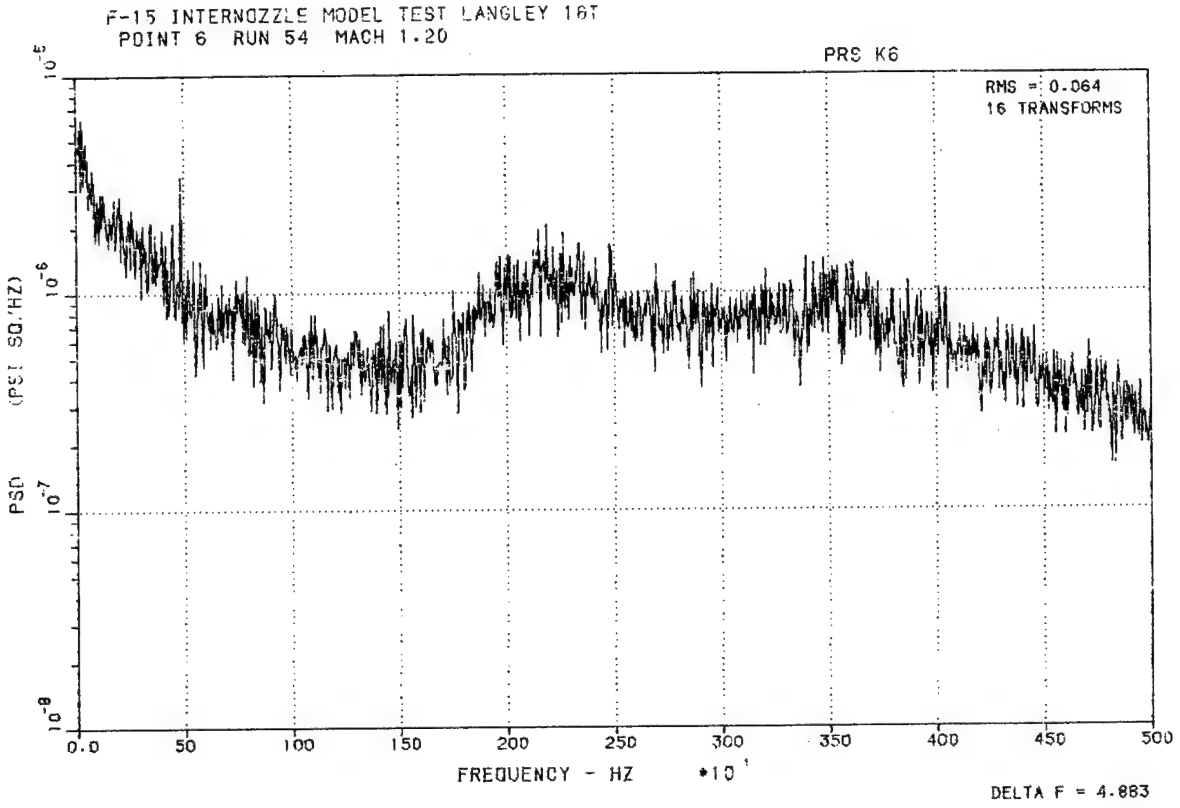

Figure 71. Power Spectral Density Function-with Canards Kulite 6
MACH 1.2 EPR 1.0

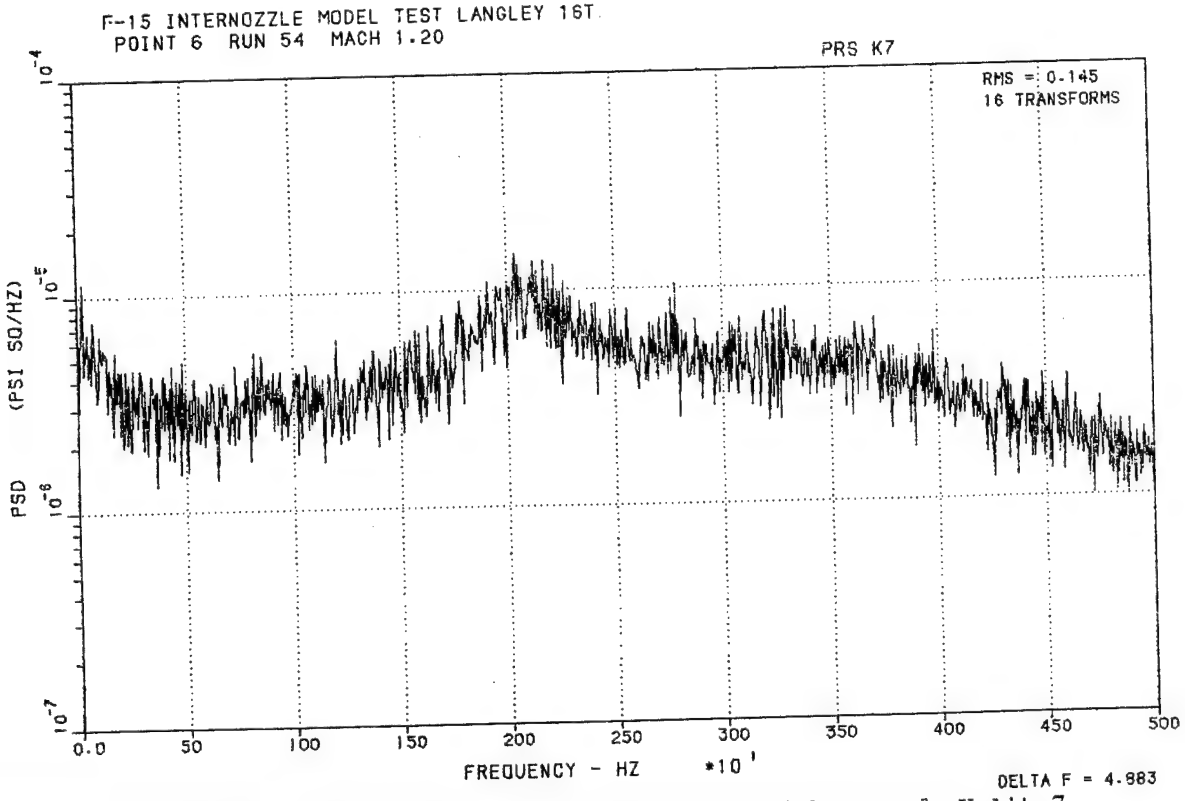

Figure 72. Power Spectral Density Function-with Canards Kulite 7
MACH 1.2 EPR 1.0

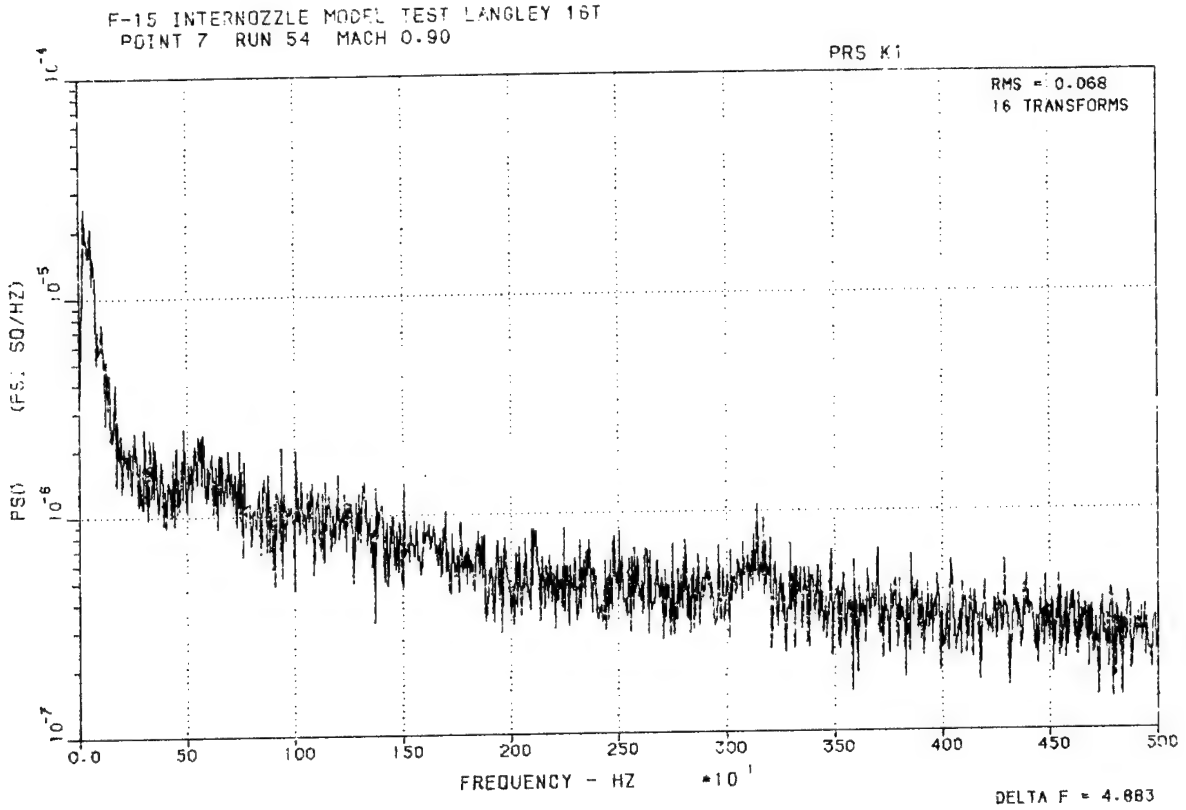

Figure 73. Power Spectral Density Function-with Canards Kulite 1 MACH 0.9 EPR 1.0

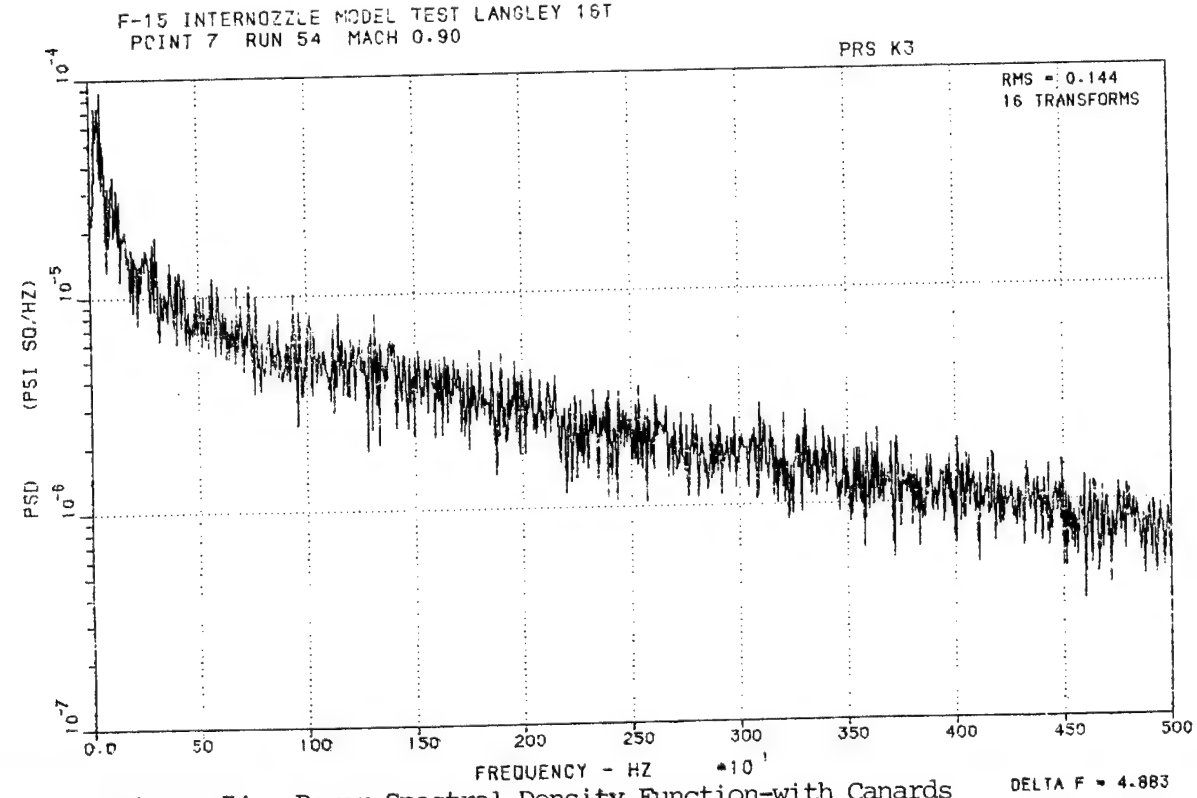

Figure 74. Power Spectral Density Function-with Canards Kulite 3 MACH 0.9 EPR 1.0

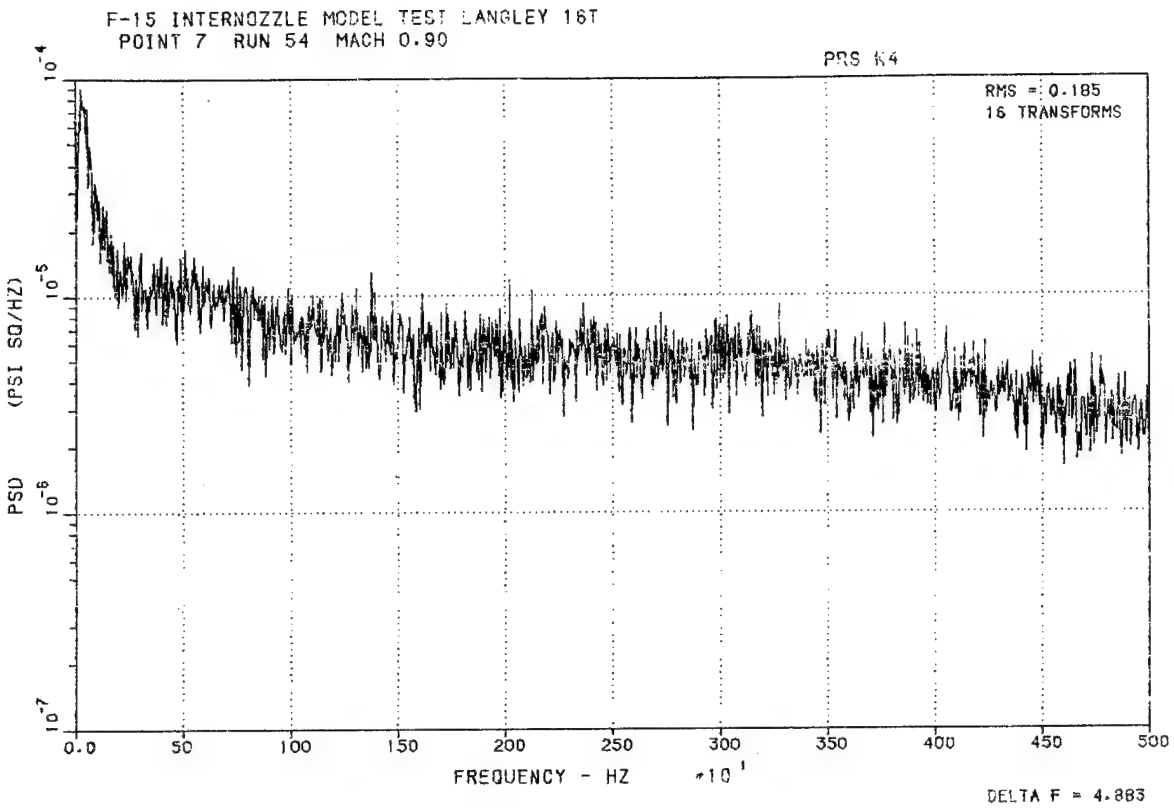

Figure 75. Power Spectral Density Function-with Canards Kulite 4 MACH 0.9 epr 1.0

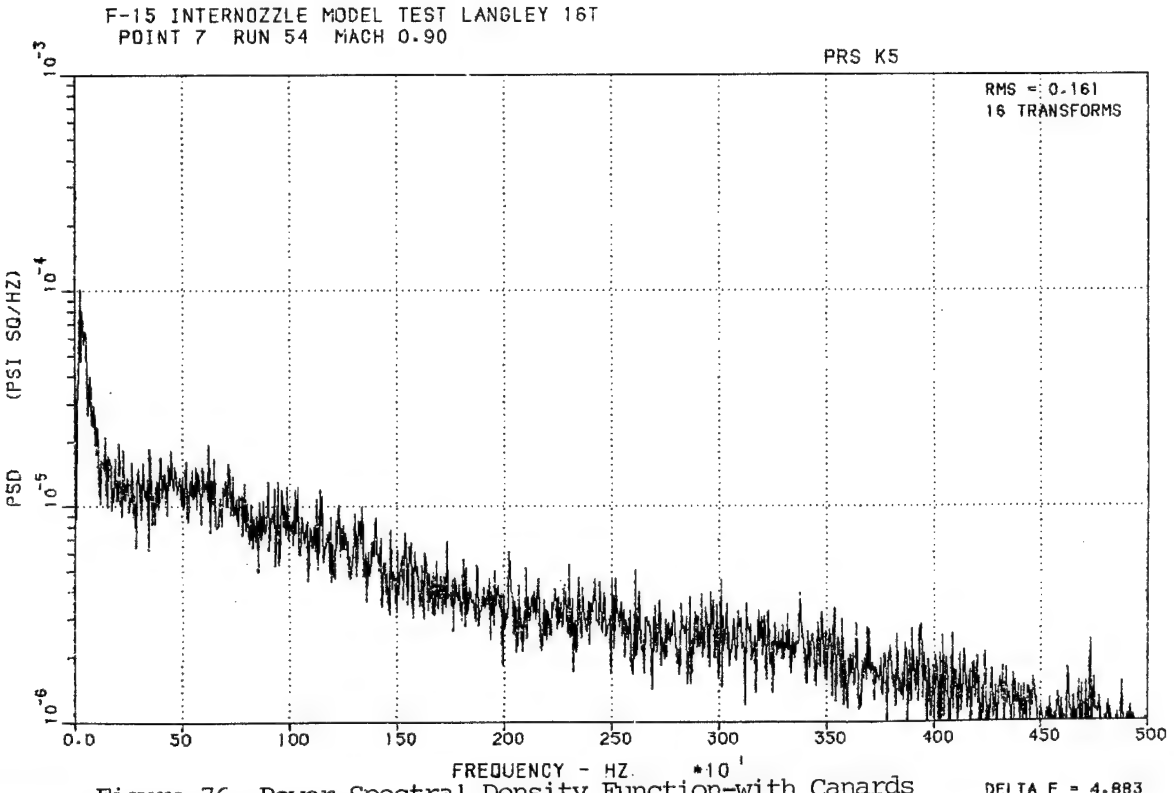

Figure 76 Power Spectral Density Function-with Canards Kulite 5 MACH 0.9 EPR 1.0

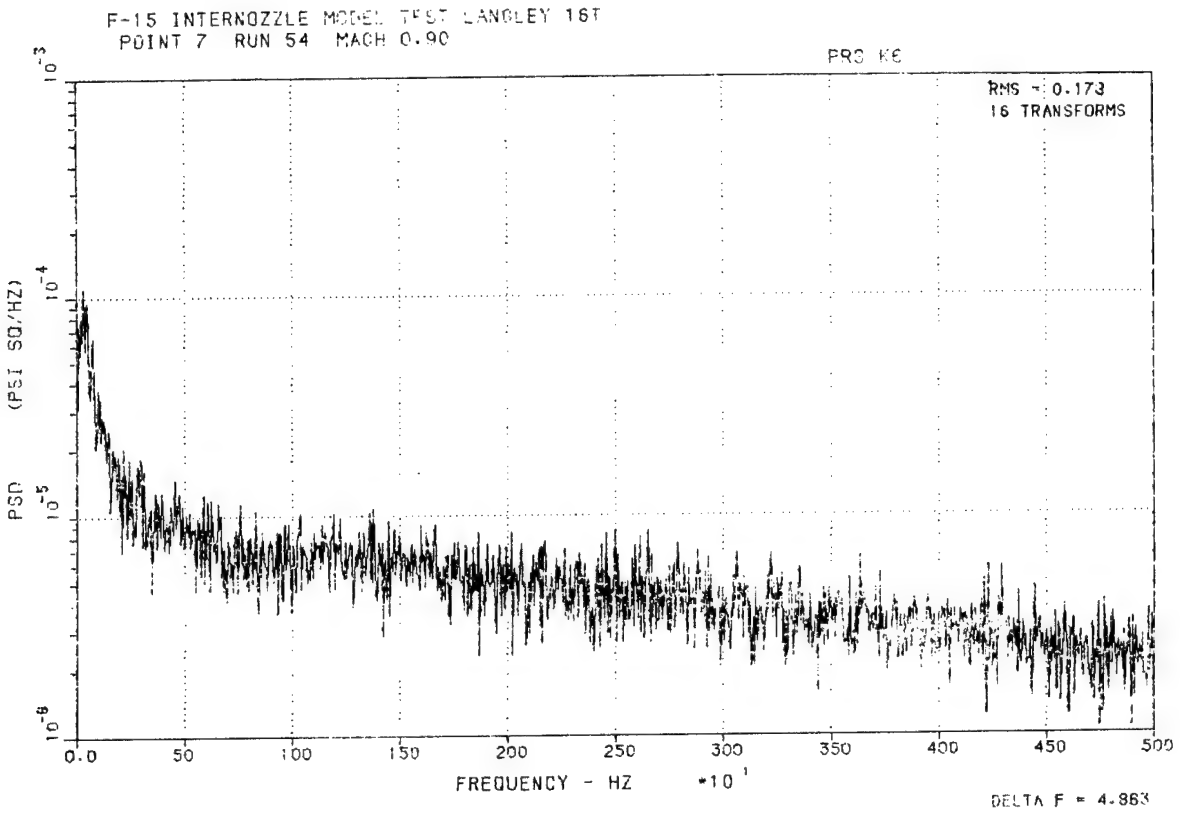

Figure 77. Power Spectral Density Function-with Canards Kulite 6 MACH 0.9 EPR 1.0

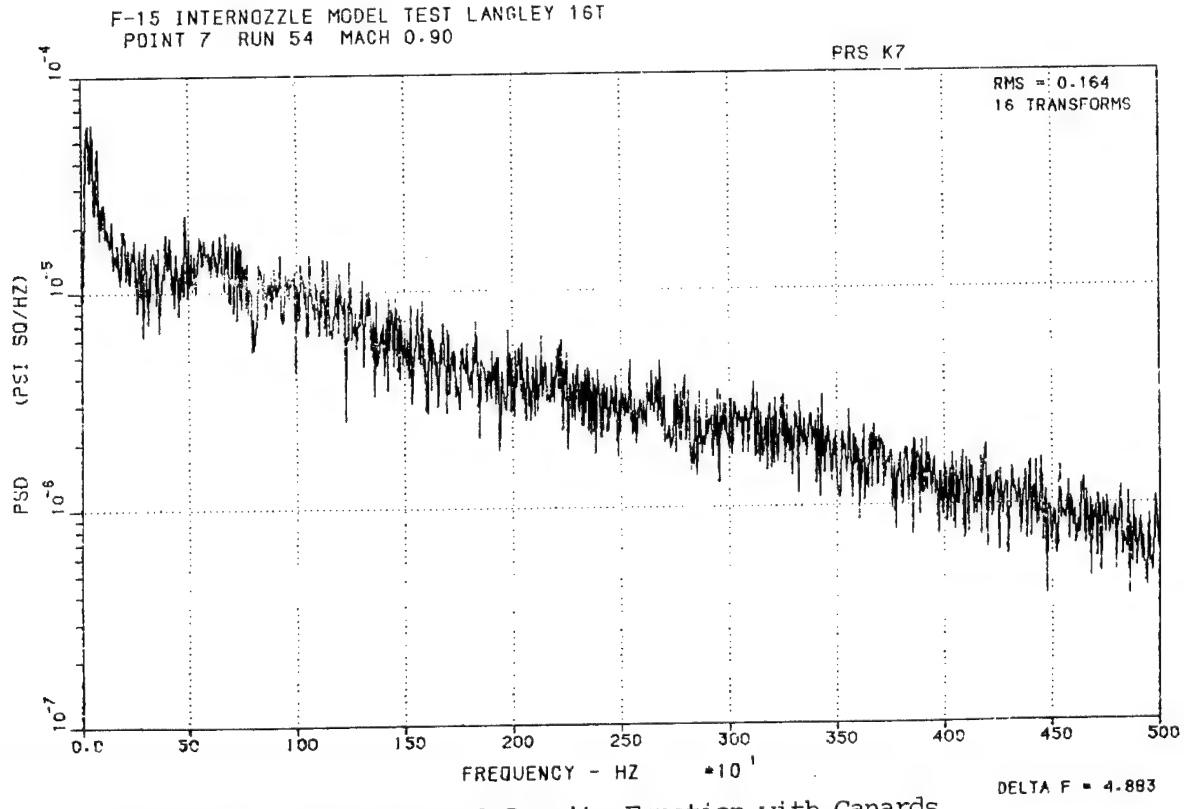

Figure 78. Power Spectral Density Function-with Canards Kulite 7 MACH 0.9 EPR 1.0

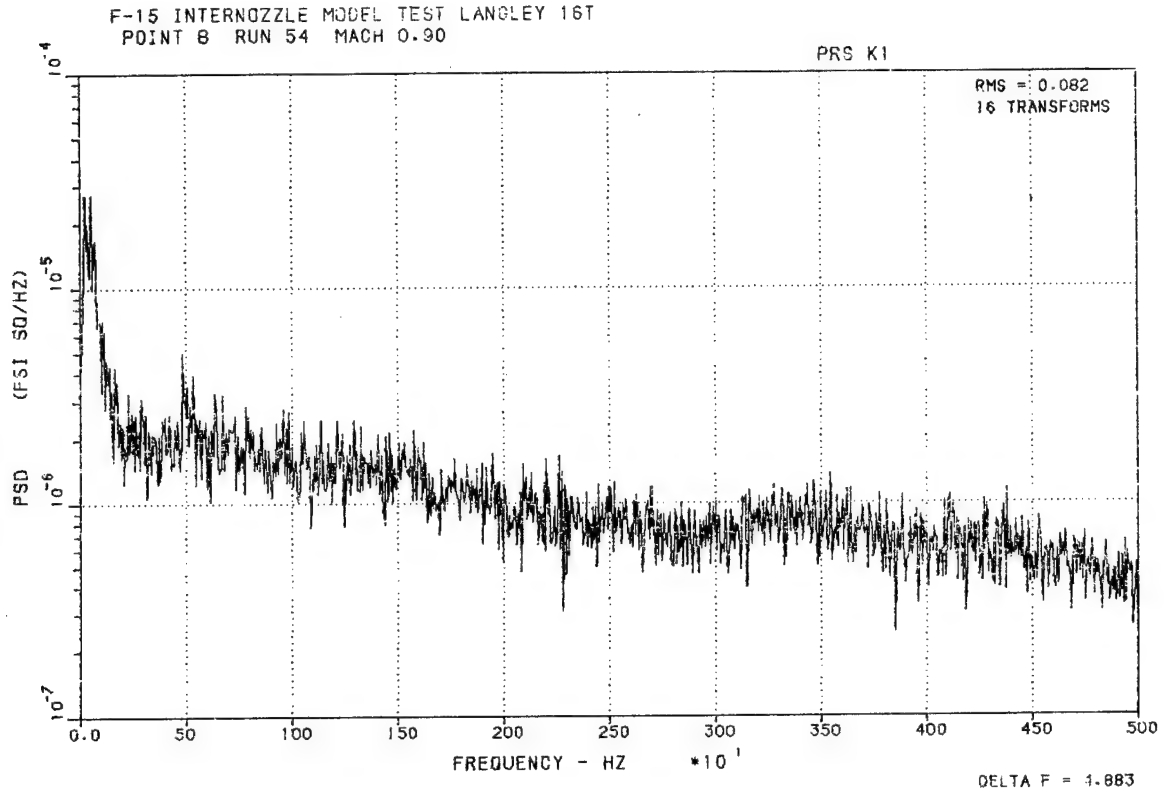

Figure 79. Power Spectral Density Function-with Canards Kulite 1 MACH 0.9 EPR 1.0

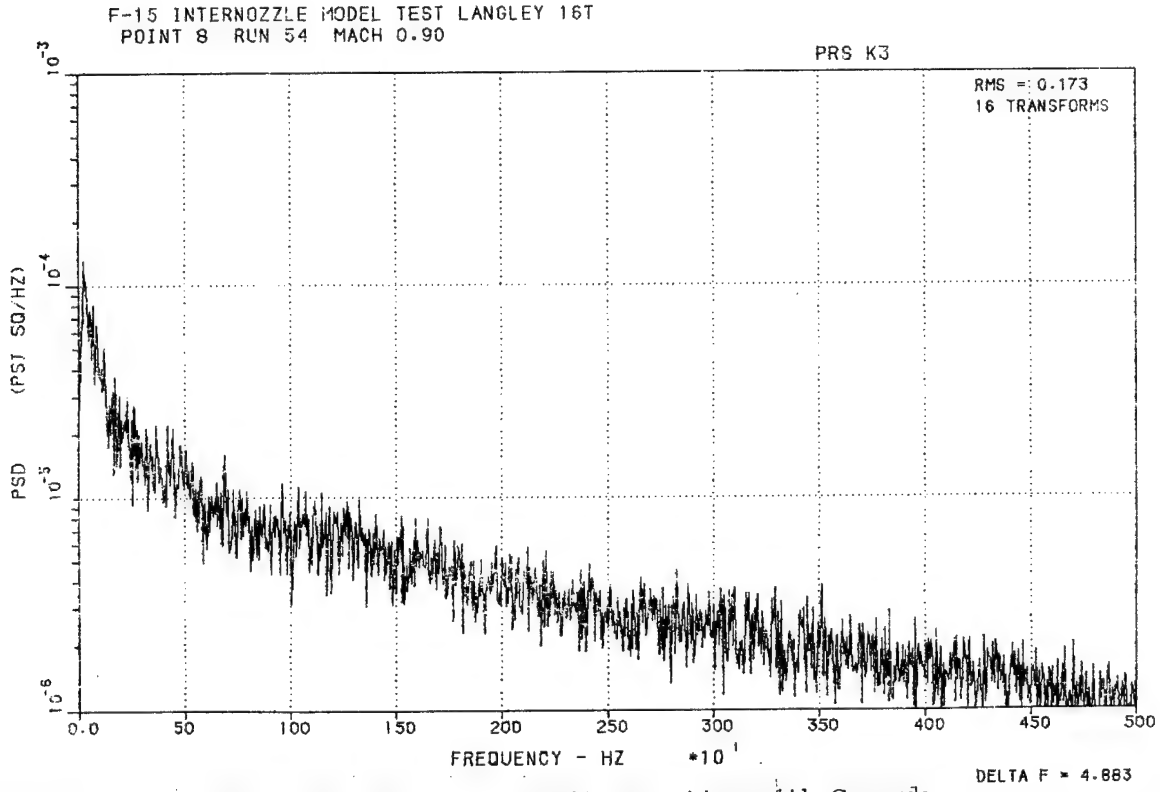

Figure 80. Power Spectral Density Function-with Canards Kulite 3 MACH 0.9 EPR 1.0

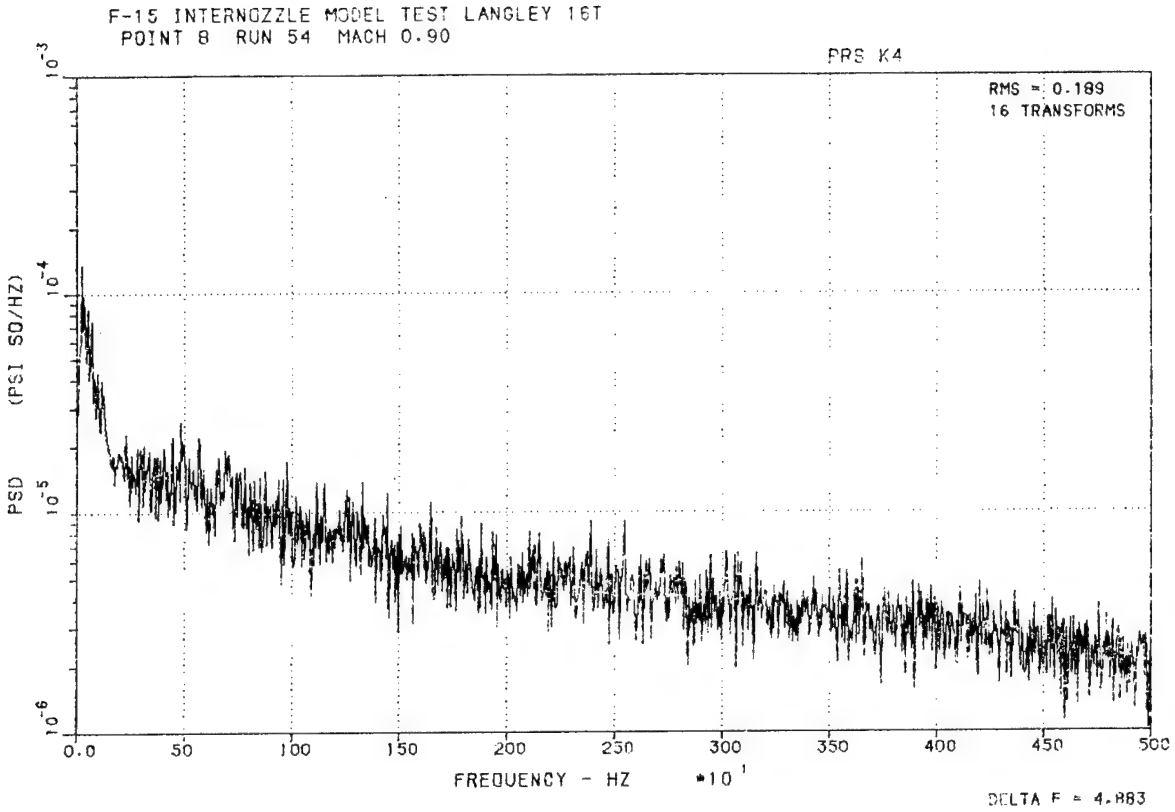

Figure 81. Power Spectral Density Function-with Canards Kulite 4 MACH 0.9 EPR 1.0

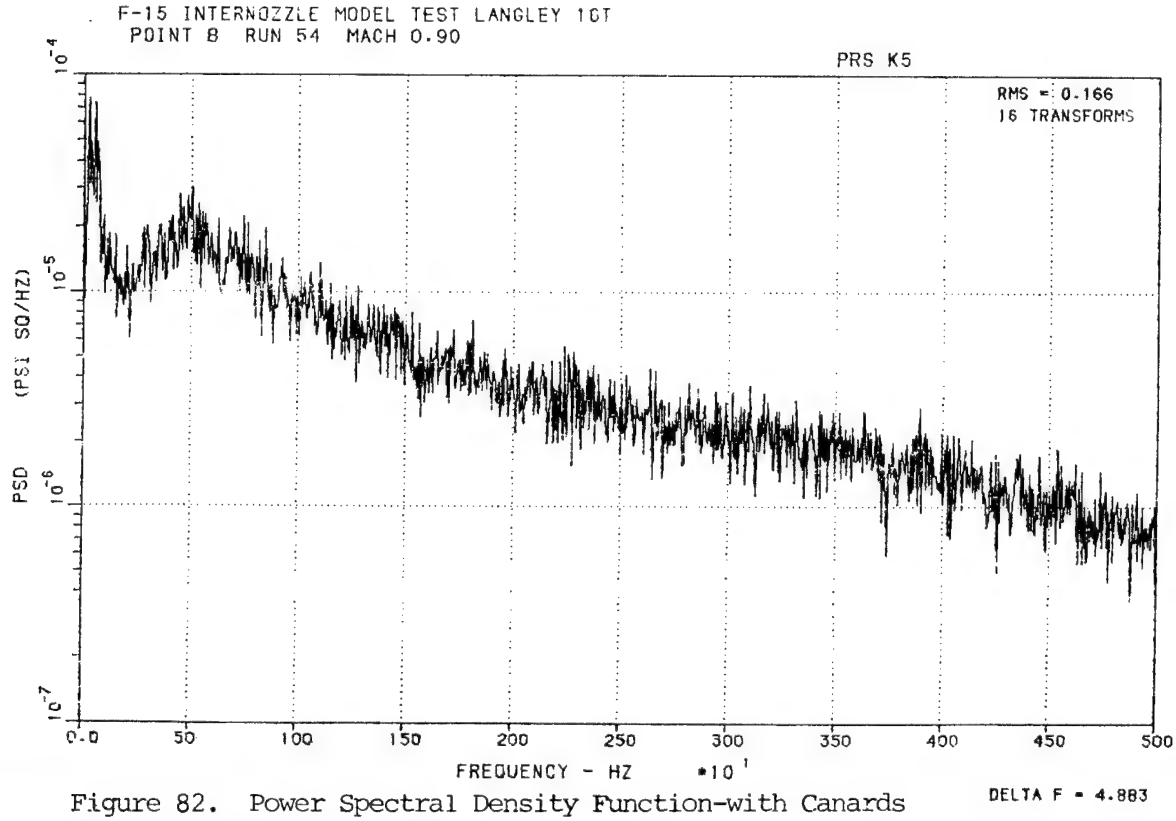

Figure 82. Power Spectral Density Function-with Canards Kulite 5 MACH 0.9 EPR 1.0

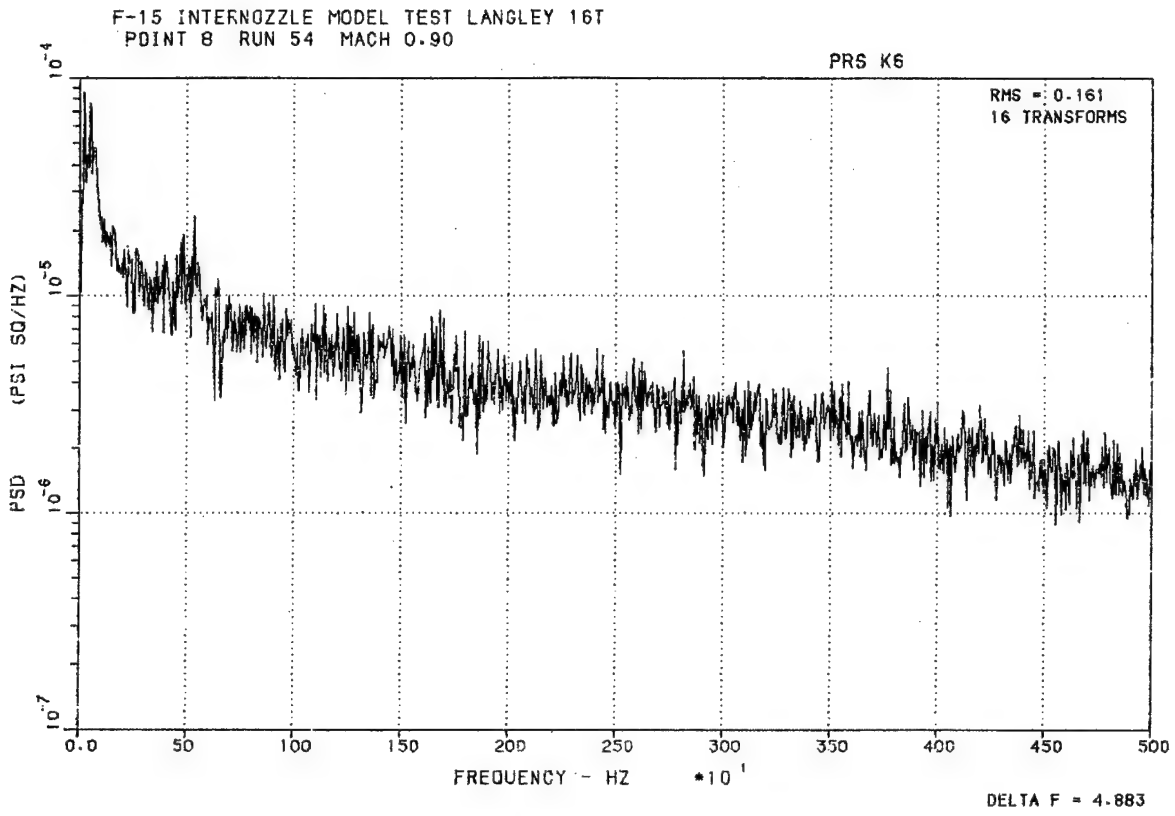

Figure 83. Power Spectral Density Function-Canards Kulite 6
MACH 0.9 EPR 1.0

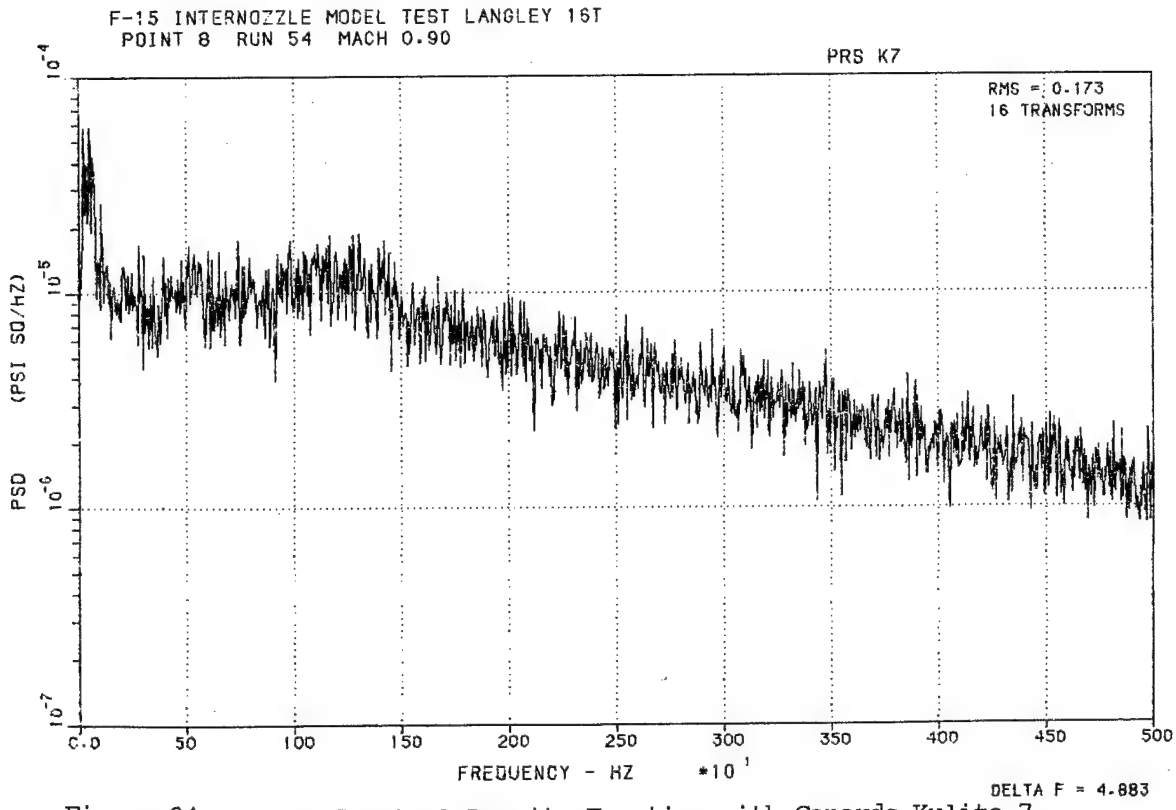

Figure 84. power Spectral Density Function-with Canards Kulite 7
MACH 0.9 EPR 1.0

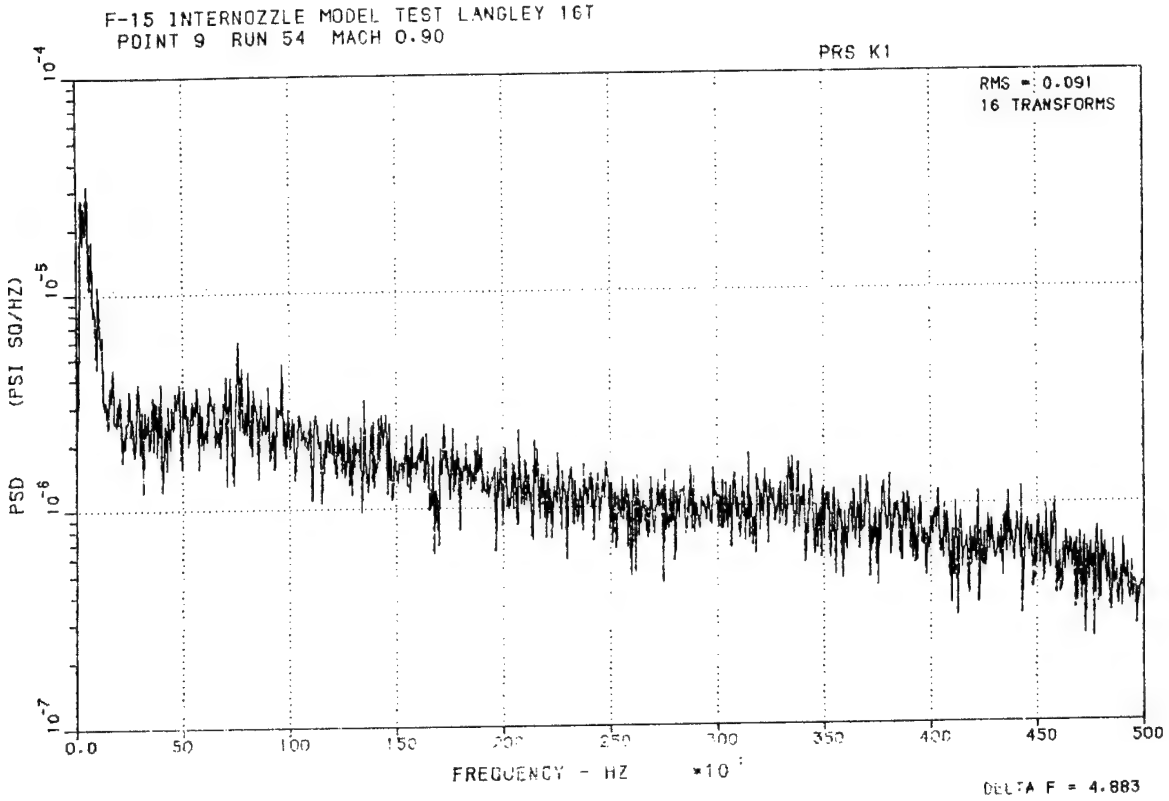

Figure 85. Power Spectral Density Function-with Canards Kulite 1 MACH 0.9 EPR 1.0

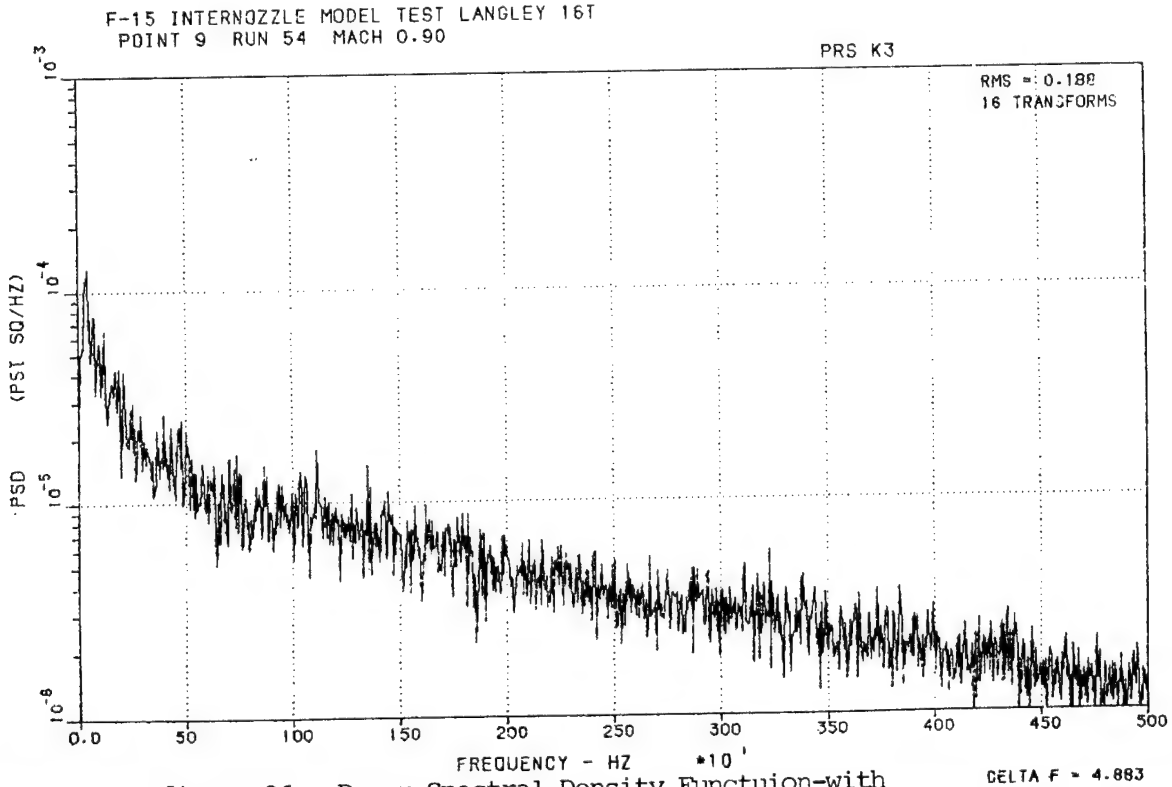

Figure 86. Power Spectral Density Functuion-with Canards Kulite 3 MACH 0.9 EPR 1.0

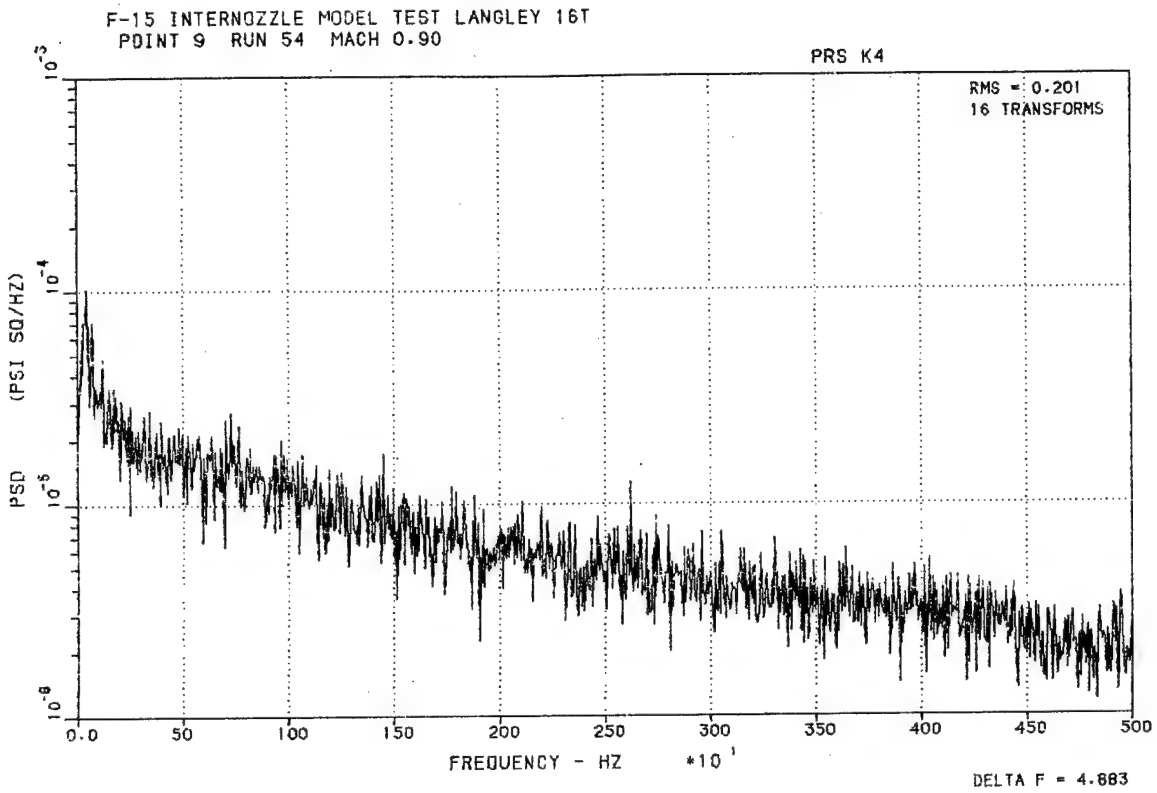

Figure 87. Power spectral Density Function-with Canards Kulite 4 MACH 0.9 EPR 1.0

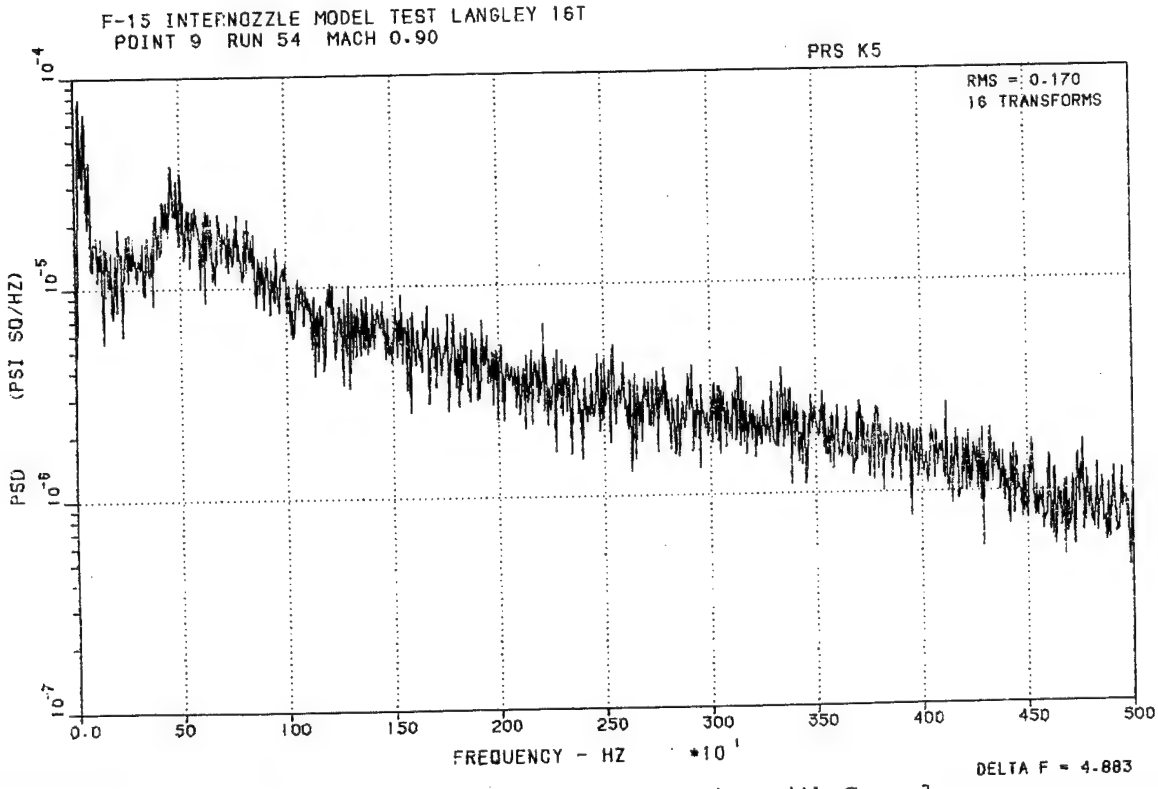

Figure 88. Power spectral Density Function-with Canards Kulite 5 MACH MACH 0.9 EPR 1.0

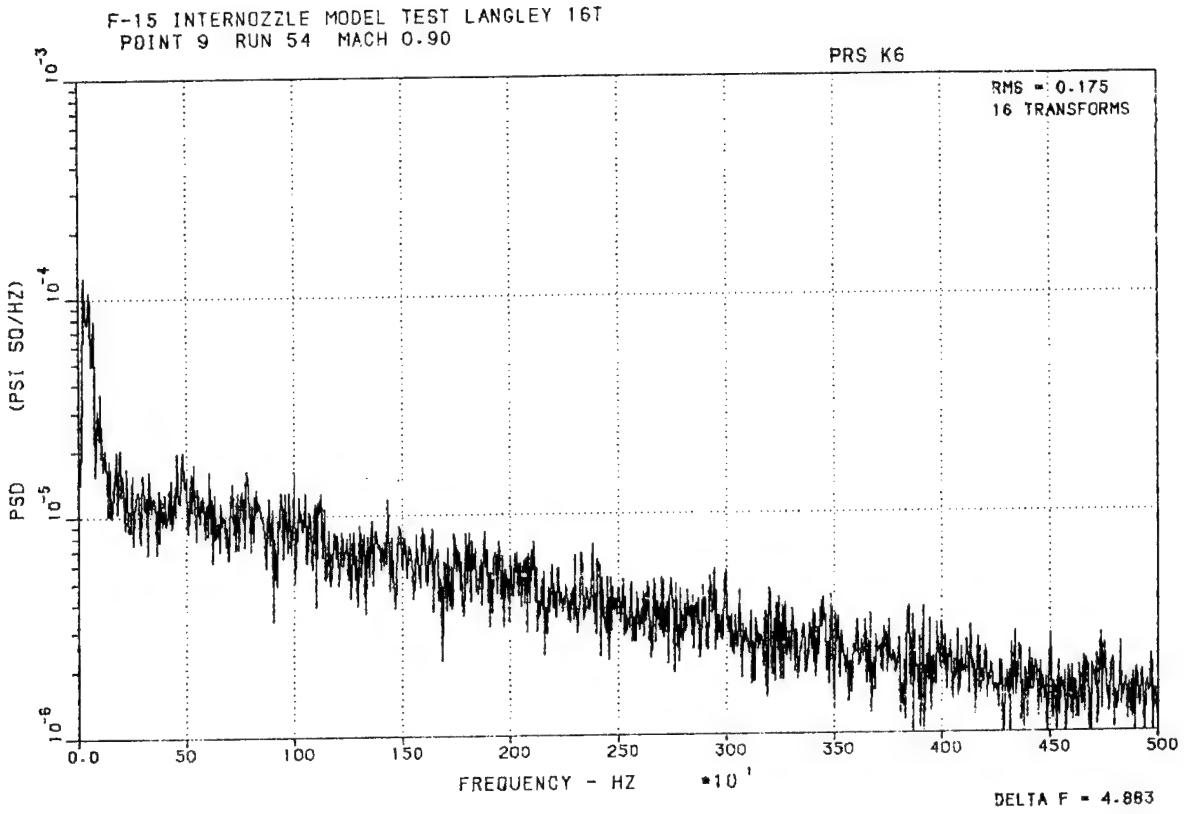

Figure 89. Power Spectral Density Function-with Canards Kulite 6 MACH 0.9 EPR 1.0

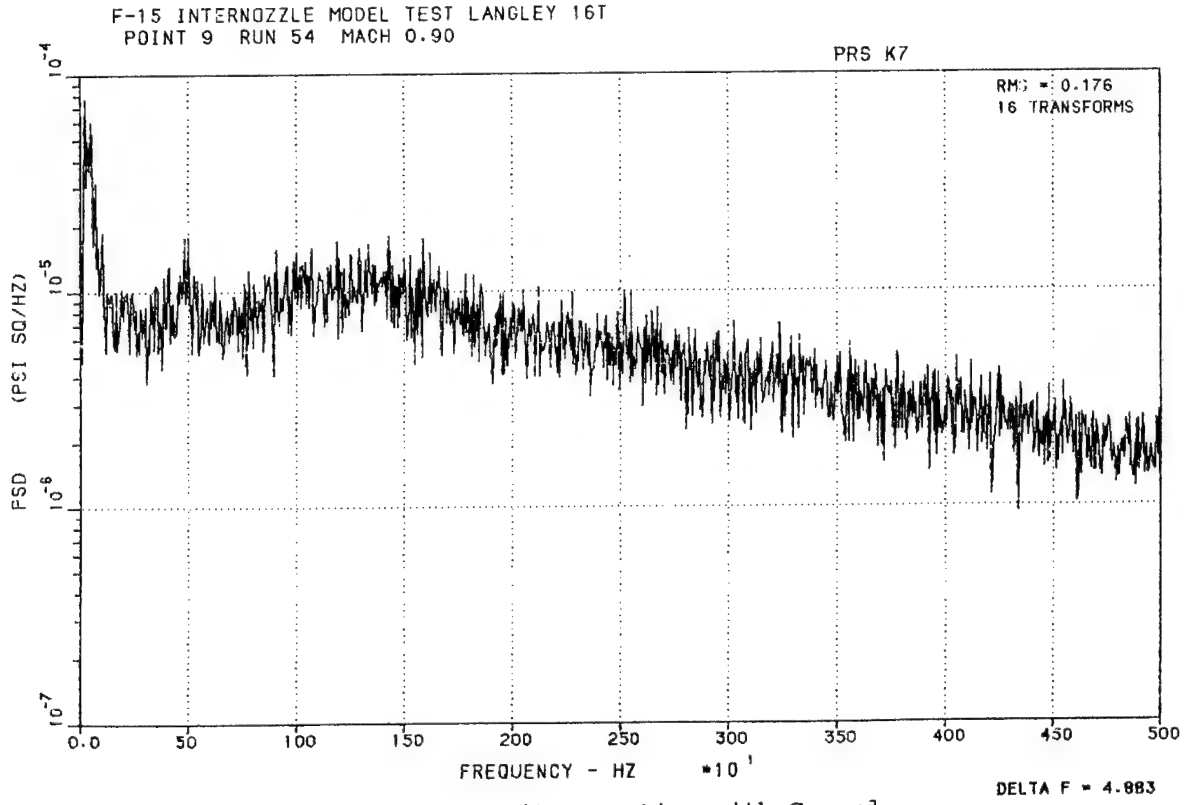

Figure 90. Power Spectral Density Function-with Canards Kulite 7 MACH 0.9 EPR 1.0

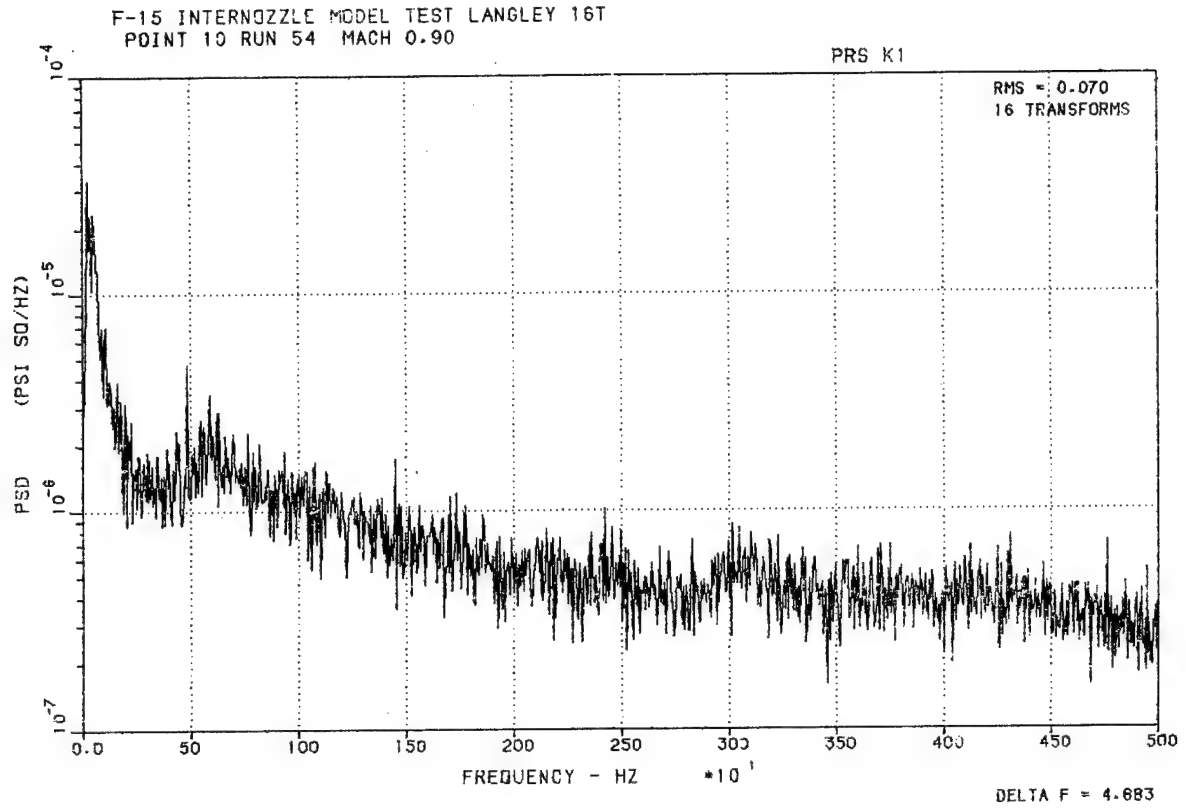

Figure 91. Power Spectral Density Function-with Canards Kulite 1 MACH 0.9 EPR 3.5

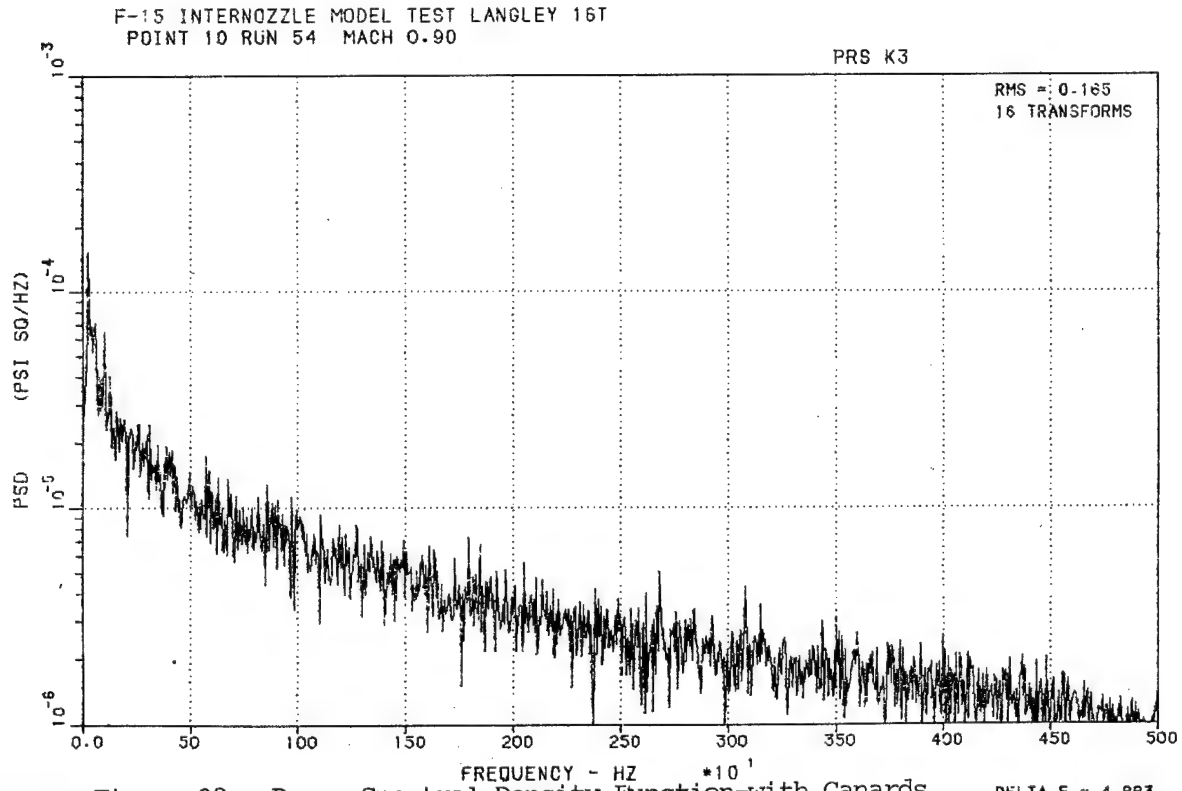

Figure 92. Power Spectral Density Function-with Canards Kulite 3 MACH 0.9 EPR 3.5

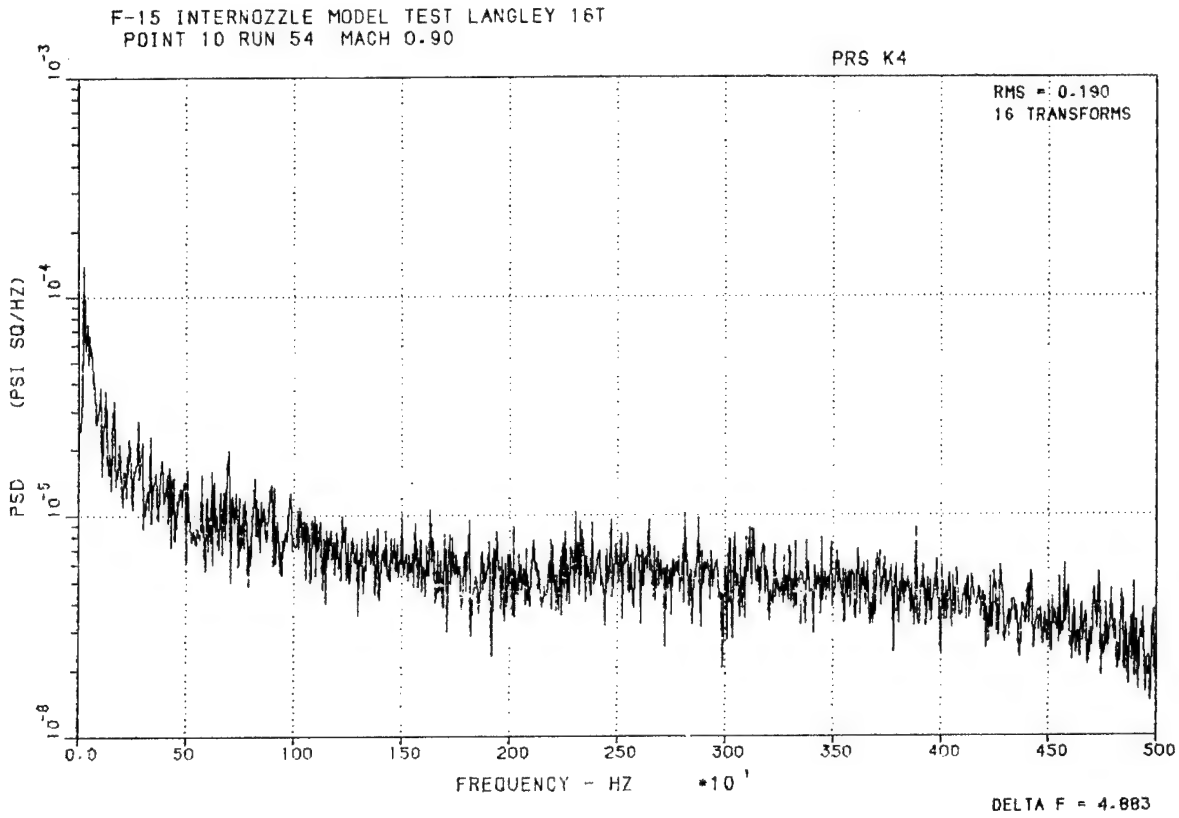

Figure 93. Power Spectral Density Function-with Canards Kulite 4
MACH 0.9 EPR 3.5

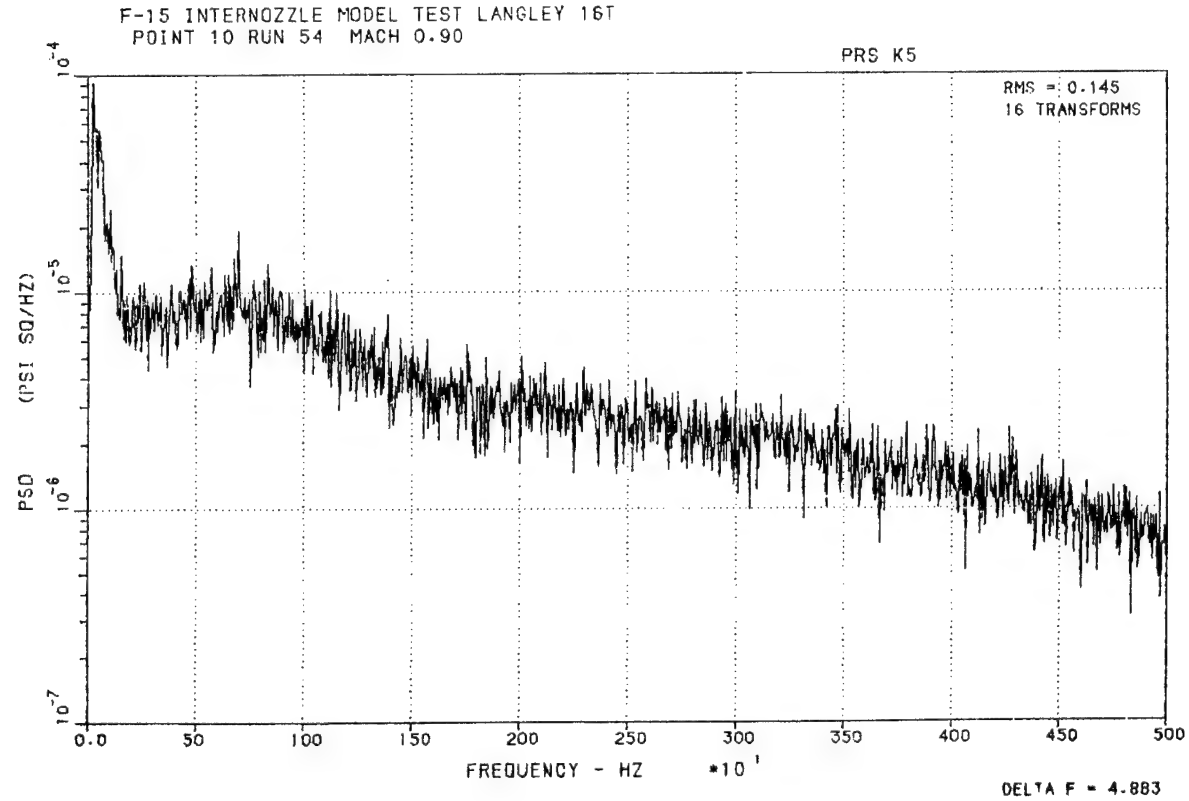

Figure 94. Power Spectral Density Function-with Canards Kulite 5
MACH 0.9 EPR 3.5

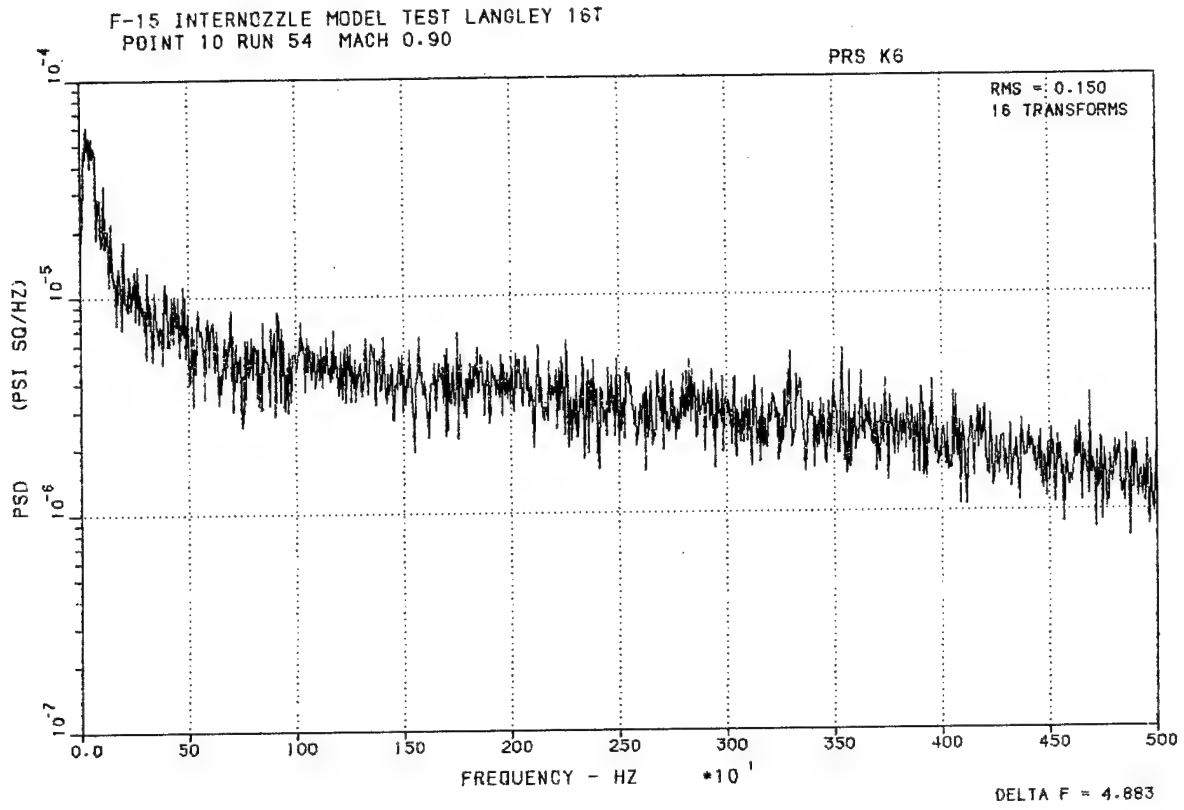

Figure 95. Power Spectral Density Function-with Canards Kulite 6
MACH 0.9 EPR 3.5

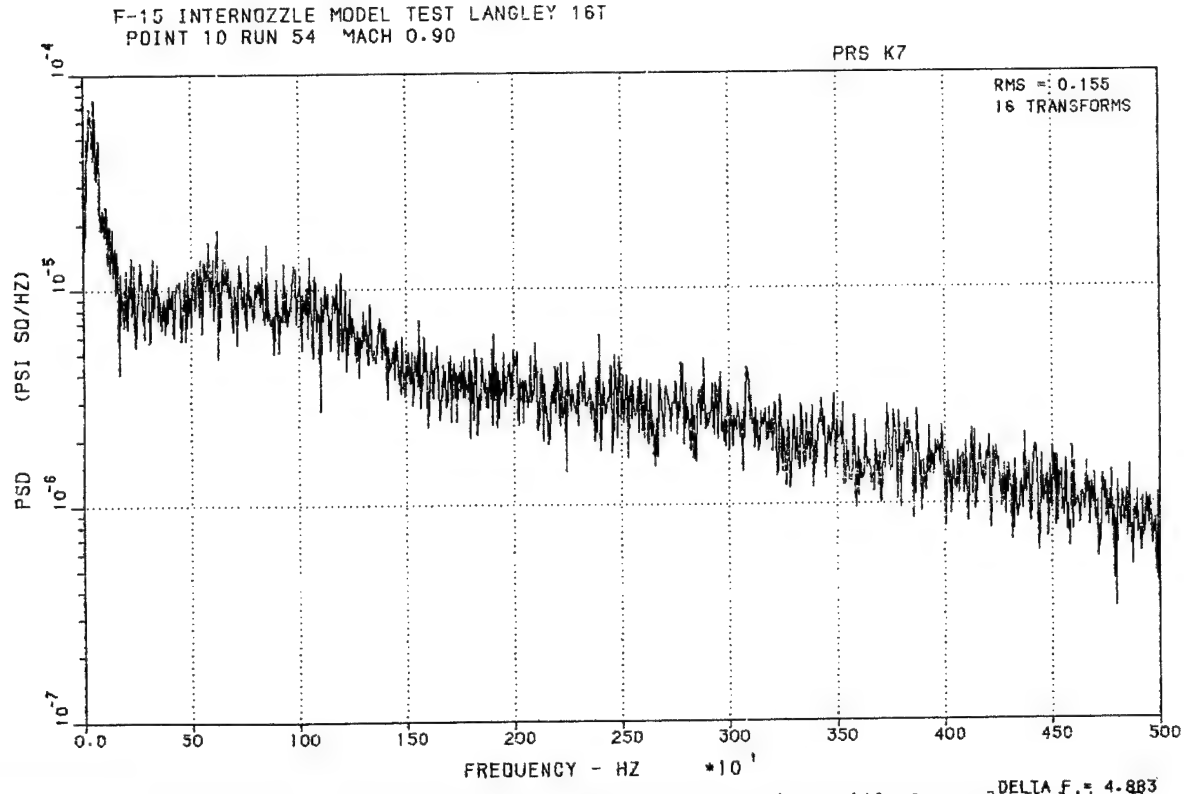

Figure 96. Power Spectral Density Function-with Canards Kulite 7
MACH 0.9 EPR 3.5

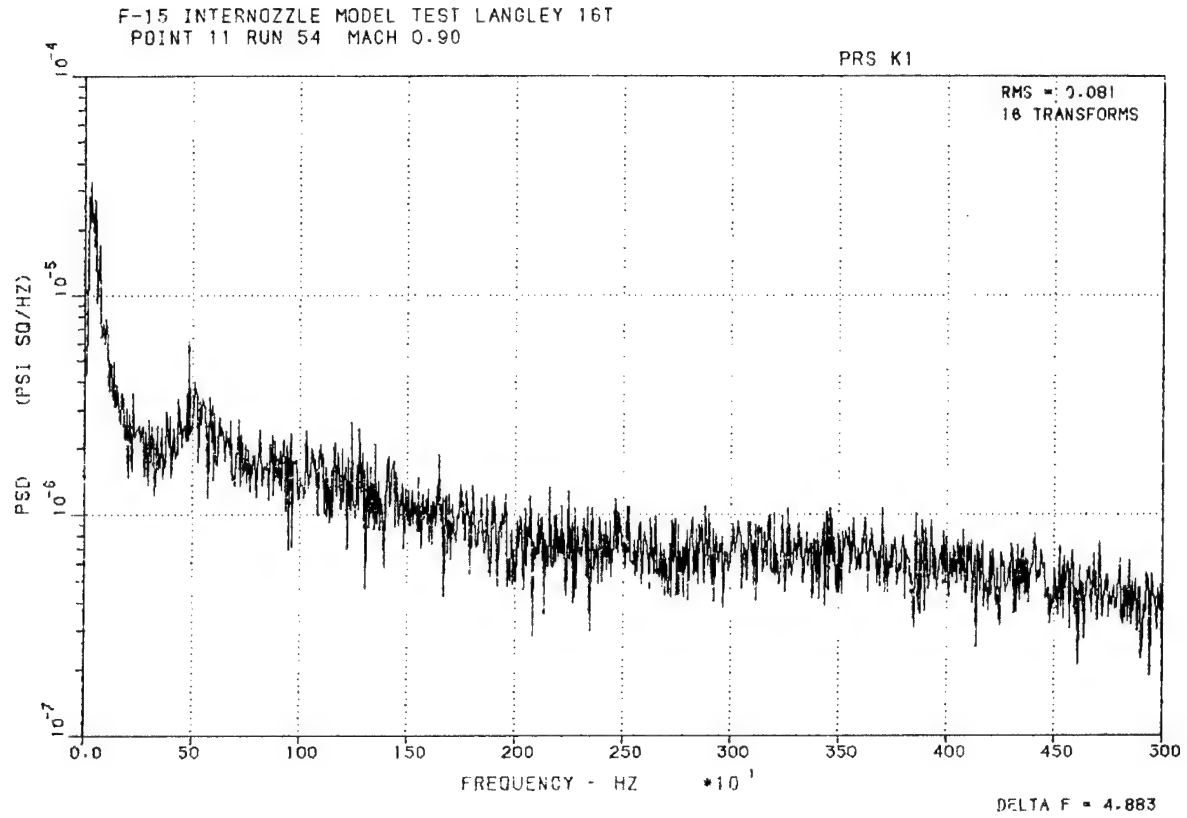

Figure 97. Power Spectral Density Function-with Canards Kulite 1 MACH 0.9 EPR 3.5

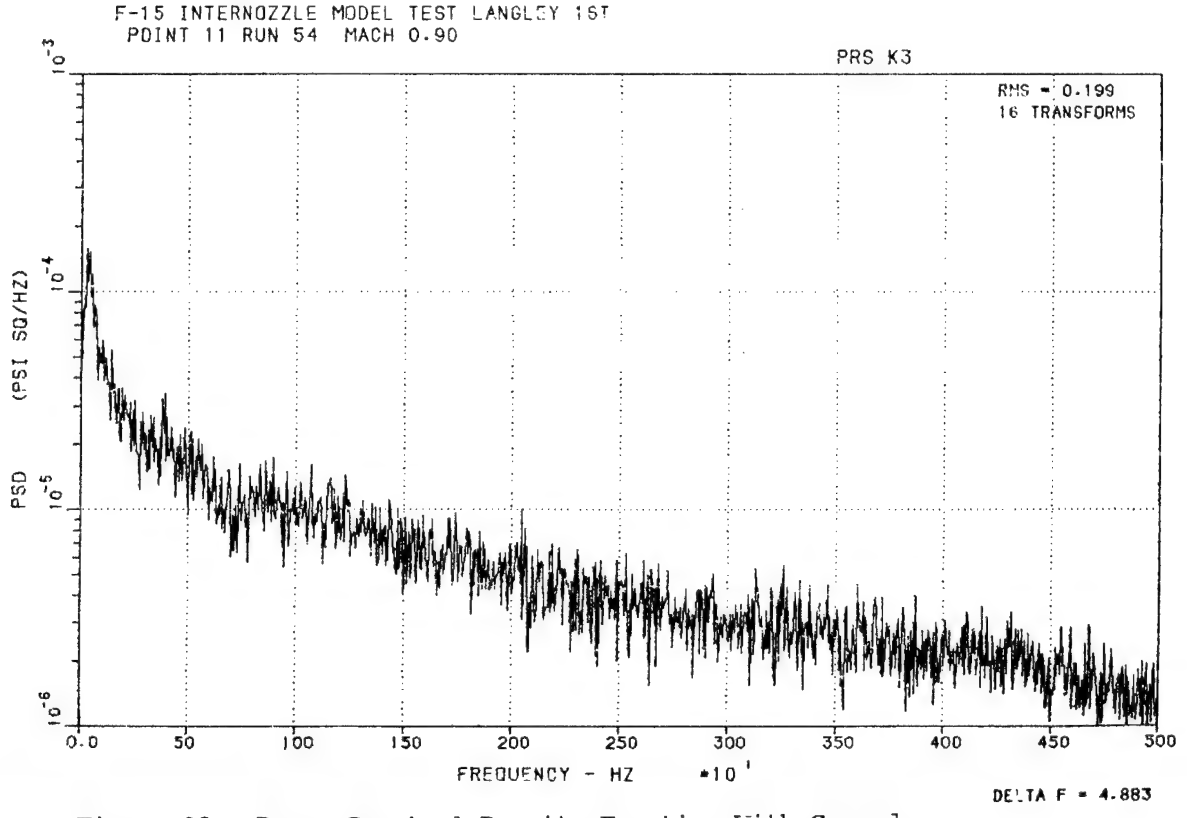

Figure 98. Power Spectral Density Function-With Canards Kulite 3 MACH 0.9 EPR 3.5

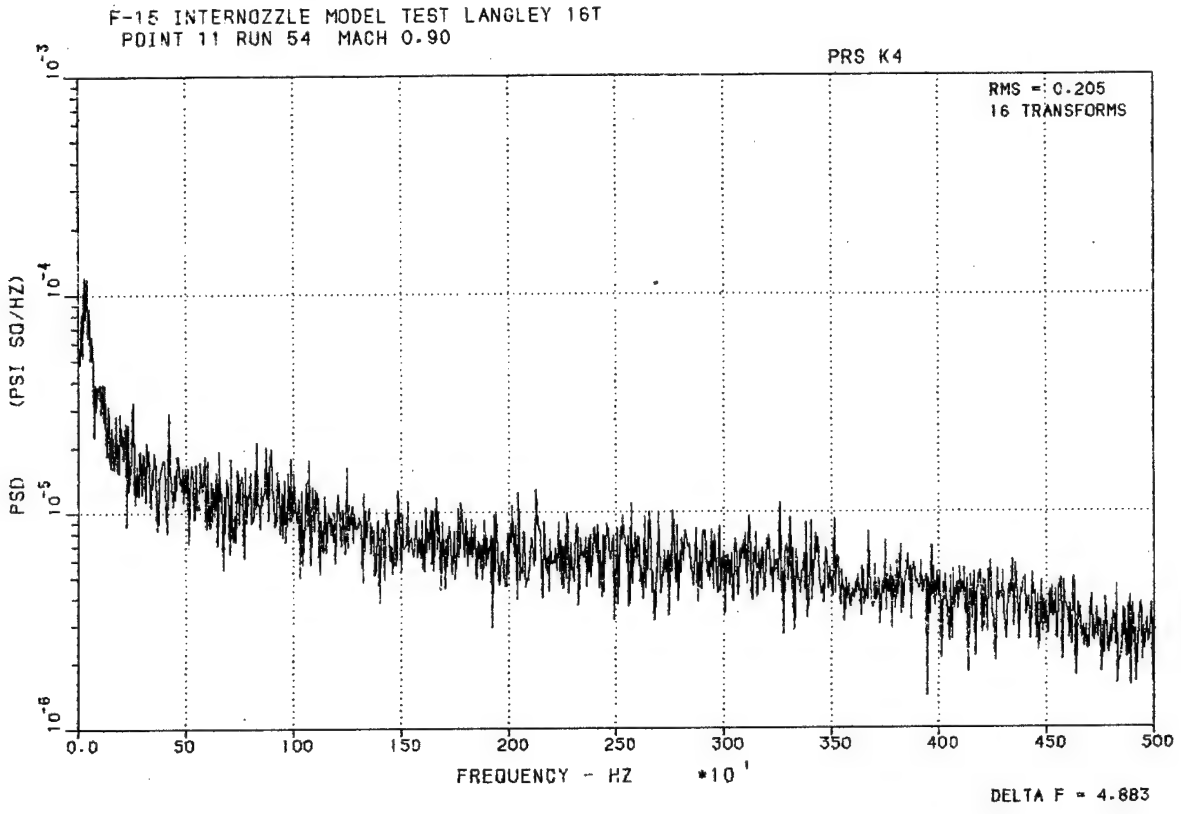

Figure 99. Power Spectral Density Function-with Canards Kulite 5 MACH 0.9 EPR 3.5

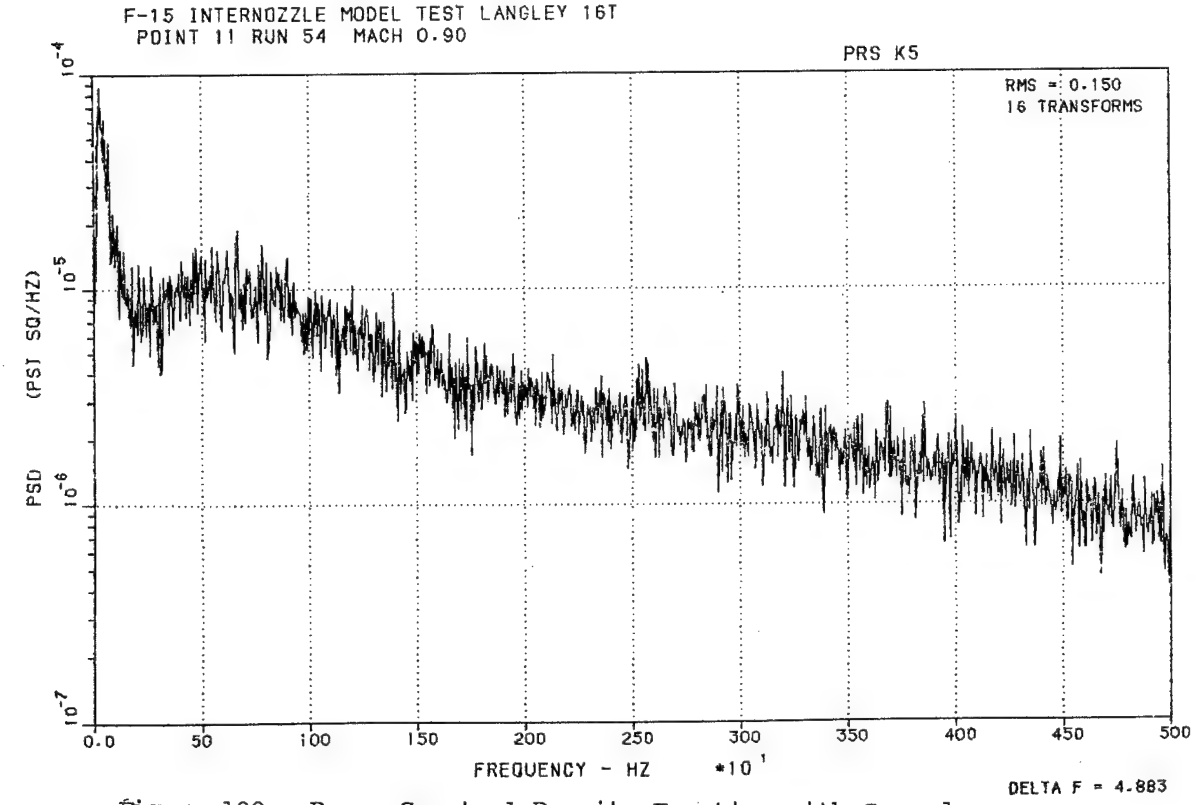

Figure 100. Power Spectral Density Function-with Canards Kulite 5 MACH 0.9 EPR 3.5

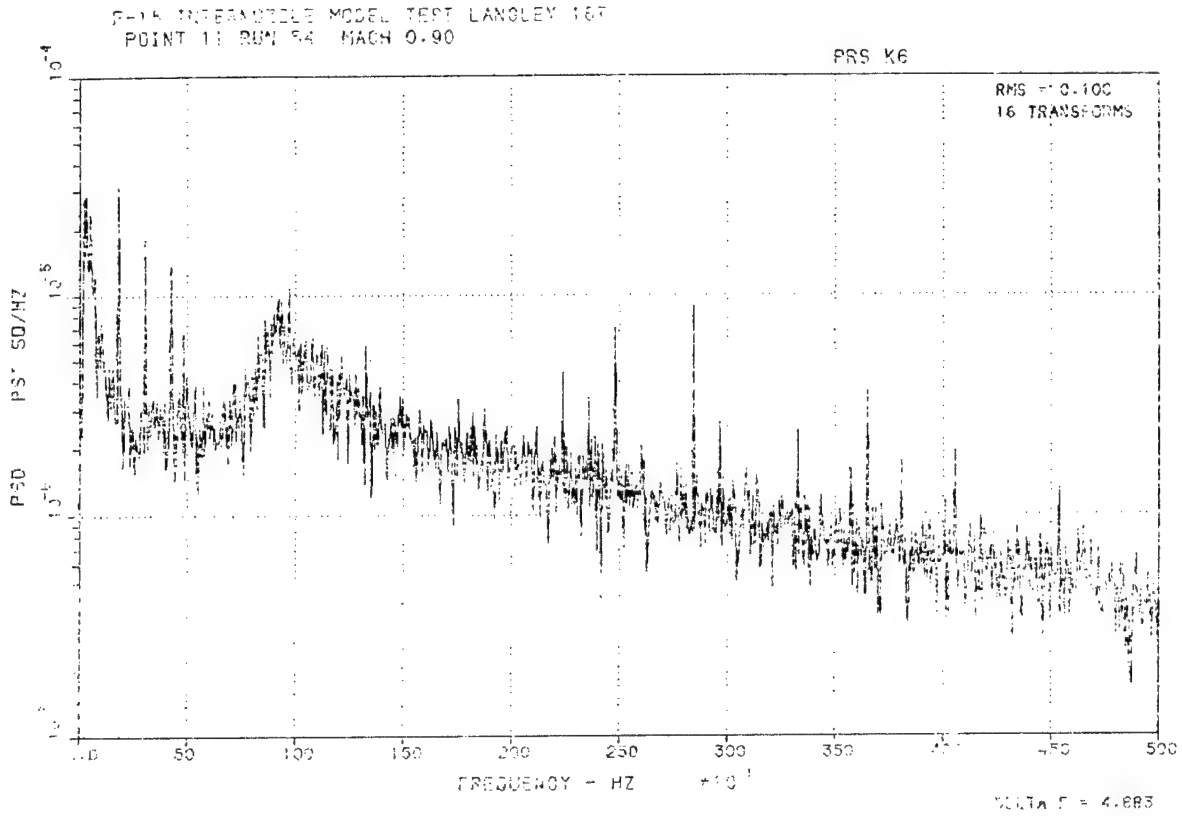

Figure 101. Power Spectral Density Function-with Canards Kulite 6 MACH 0.9 EPR 3.5

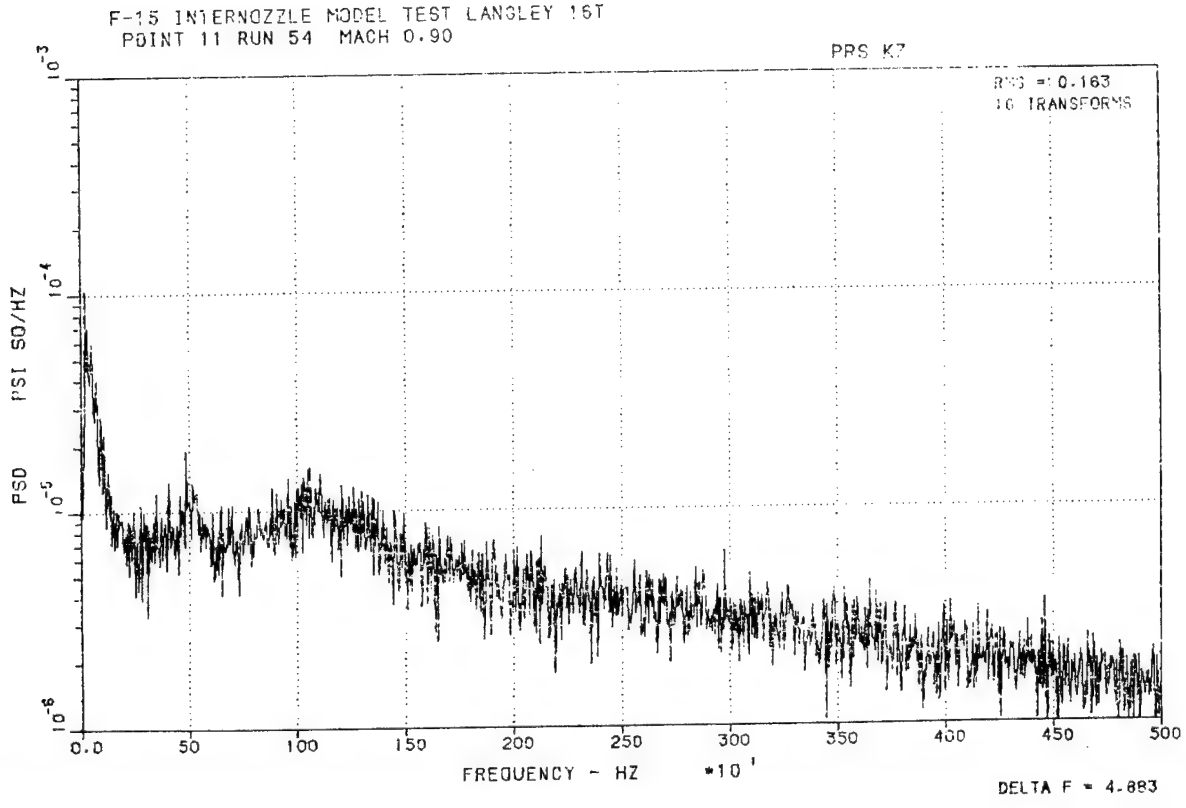

Figure 102. Power Spectral Density Fucntion-with Canards Kulite 7 MACH 0.9 EPR 3.5

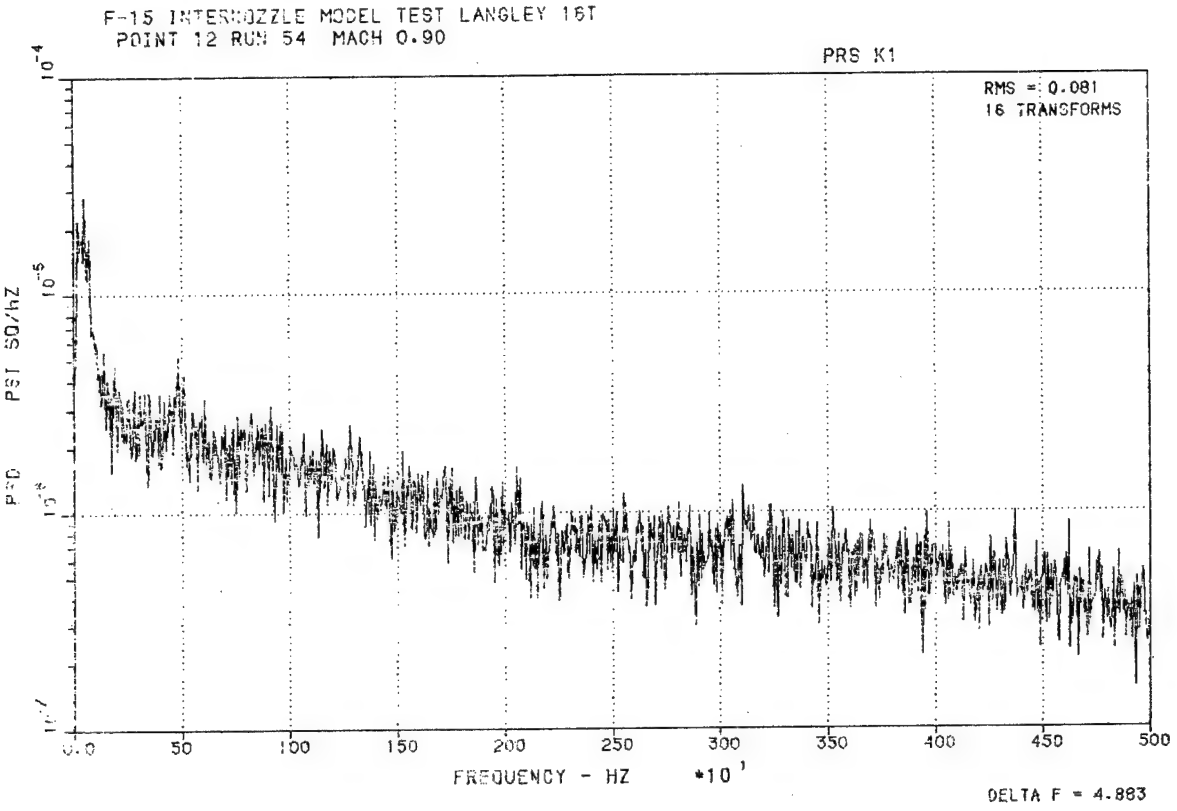

Figure 103. Power Spectral Density Function-with Canards Kulite 1 MACH 0.9 EPR 3.5

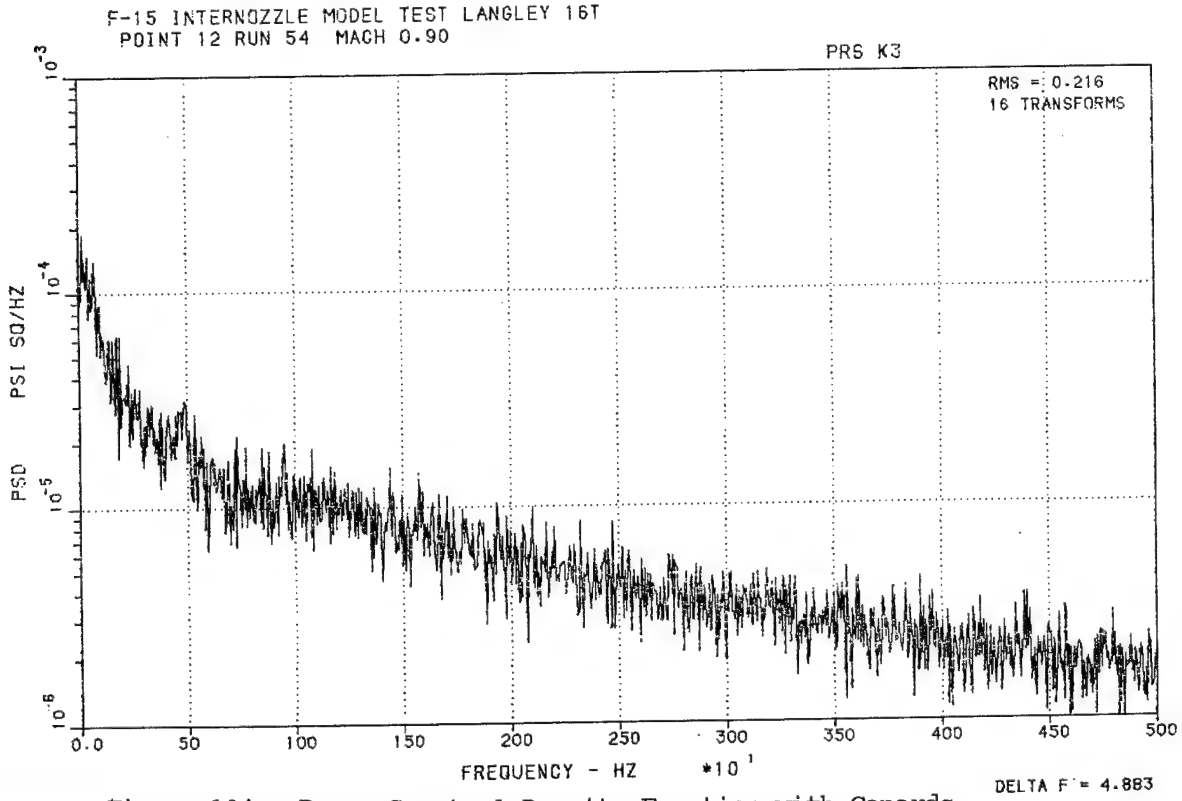

Figure 104. Power Spectral Density Function-with Canards Kulite 3 MACH 0.9 EPR 3.5

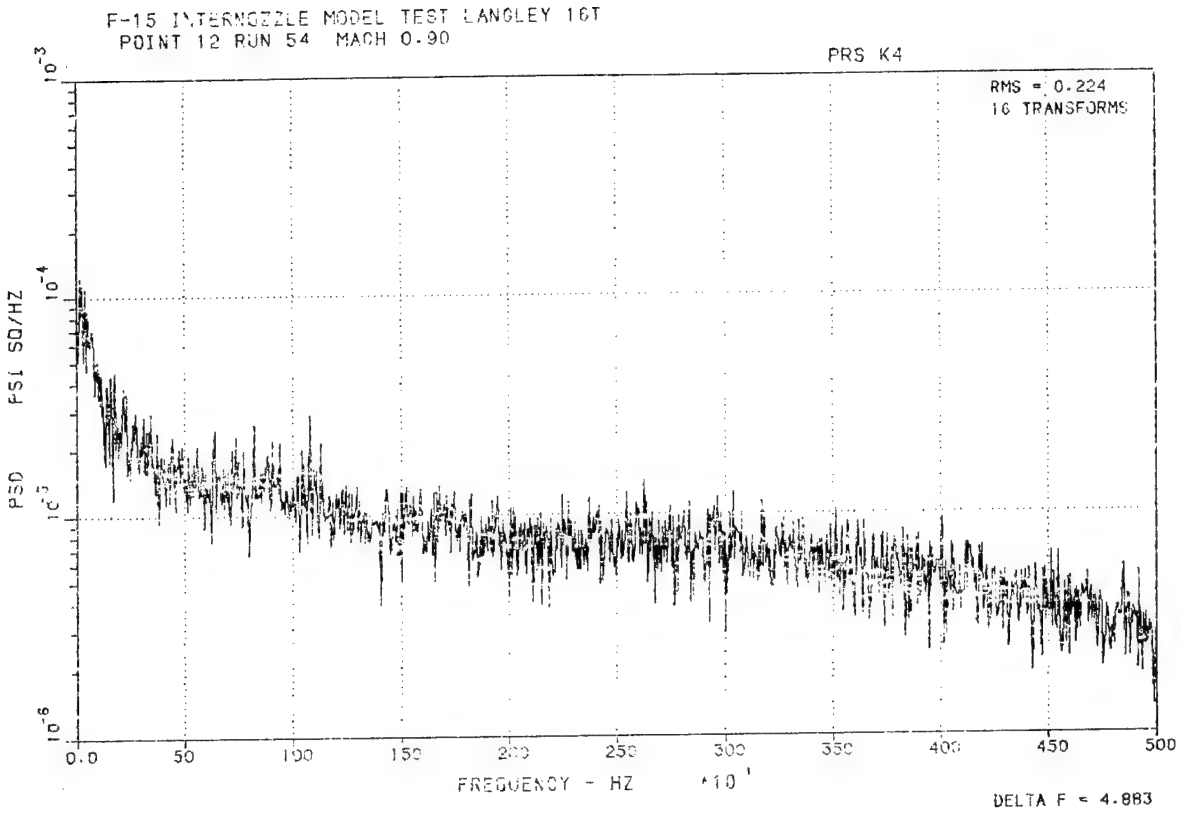

Figure 105. Power Spectral Density Function-with Canards Kulite 4 MACH 0.9 EPR 3.5

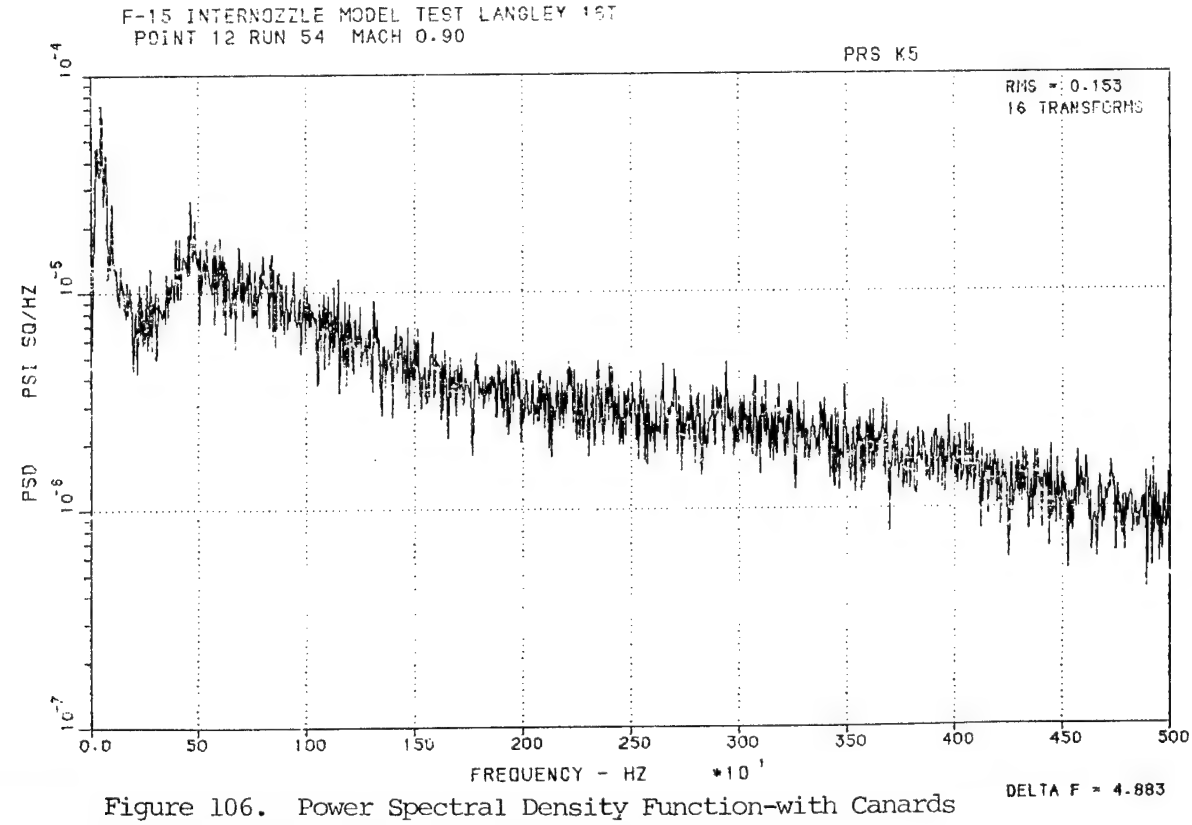

Figure 106. Power Spectral Density Function-with Canards Kulite 5 MACH 0.9 EPR 3.5

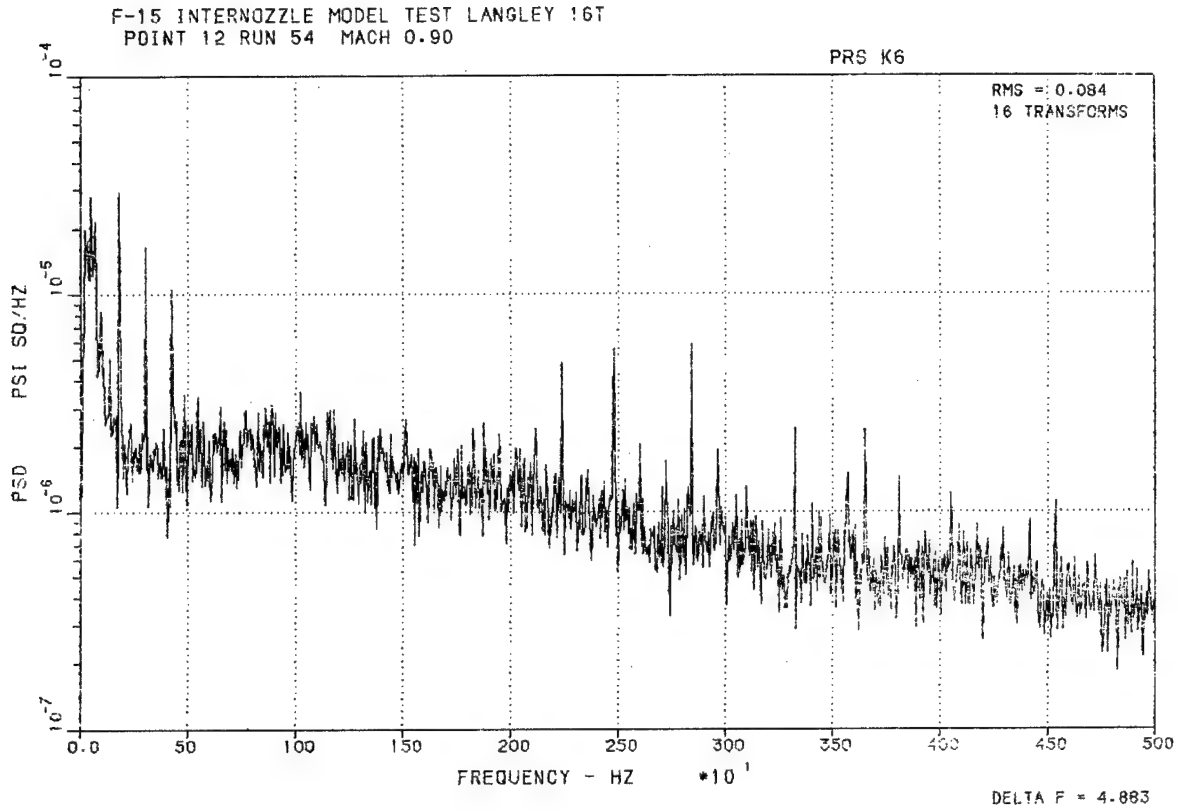

Figure 107. Power Spectral Density Funtion-with Canards Kulite 6 MACH 0.9 EPR 3.5

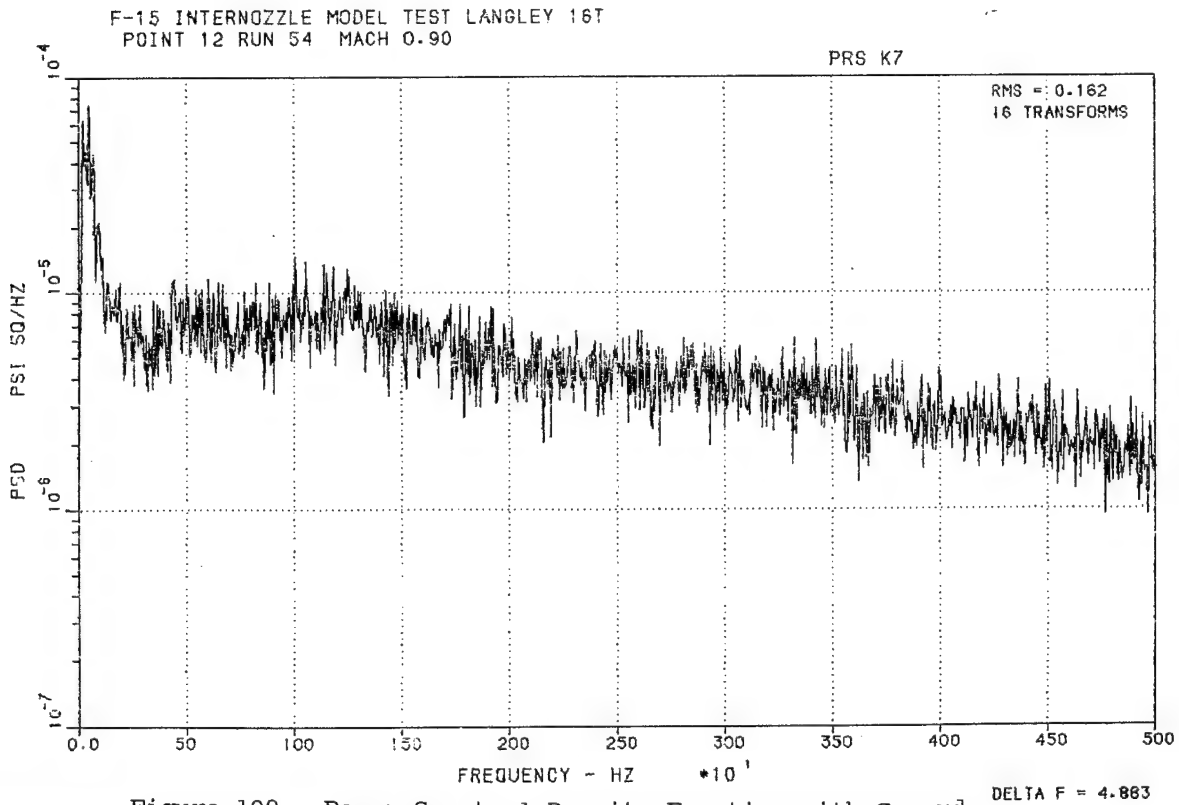

Figure 108. Power Spectral Density Function-with Canards Kulite 7 MACH 0.9 EPR 3.5

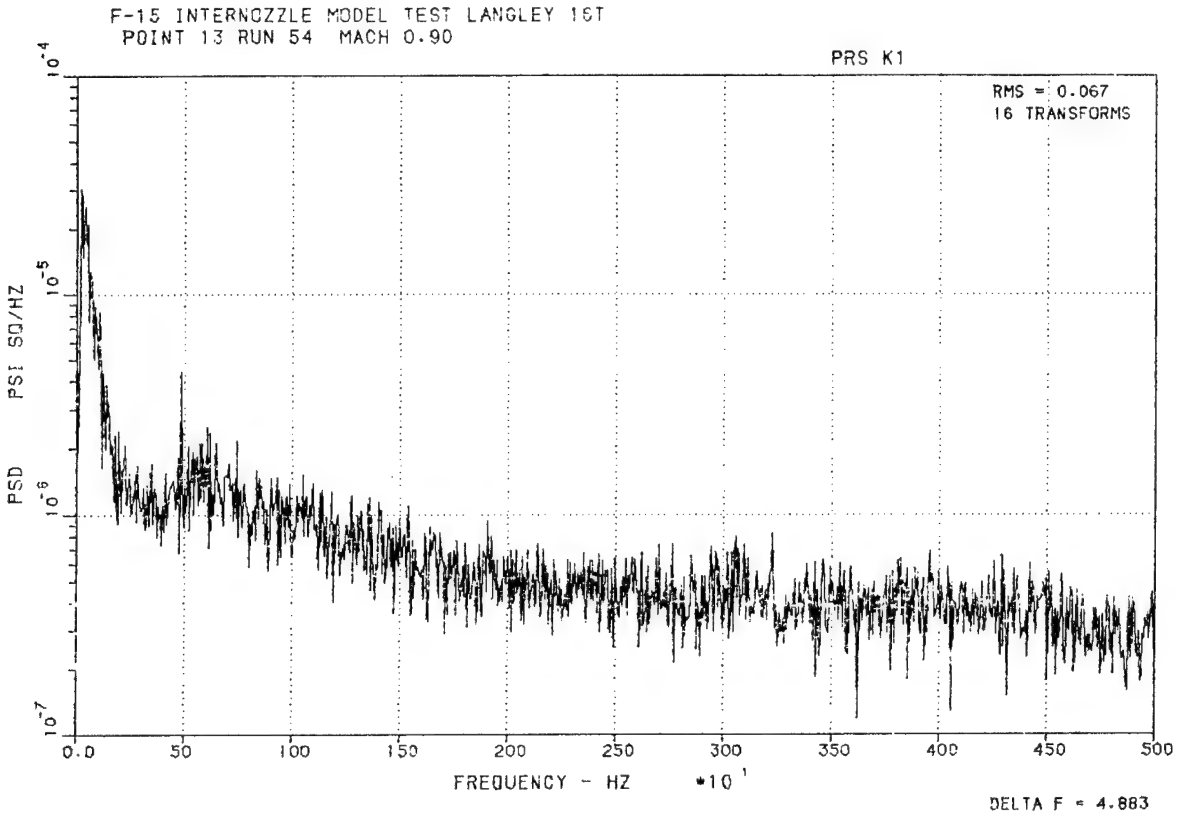

Figure 109. Power Spectral Density Function-with Canards Kulite 1 MACH 0.9 EPR 5.0

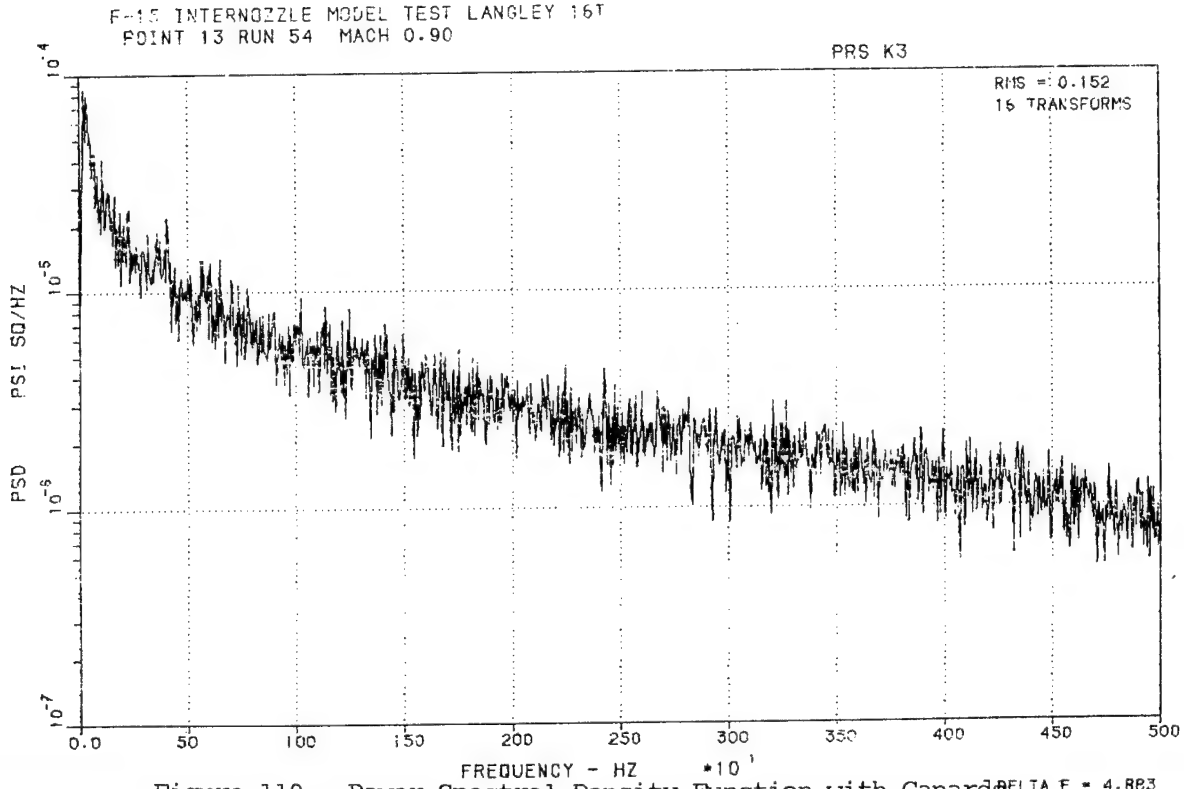

Figure 110. Power Spectral Density Function-with Canards Kulite 3 MACH 0.9 EPR 5.0

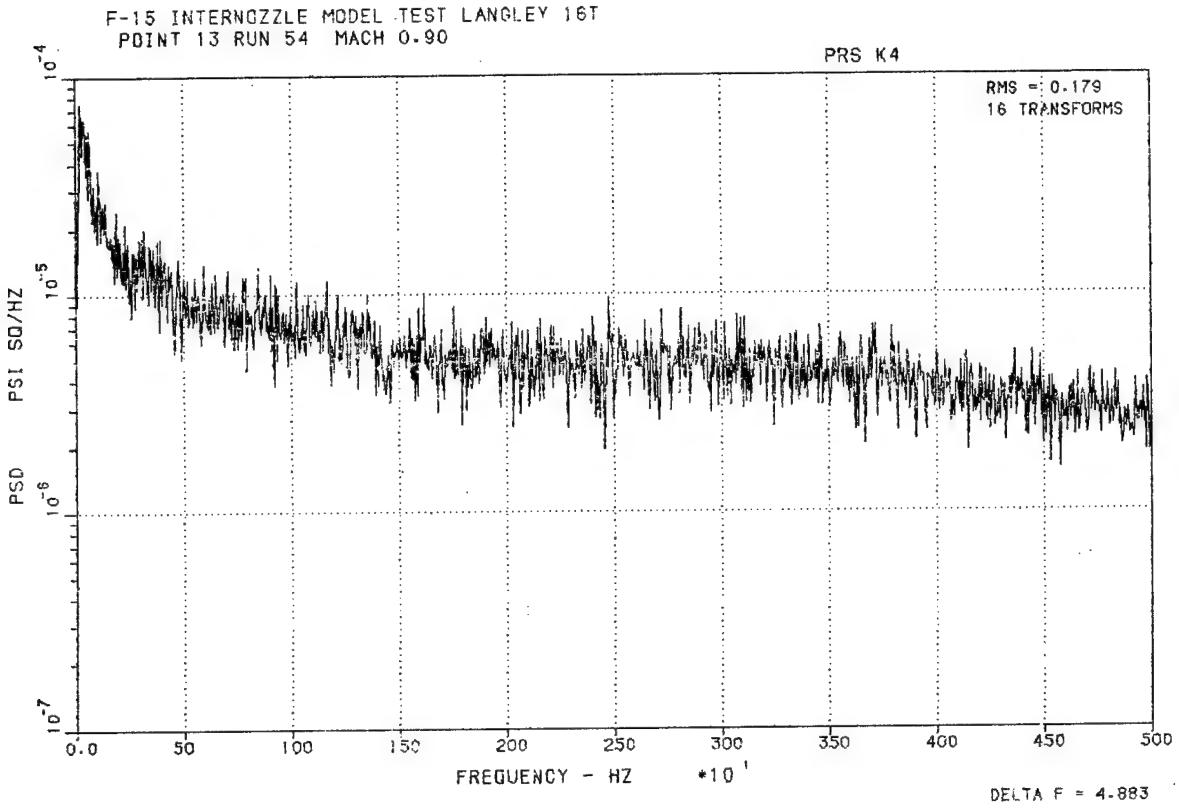

Figure 111. PSDF-with Canards Kulite 4 MACH 0.9 EPR 5.0

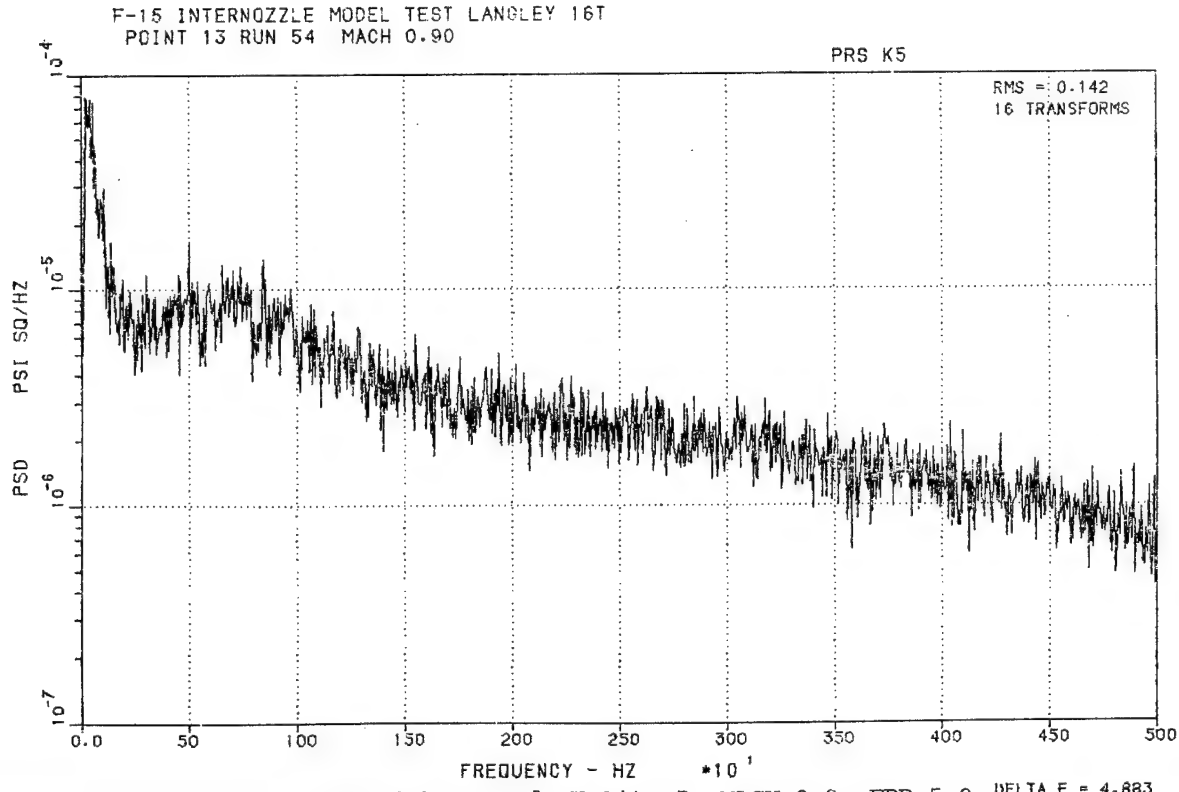

Figure 112. PSDF-with Canards Kulite 5 MACH 0.9 EPR 5.0

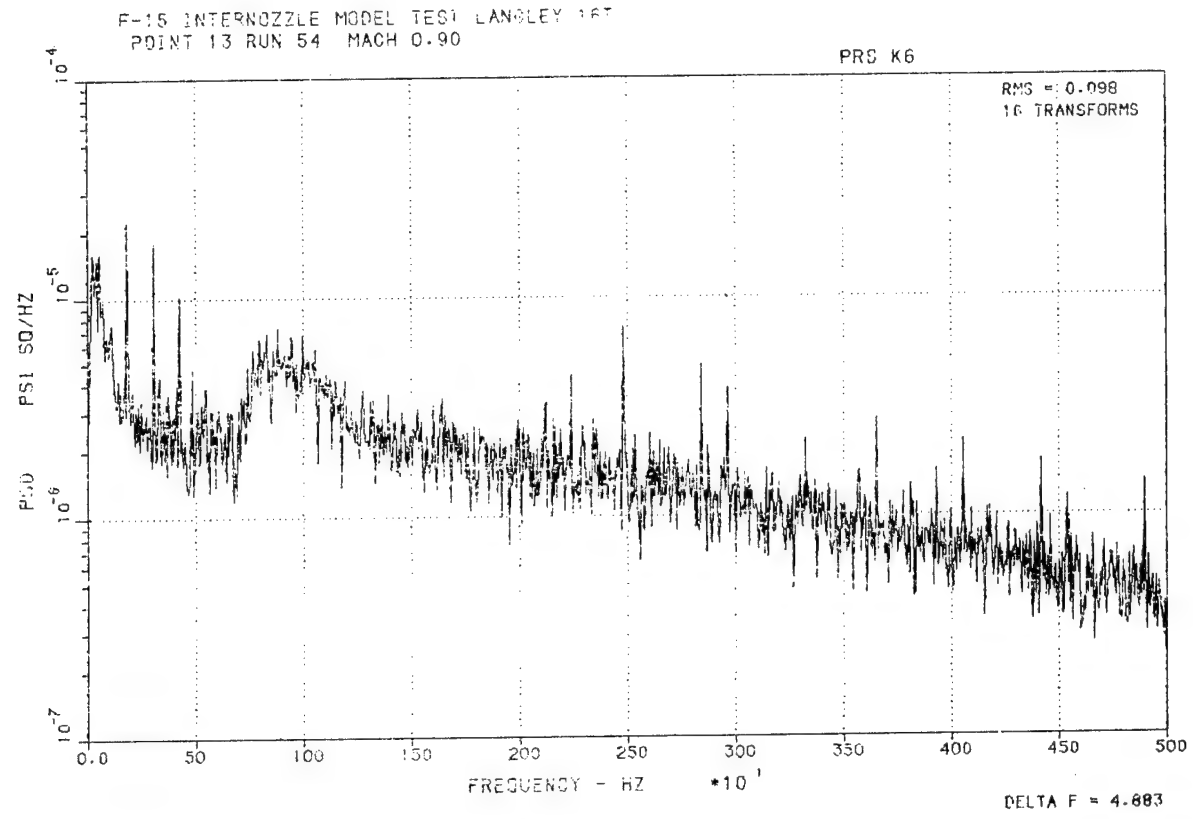

Figure 113. PSDF-with Canards Kulite 6 MACH 0.9 EPR 5.0

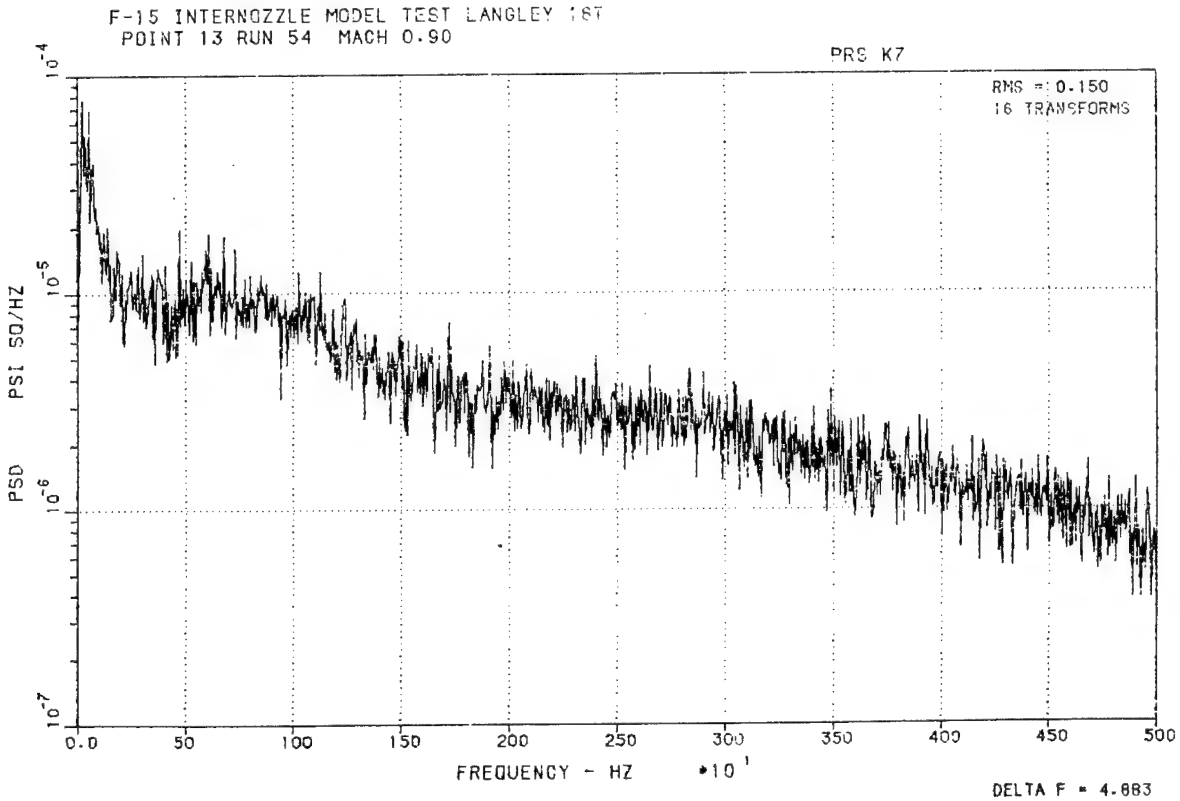

Figure 114. PSDF-with Canards Kulite 6 MACH 0.9 EPR 5.0

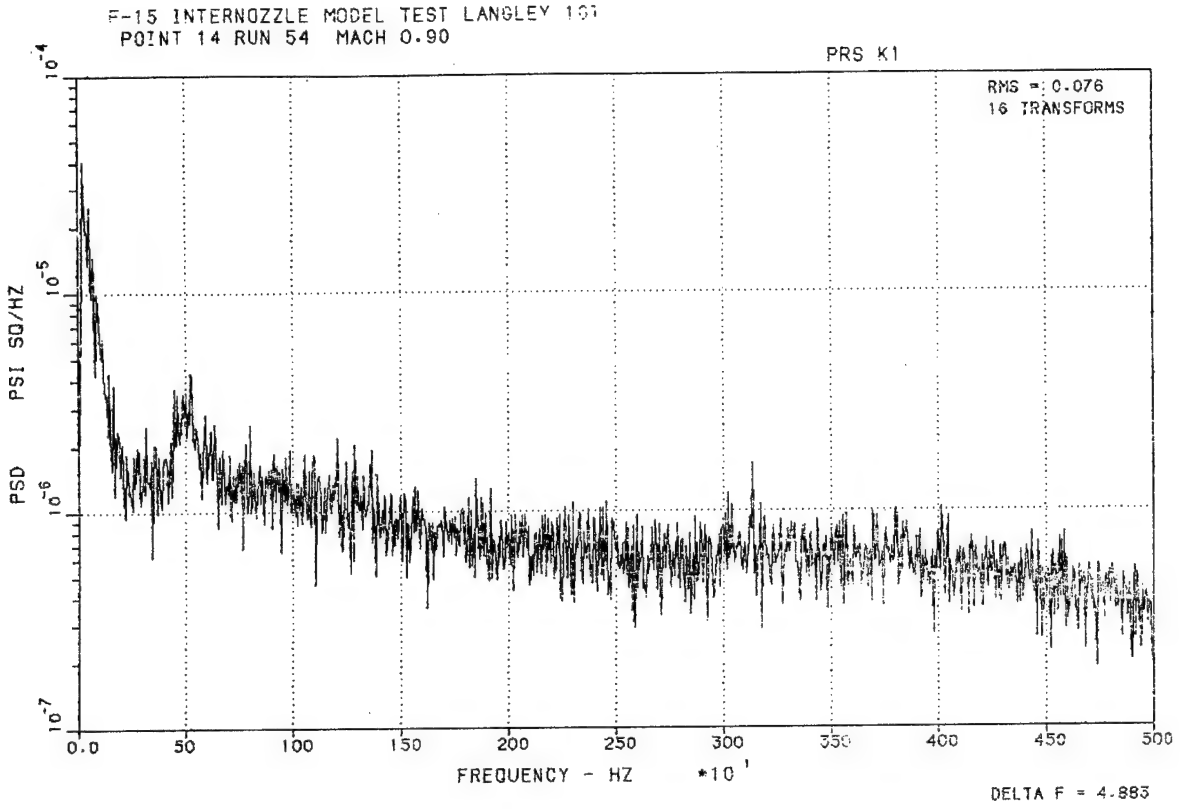

Figure 115. PSDF-with Canards Kulite 1 MACH 0.9 EPR 5.0

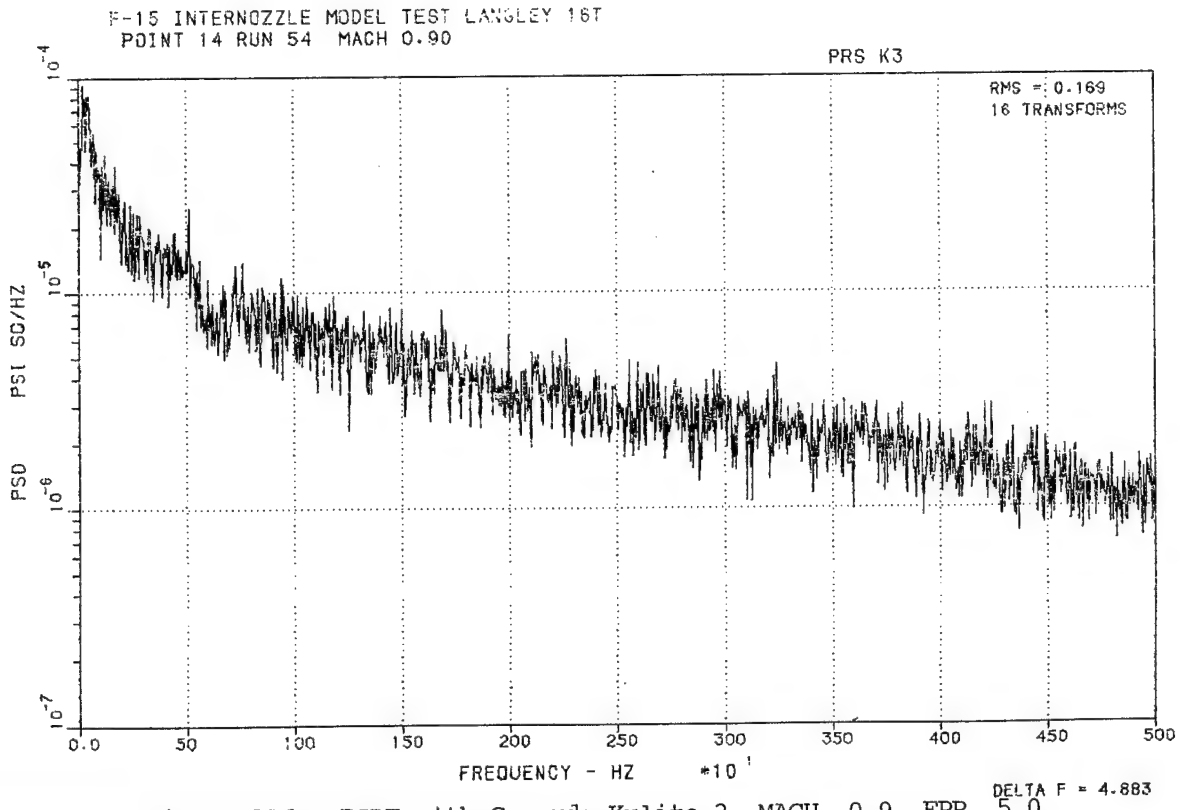

Figure 116. PSDF-with Canards Kulite 3 MACH 0.9 EPR 5.0

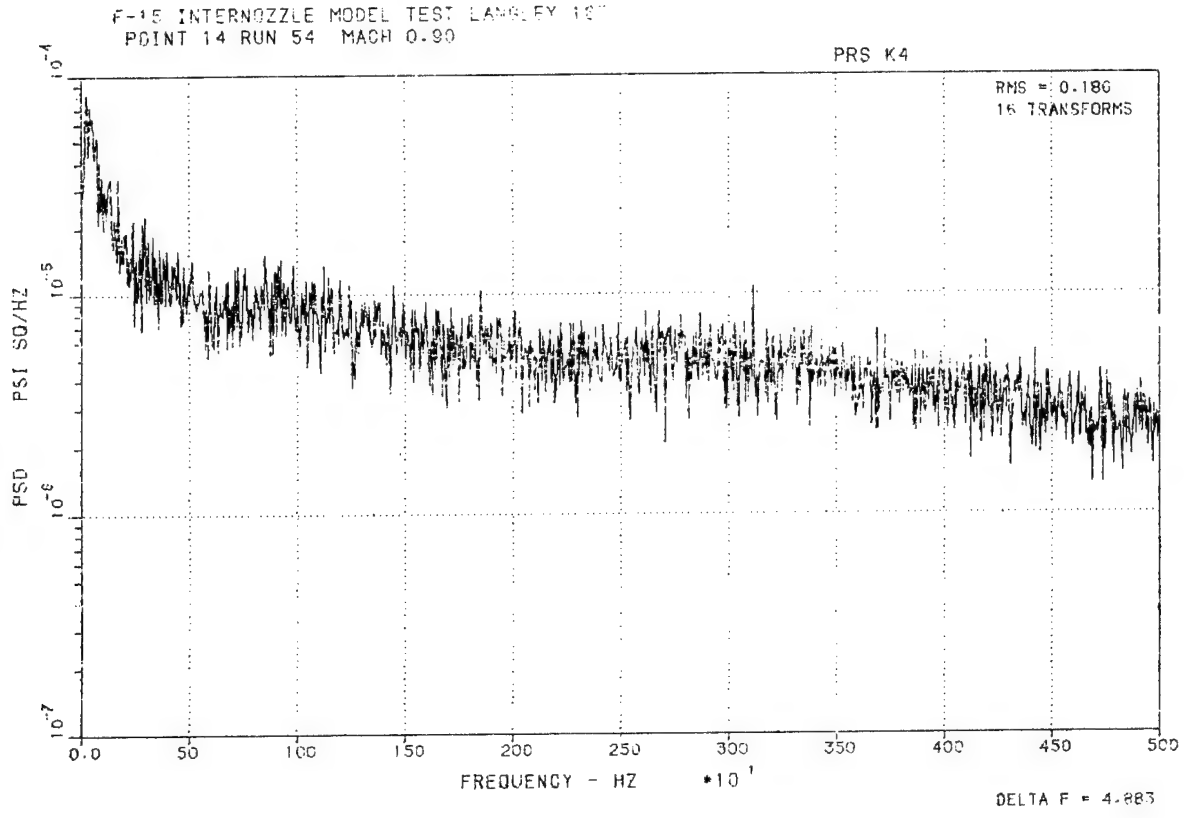

Figure 117. PSDF-with Canards Kulite 4 MACH 0.9 EPR 5.0

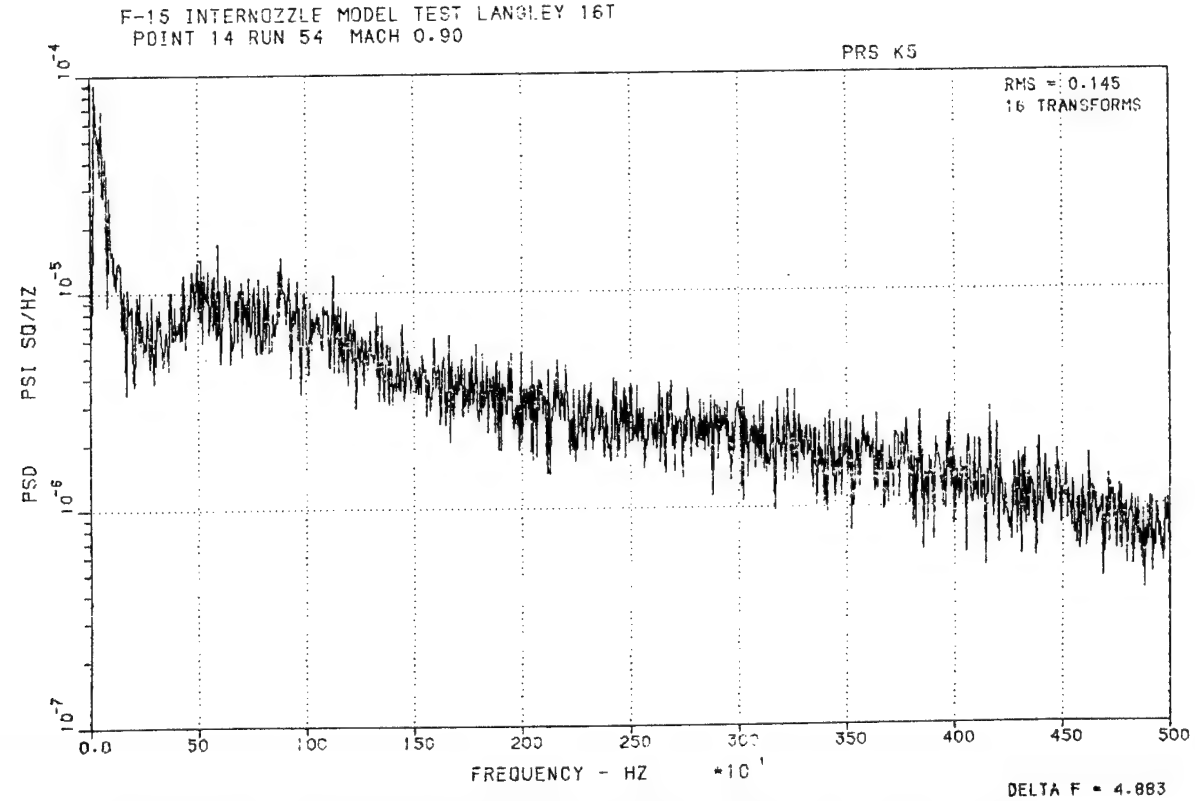

Figure 118. PSDF-with Canards Kulite 5 MACH 0.9 EPR 5.0

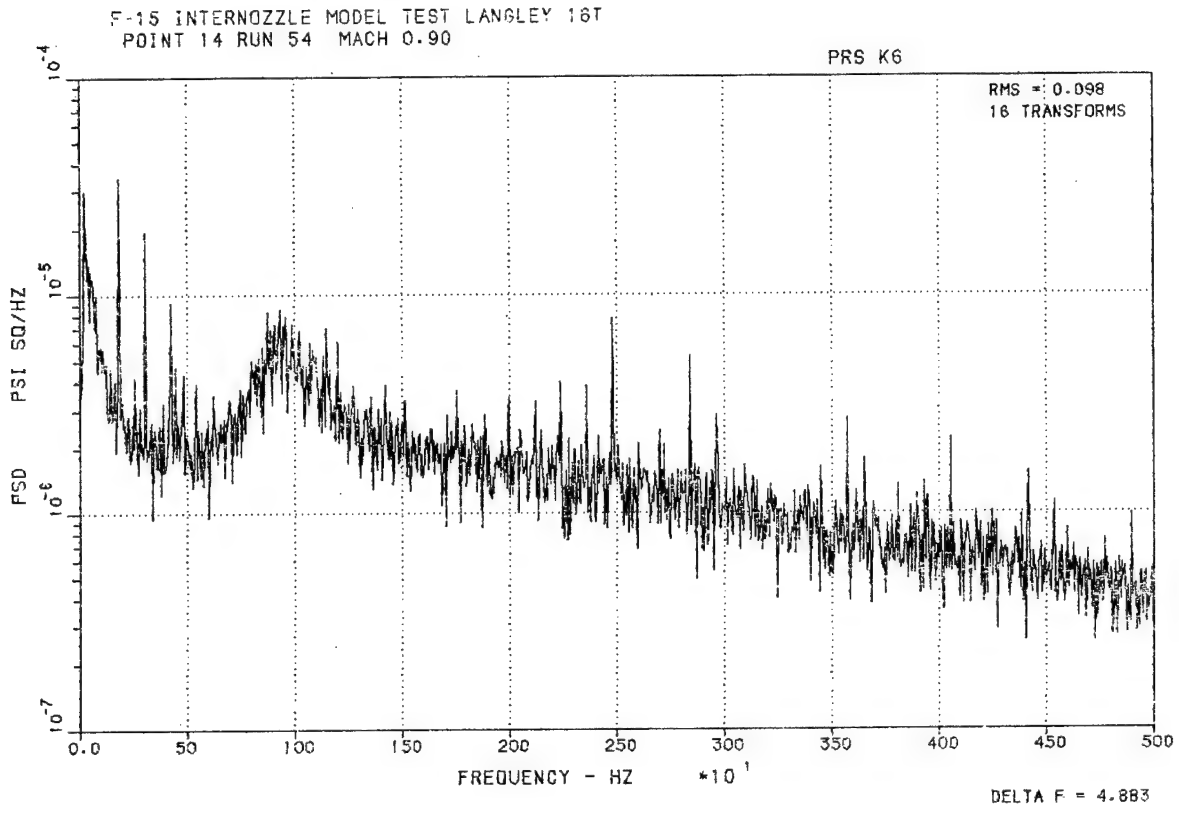

Figure 119. PSDF-with Canards Kulite 7 MACH 0.9 EPR 5.0

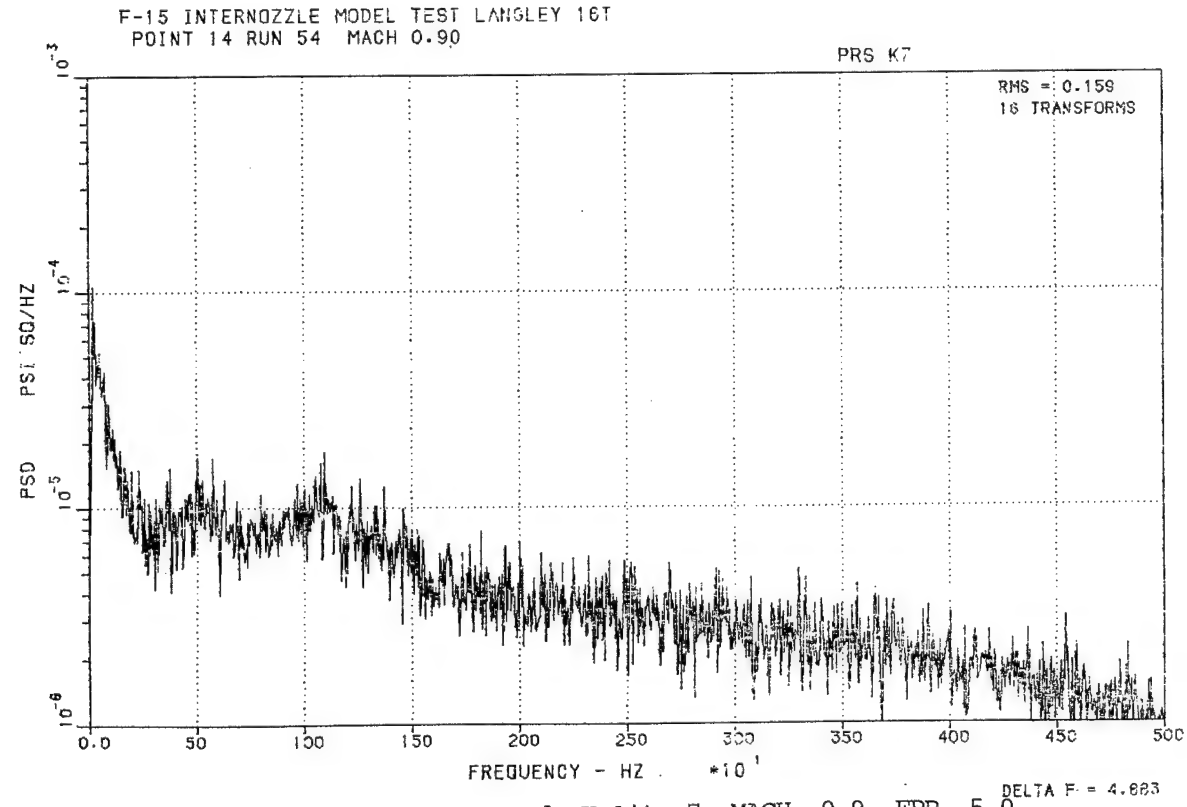

Figure 120. PSDF-with Canards Kulite 7 MACH 0.9 EPR 5.0

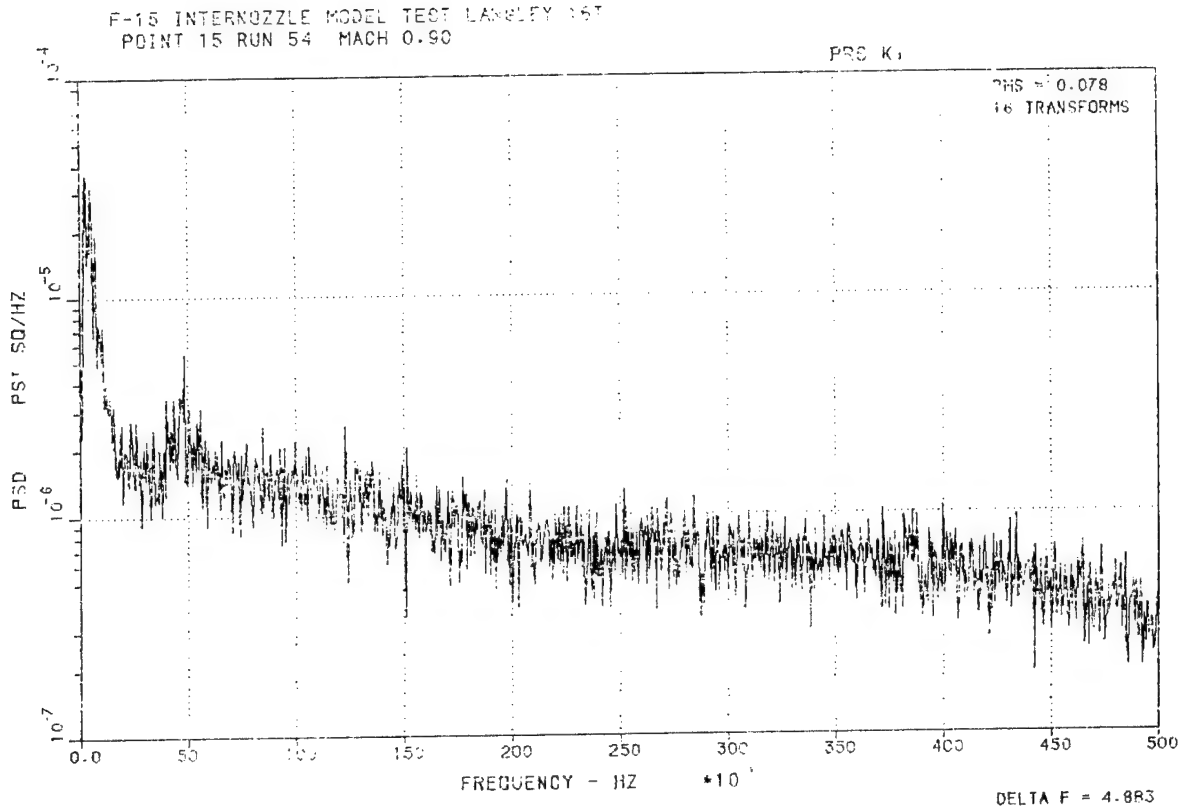

Figure 121. PSDF-with Canards Kulite 1 MACH 0.9 EPR 5.0

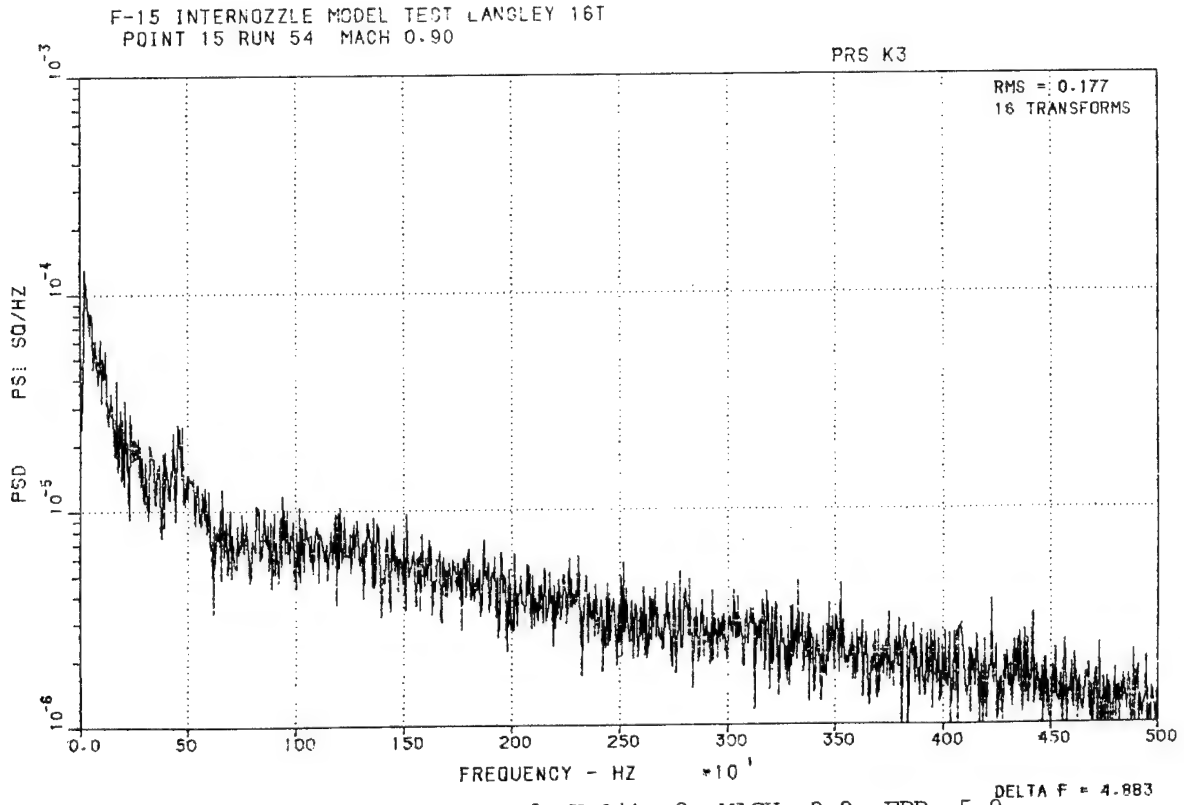

Figure 122. PSDF-with Canards Kulite 3 MACH 0.9 EPR 5.0

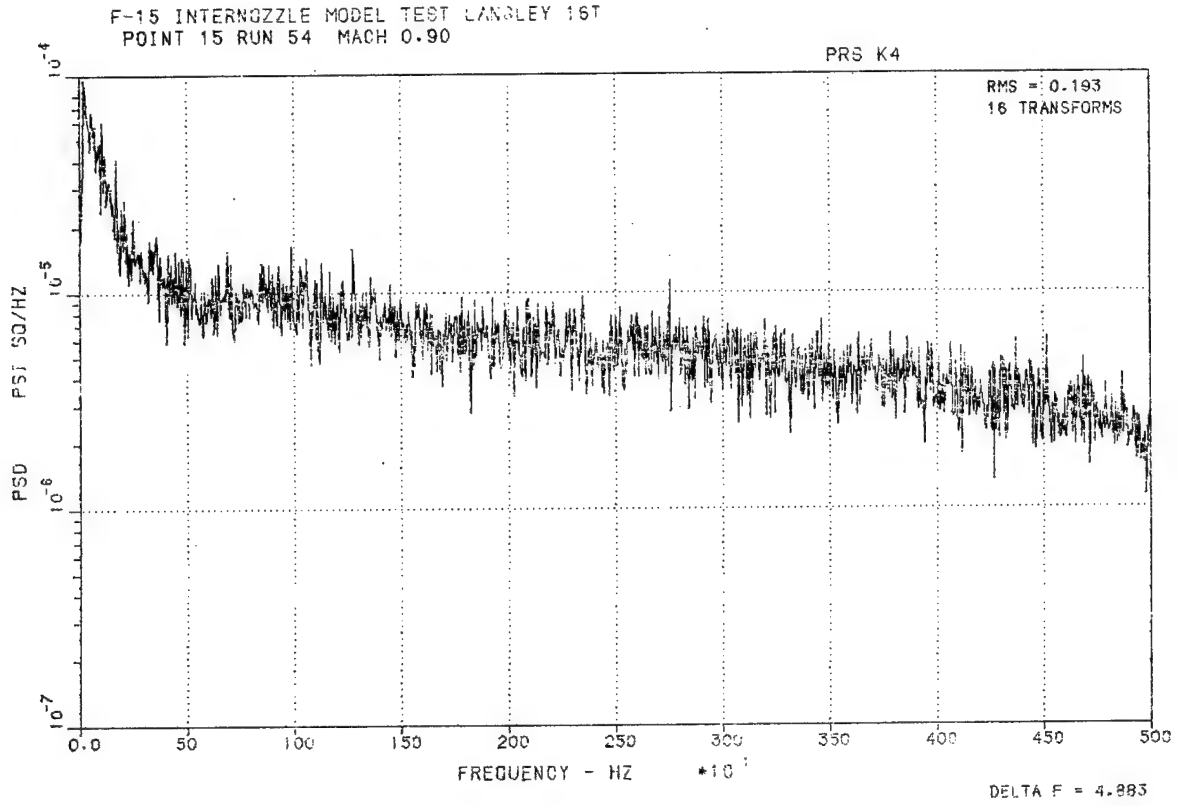

Figure 123. PSDF-with Canards Kulite 4 MACH 0.9 EPR 5.0

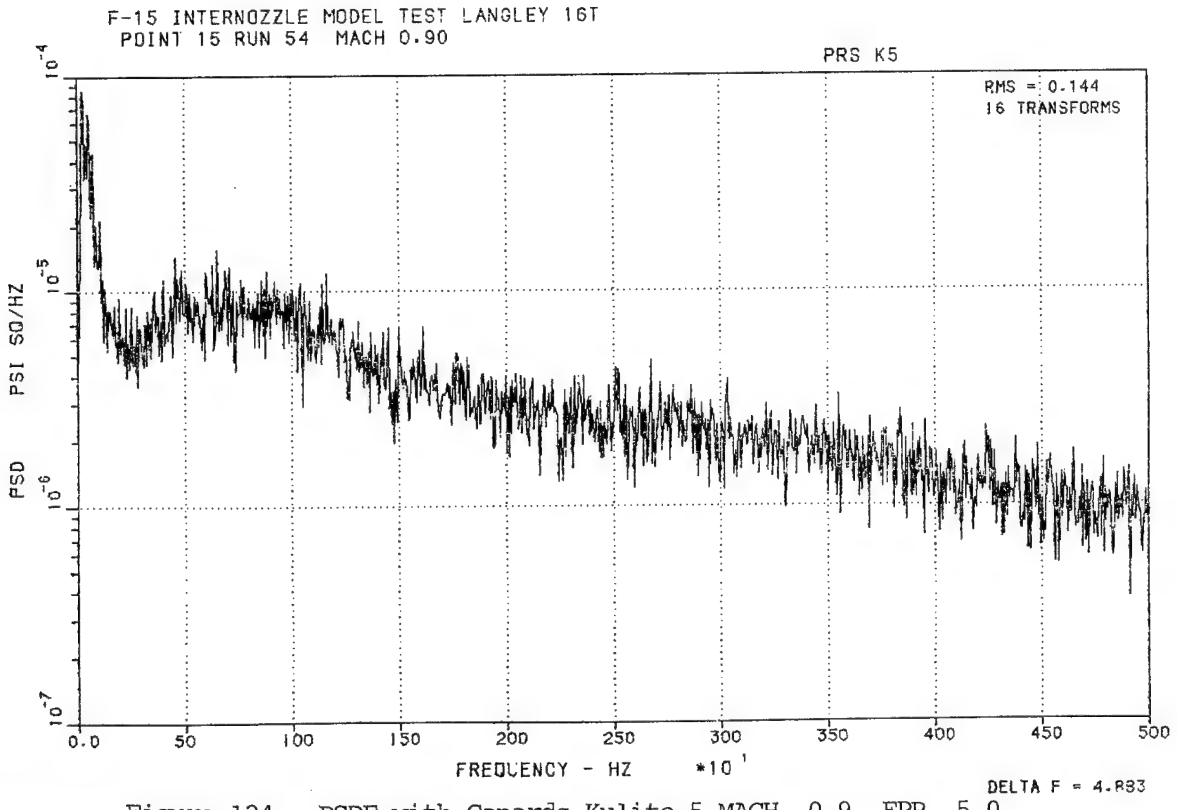

Figure 124. PSDF-with Canards Kulite 5 MACH 0.9 EPR 5.0

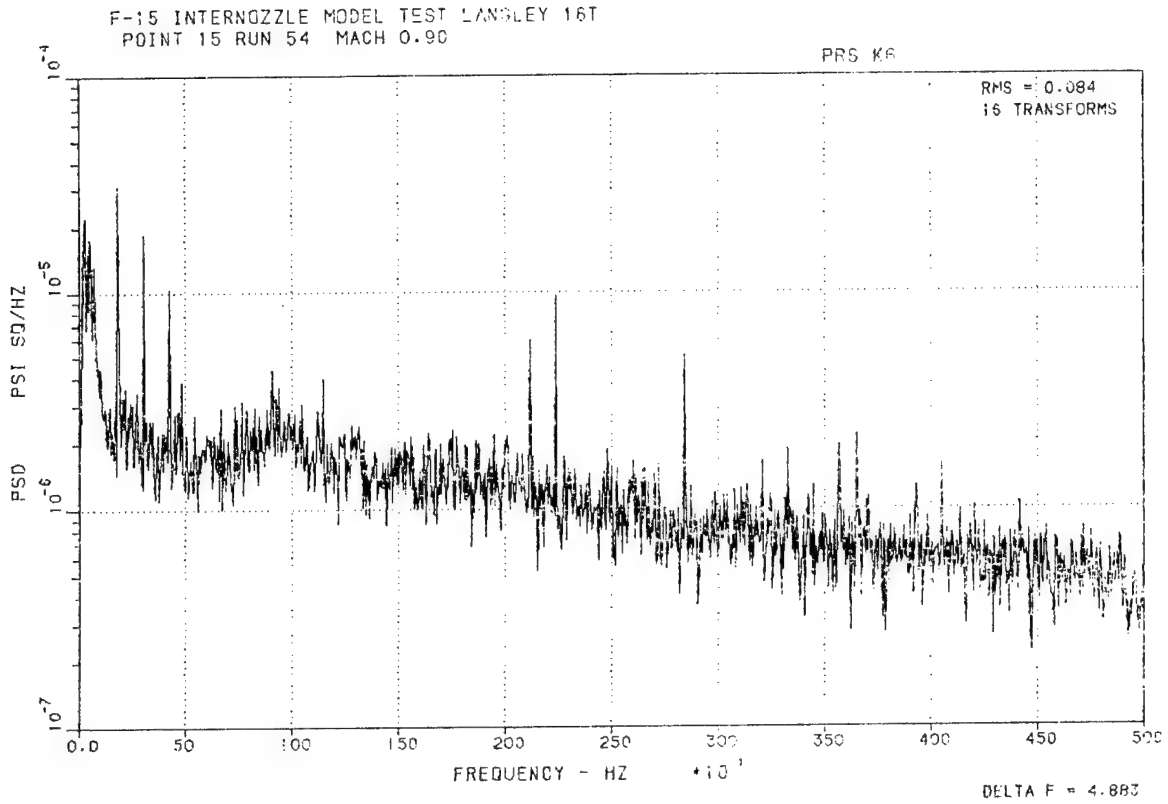

Figure 125. PSDF-with Canards Kulite 6 MACH 0.9 EPR 5.0

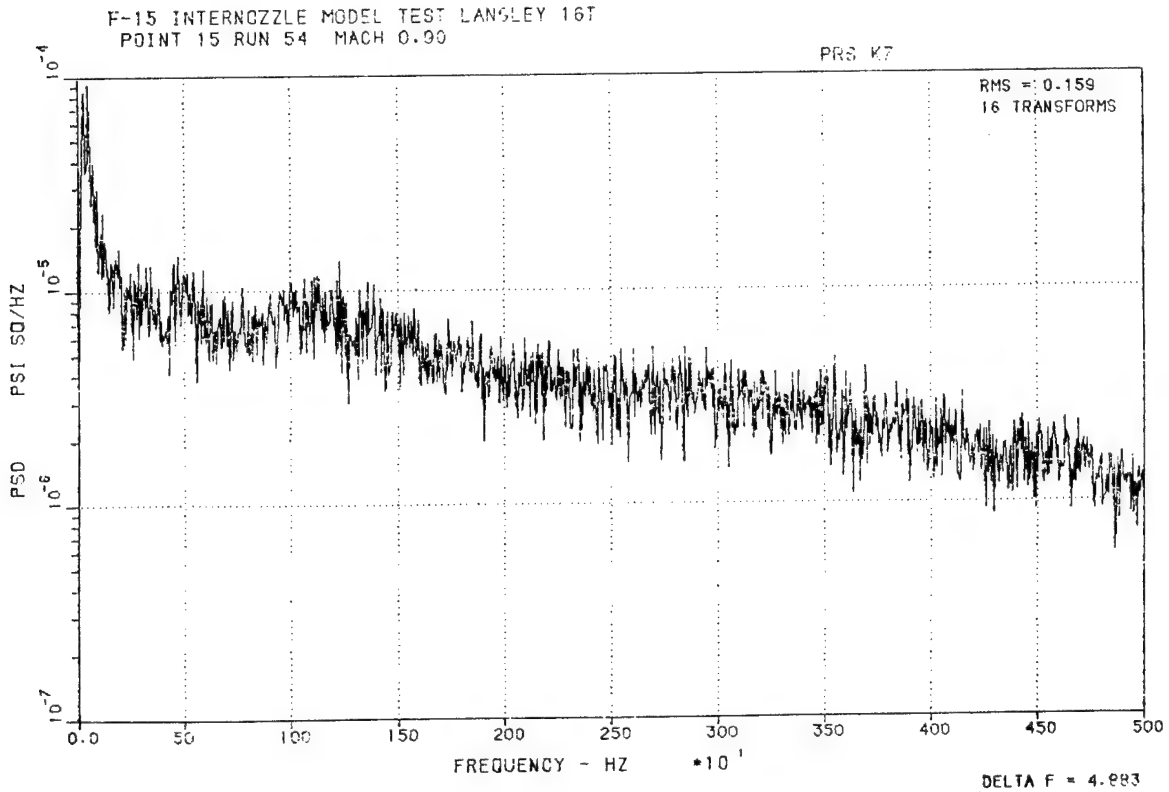

Figure 126. PSDF-with Canards Kulite 7 MACH 0.9 EPR 5.0

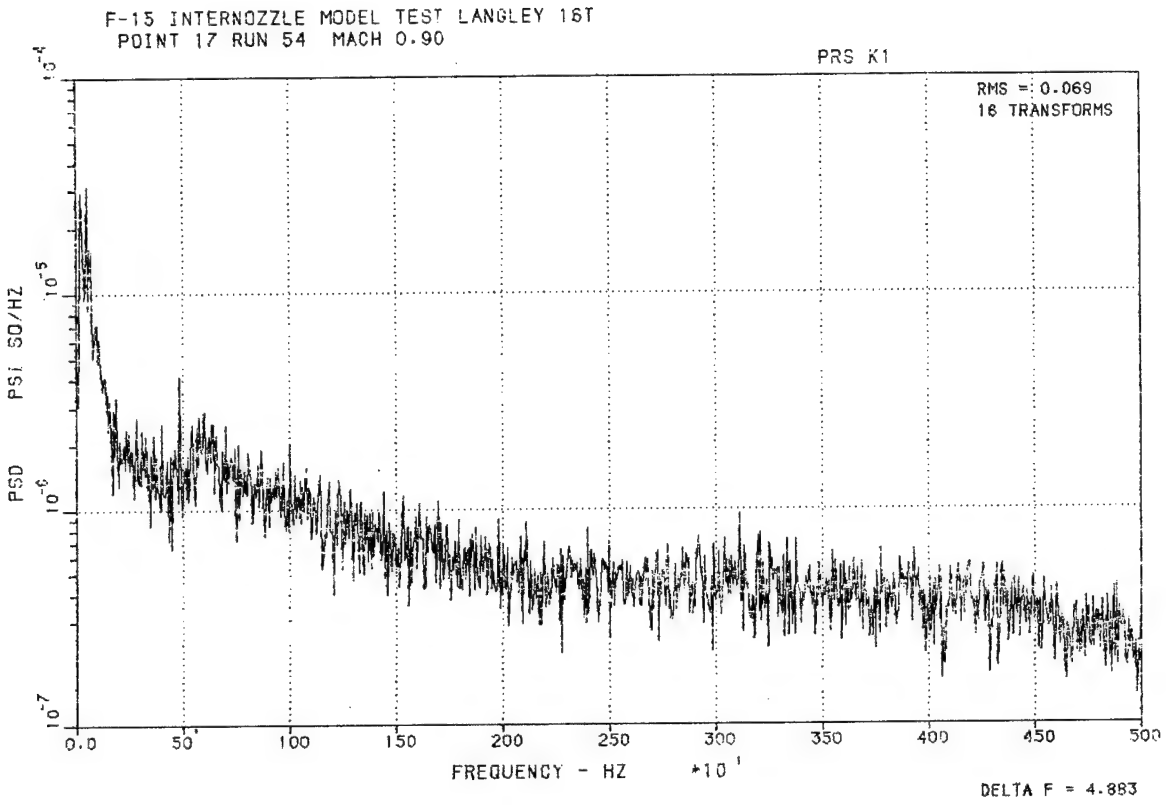

Figure 127. PSDF-with Canards Kulite 1 MACH 0.9 EPR 2.0

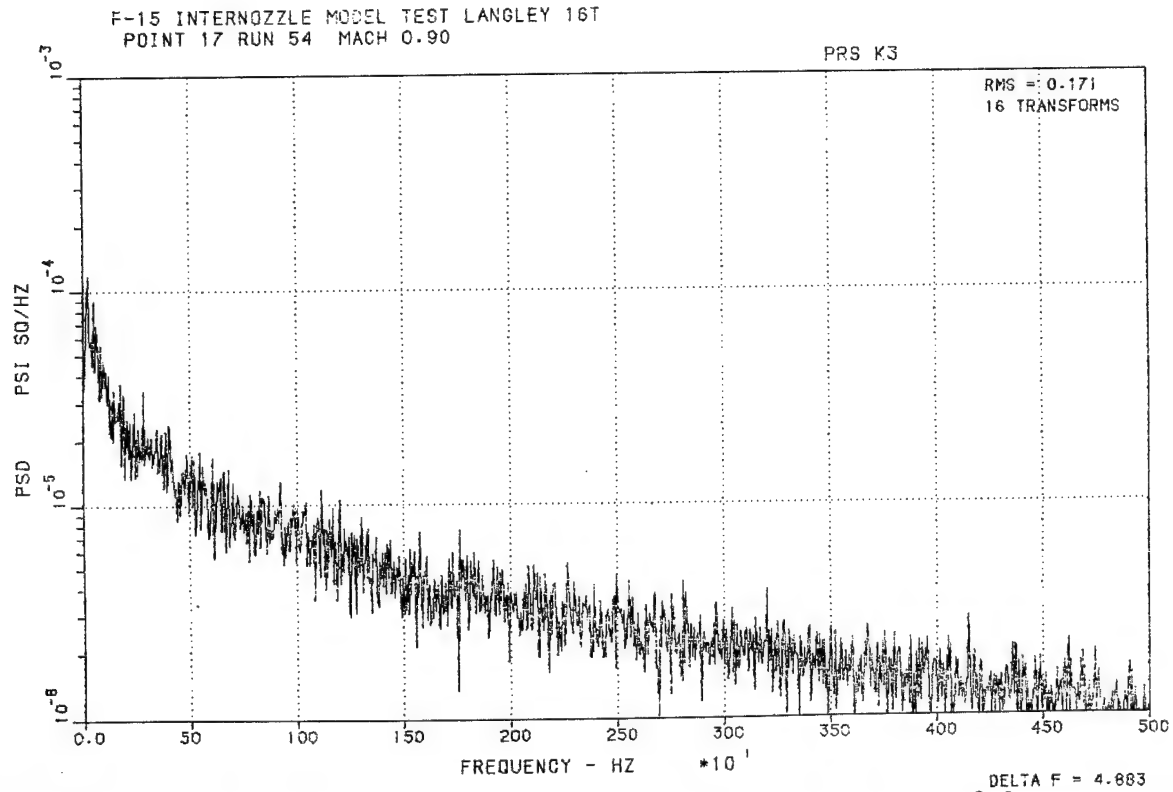

Figure 128. PSDF-with Canards Kulite 3 MACH 0.9 EPR 2.0

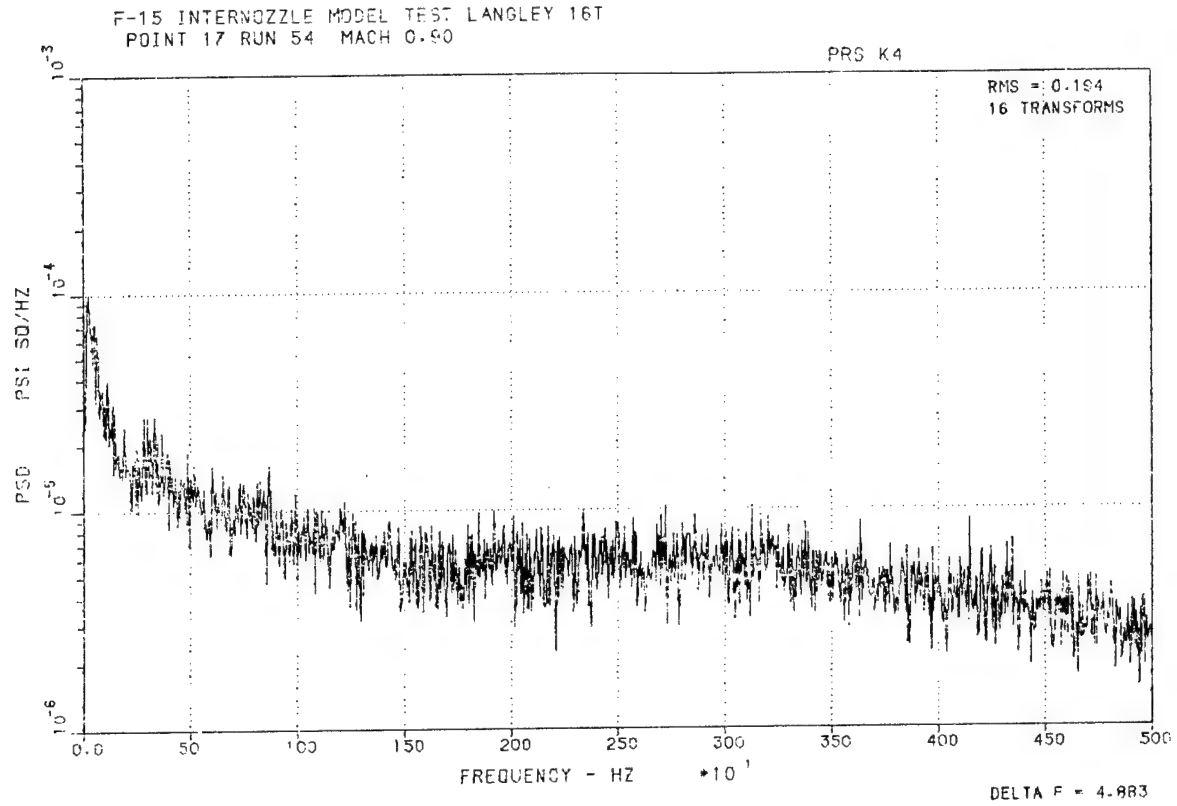

Figure 129. PSDF-with Canards Kulite 4 MACH 0.9 EPR 2.0

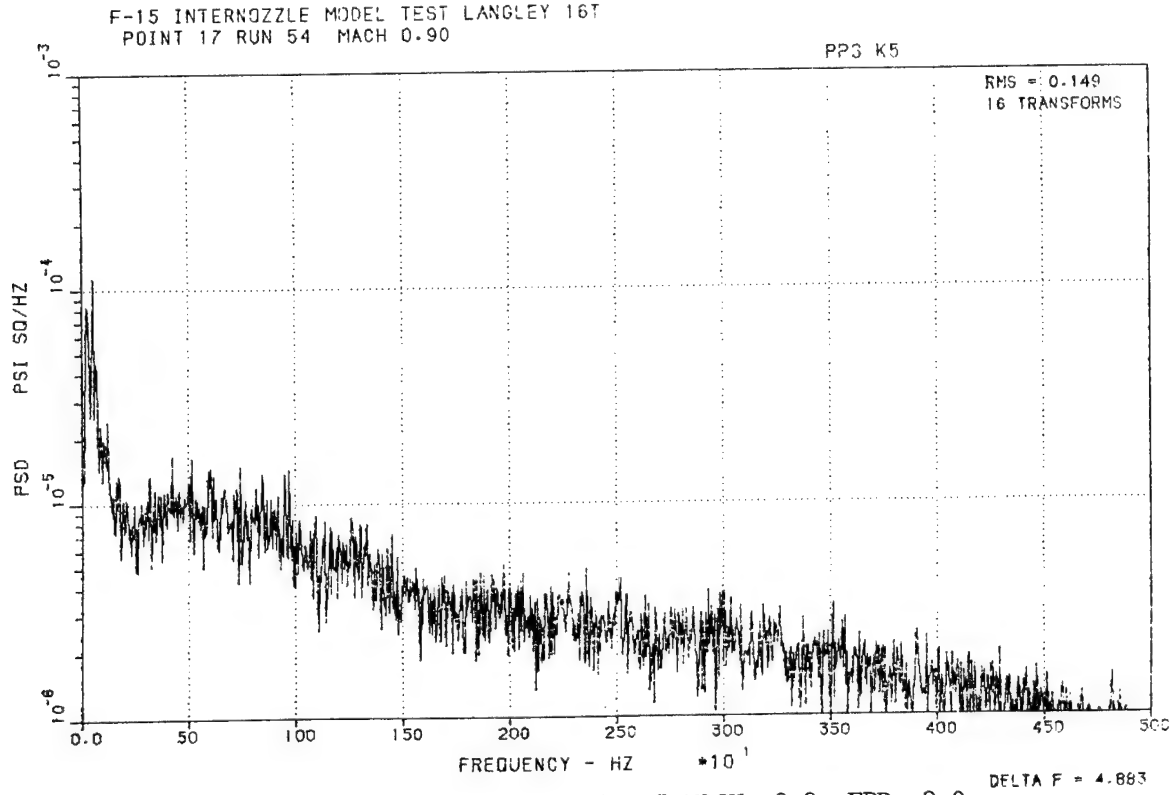

Figure 130. PSDF-with Canards Kulite 5 MACH 0.9 EPR 2.0

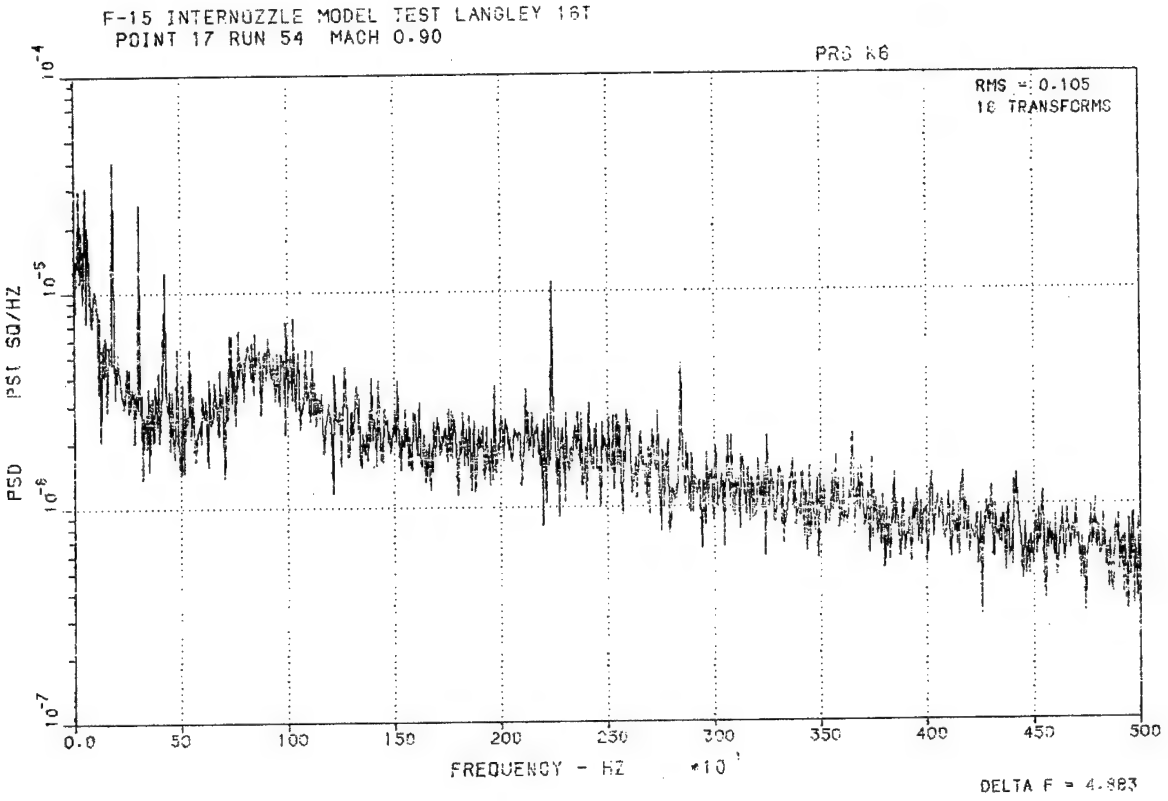

Figure 131. PSDF-with Canards Kulite 6 MACH 0.9 EPR 2.0

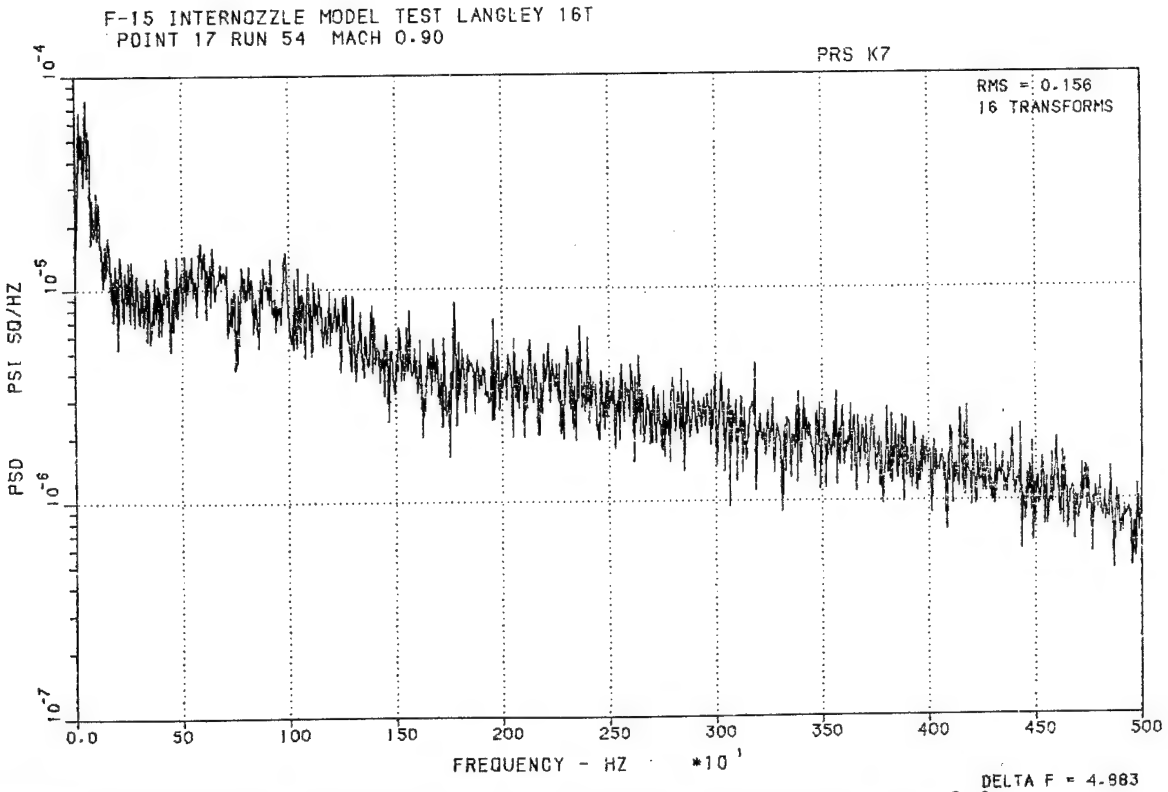

Figure 132. PSDF-with Canards Kulite 7 MACH 0.9 EPR 2.0

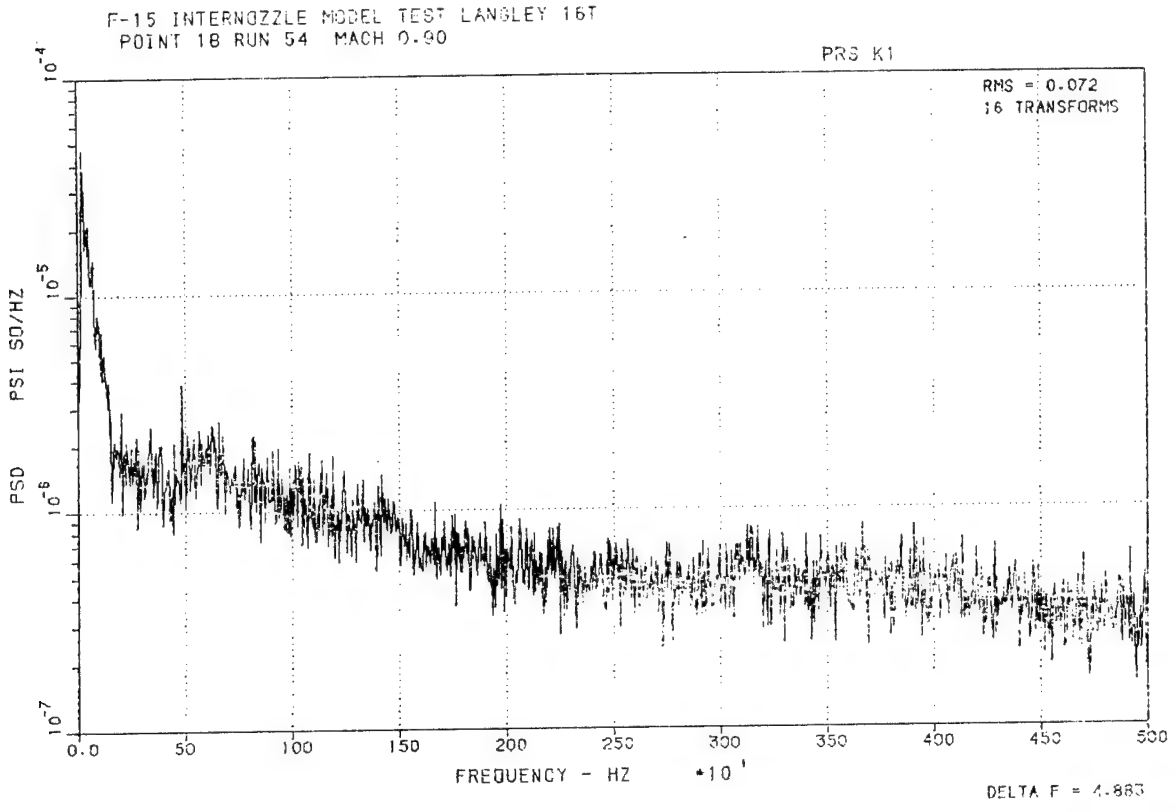

Figure 133. PSDF-with Canards Kulite 1 MACH 0.9 EPR 2.0

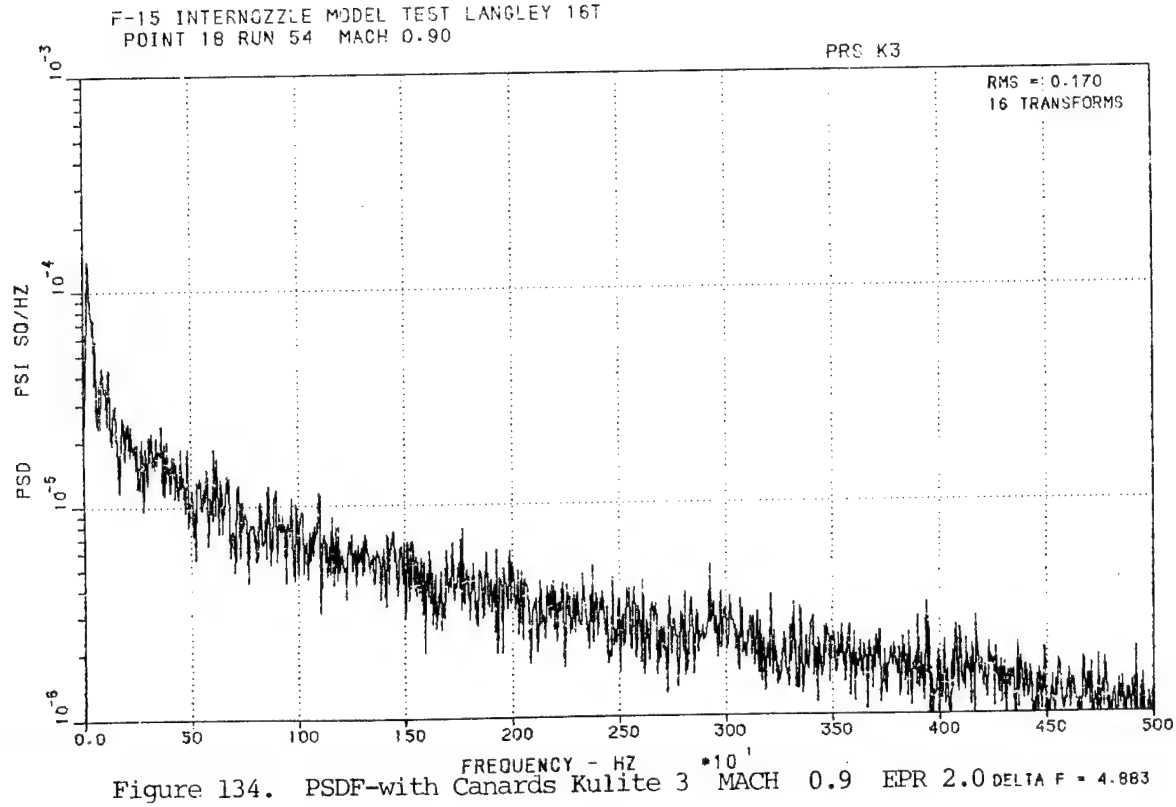

Figure 134. PSDF-with Canards Kulite 3 MACH 0.9 EPR 2.0

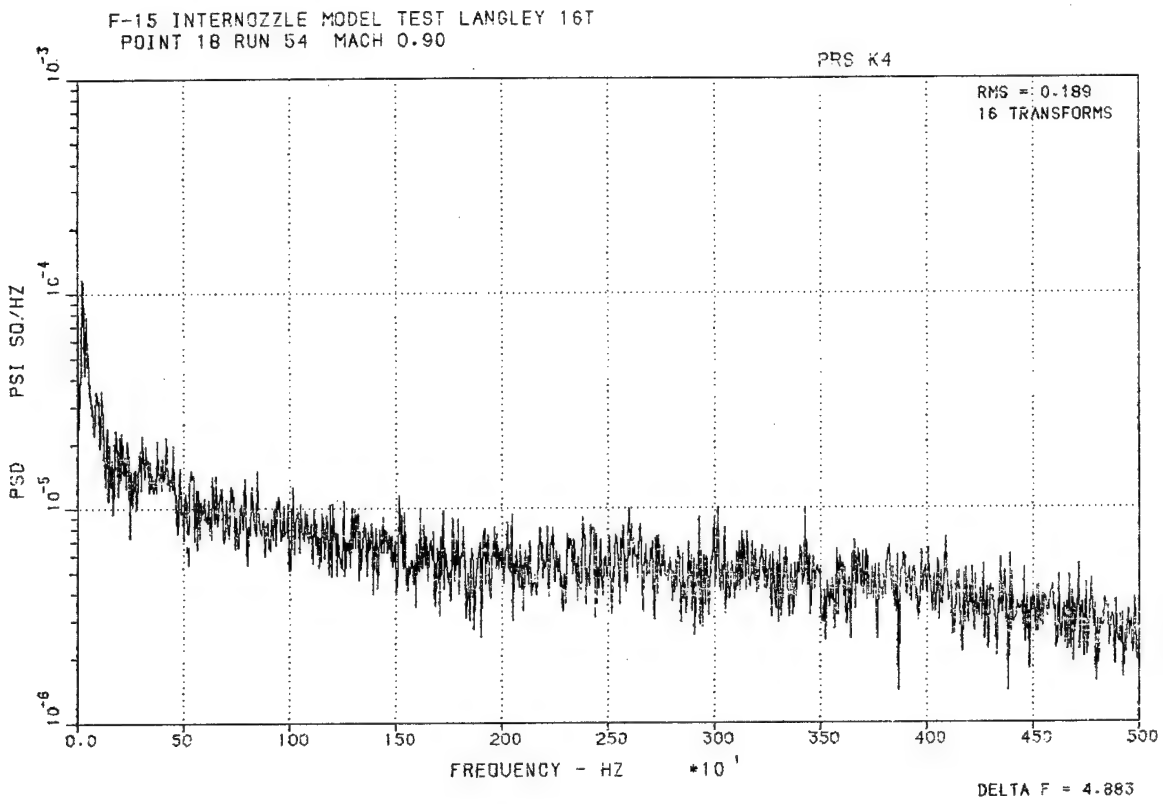

Figure 135. PSDF-with Canards Kulite 4 MACH 0.9 EPR 2.0

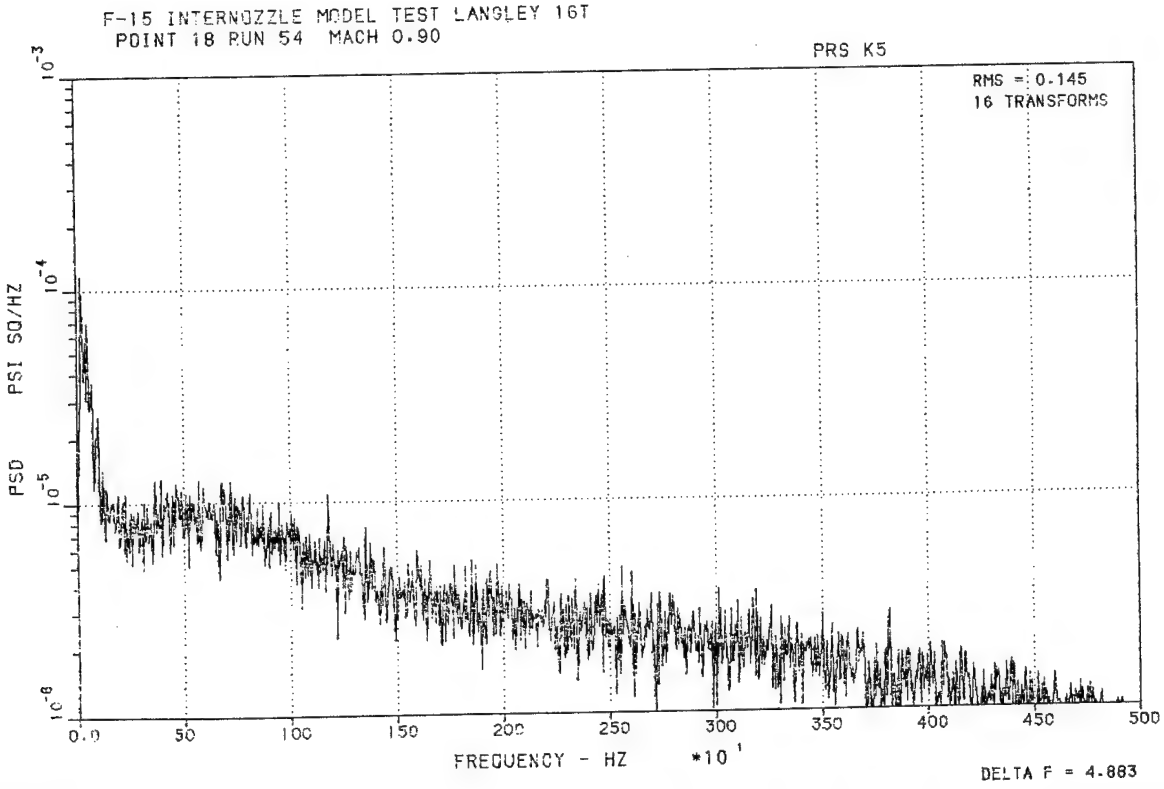

Figure 136. PSDF-with Canards Kulite 5 MACH 0.9 EPR 2.0

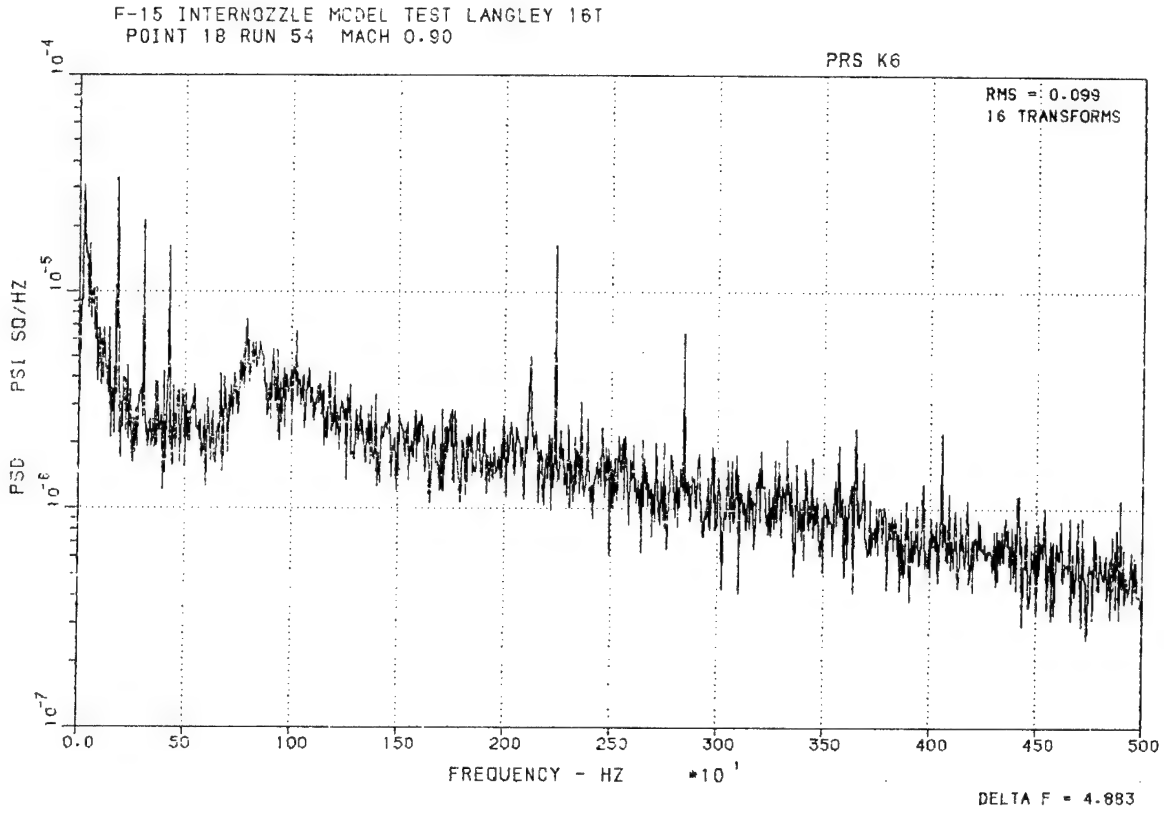

Figure 137. PSDF-with Canards Kulite 4 MACH 0.9 EPR 3.5

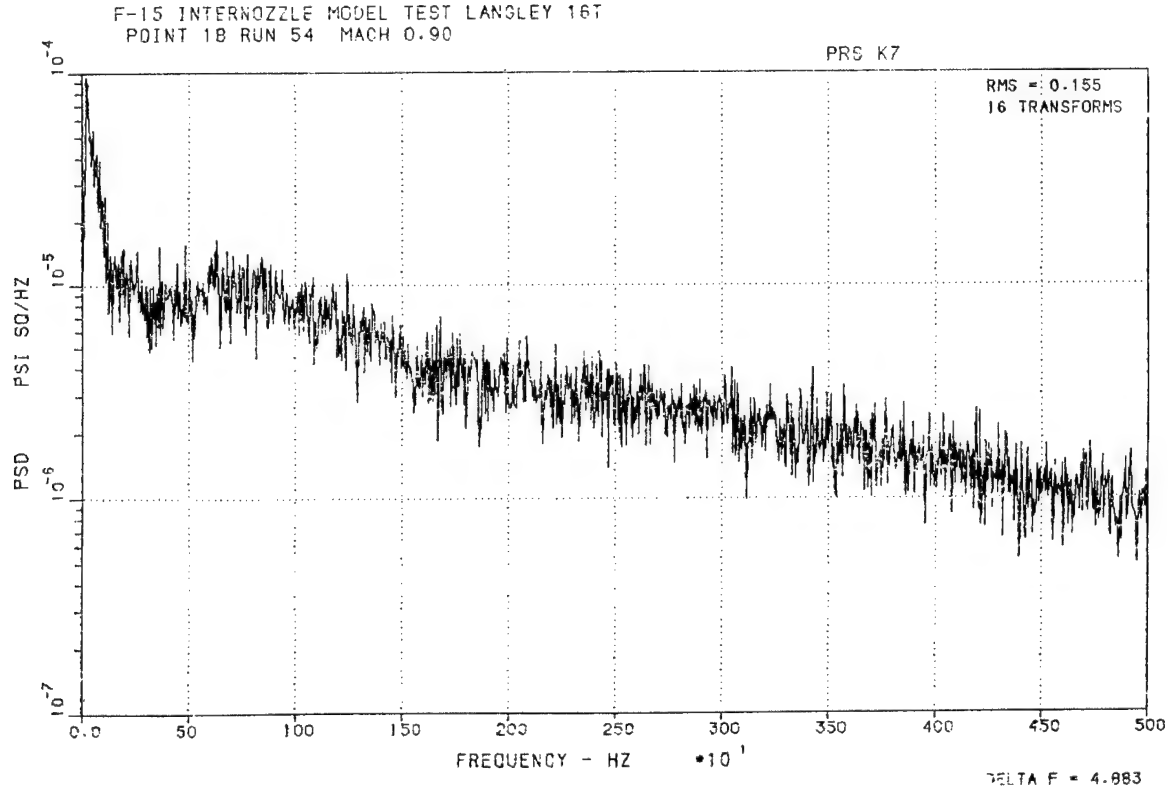

Figure 138. PSDF-with Canards Kulite 5 MACH 0.9 EPR 3.5

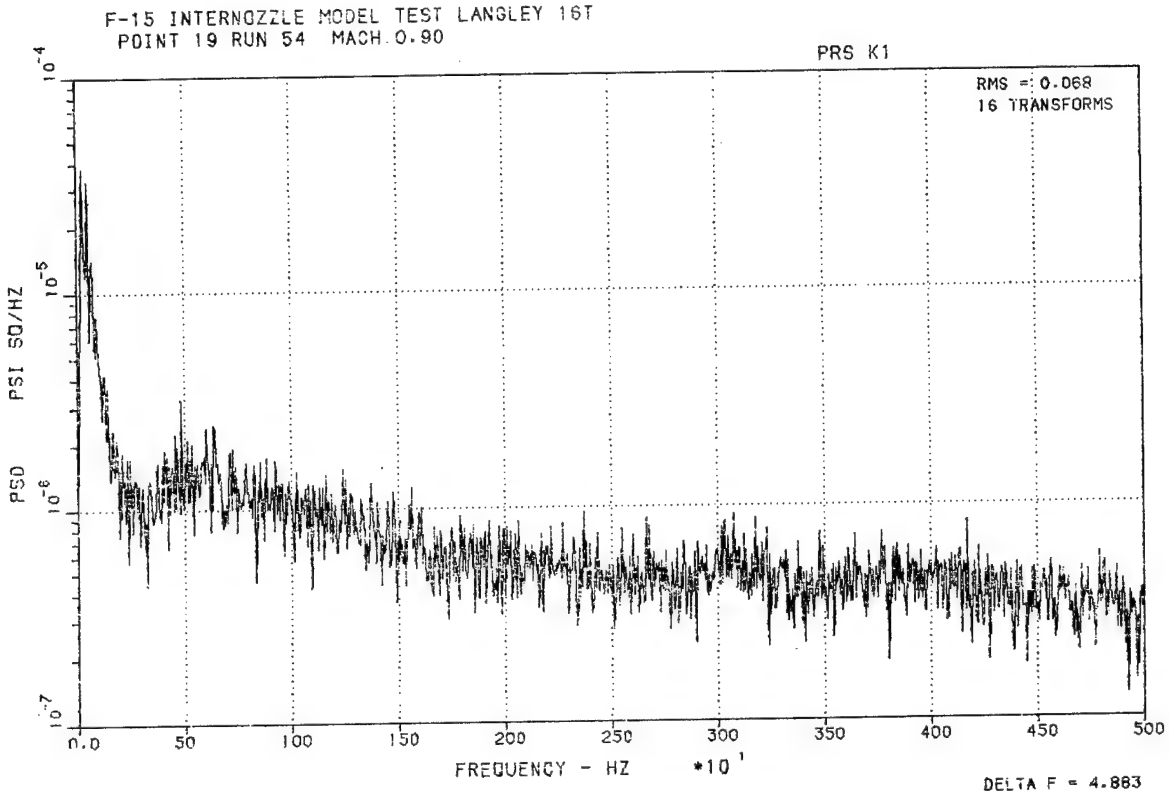

Figure 139. PSDF-with Canards Kulite 1, MACH 0.9 EPR 5.0

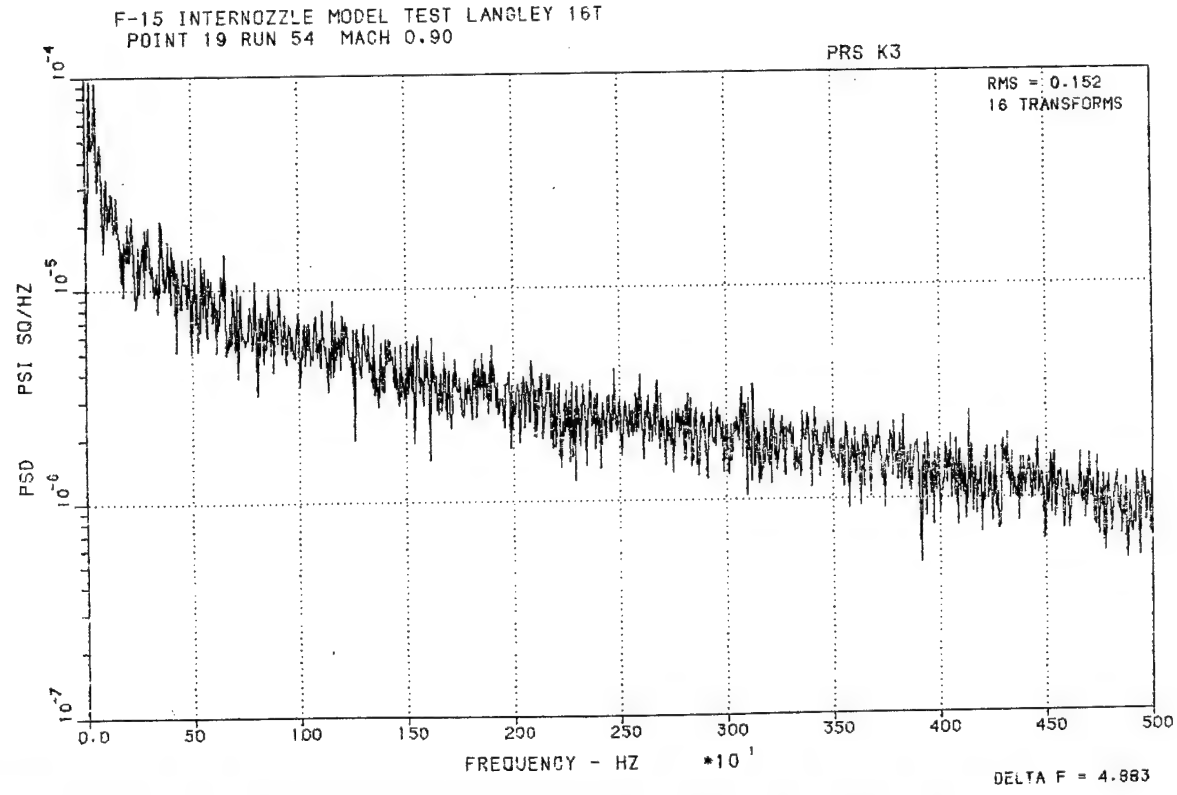

Figure 140. PSDF-with Canards Kulite 3 MACH 0.9 EPR 5.0

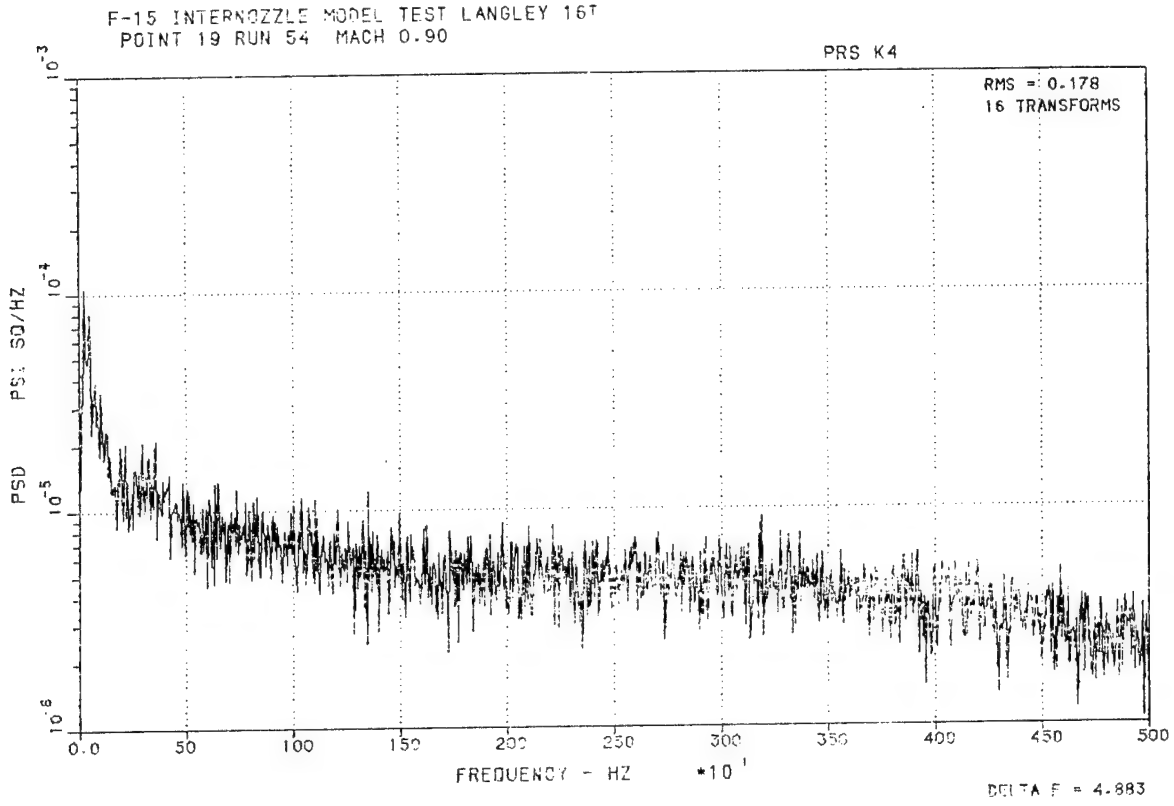

Figure 141. PSDF-with Canards Kulite 4 MACH 0.9 EPR 5.0

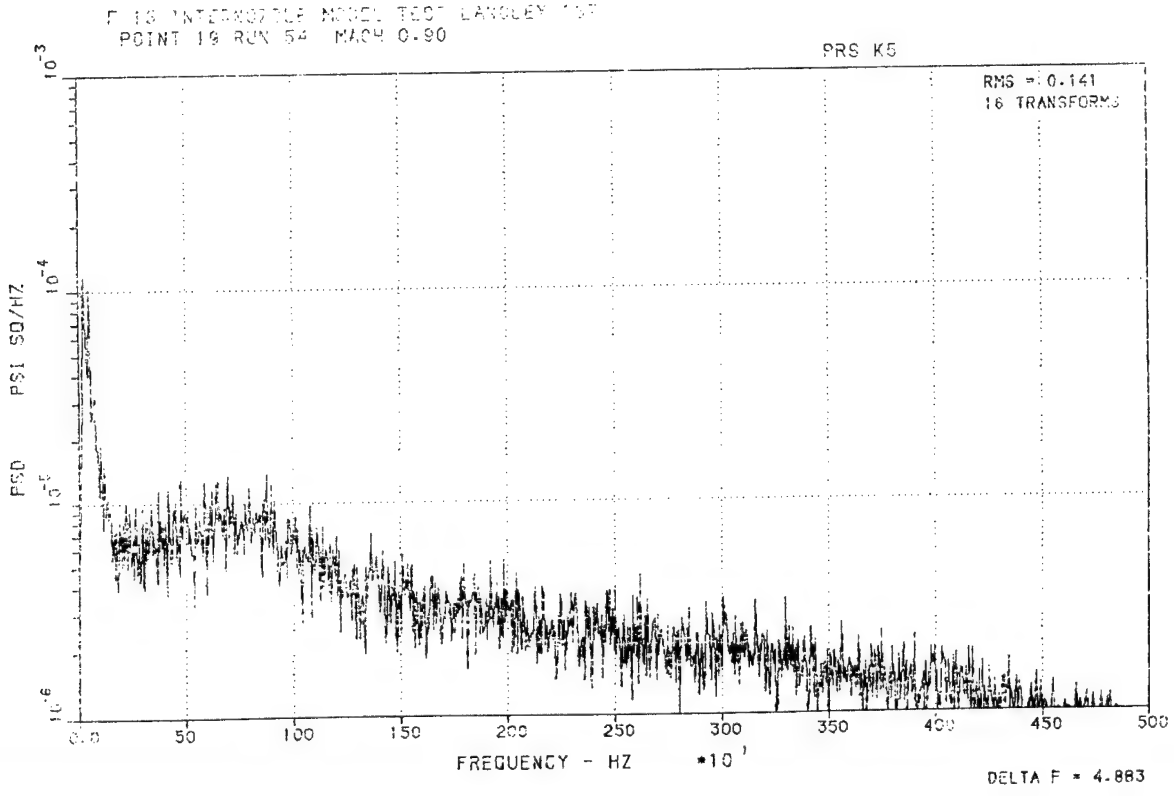

Figure 142. PSDF-with Canards Kulite 5 MACH 0.9 EPR 5.0

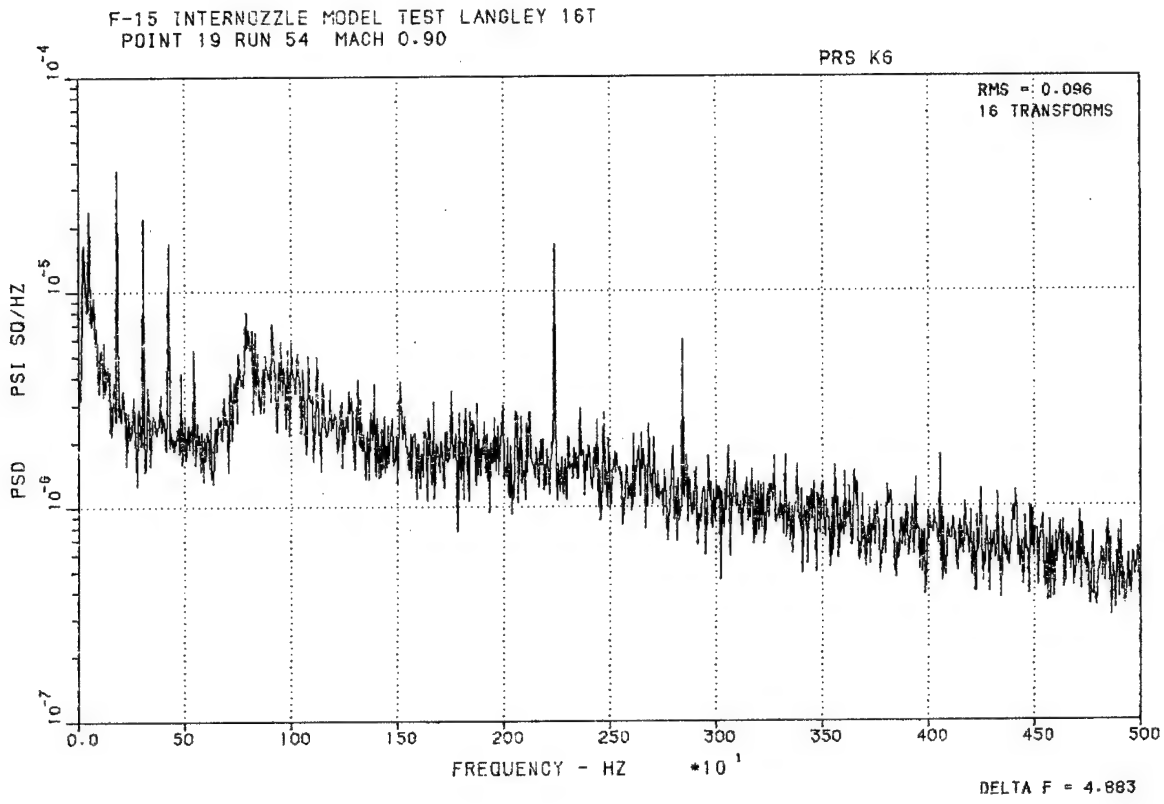

Figure 143. PSDF-with Canards Kulite 6 MACH 0.9 EPR 5.0

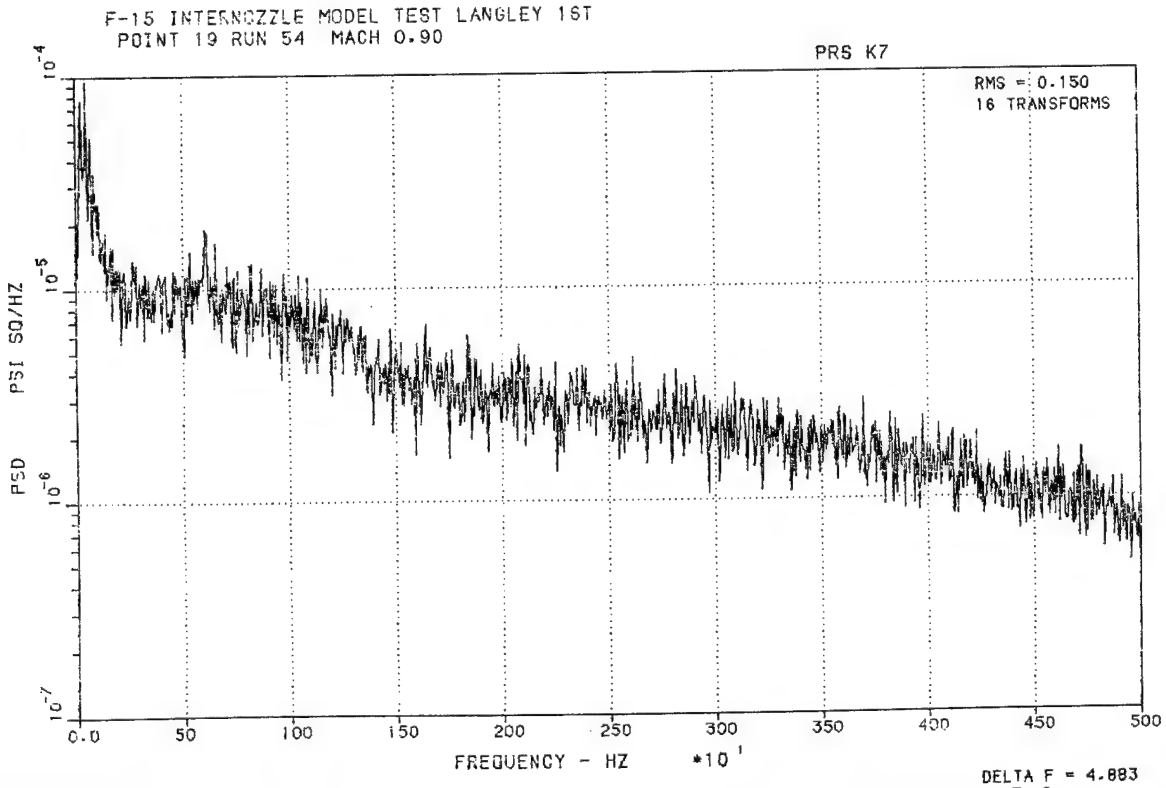

Figure 144. PSDF-with Canards Kulite 7 MACH 0.9 EPR 5.0

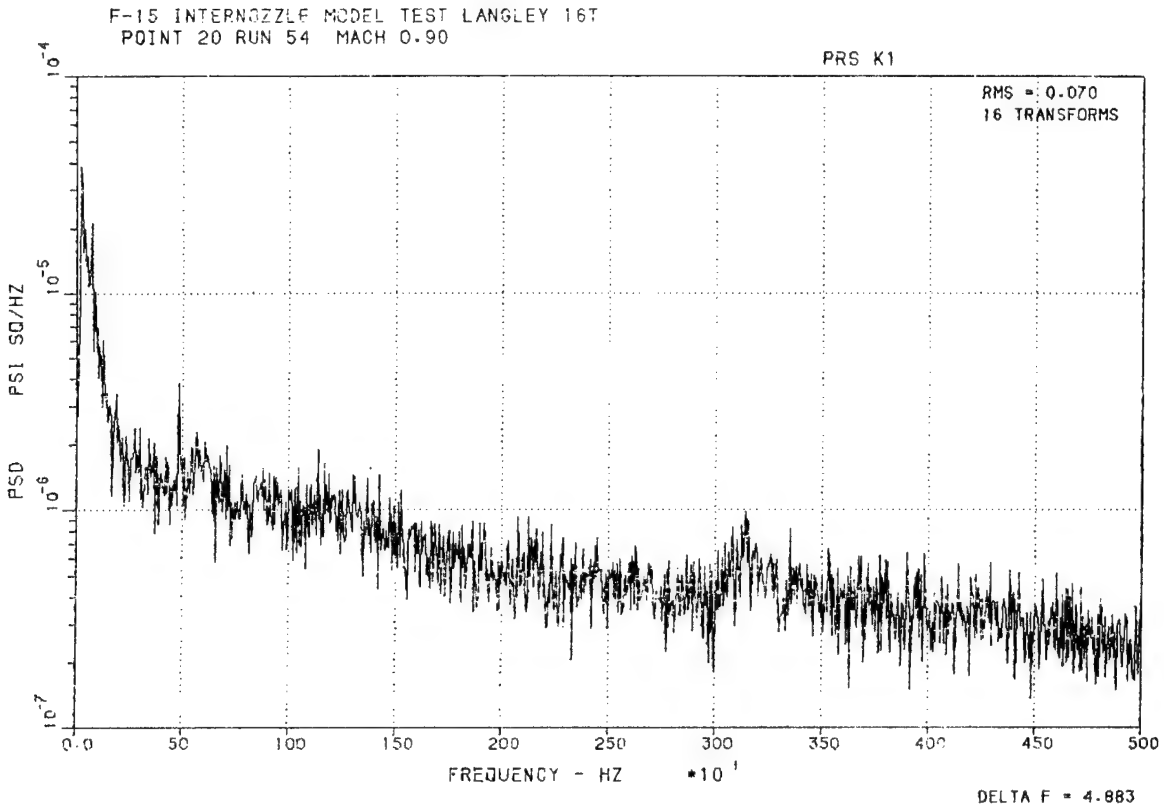

Figure 145. PSDF-with Canards Kulite 1 MACH 0.9 EPR 1.0

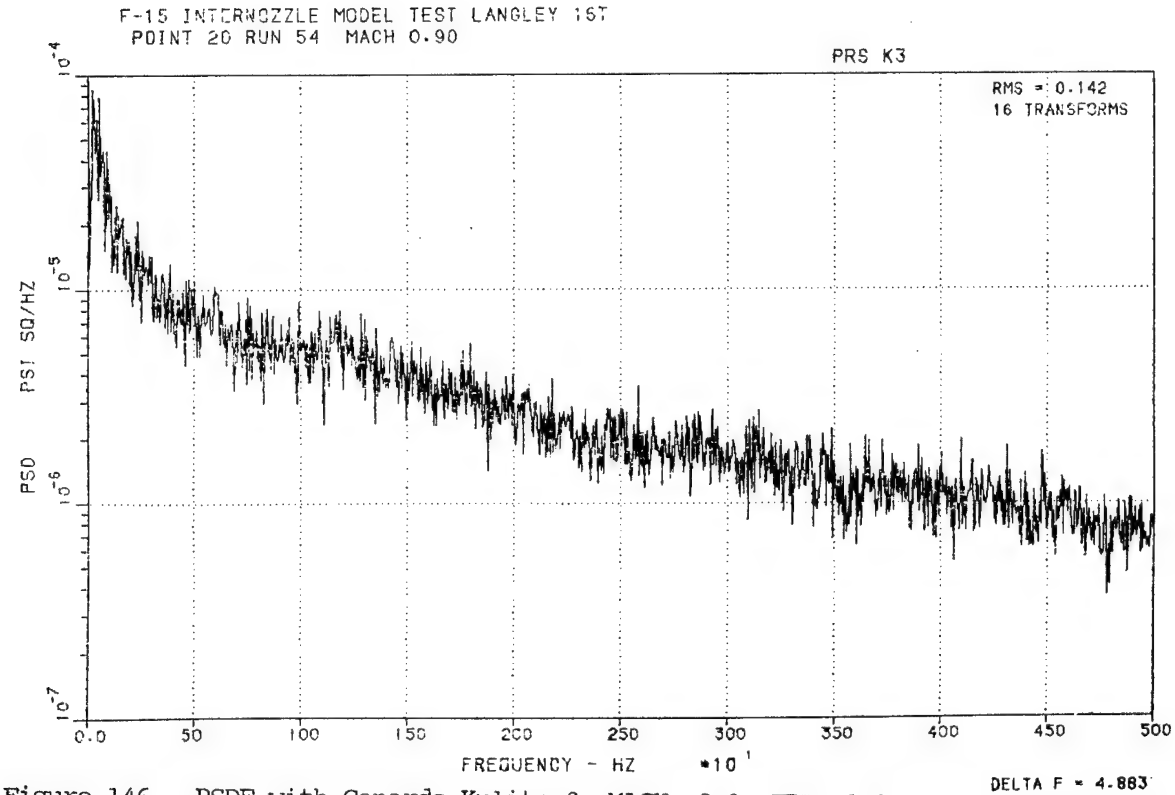

Figure 146. PSDF-with Canards Kulite 3 MACH 0.9 EPR 1.0

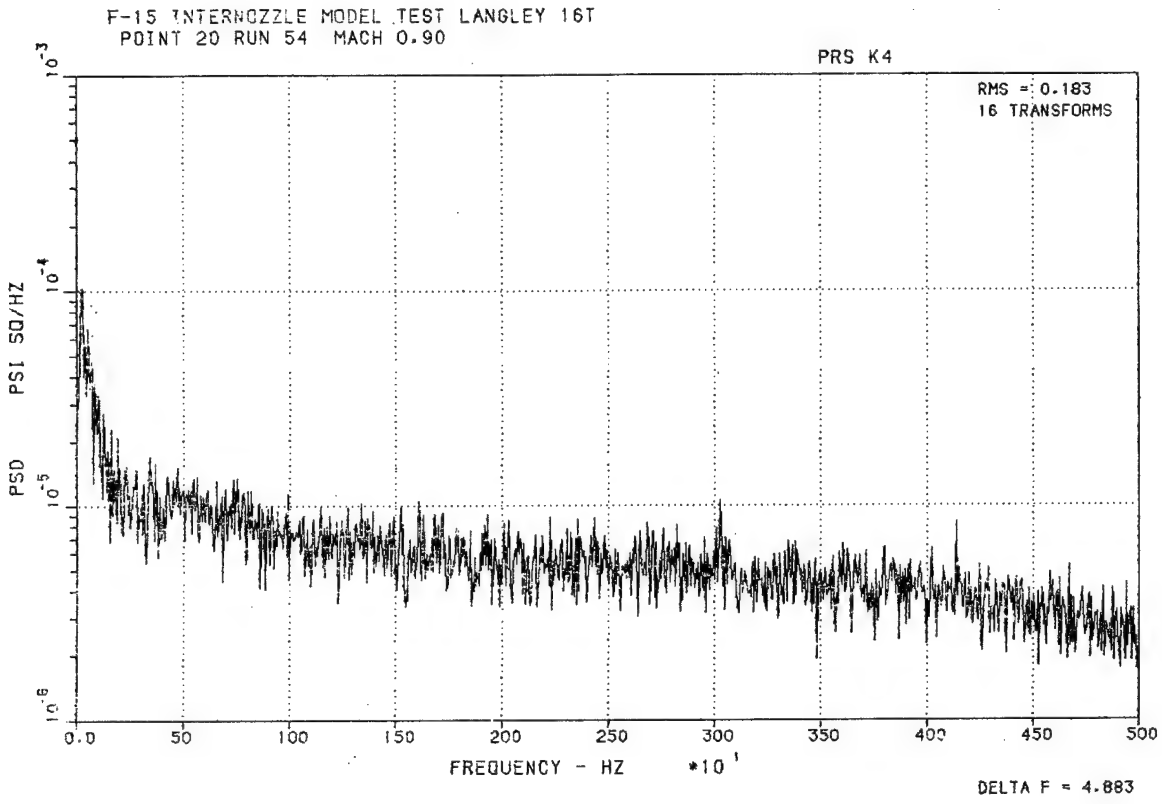

Figure 147. PSDF-with Canards Kulite 4 MACH 0.9 EPR 1.0

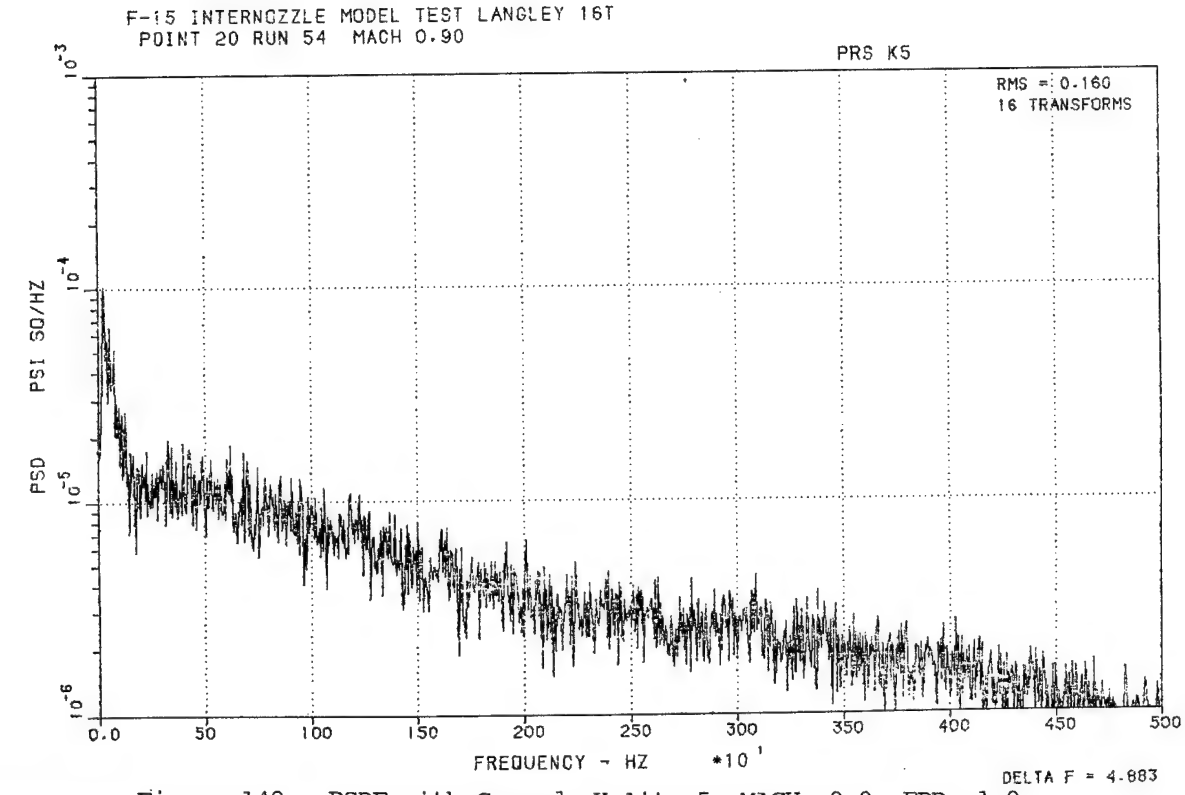

Figure 148. PSDF-with Canards Kulite 5 MACH 0.9 EPR 1.0

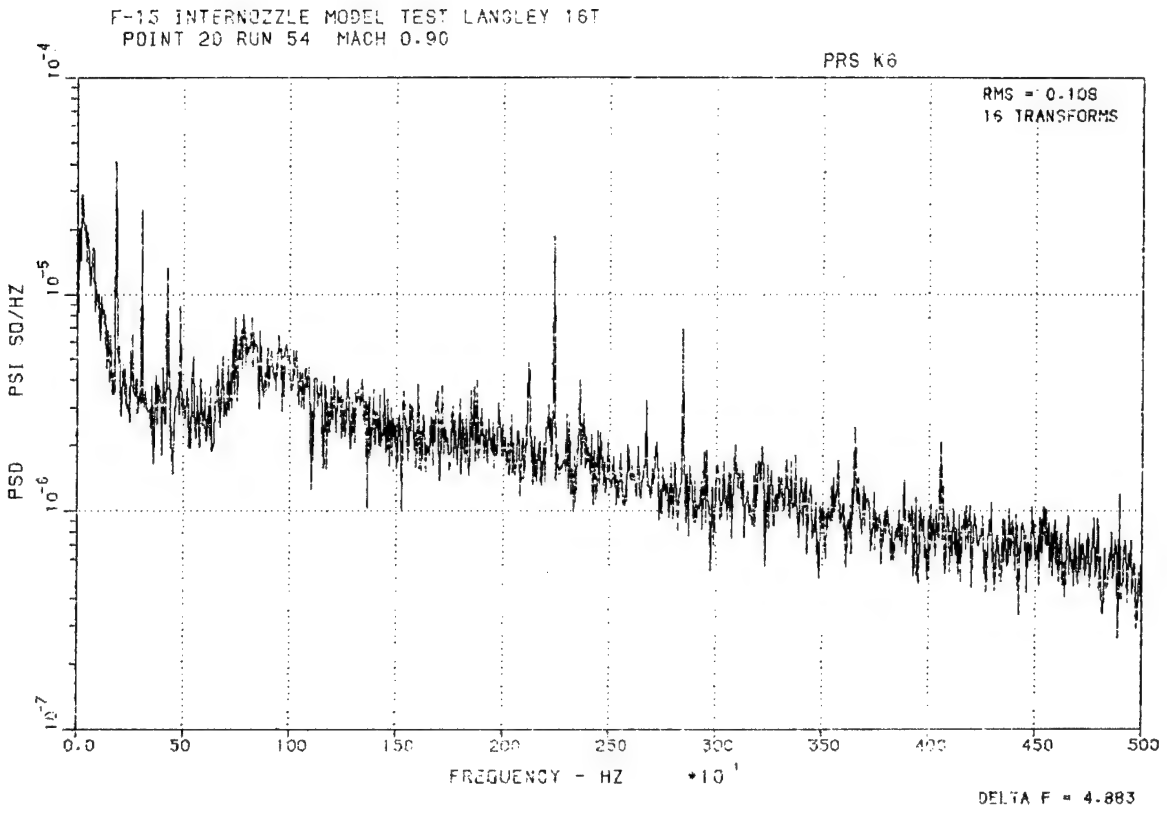

Figure 149. PSDF-with Canards Kulite 6 MACH 0.9 EPR 1.0

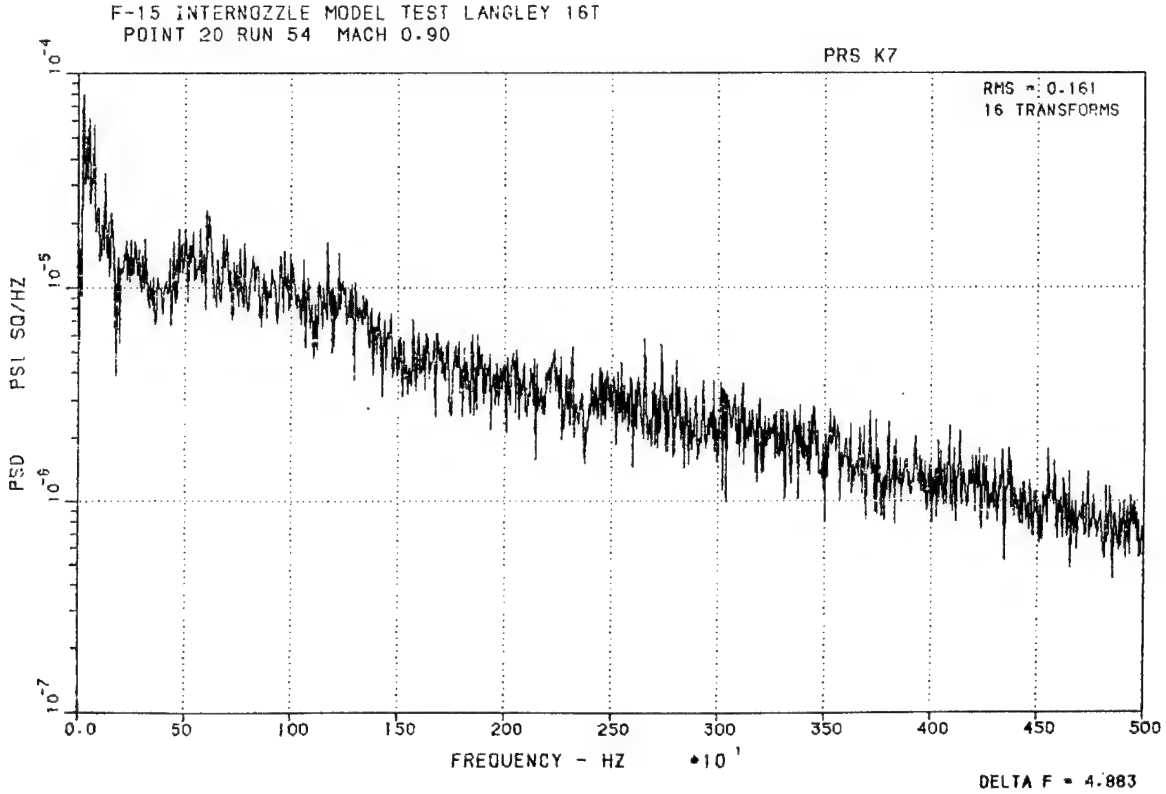

Figure 150. PSDF-with Canards Kulite 7 MACH 0.9 EPR 1.0

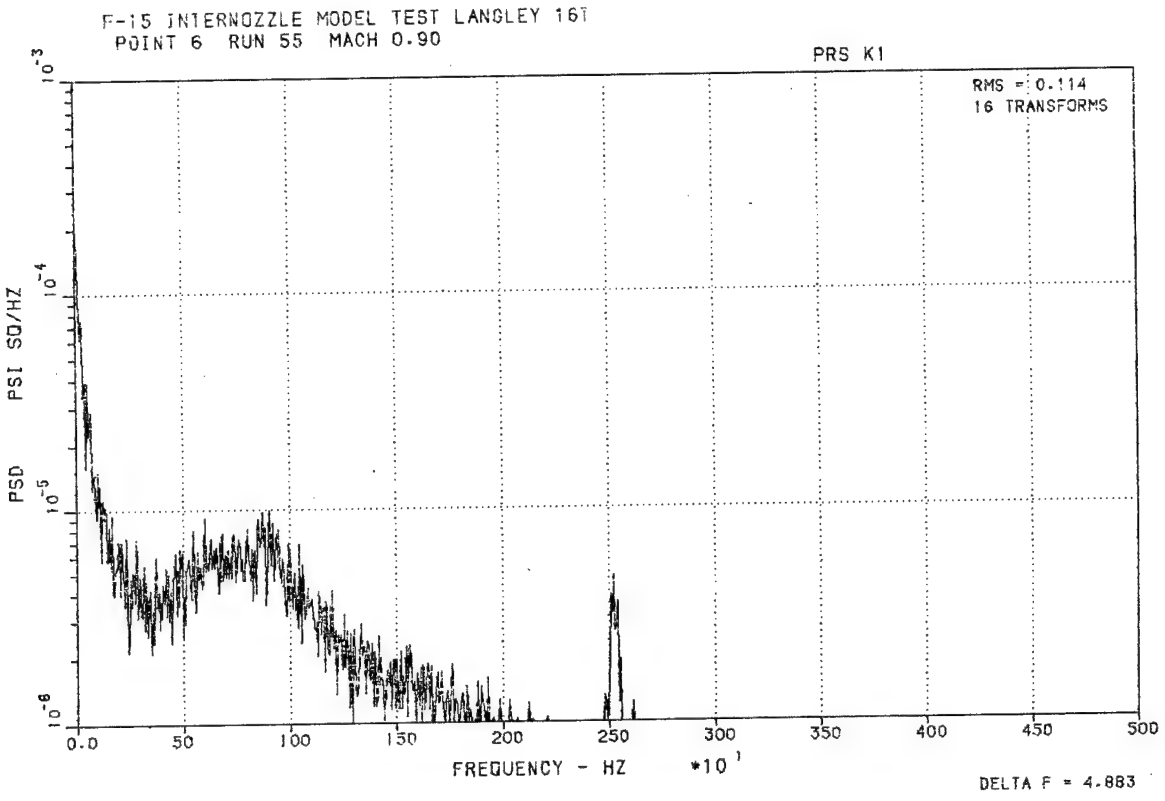

Figure 151. PSDF-No Vertical Tails Kulite 1 MACH 0.9 EPR 3.5

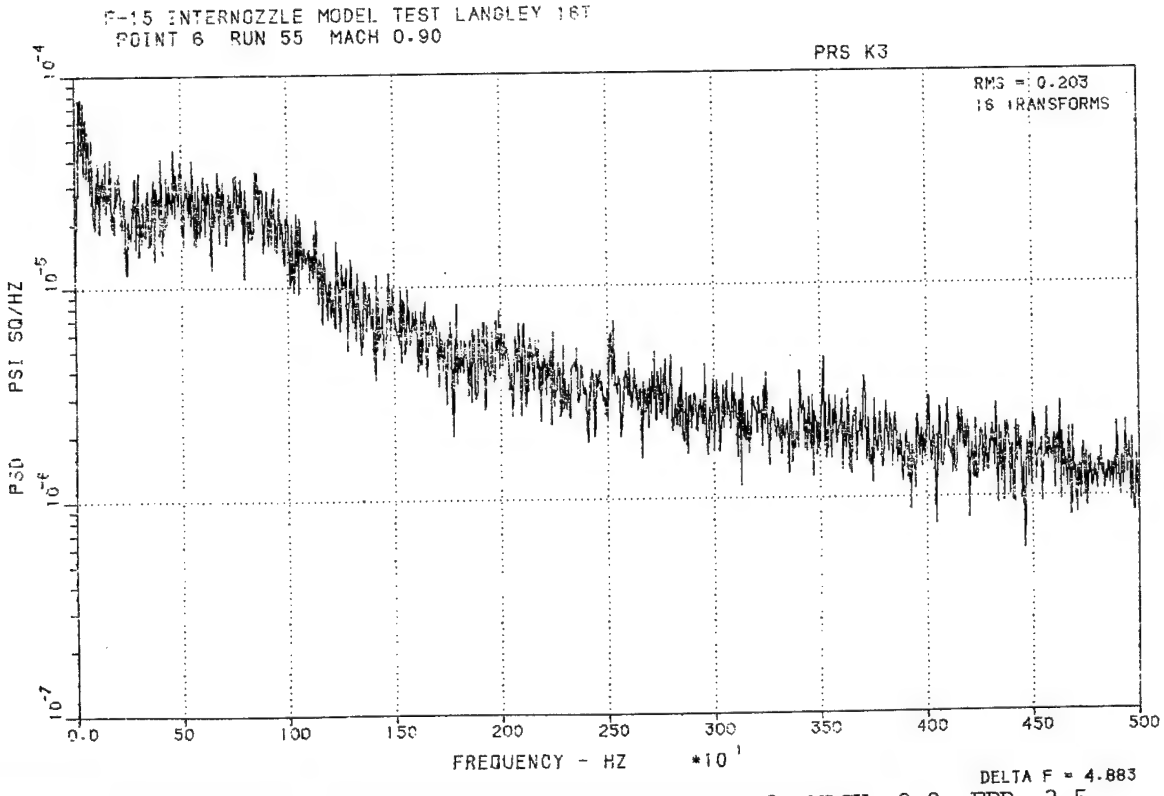

Figure 152. PSDF-No Vertical Tails Kulite 3 MACH 0.9 EPR 3.5

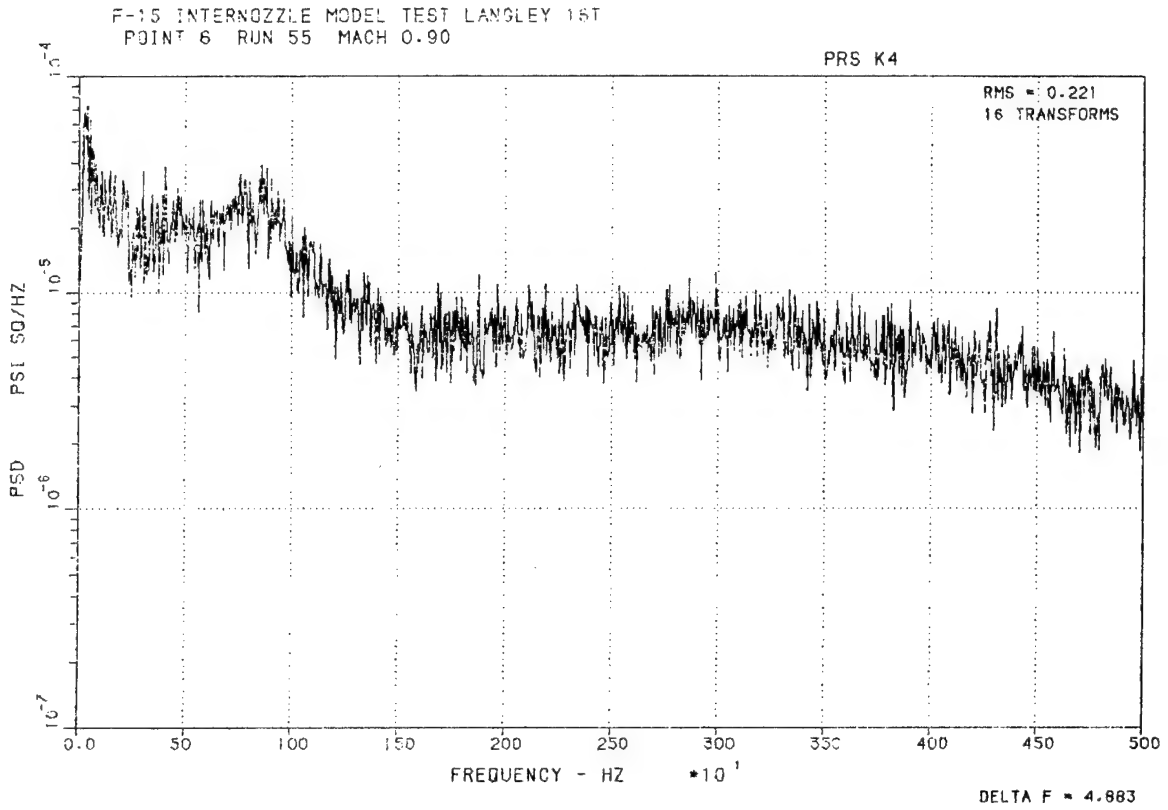

Figure 153. PSDF-No Vertical Tails Kulite 4 MACH 0.9 EPR 3.5

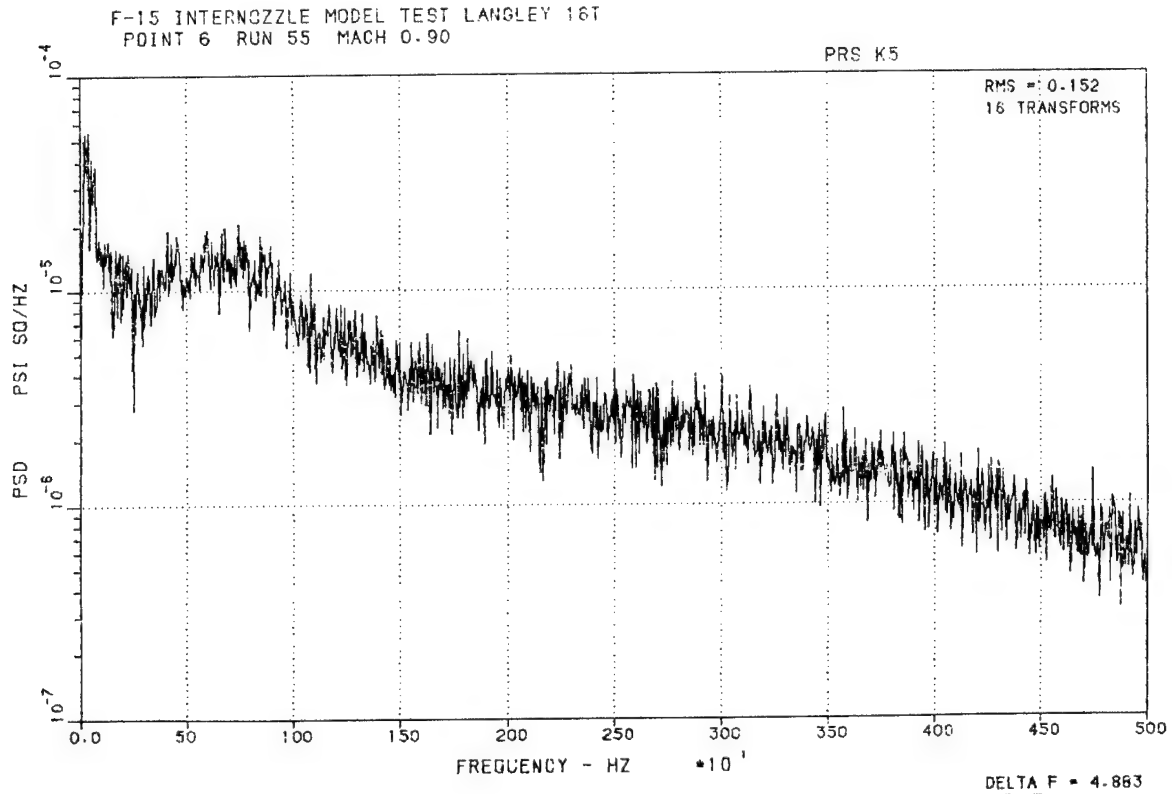

Figure 154. PSDF-No Vertical Tails Kulite 5 MACH 0.9 EPR 3.5

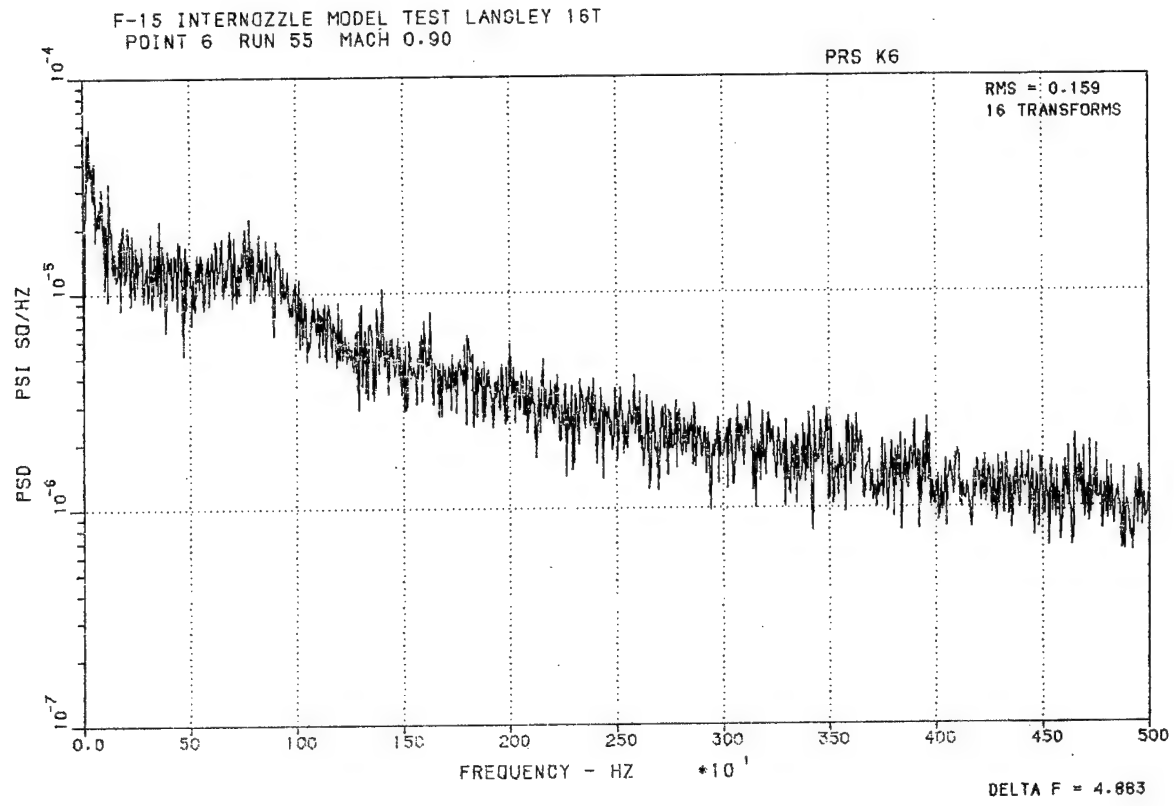

Figure 155. PSDF-No Vertical Tails Kulite 6 MACH 0.9 EPR 3.5

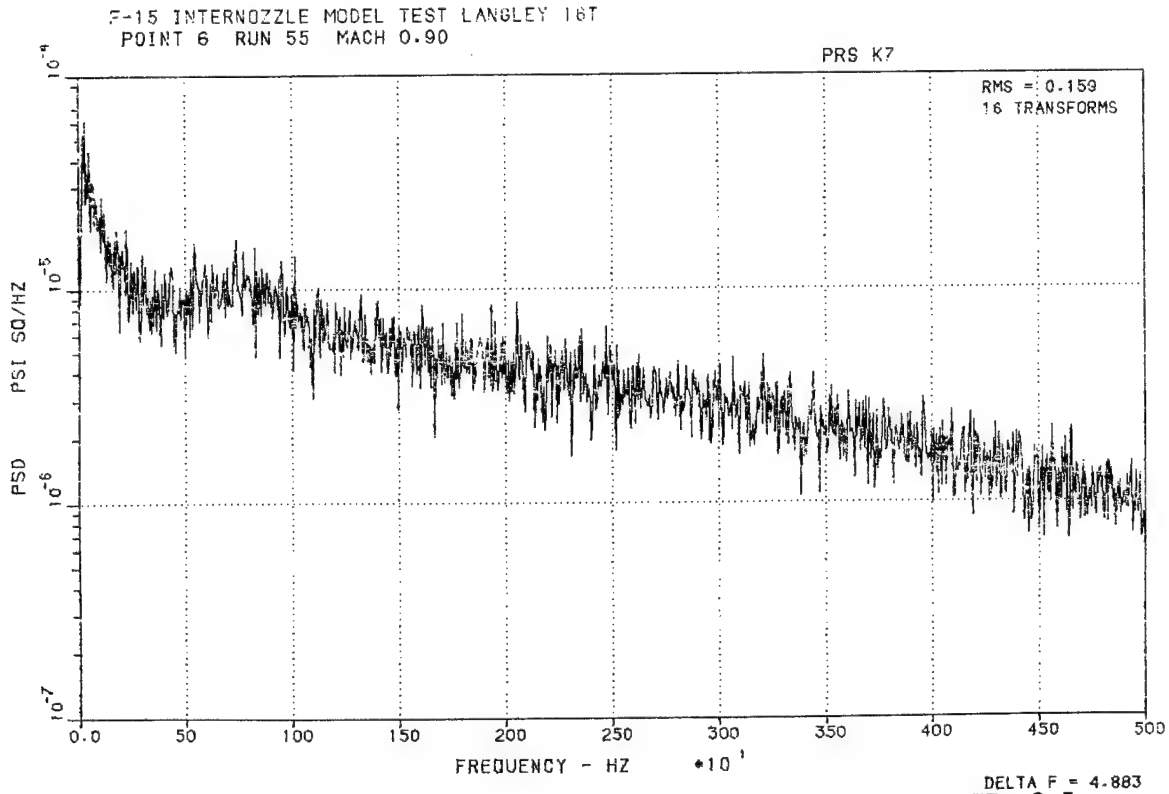

Figure 156. PSDF-No Vertical Tails Kulite 7 MACH 0.9 EPR 3.5

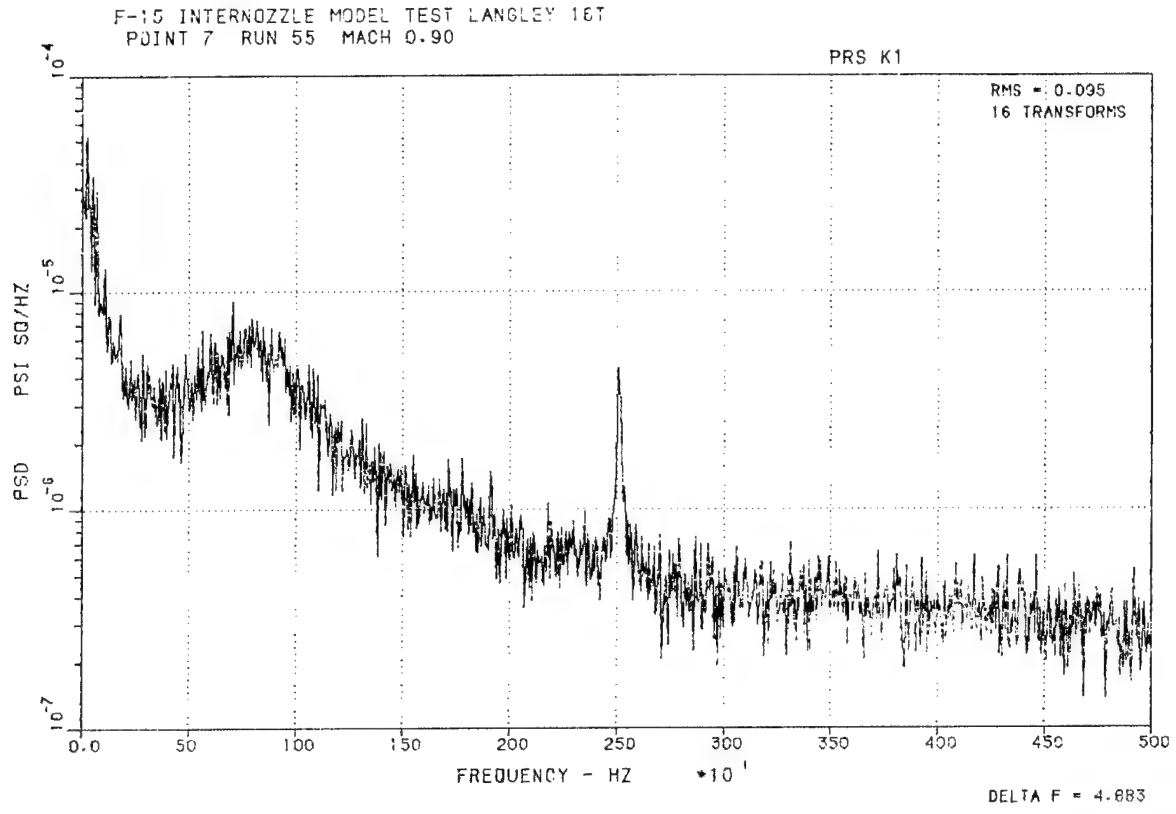

Figure 157. PSDF- No Vertical Tails Kulite 1 MACH 0.9 EPR 5.0

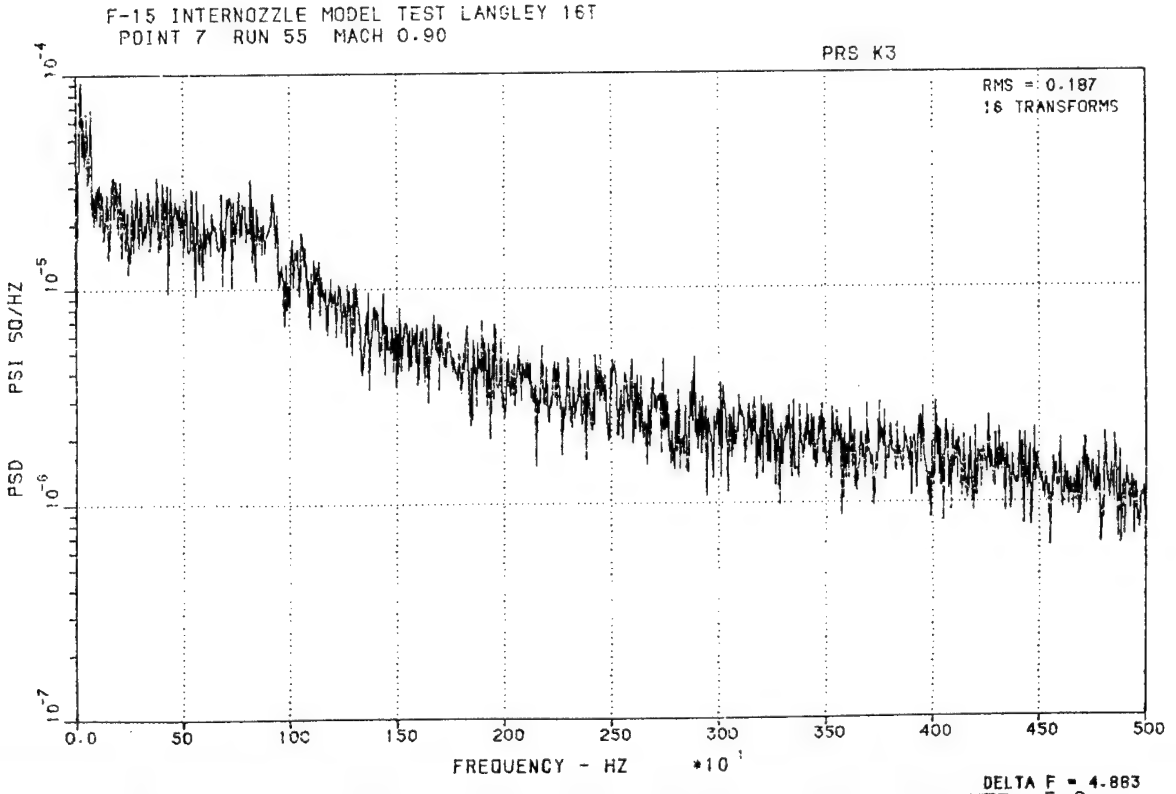

Figure 158. PSDF-No Vertical Tails Kulite 3 MACH 0.9 EPR 5.0

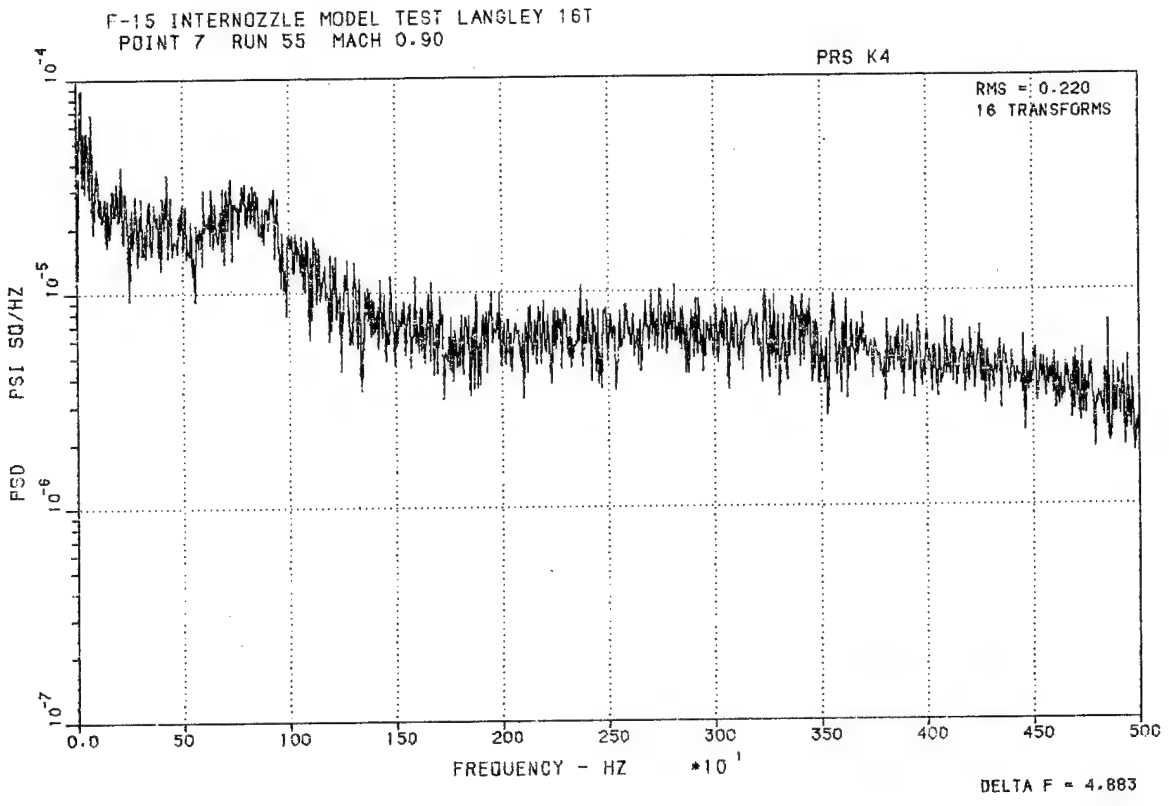

Figure 159. PSDF-No Vertical Tails Kulite 4 MACH 0.9 EPR 5.0

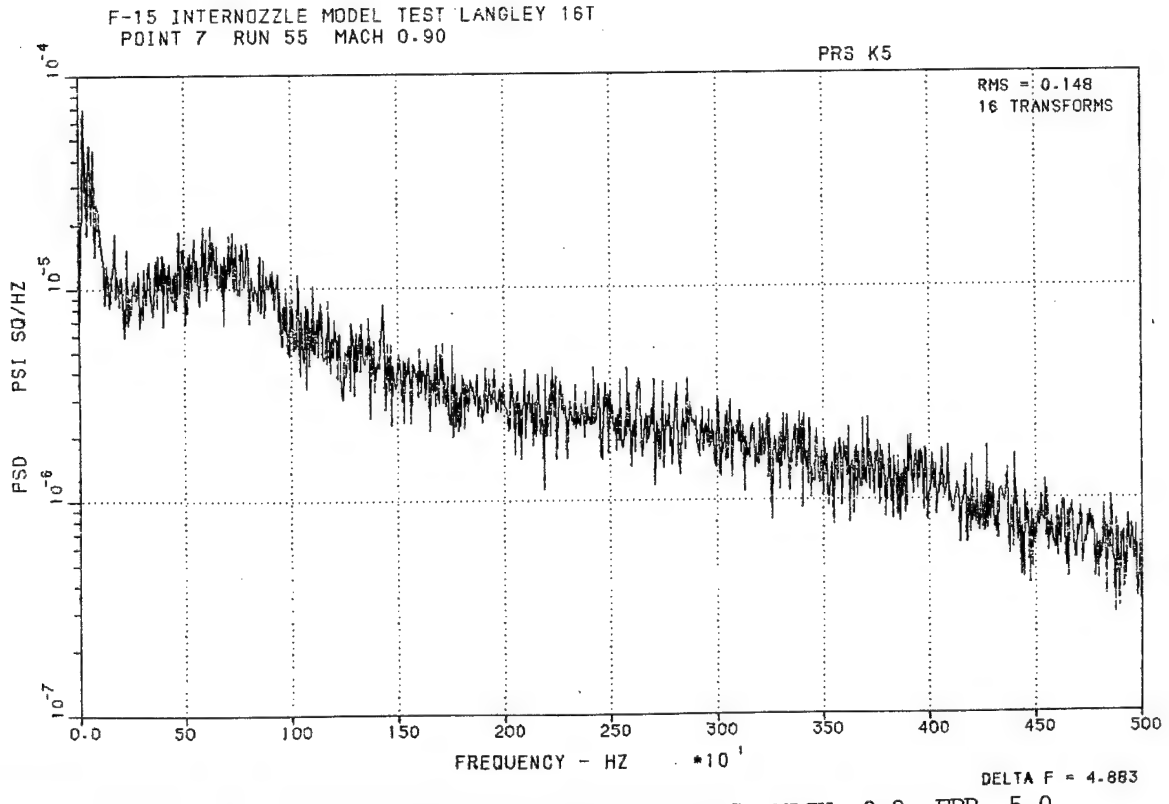

Figure 160. PSDF-No Vertical Tails Kulite 5 MACH 0.9 EPR 5.0

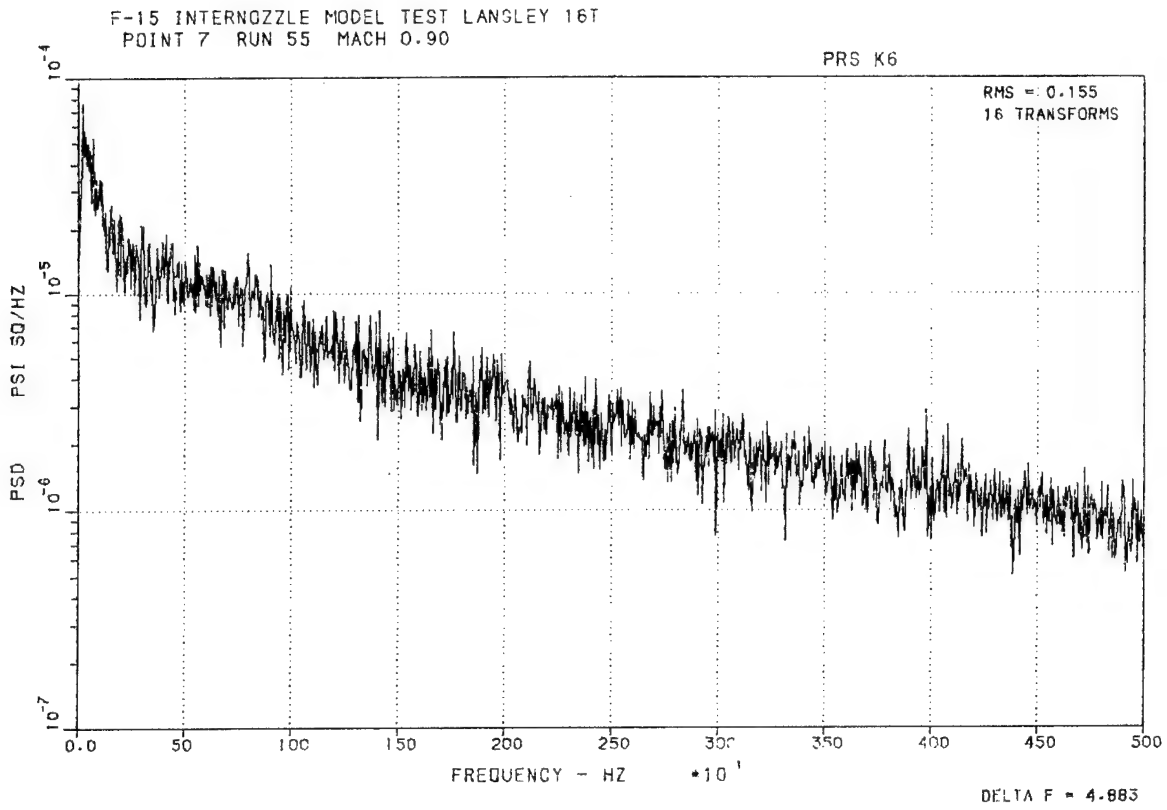

Figure 161. PSDF-No Vertical Tails Kulite 6 MACH 0.9 EPR 5.0

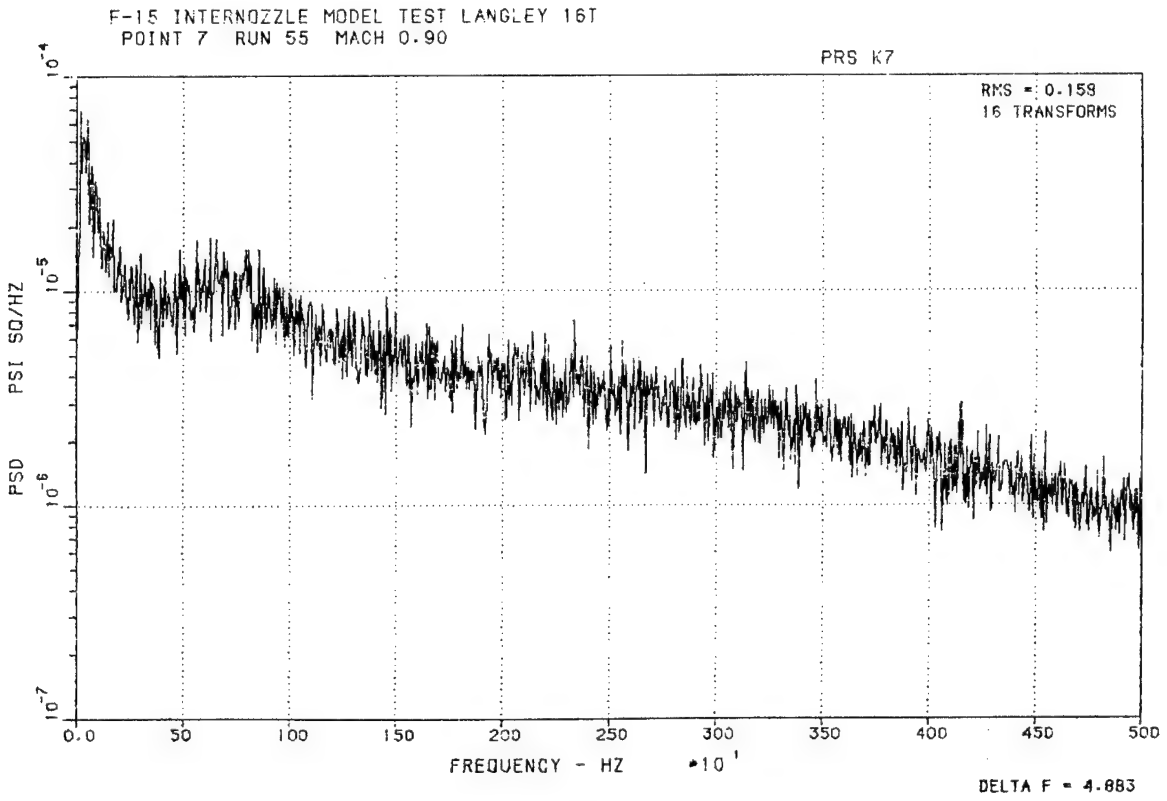

Figure 162. PSDF-No Vertical Tails Kulite 7 MACH 0.9 EPR 5.0

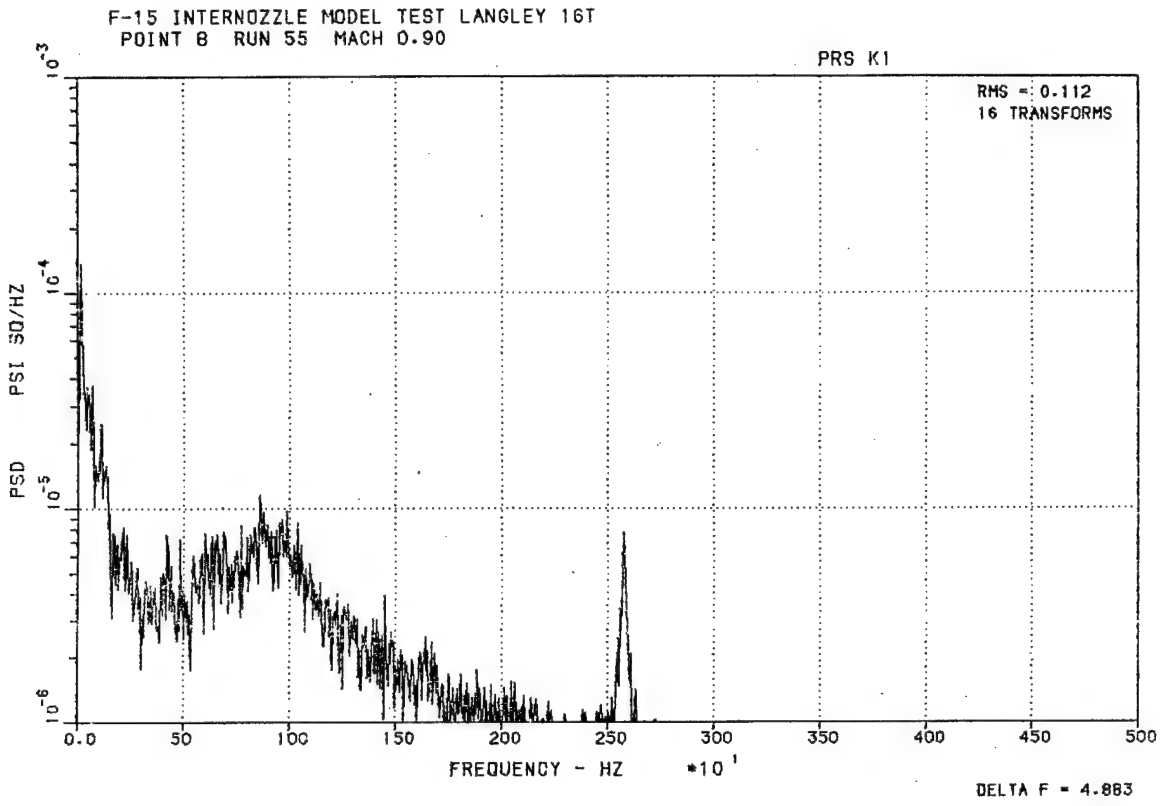

Figure 163. PSDF-No Vertical Tails Kulite 1 MACH 0.9 EPR 1.0

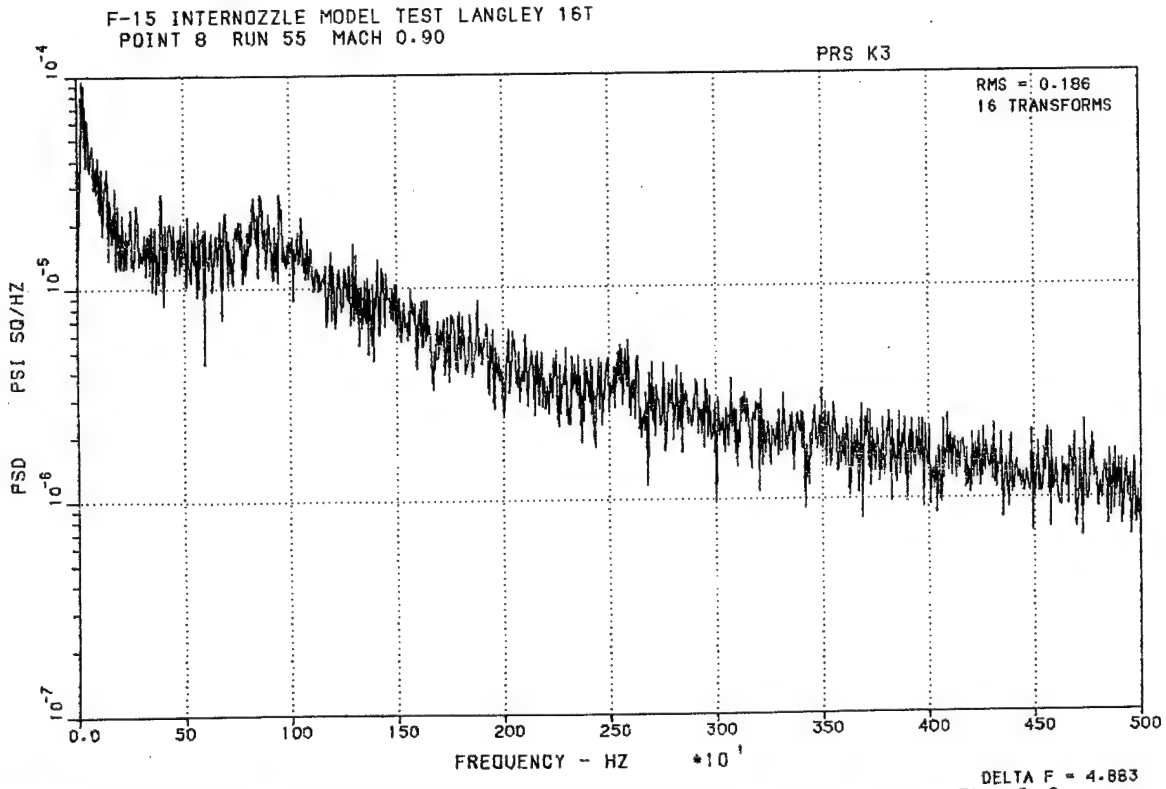

Figure 164. PSDF-No Vertical Tails Kulite 3 MACH 0.9 EPR 1.0

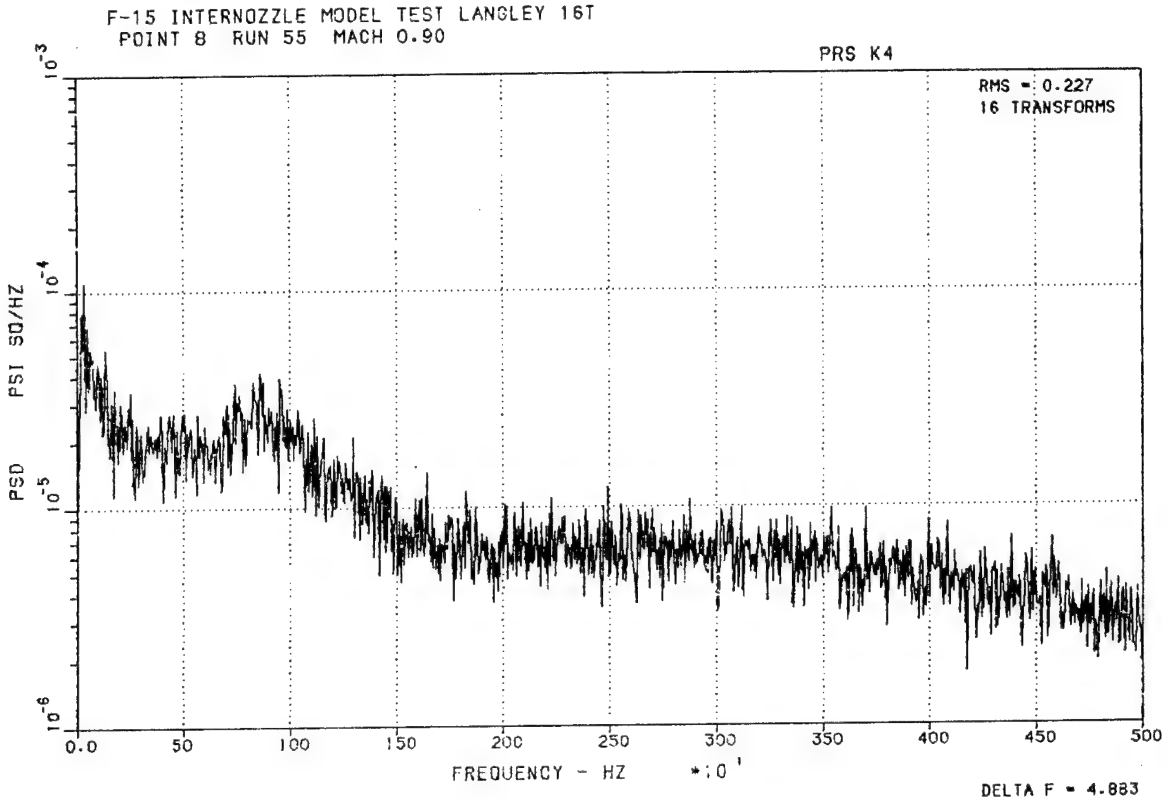

Figure 165. PSDF-No Vertical Tails Kulite 4 MACH 0.9 EPR 1.0

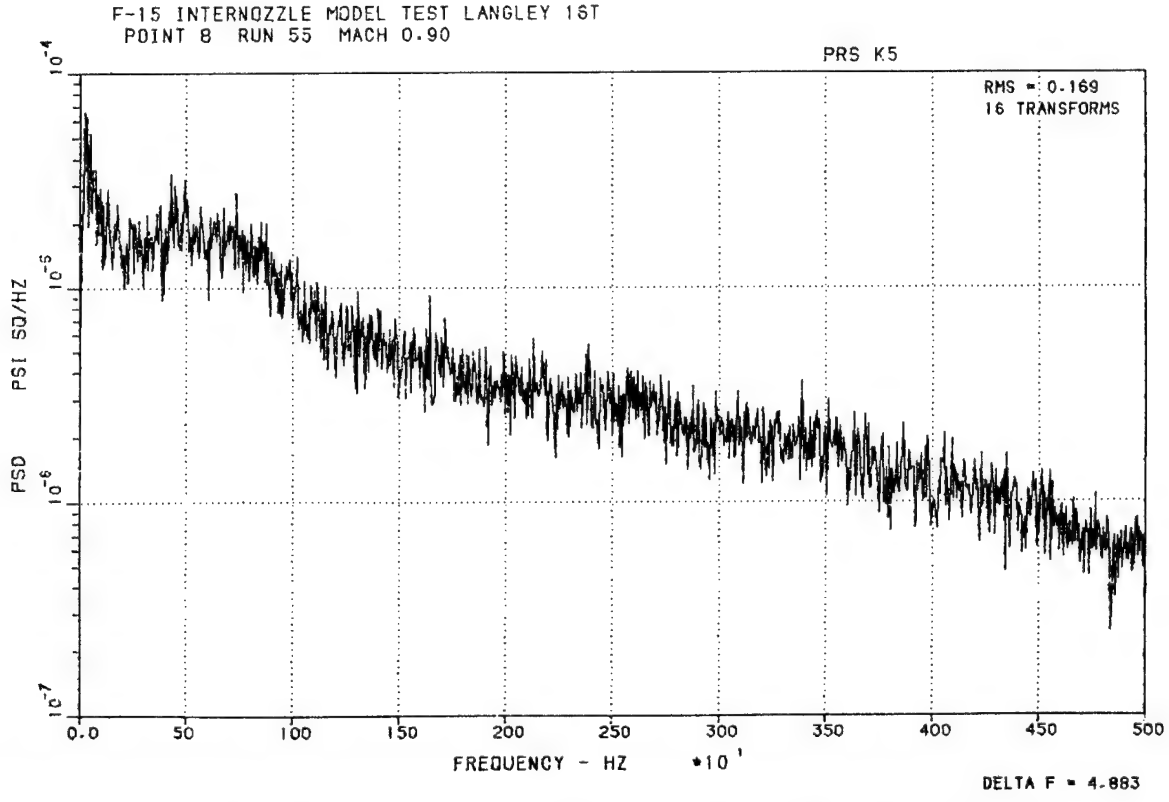

Figure 166. PSDF-No Vertical Tails Kulite 5 MACH 0.9 EPR 1.0

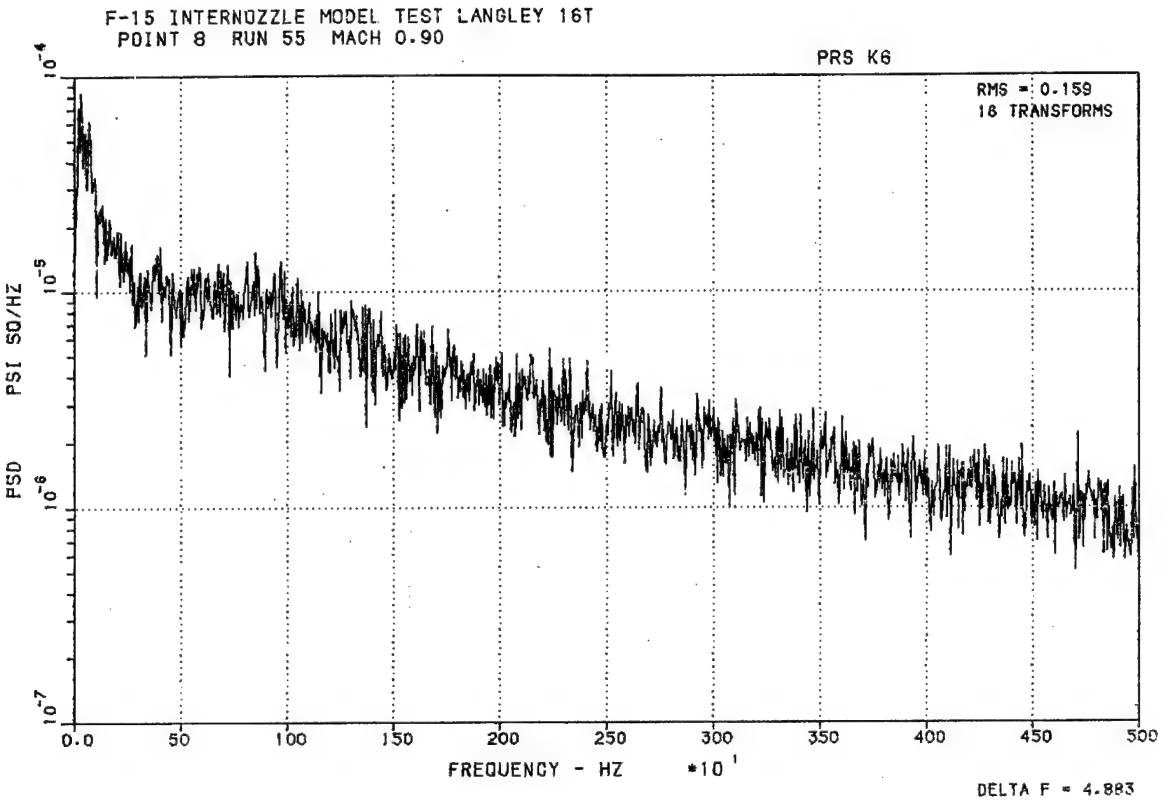

Figure 167. PSDF-No Vertical Tails Kulite 6 MACH 0.9 EPR 1.0

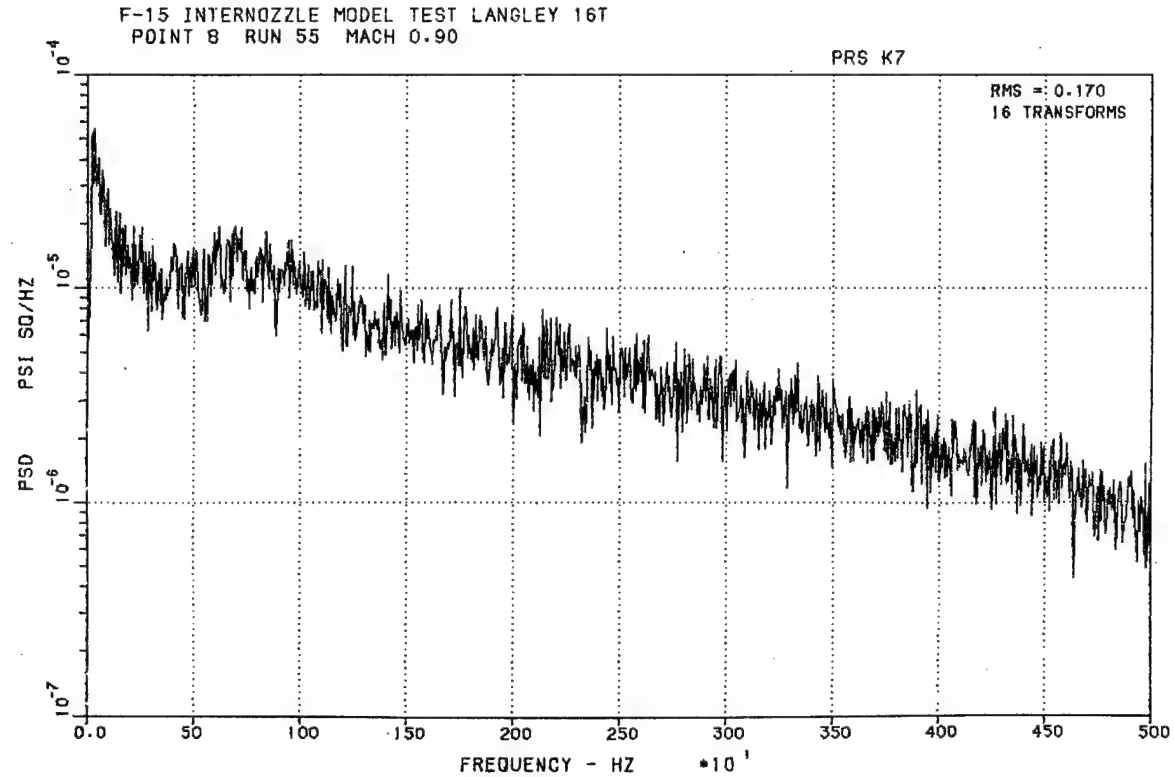

Figure 168. PSDF-No Vertical Tails Kulite 6 MACH 0.9 EPR 1.0

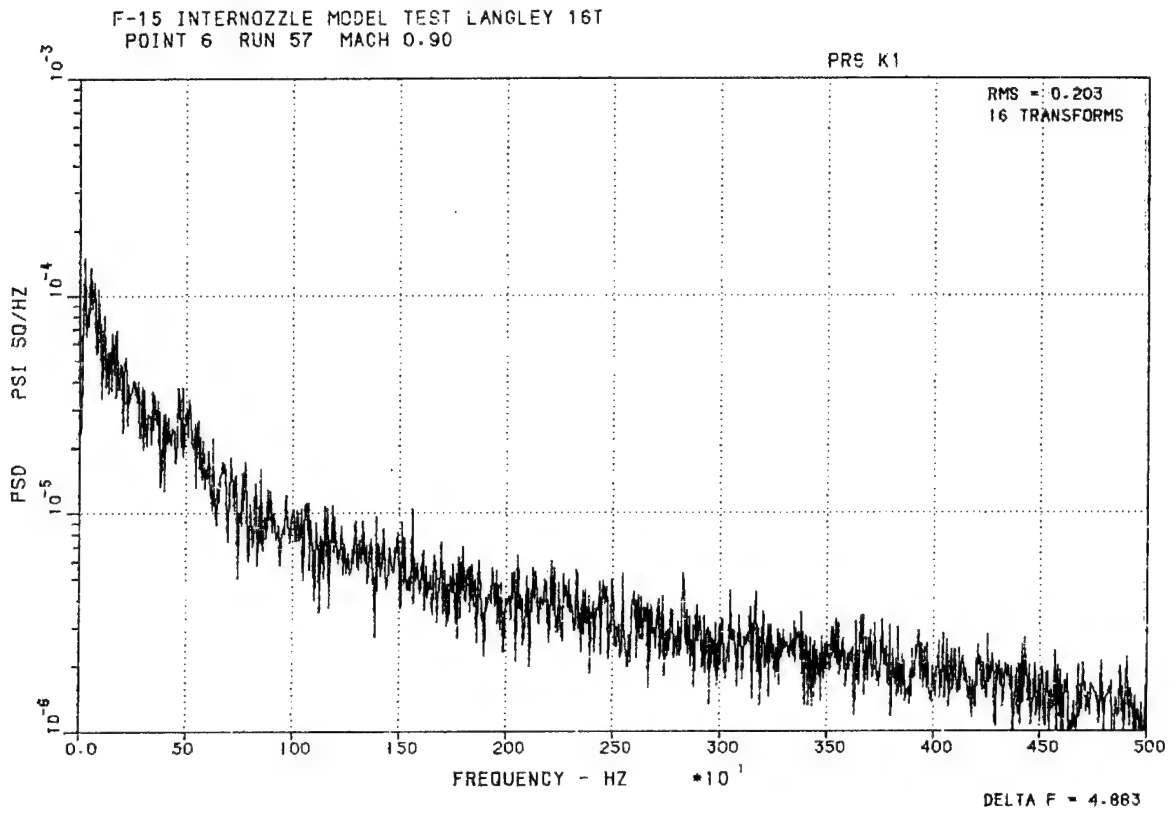

Figure 169. PSDF-Baseline Kulite 1 MACH 0.9 EPR 3.5

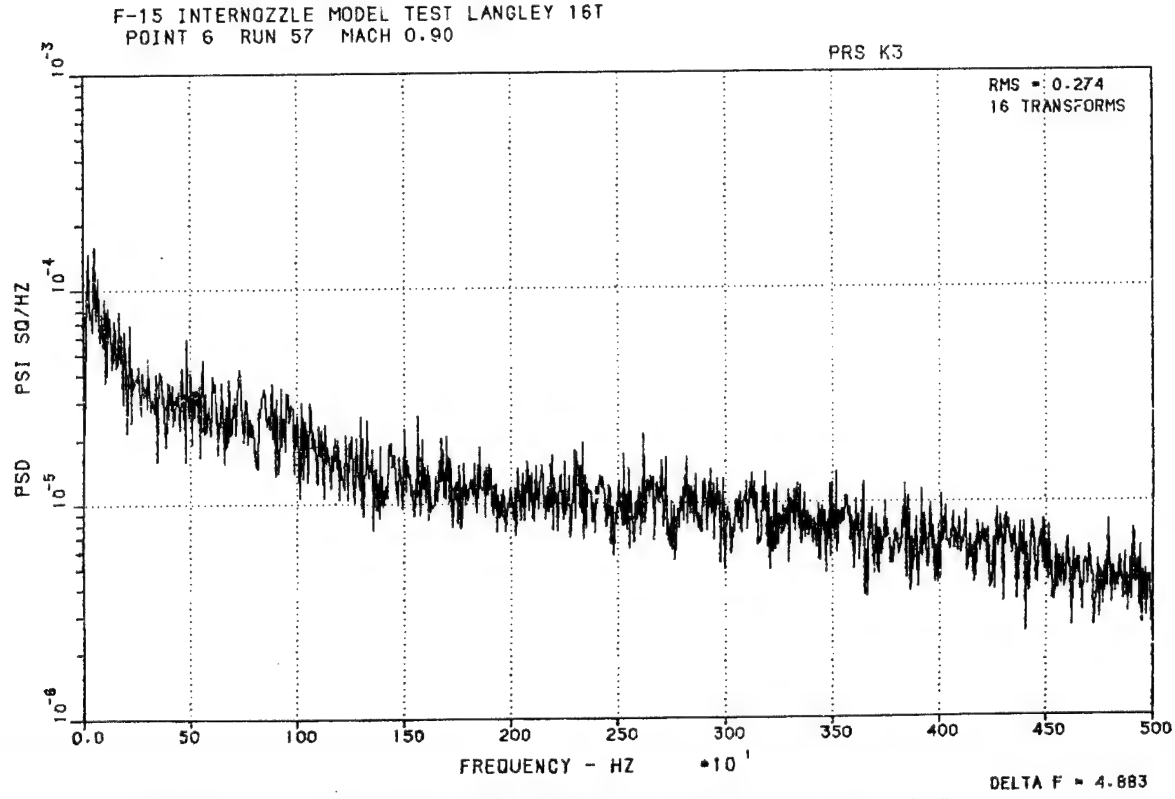

Figure 170 PSDF-Baseline Kulite 3 MACH 0.9 EPR 3.5

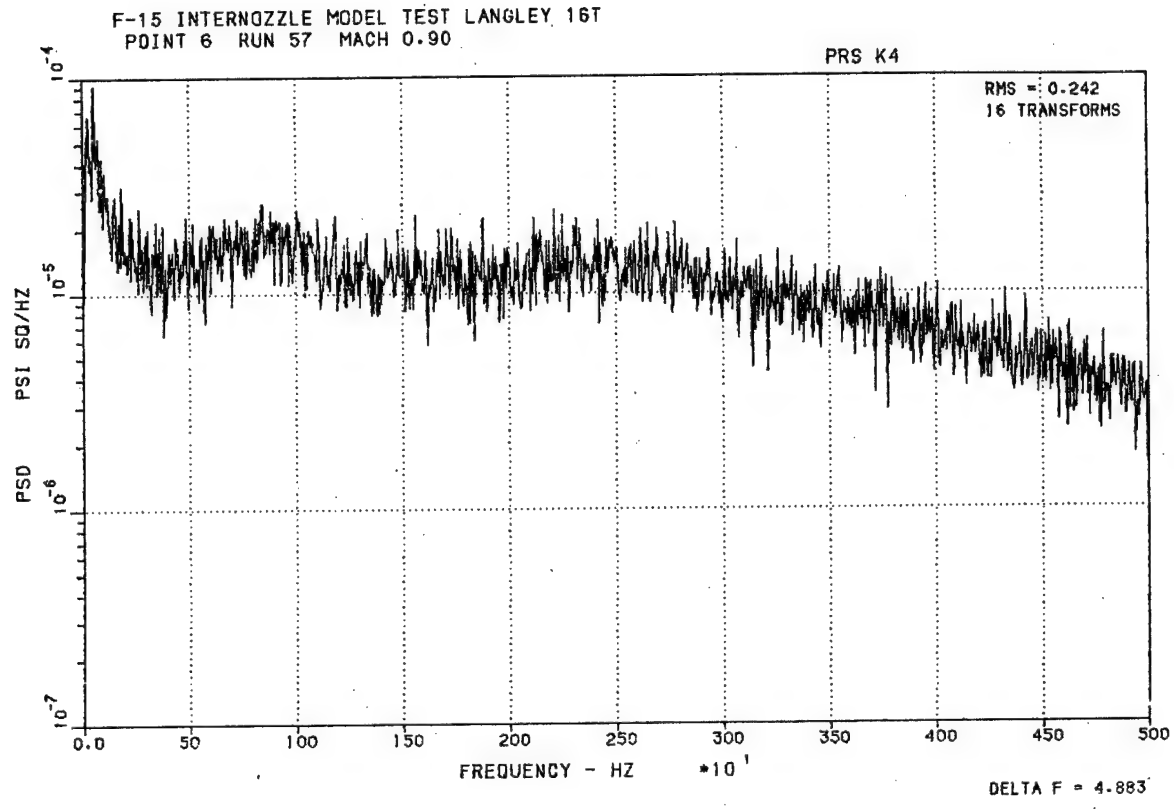

Figure 171. PSDF-Baseline KUlite 4 MACH 0.9 EPR 3.5

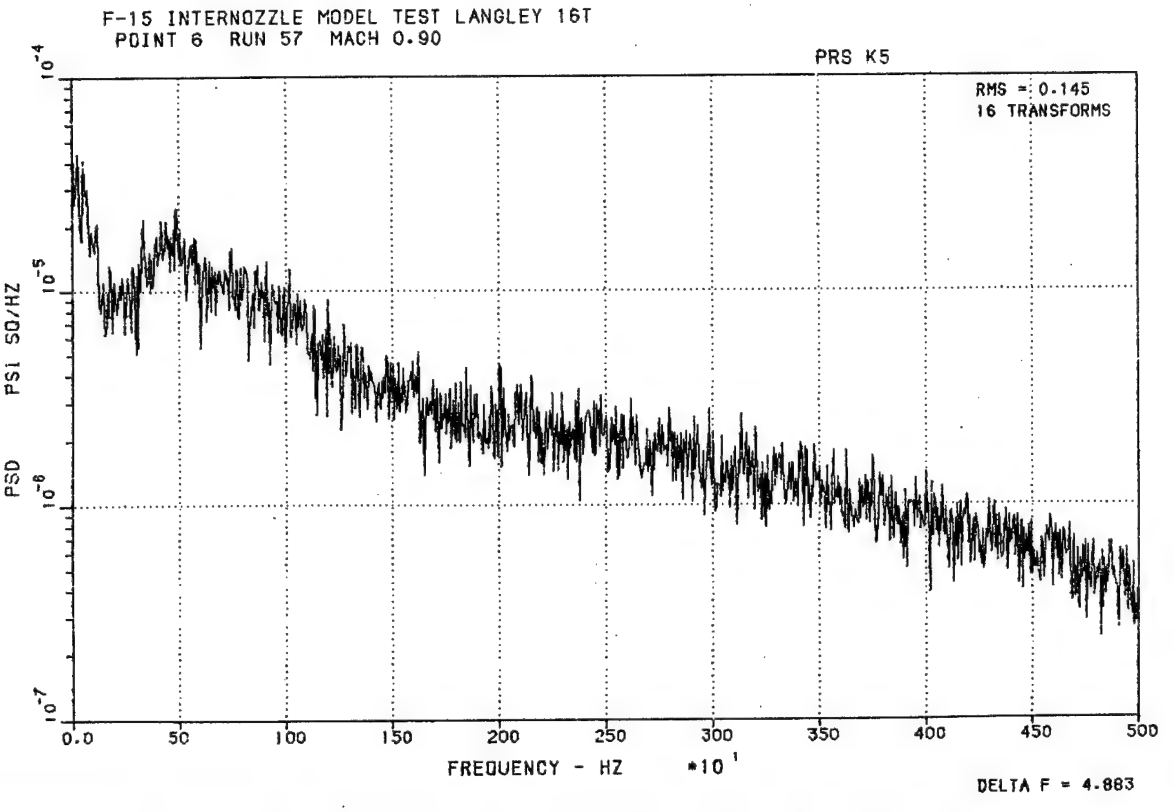

Figure 172. PSDF-Baseline Kulite 5 MACH 0.9 EPR 3.5

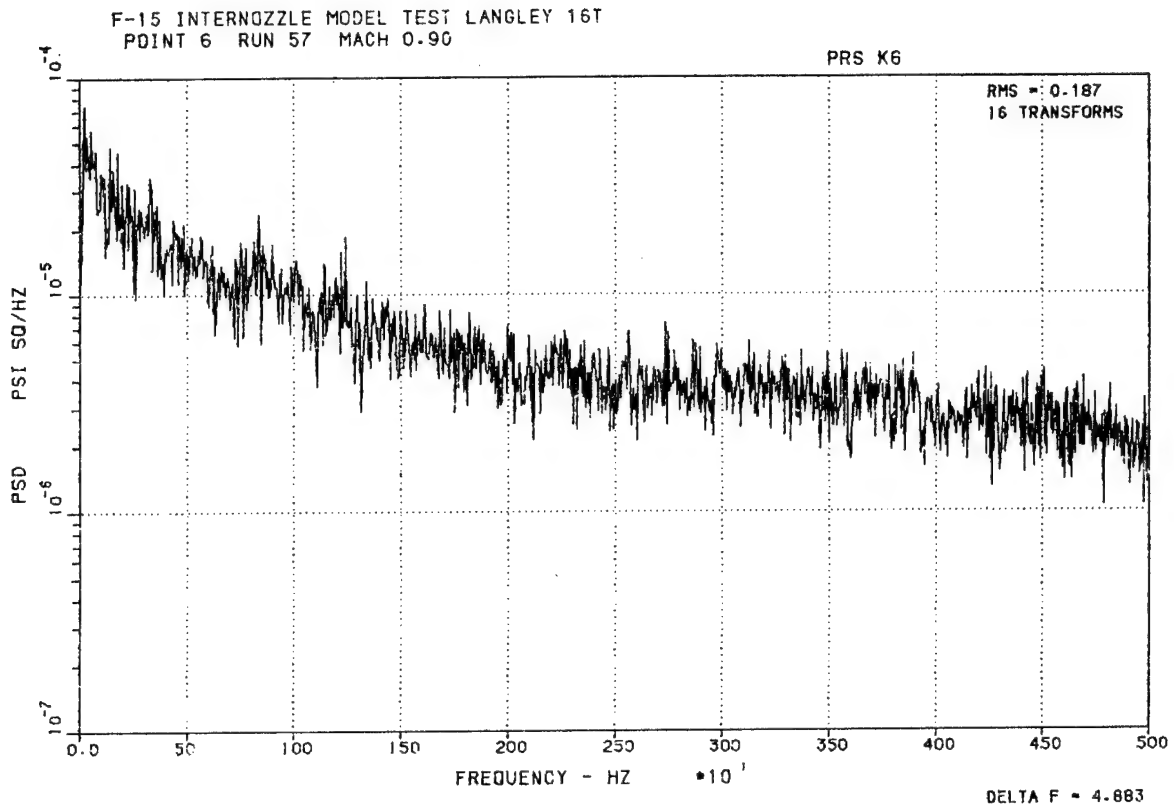

Figure 173. PSDF-Baseline Kulite 6 MACH 0.9 EPR 3.5

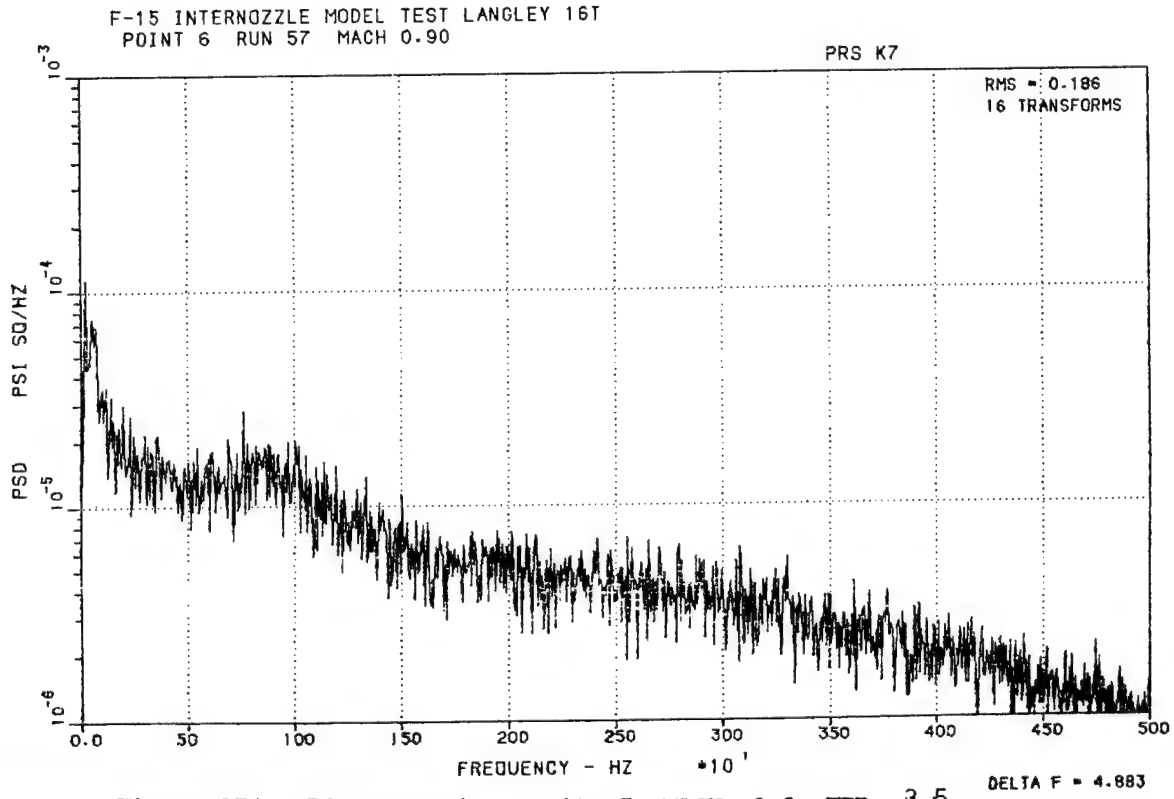

Figure 174. PSDF-Baseline Kulite 7 MACH 0.9 EPR 3.5

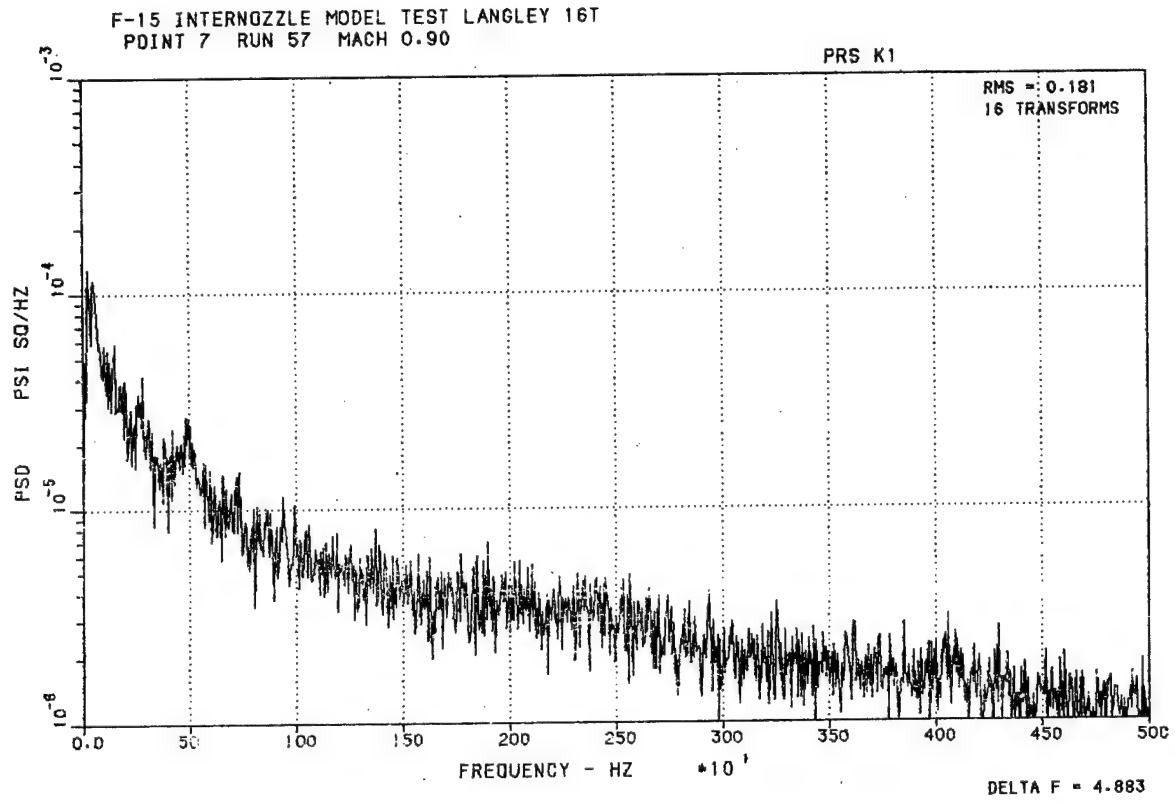

Figure 175. PSDF-Baseline Kulite 1 MACH 0.9 EPR 5.0

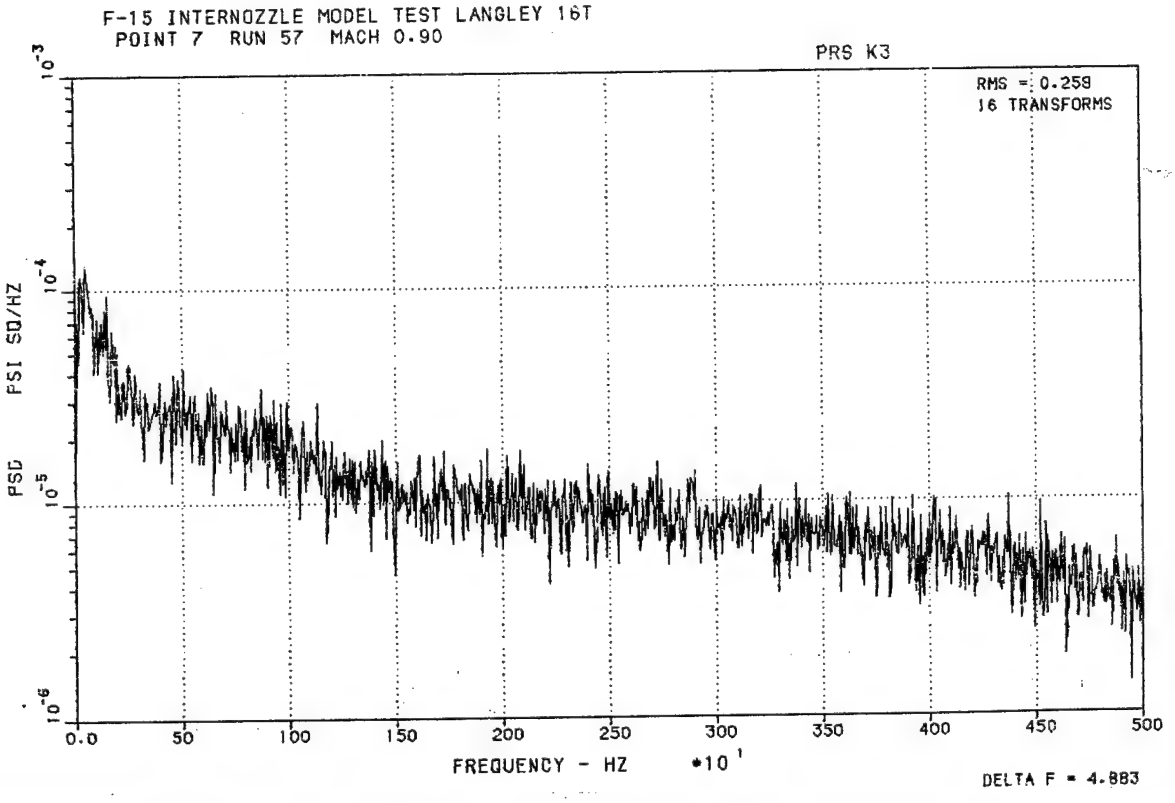

Figure. 176. PSDF-Baseline Kulite 3 Mach 0.9 EPR 5.0

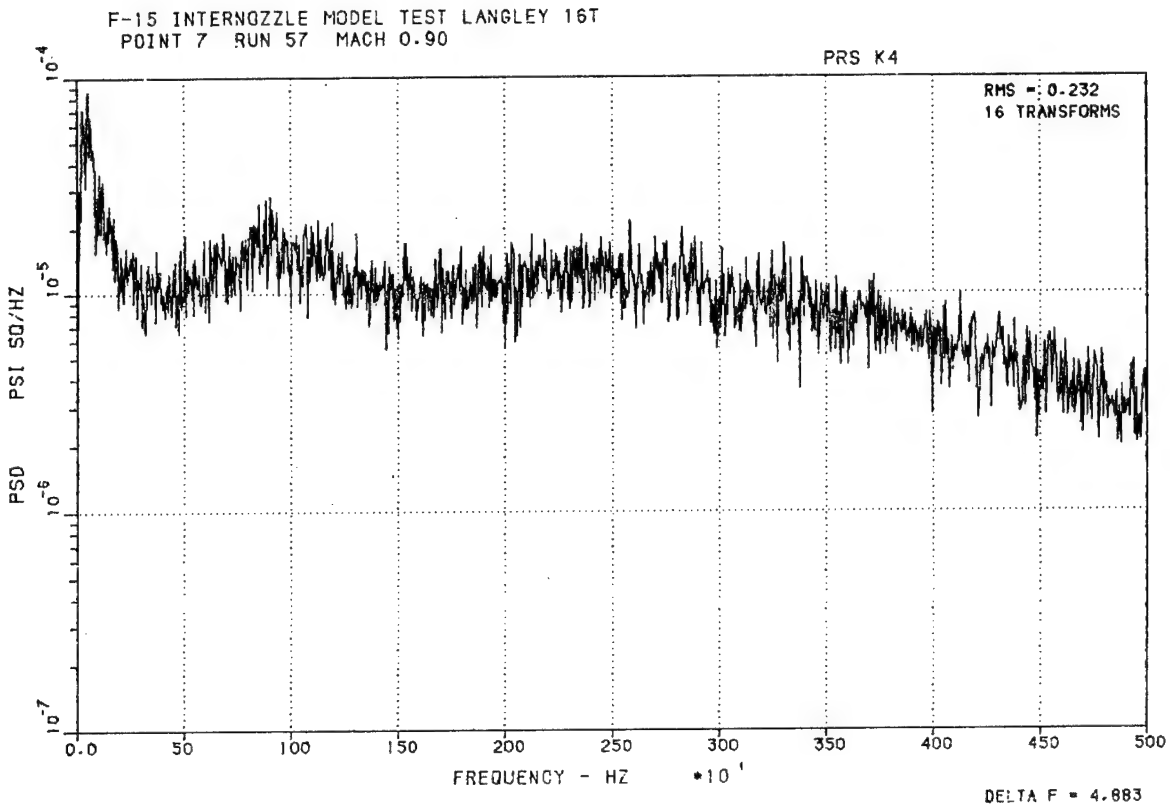

Figure 177. PSDF-Baseline Kulite 4 MACH 0.9 EPR 5.0

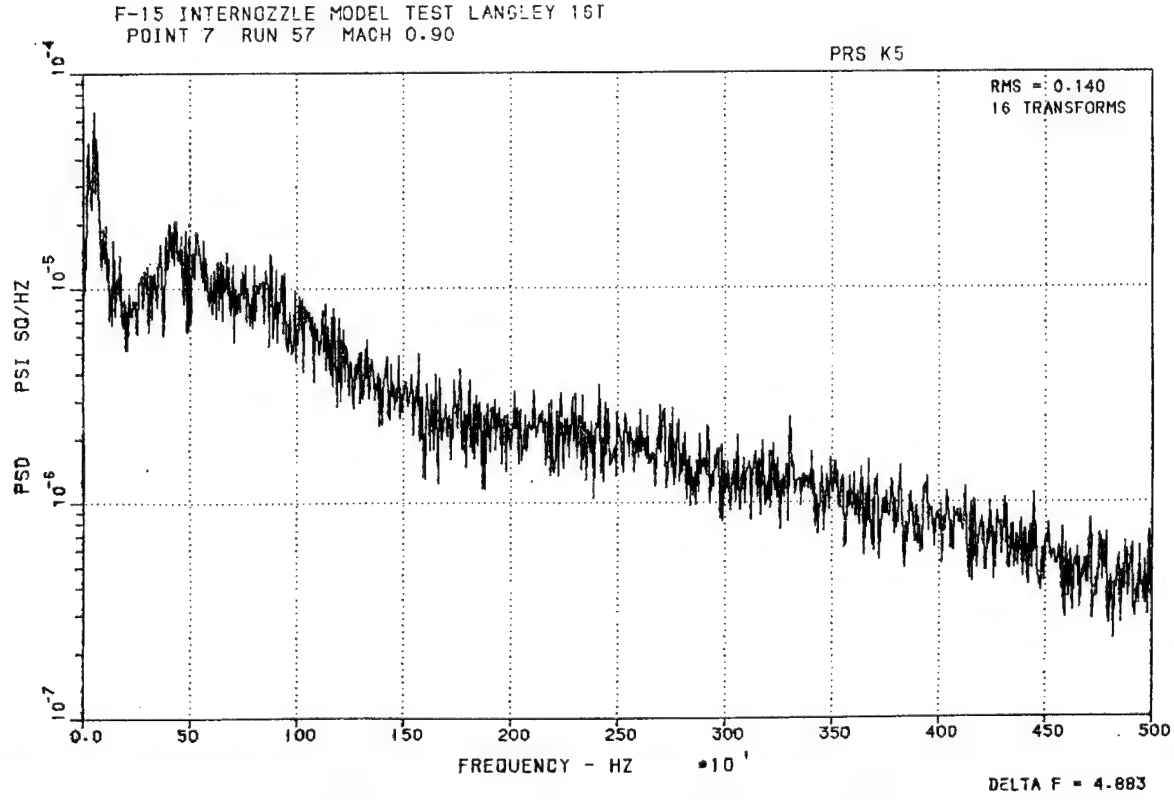

Figure 178. PSDF-Baseline Kulite 5 MACH 0.9 EPR 5.0

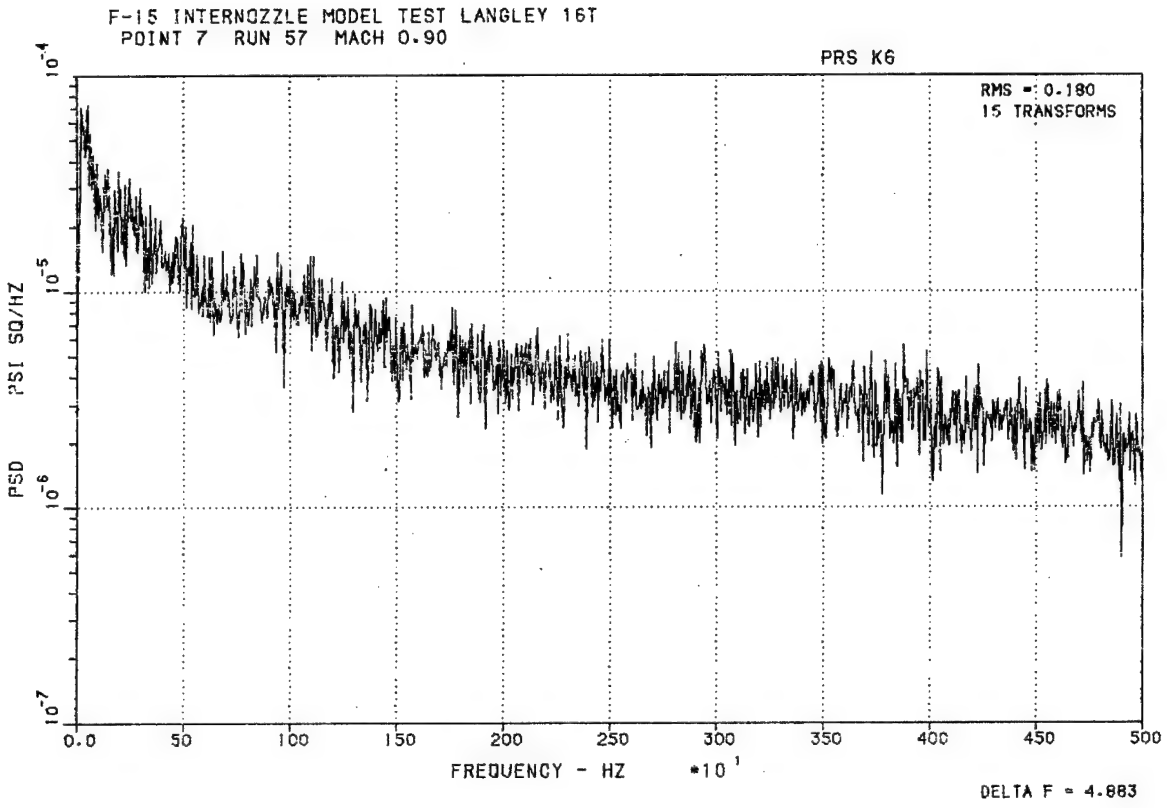

Figure 179. PSDF-Baseline Kulite 6 MACH 0.9 EPR 5.0

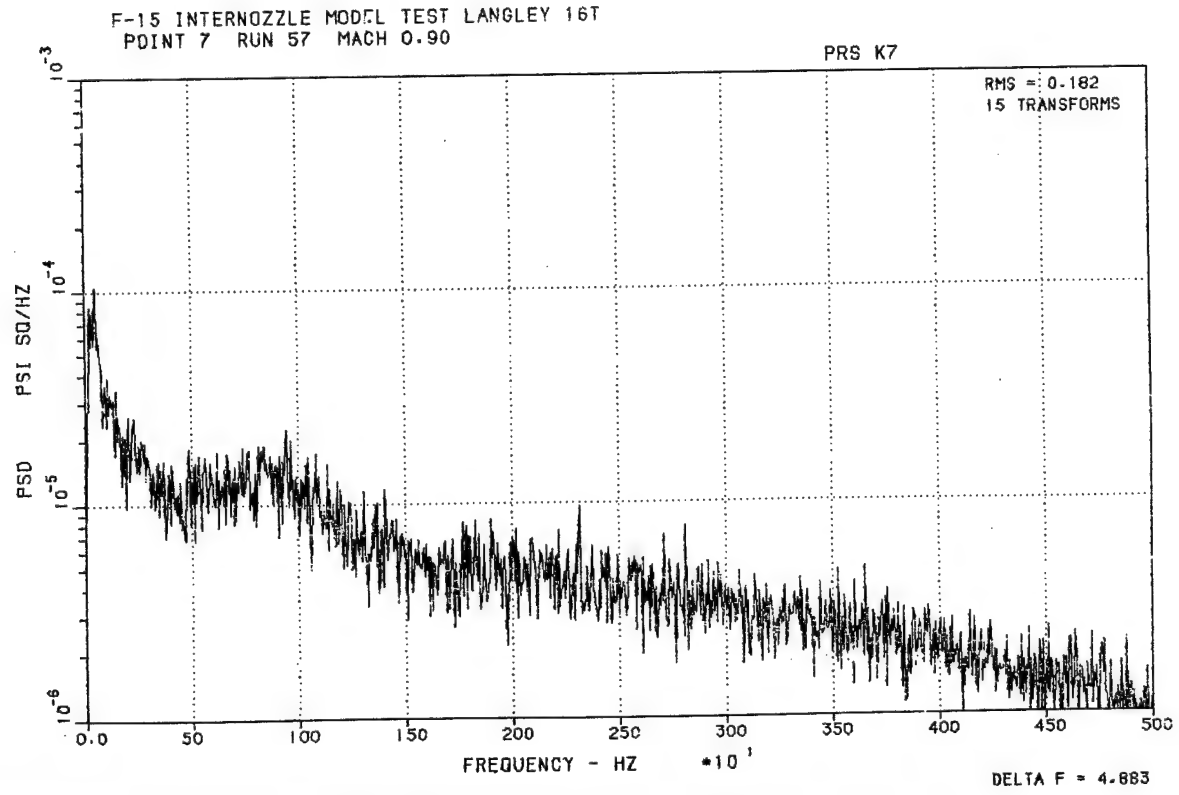

Figure 180. PSDF-Baseline Kulite 7 MACH 0.9 EPR 5.0

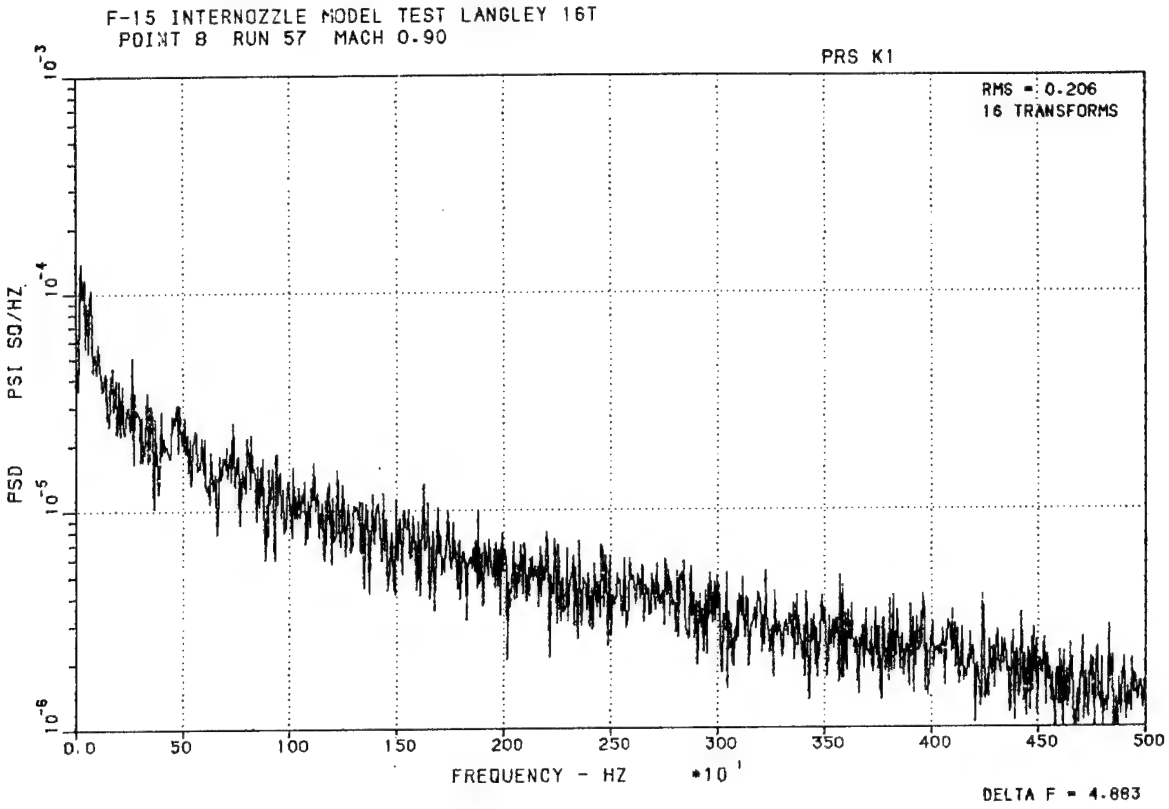

Figure 181. PSDF-Baseline Kulite 1 MACH 0.9 EPR 1.0

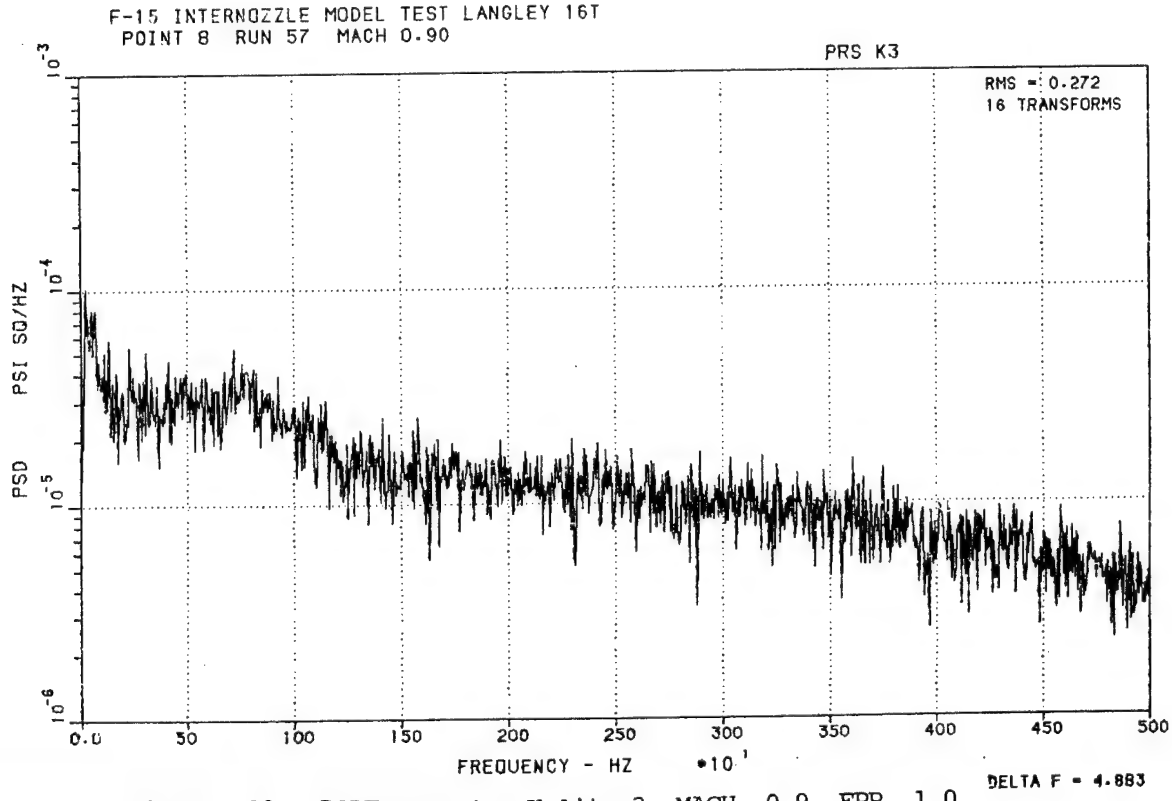

Figure 182. PSDF-Baseline Kulite 3 MACH 0.9 EPR 1.0

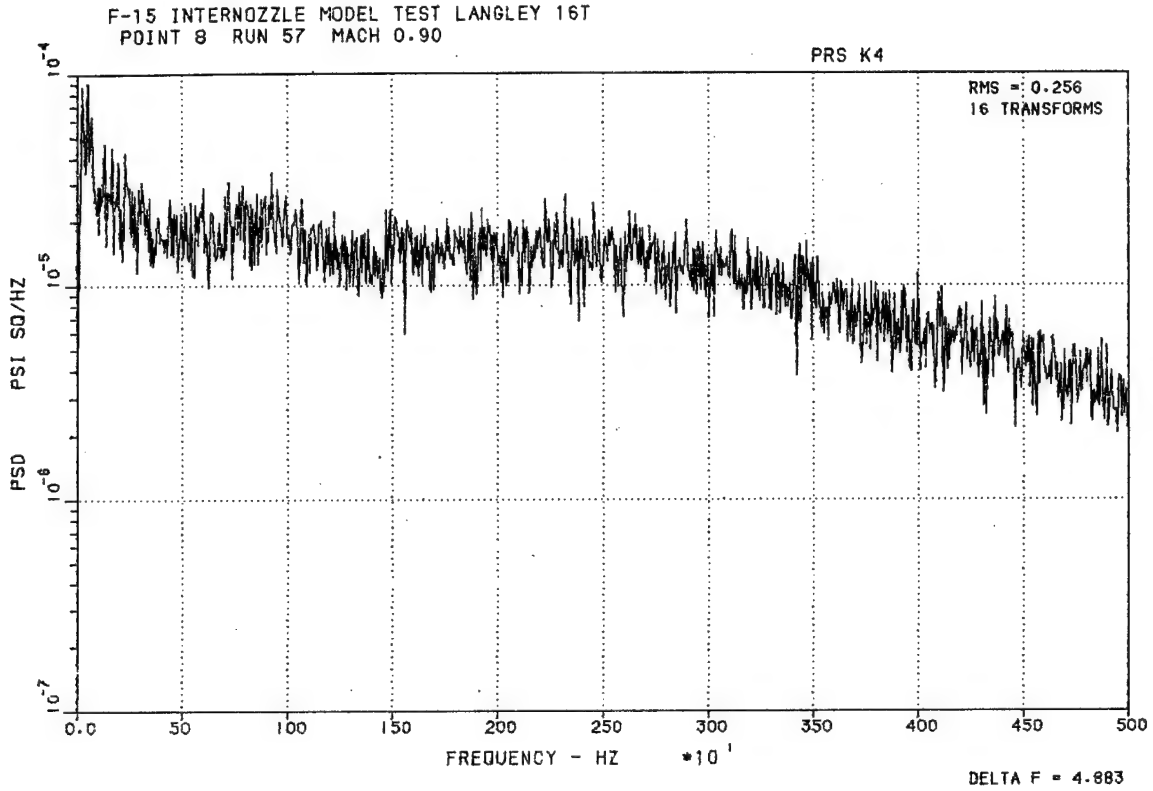

Figure 183. PSDF-Baseline Kulite 4 MACH 0.9 EPR 1.0

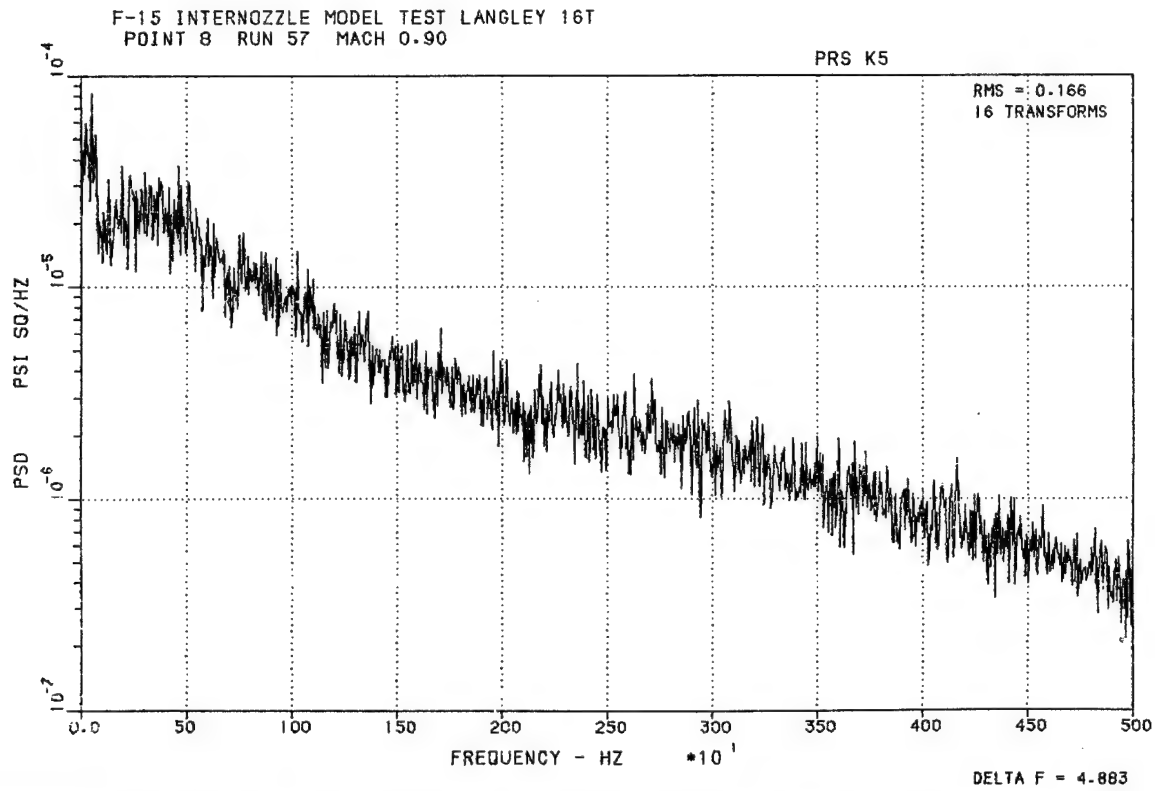

Figure 184. PSDF-Baseline Kulite 5 MACH 0.9 EPR 1.0

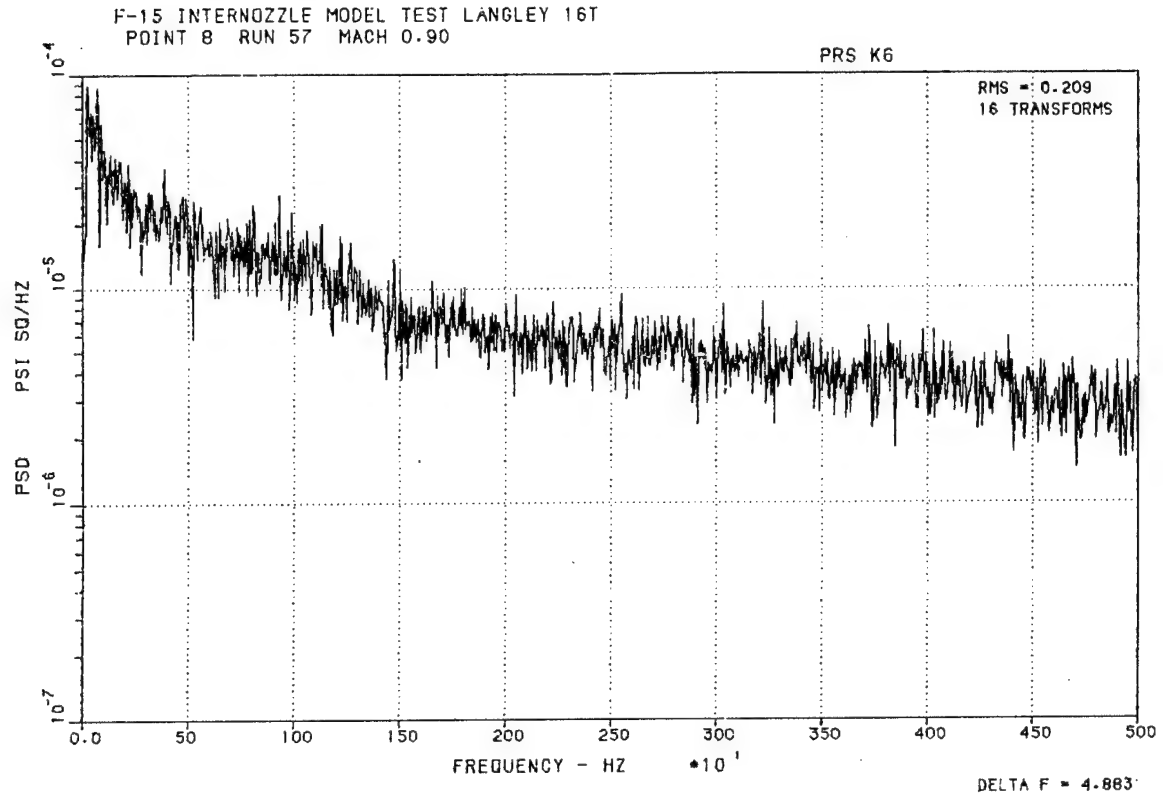

Figure 185. PSDF-Baseline Kulite 6 MACH 0.9 EPR 1.0

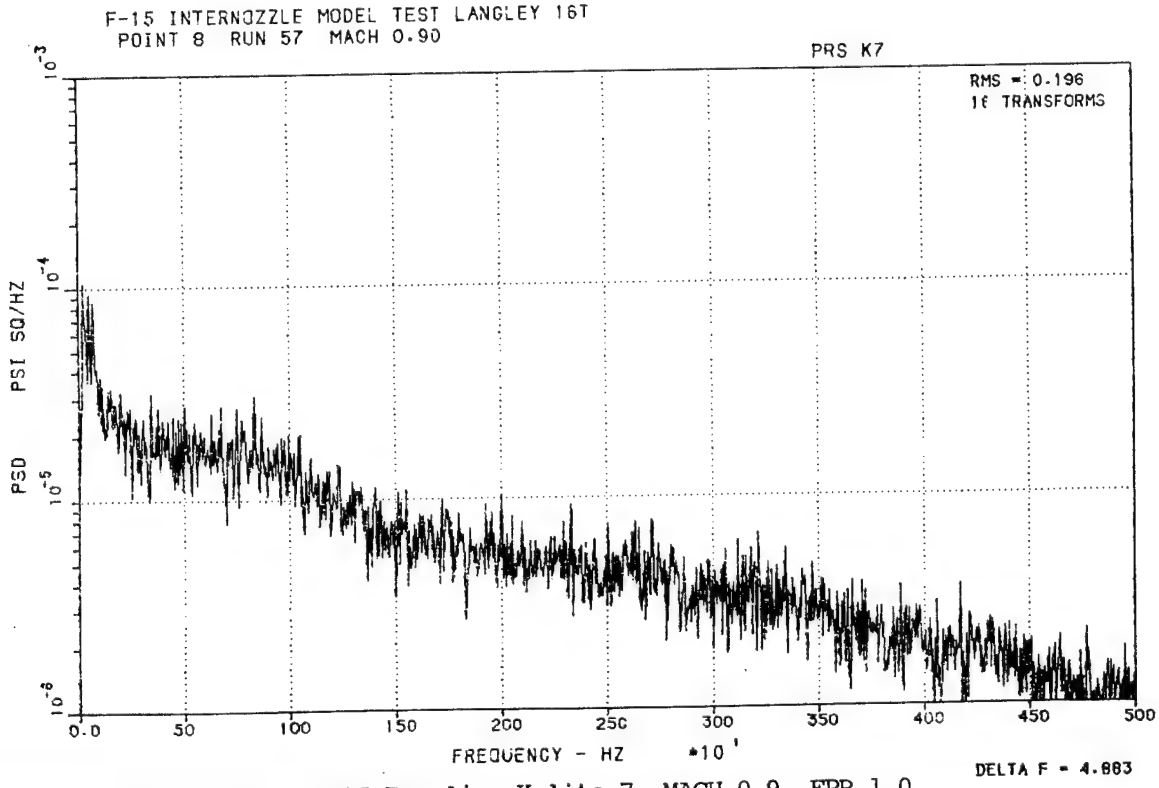

Figure 186. PSDF-Baseline Kulite 7 MACH 0.9 EPR 1.0

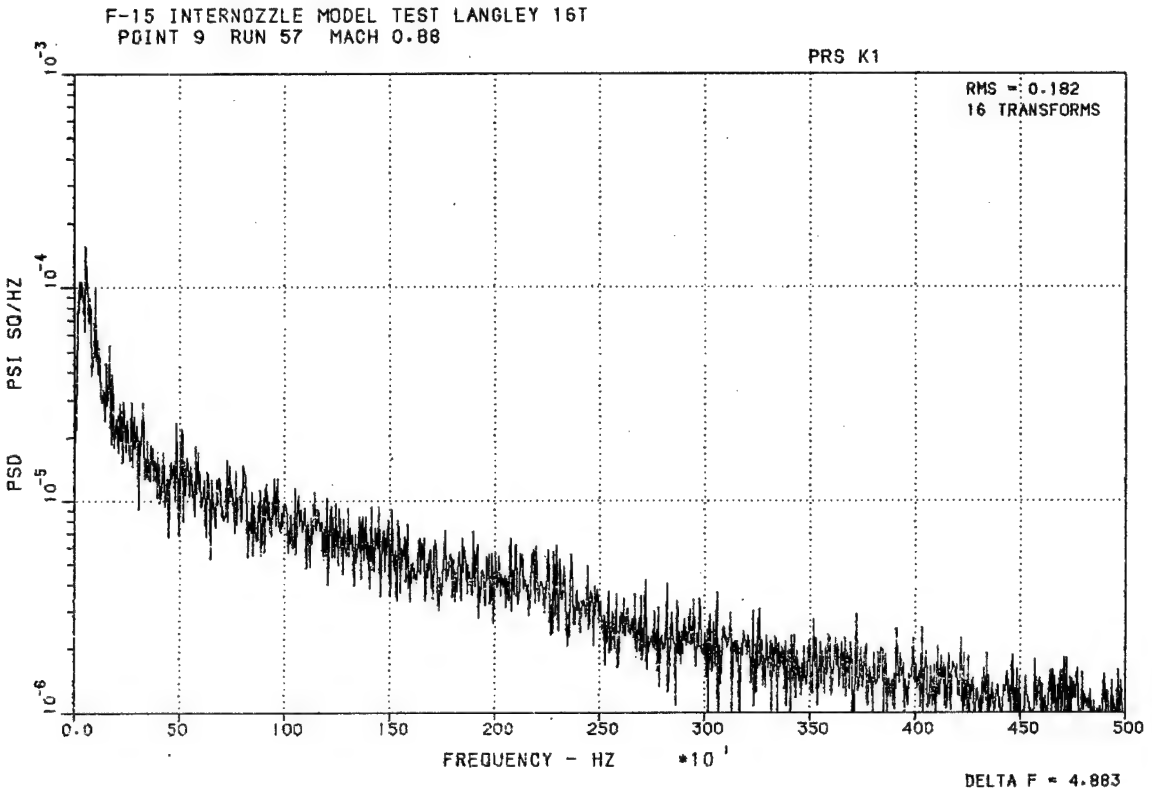

Figure 187. PSDF-Baseline Kulite 1 MACH 0.88 EPR 1.0

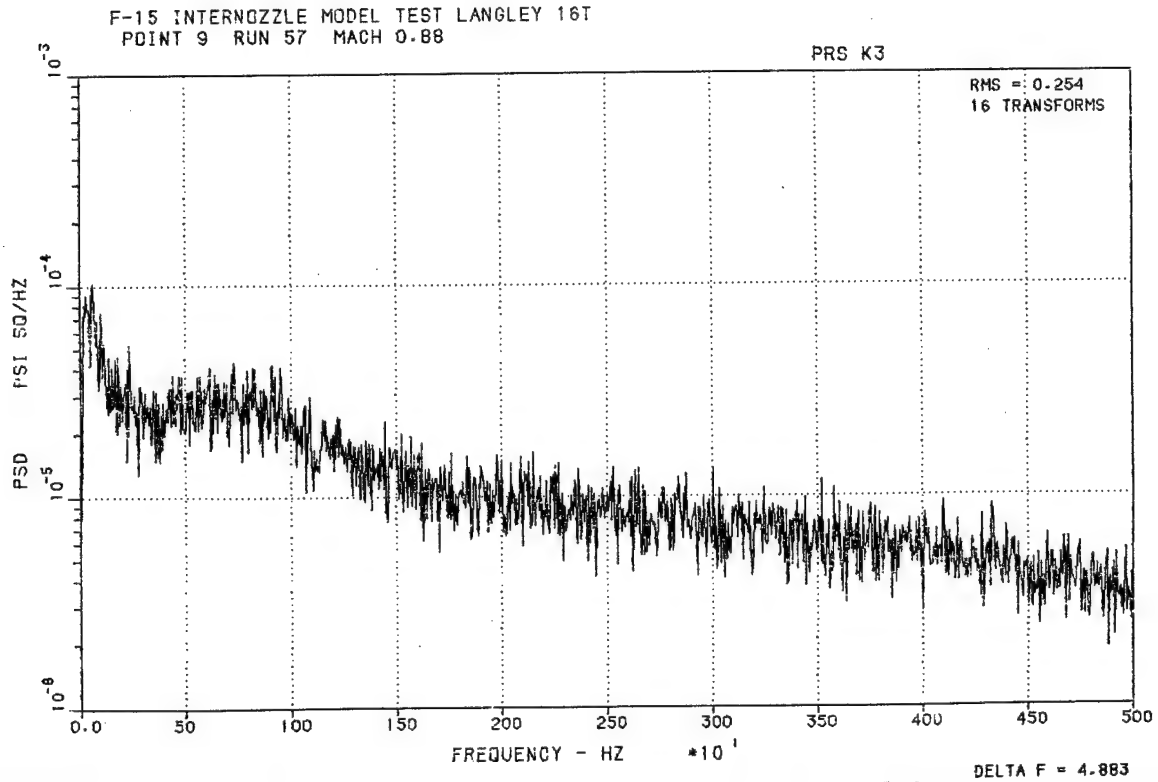

Figure 188. PSDF-Baseline Kulite 3 MACH 0.88 EPR 1.0

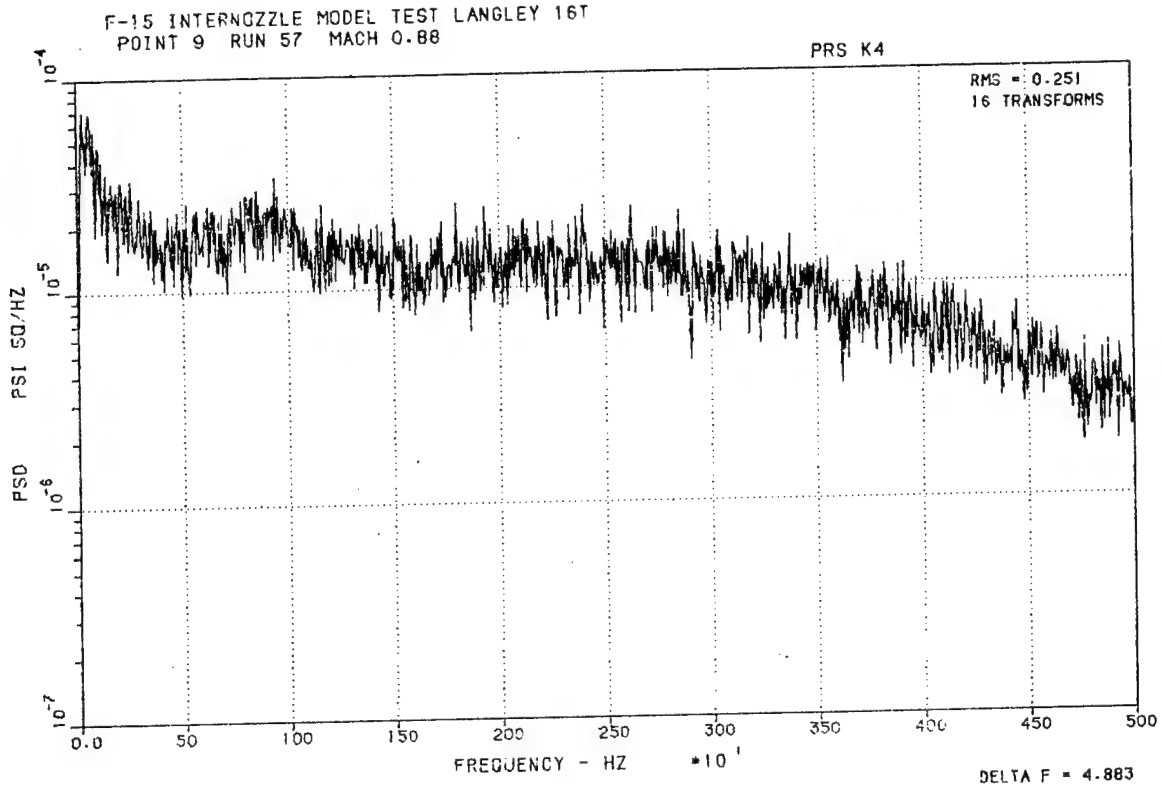

Figure 189. PSDF-Baseline Kulite 4 MACH 0.88 EPR 1.0

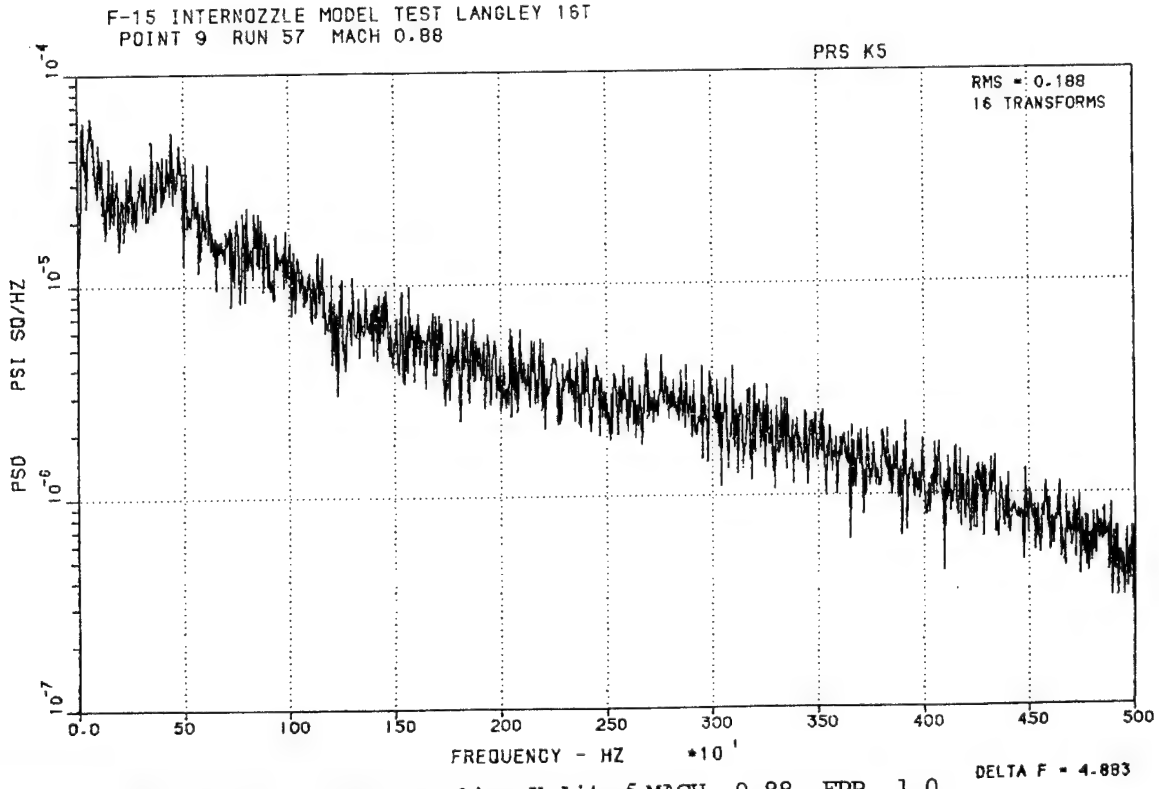

Figure 190. PSDF-Baseline Kulite 5 MACH 0.88 EPR 1.0

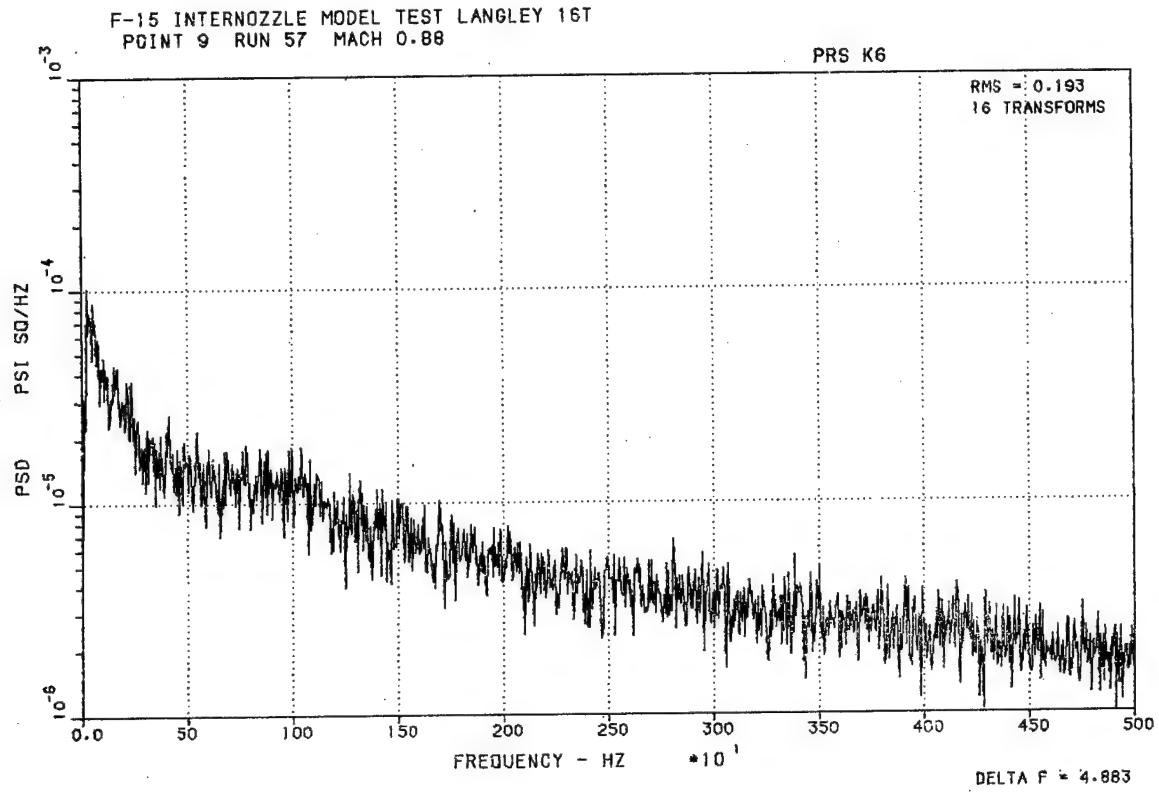

Figure 191. PSDF-Baseline Kulite 6 MACH 0.88 EPR 1.0

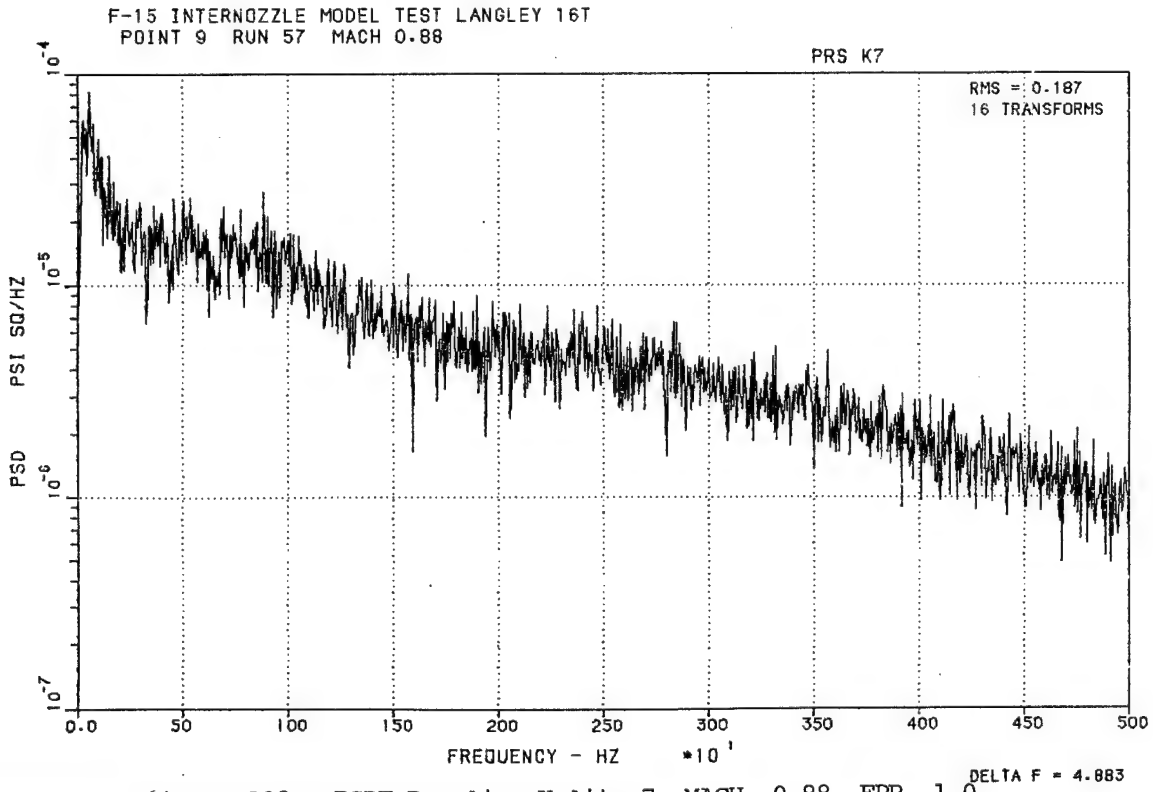

Figure 192. PSDF-Baseline Kulite 7 MACH 0.88 EPR 1.0

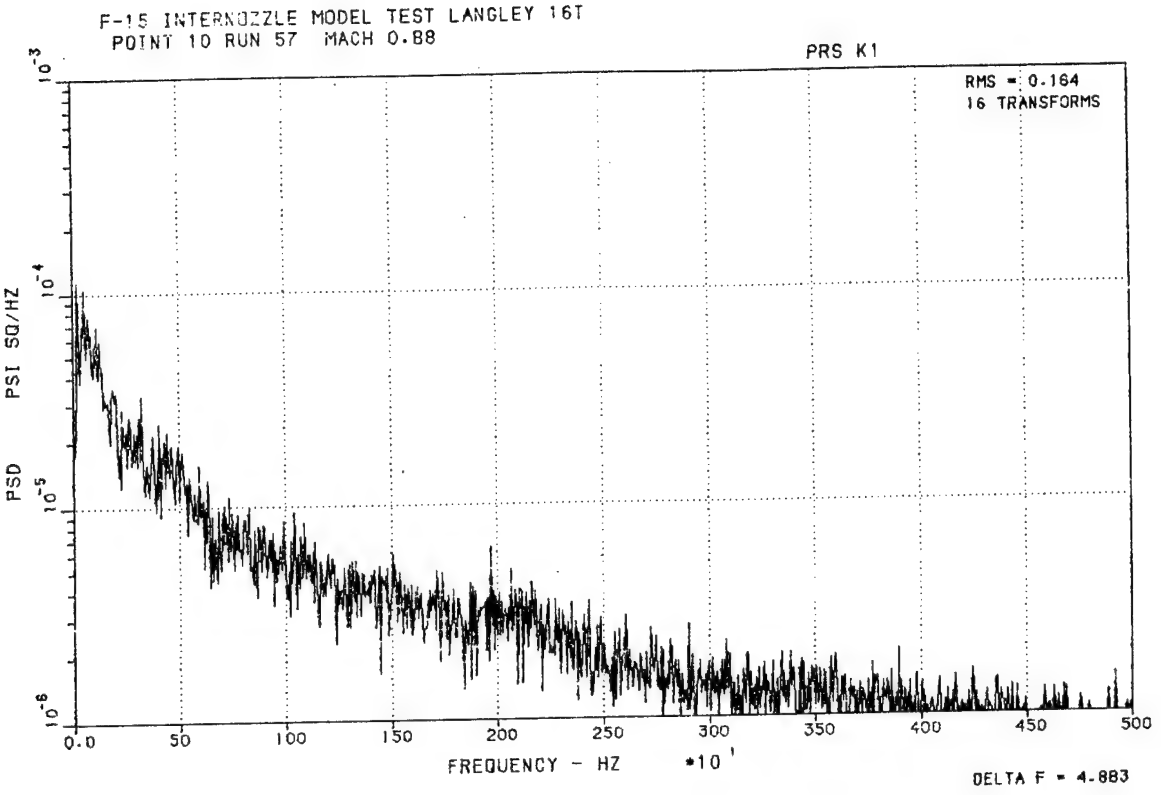

Figure 193. PSDF-Baseline Kulite 1 MACH 0.88 EPR 3.5
α 0.0

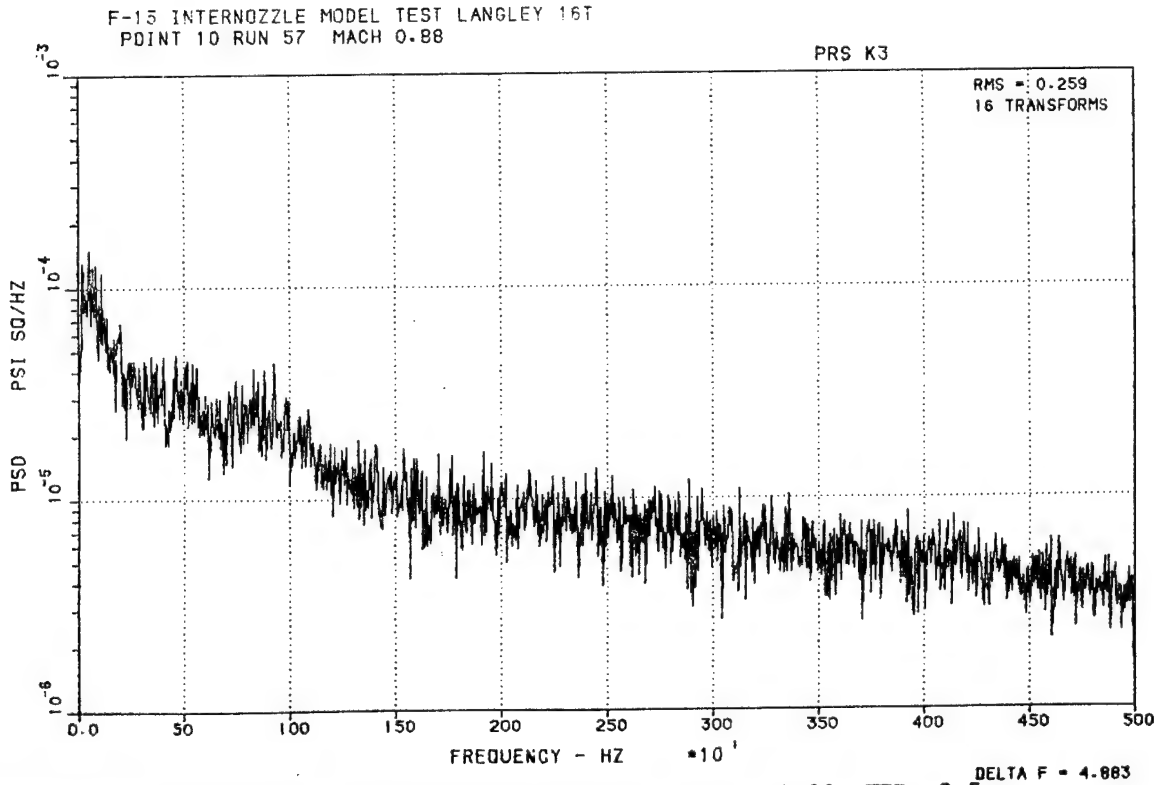

Figure 194. PSDF-Baseline Kulite 3 MACH 0.88 EPR 3.5
α 0.0

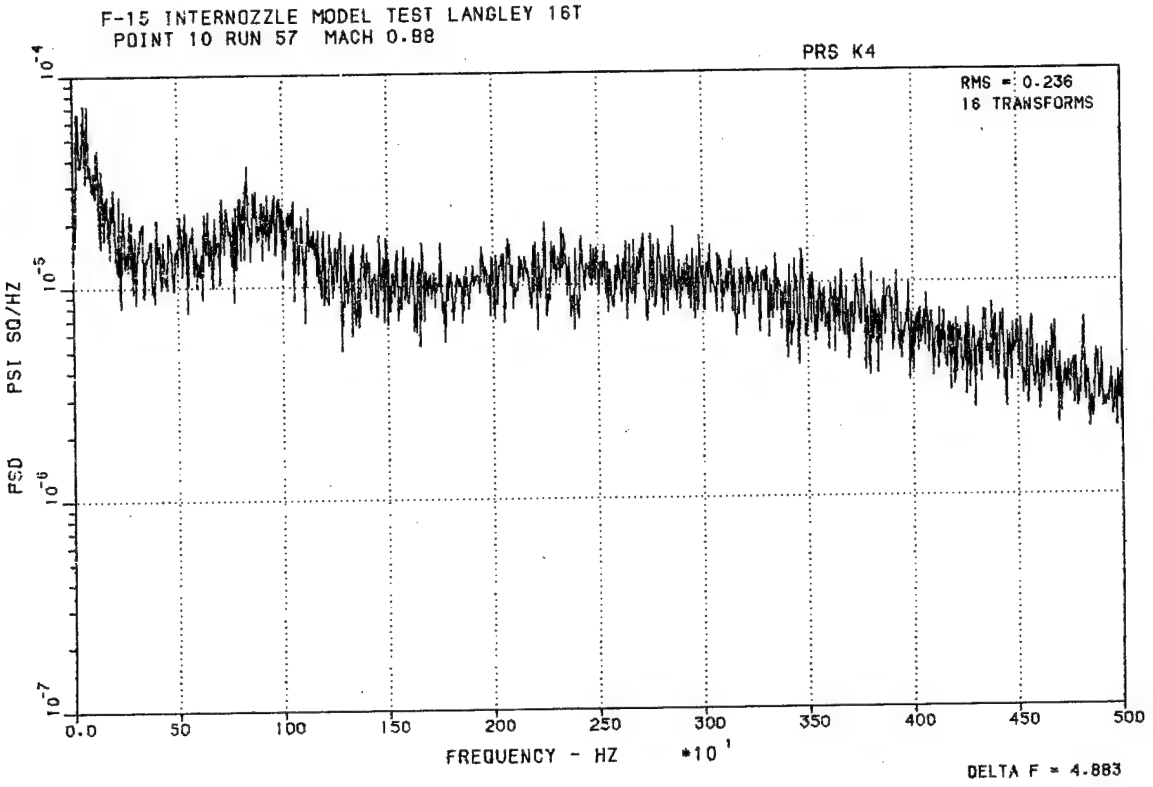

Figure 195. PSDF-Baseline Kulite 4 MACH 0.88 EPR 3.55 α 0.0

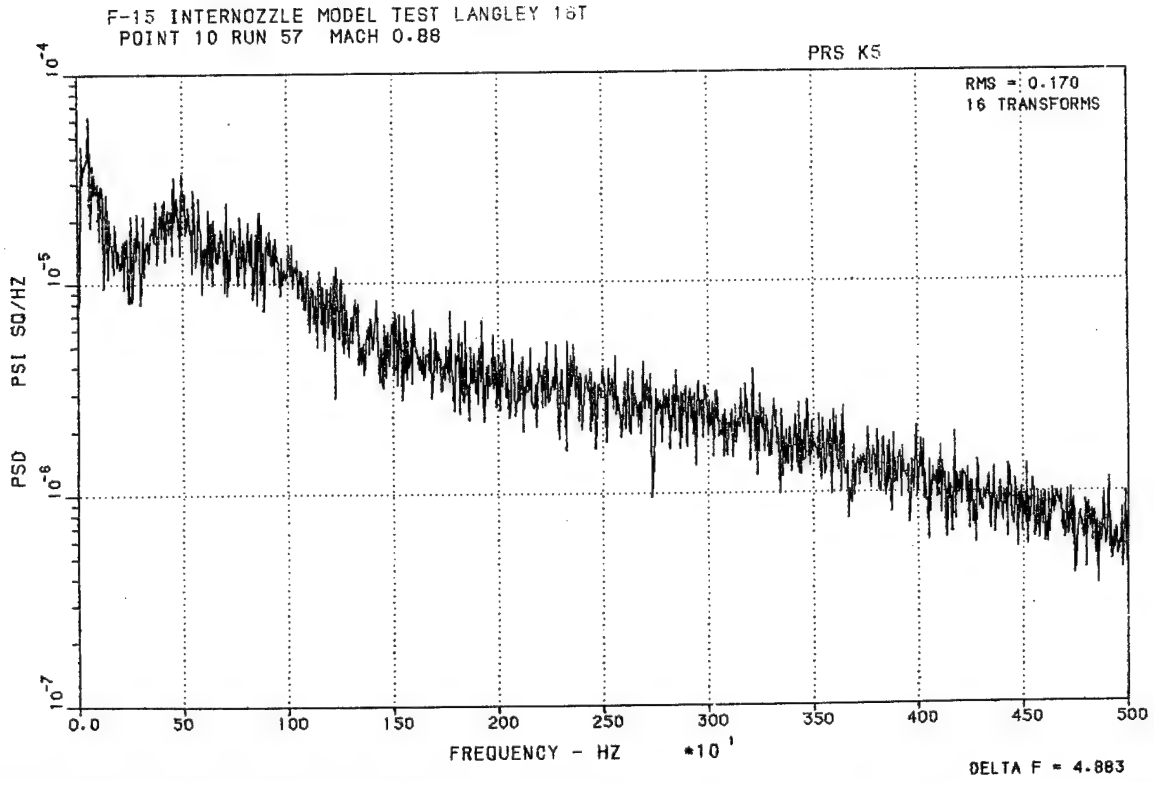

Figure 196. PSDF-Baseline Kulite 5 MACH 0.88 EPR 3.5 α 0.0

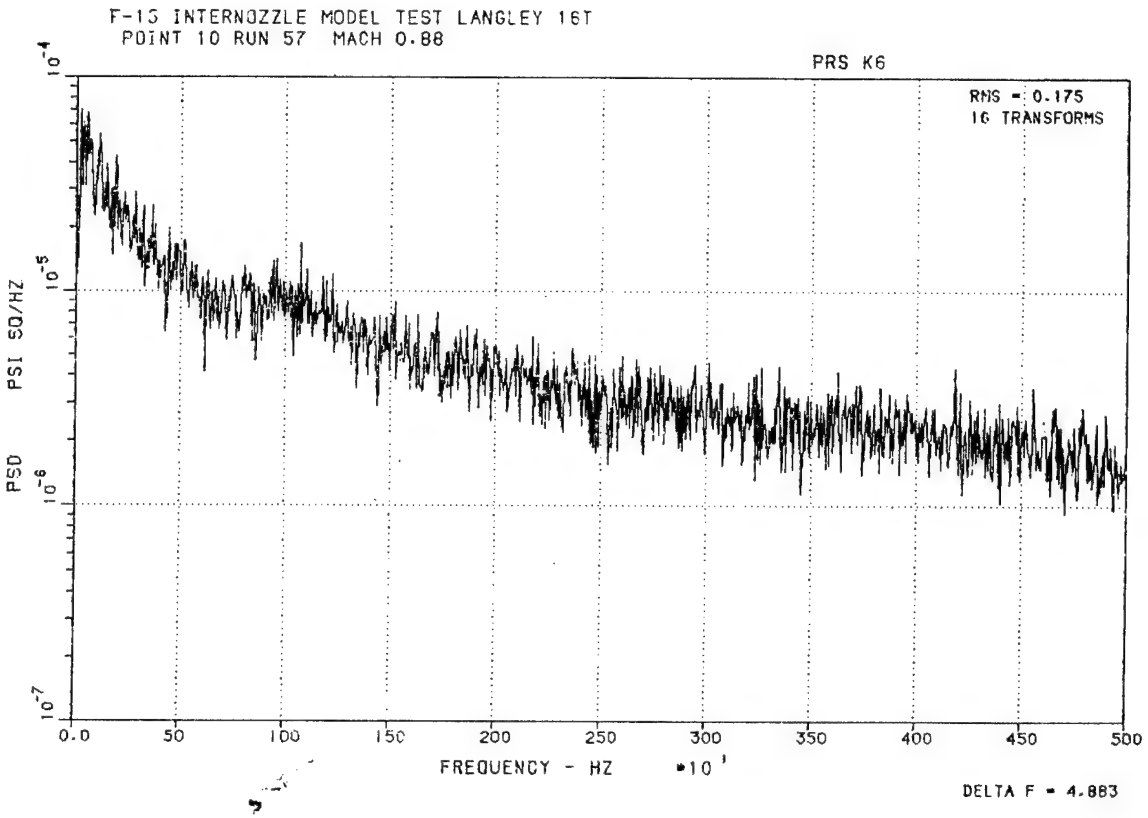

Figure 197. PSDF-Baseline Kulite 6 MACH 0.88 EPR 3.5 α 0.0

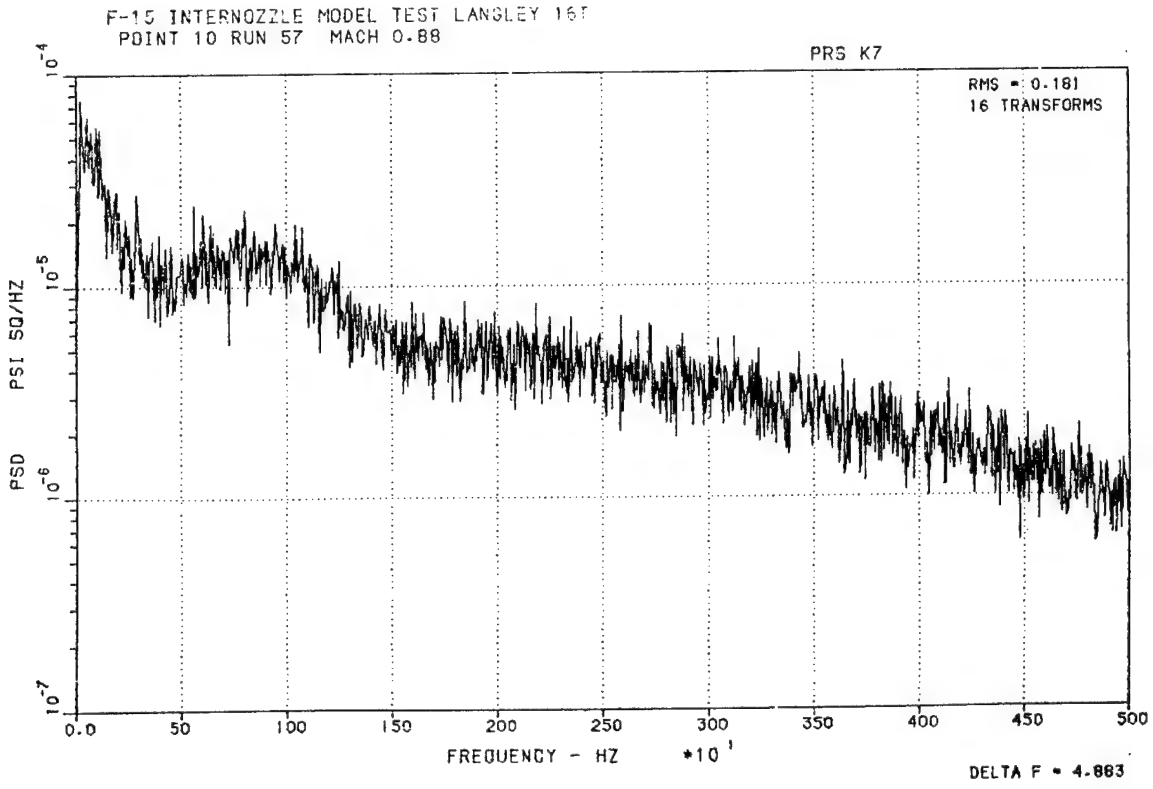

Figure 198. PSDF-Baseline Kulite 7 MACH 0.88 EPR 3.5 α 0.0

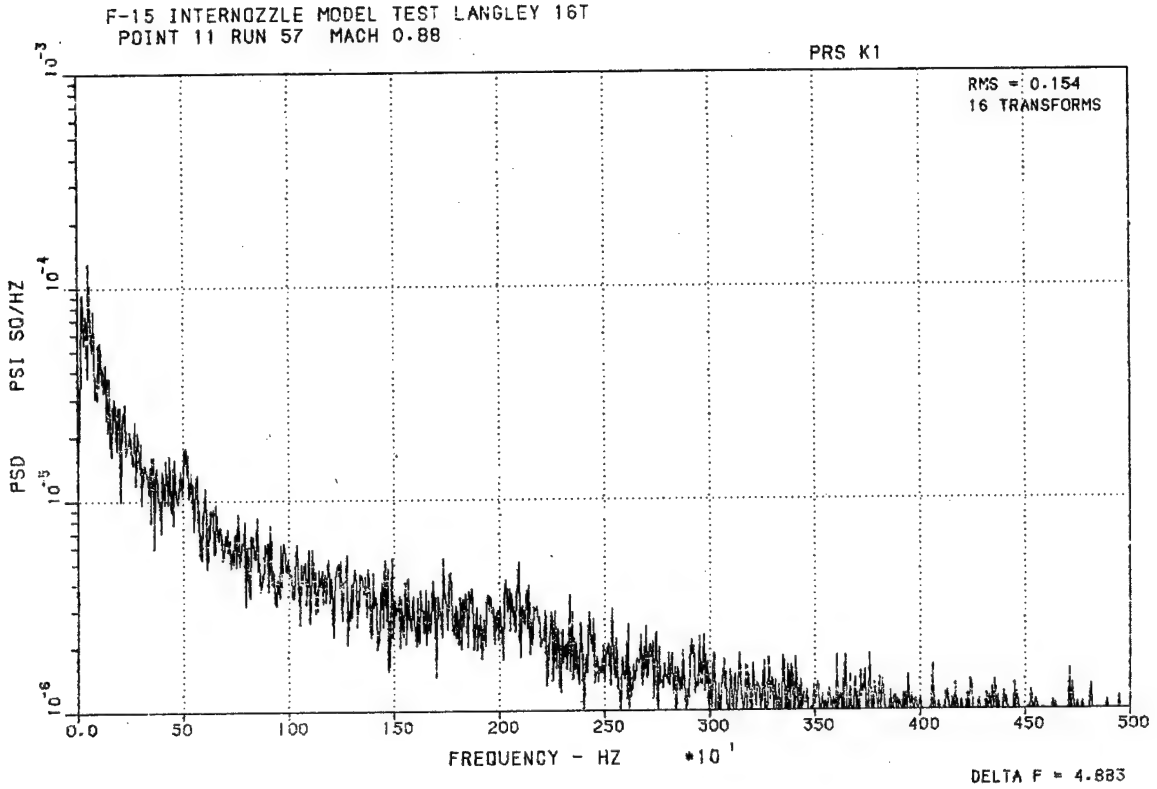

Figure 199. PSDF-Baseline Kulite 1 MACH 0.88 EPR 5.0 α 0.0

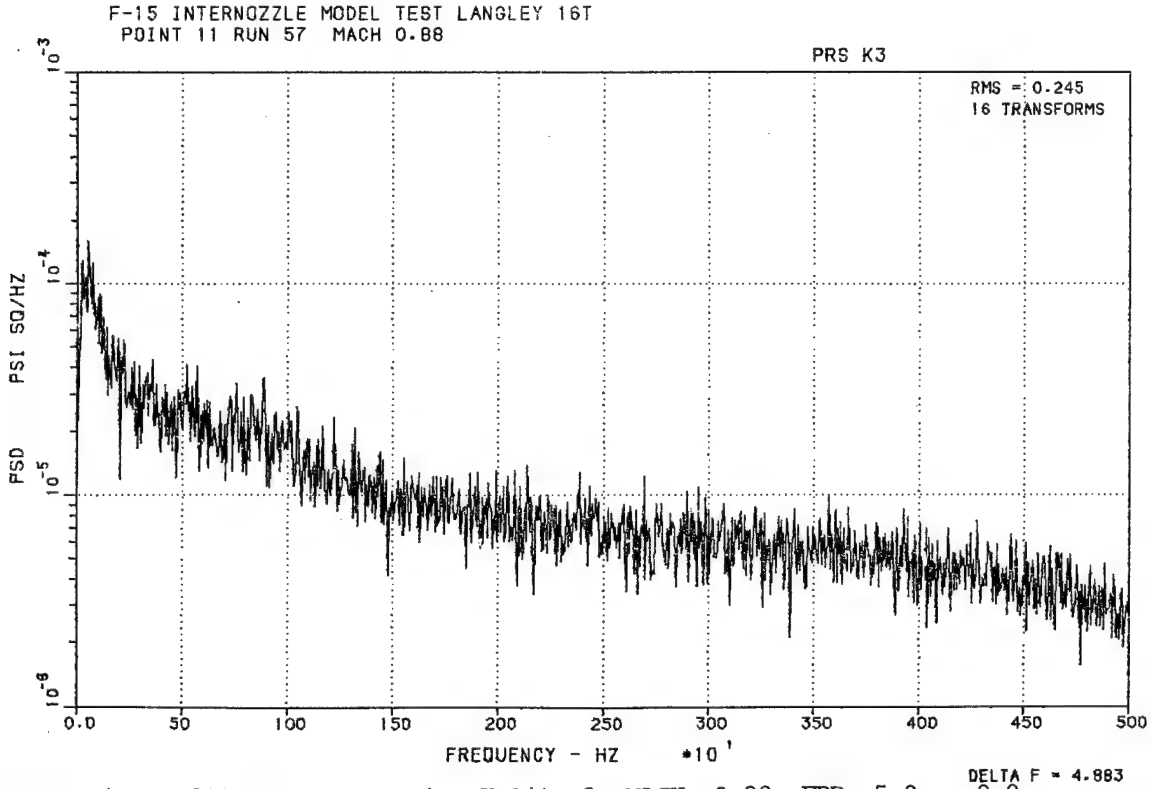

Figure 200. PSDF-Baseline Kulite 3 MACH 0.88 EPR 5.0 α 0.0

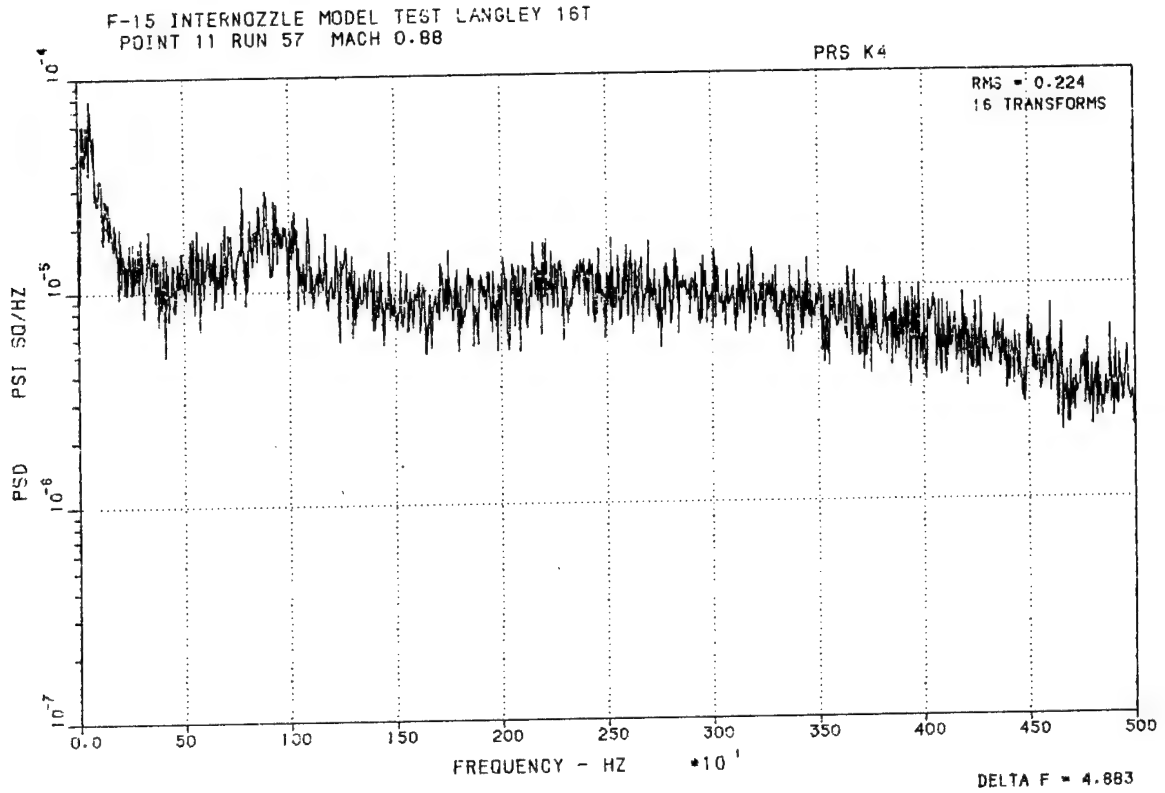

Figure 201. PSDF-Baseline Kulite 4 MACH 0.88 EPR 5.0 α 0.0

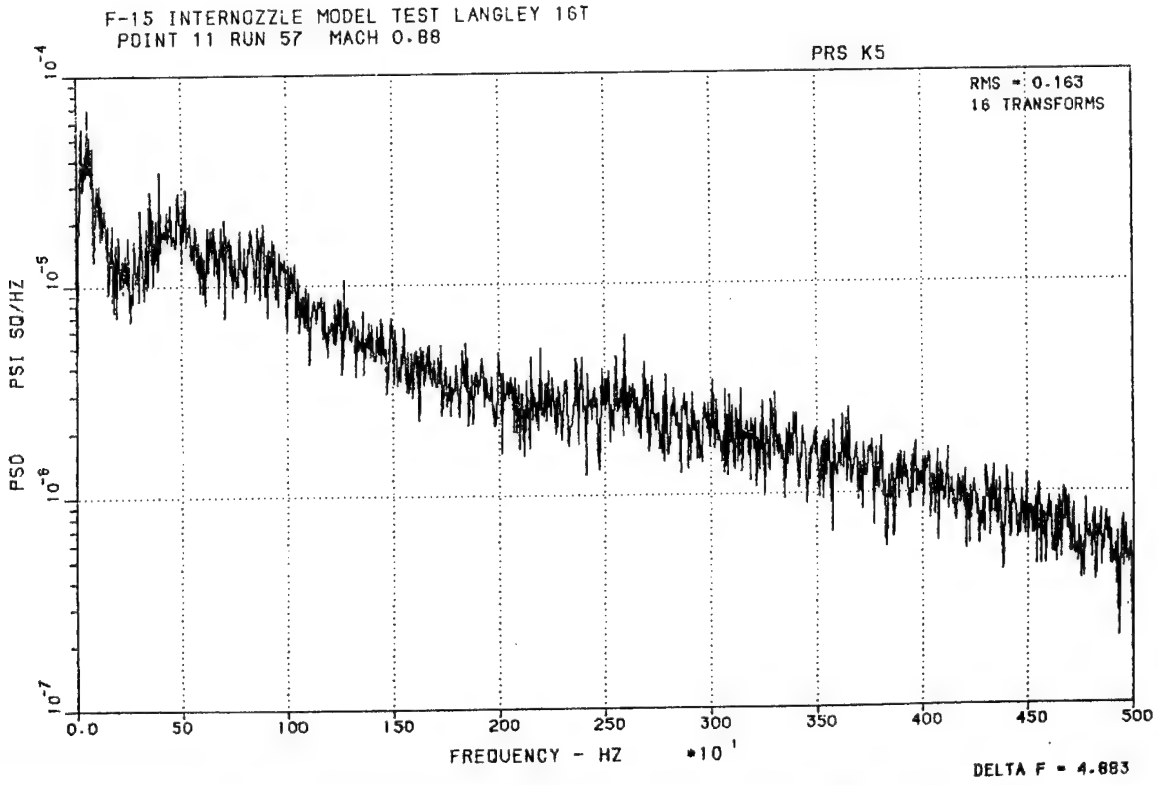

Figure 202. PSDF-Baseline Kulite 5 MACH 0.88 EPR 5.0 α 0.0

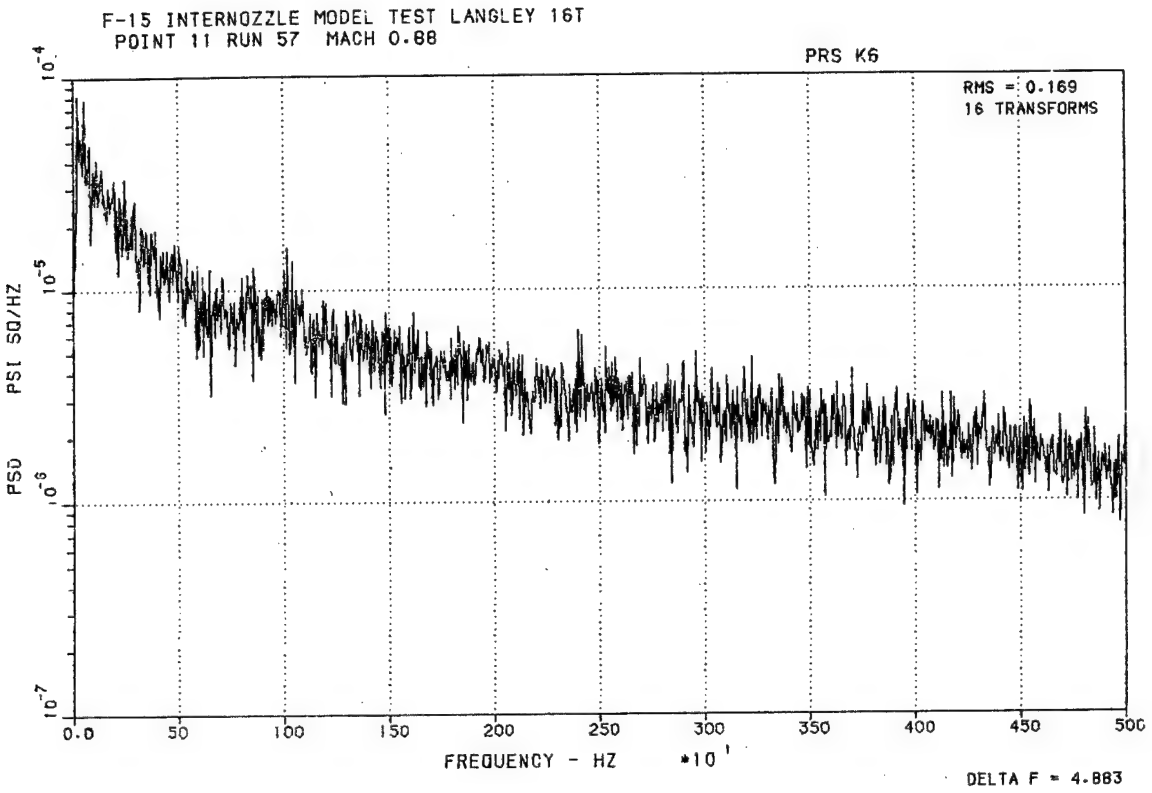

Figure 203. PSDF-Baseline Kulite 6 MACH 0.88 EPR 5.0 α0.0

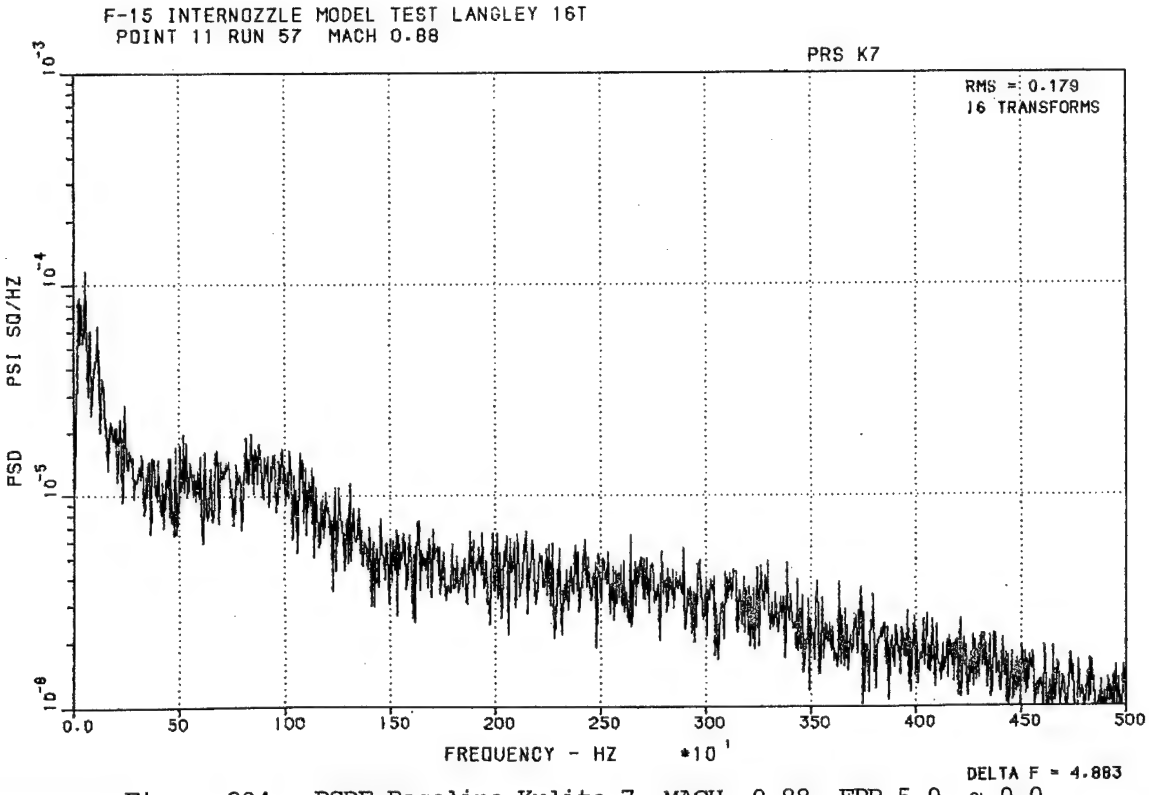

Figure 294. PSDF-Baseline Kulite 7 MACH 0.88 EPR 5.0 α 0.0

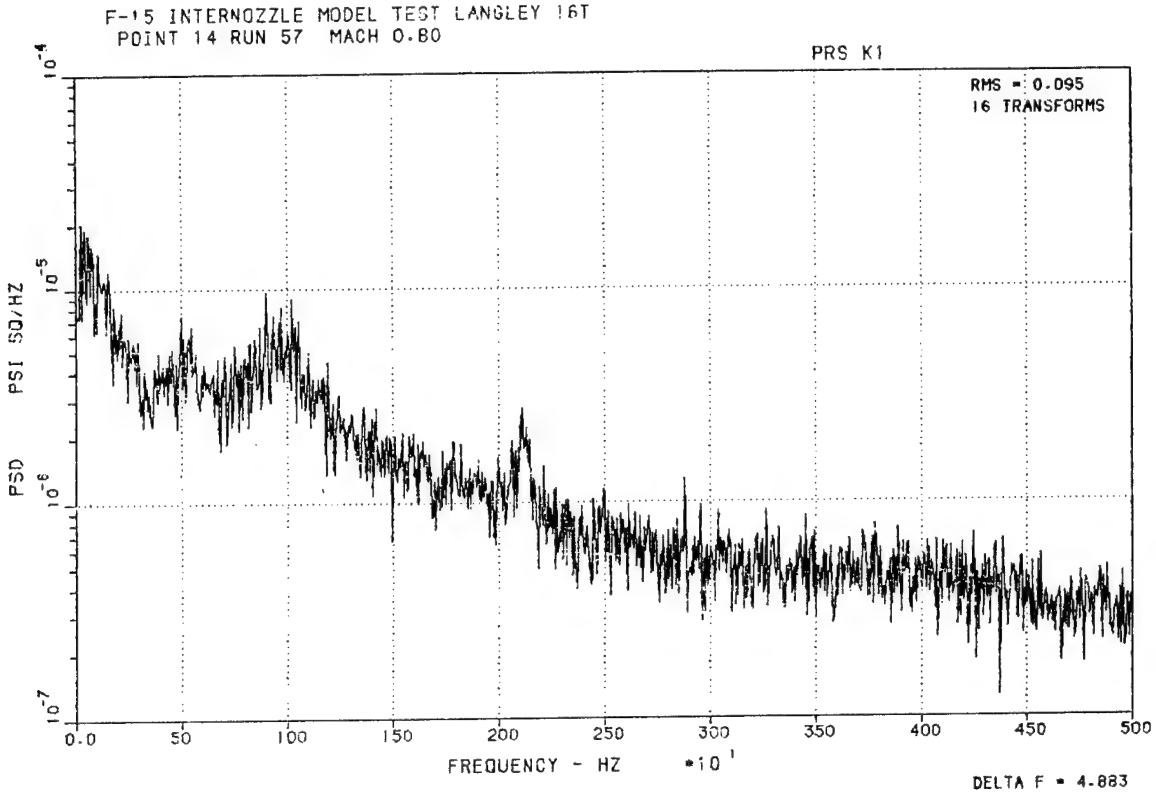

Figure 205. PSDF-Baseline Kulite 1 MACH 0.8 EPR 3.5 α0.0

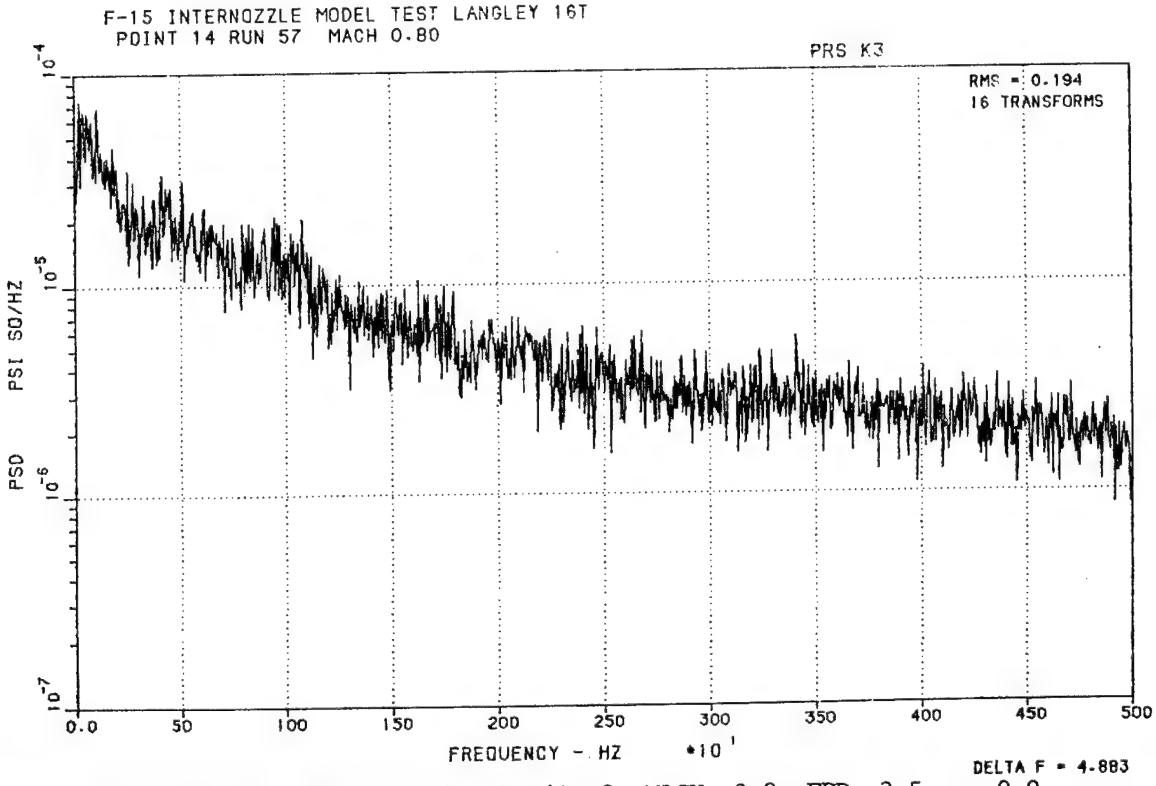

Figure 206. PSDF-Baseline Kulite 3 MACH 0.8 EPR 3.5 α 0.0

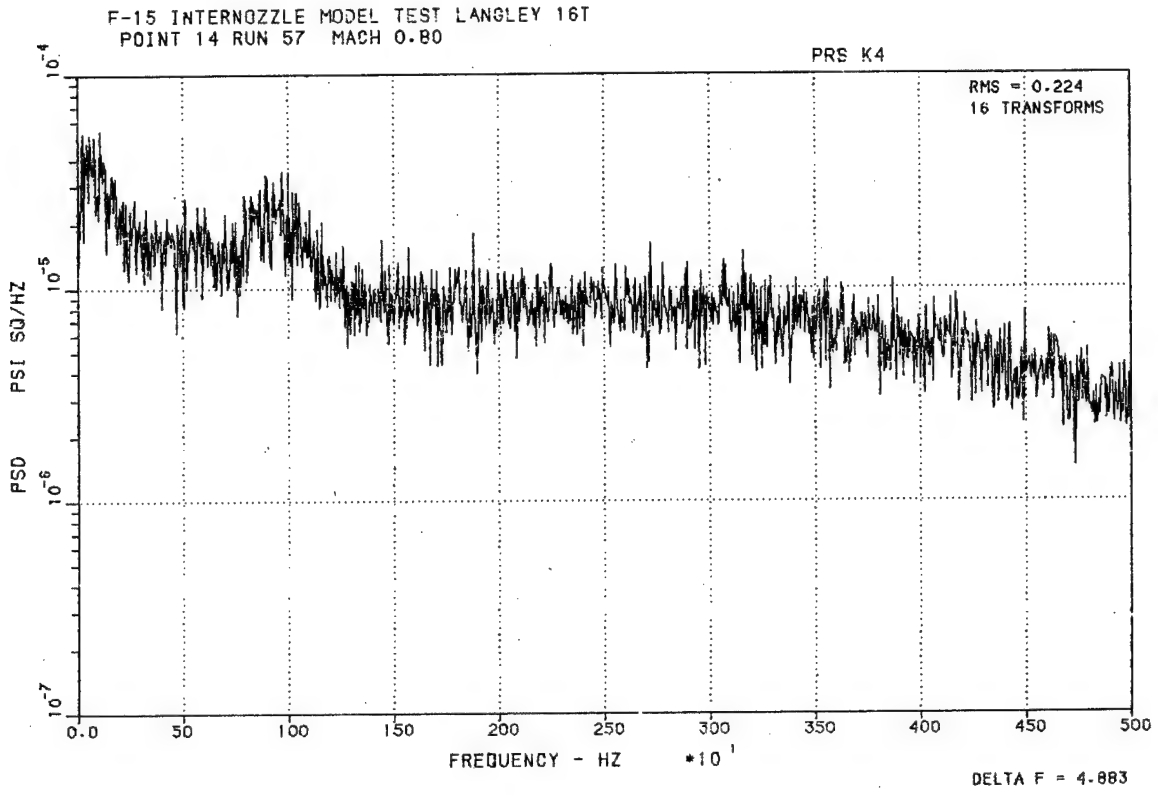

Figure 207. PSDF-Baseline Kulite 4 MACH 0.80 EPR 3.5 α 0.0

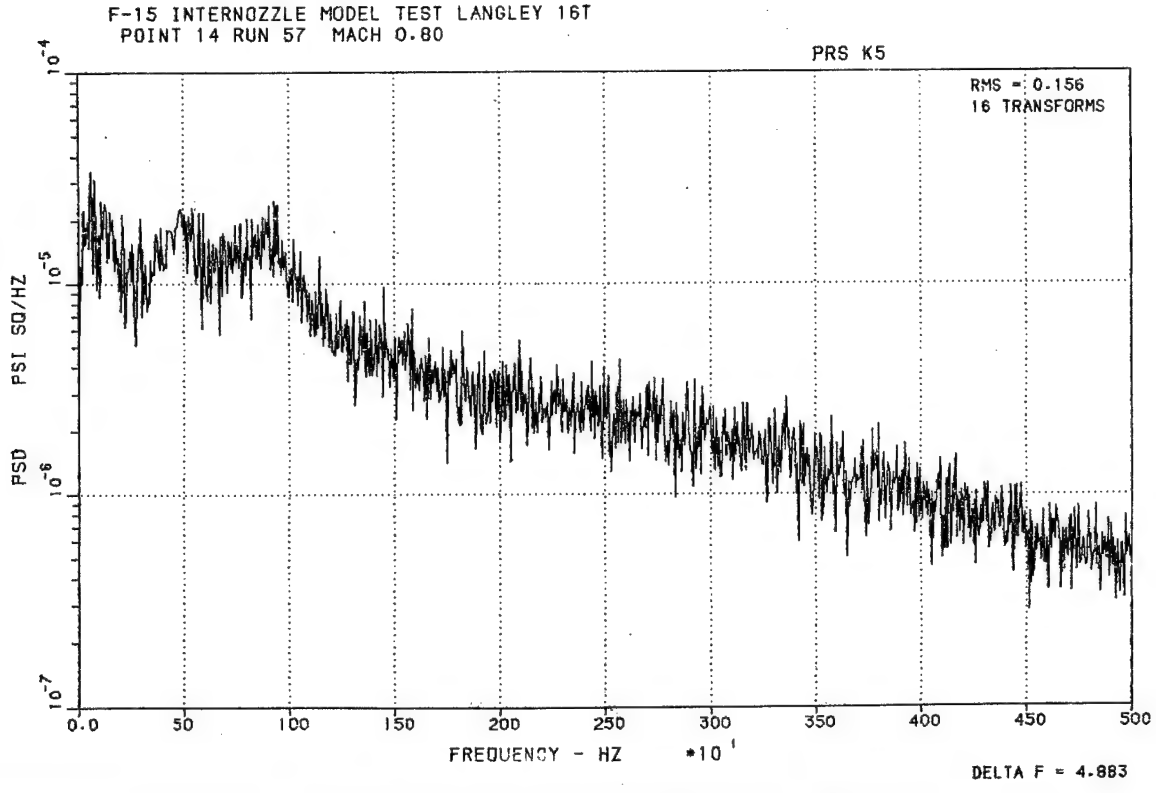

Figure 208. PSDF-Baseline Kulite 5 MACH 0.80 EPR 3.5 α 0.0

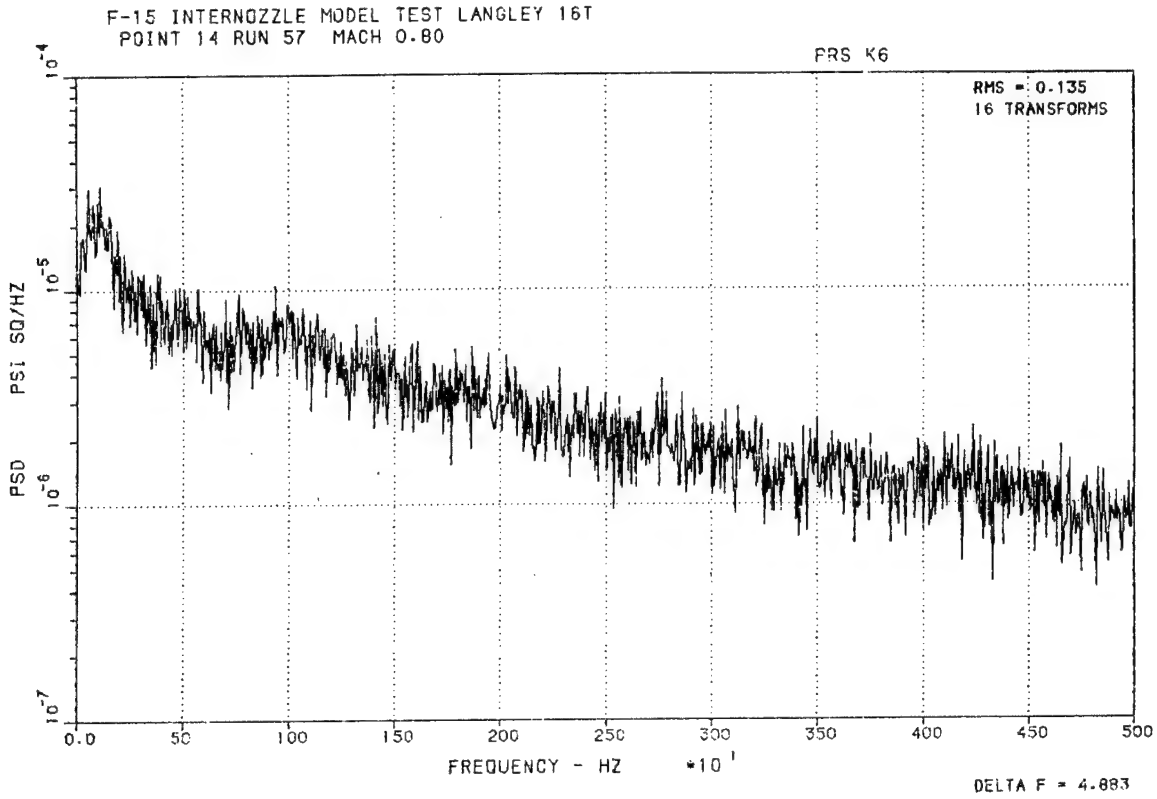

Figure 209. PSDF-Baseline Kulite 6 MACH 0.80 EPR 3.5 α 0.0

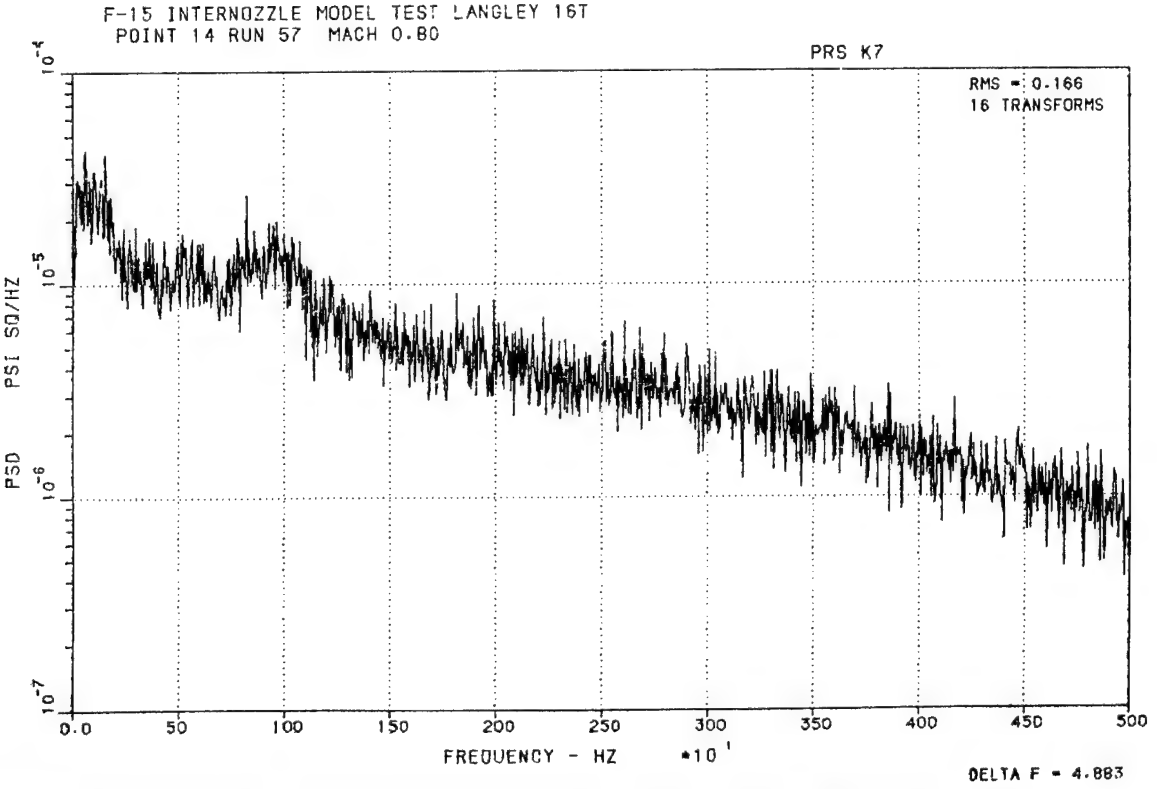

Figure 210. PSDF-Baseline Kulite 7 MACH 0.80 EPR 3.5 α 0.0

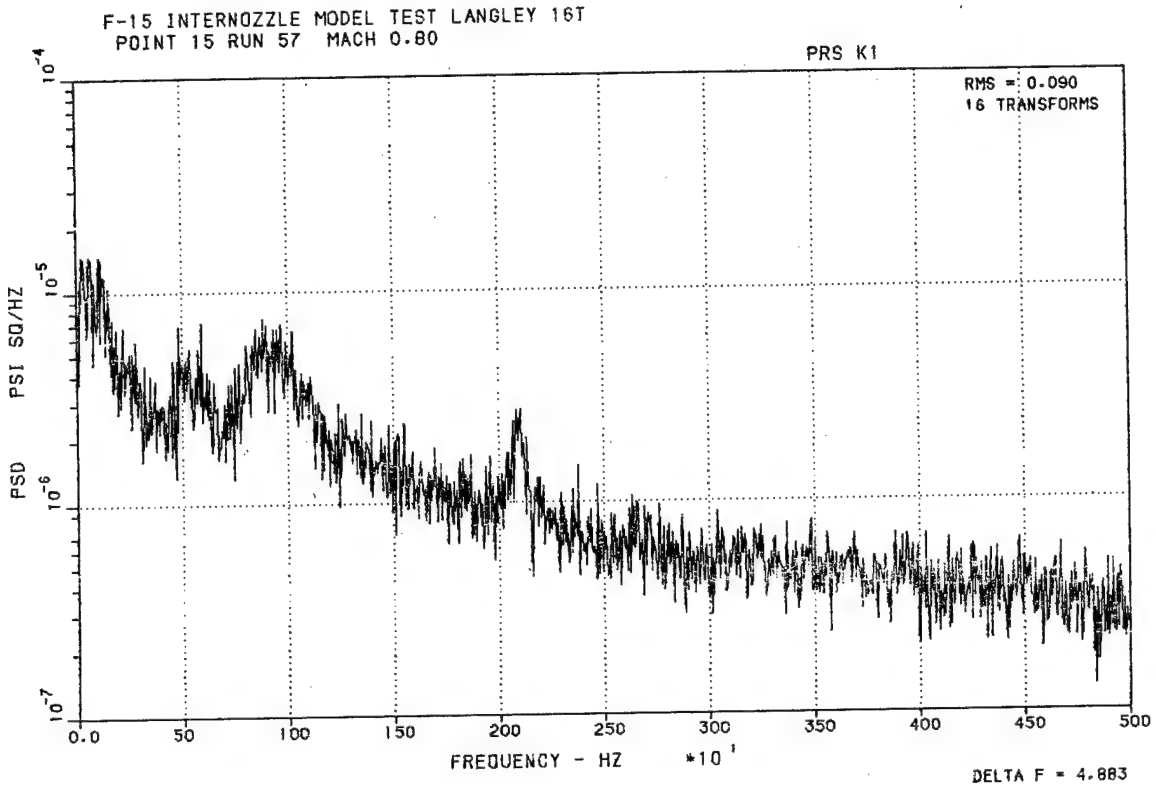

Figure 211. PSDF-Baseline Kulite 1 MACH 0.80 EPR 5.0 α 0.0

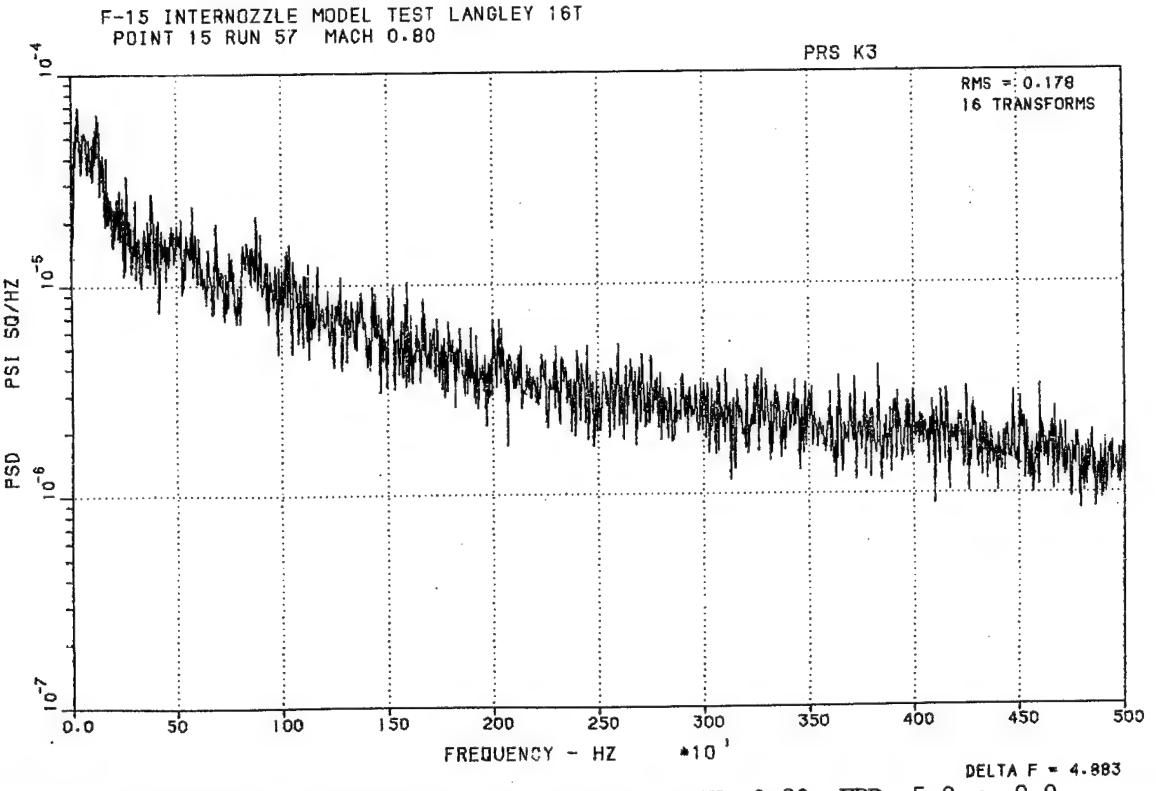

Figure 212. PSDF-Baseline Kulite 3 MACH 0.80 EPR 5.0 α 0.0

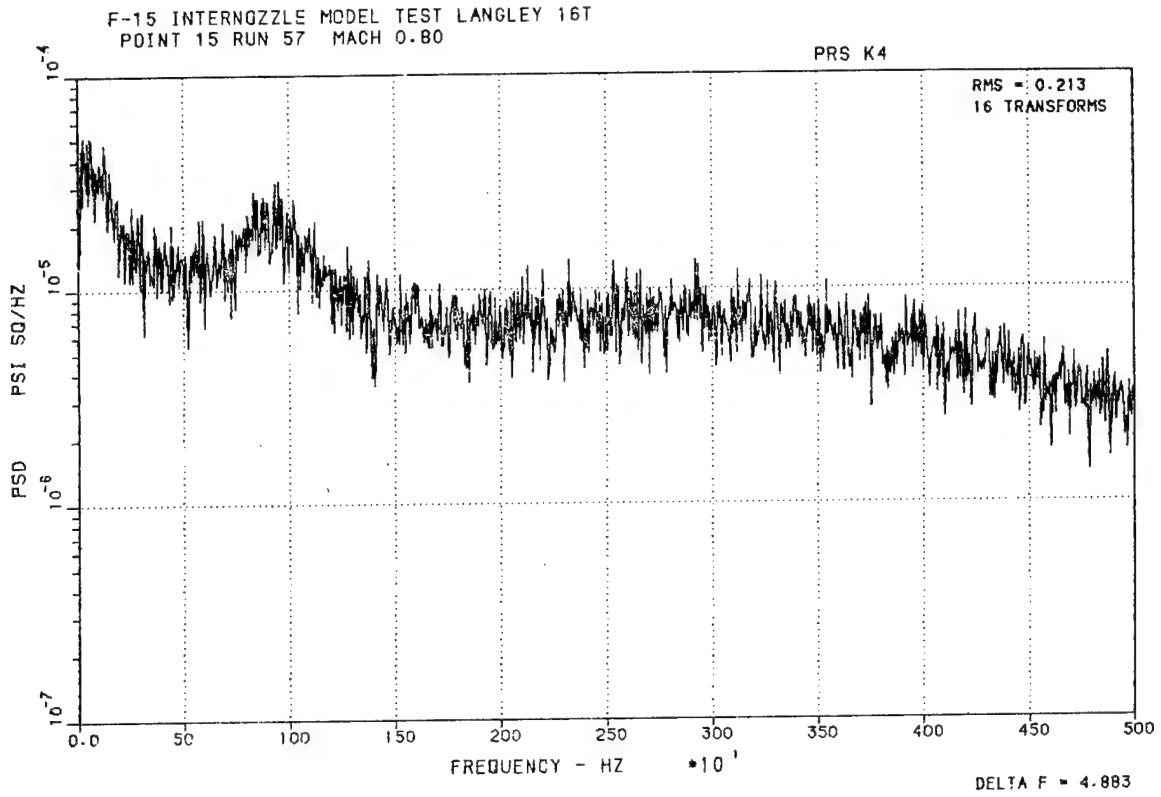

Figure 213. PSDF-Baseline Kulite 4 MACH 0.80 EPR 5.0 α 0.0

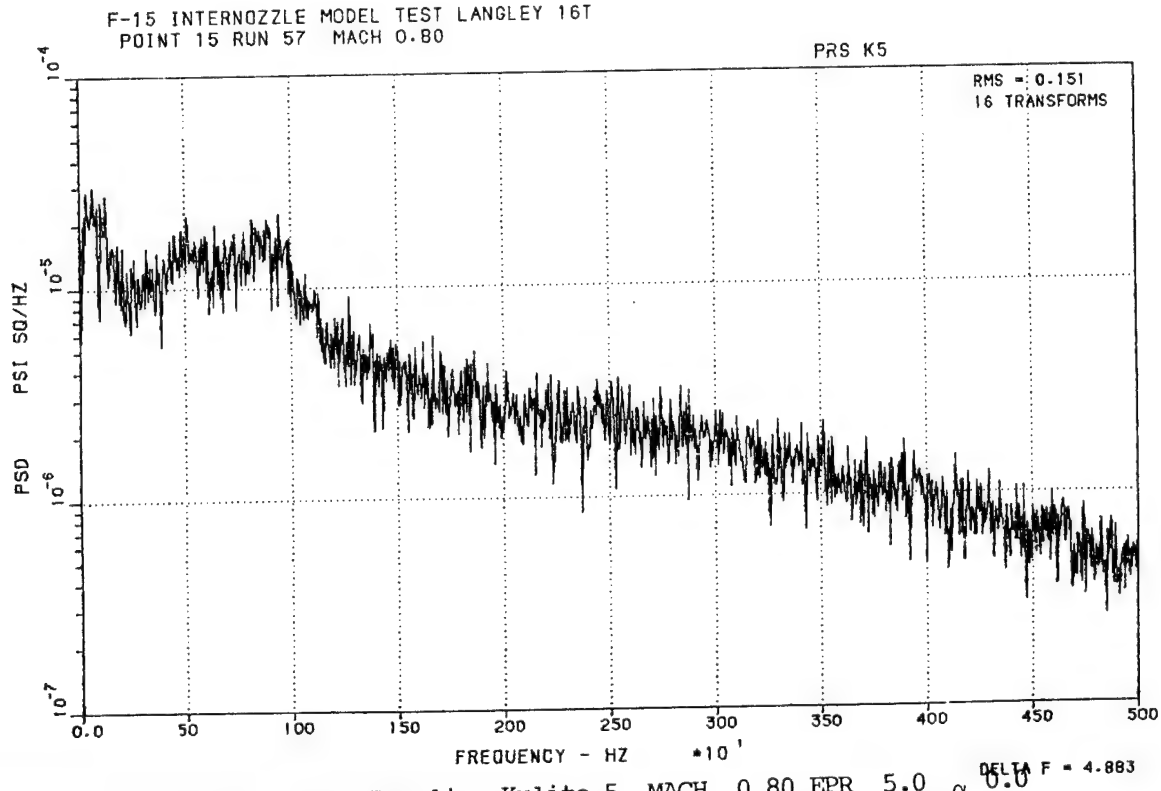

Figure 214. PSDF-Baseline Kulite 5 MACH 0.80 EPR 5.0 α 0.0

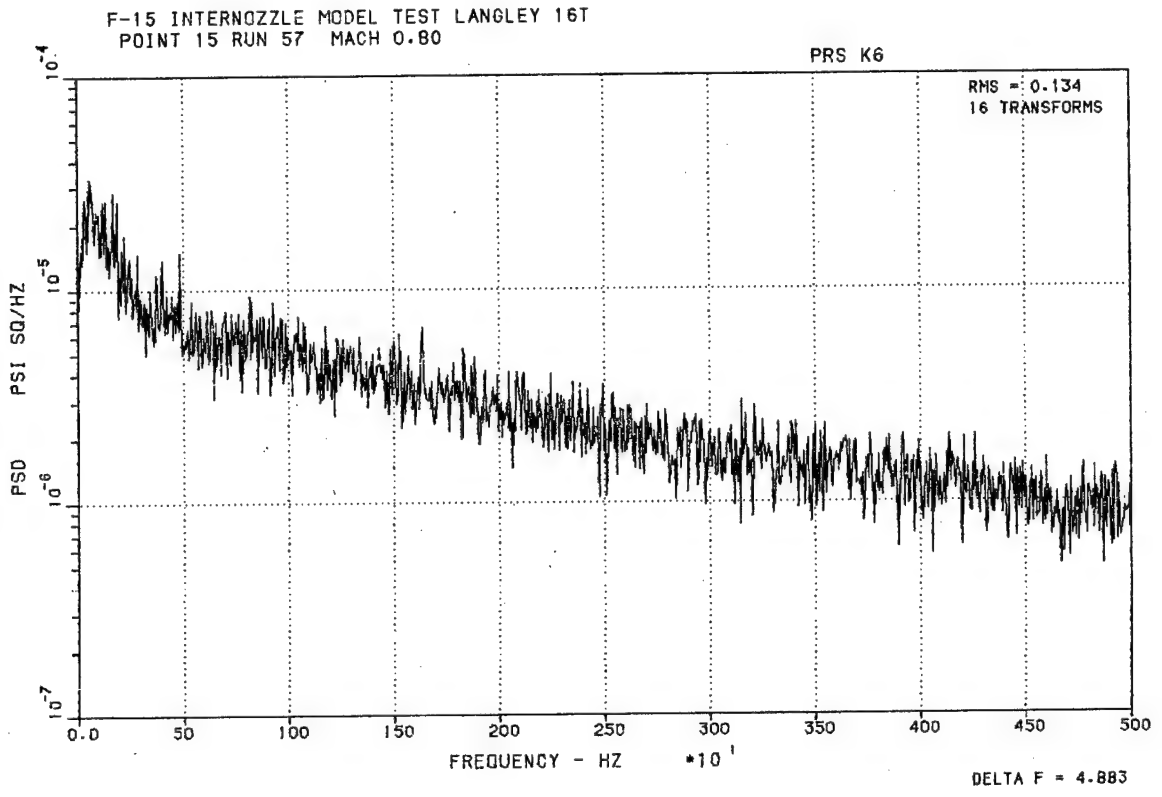

Figure 215. PSDF-Baseline Kulite 6 MACH 0.80 EPR 5.0 α0.0

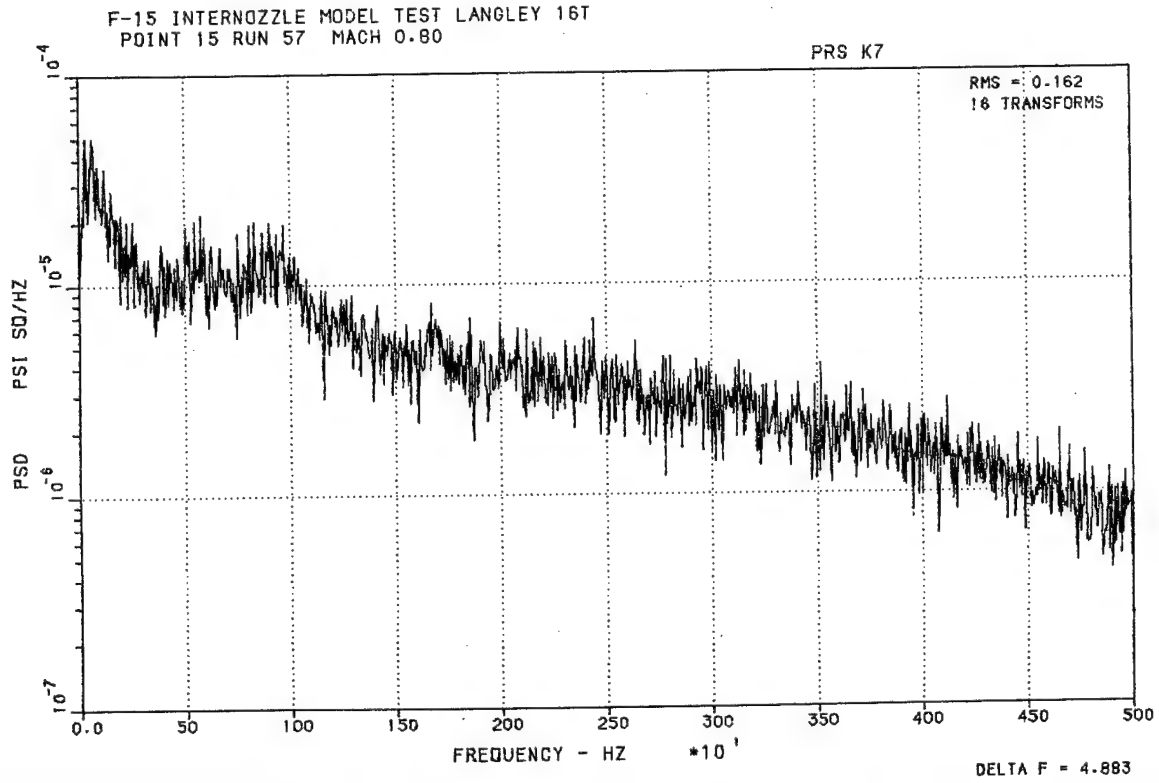

Figure 216. PSDF-Baseline Kulite 7 MACH 0.80 EPR 5.0 α0.0

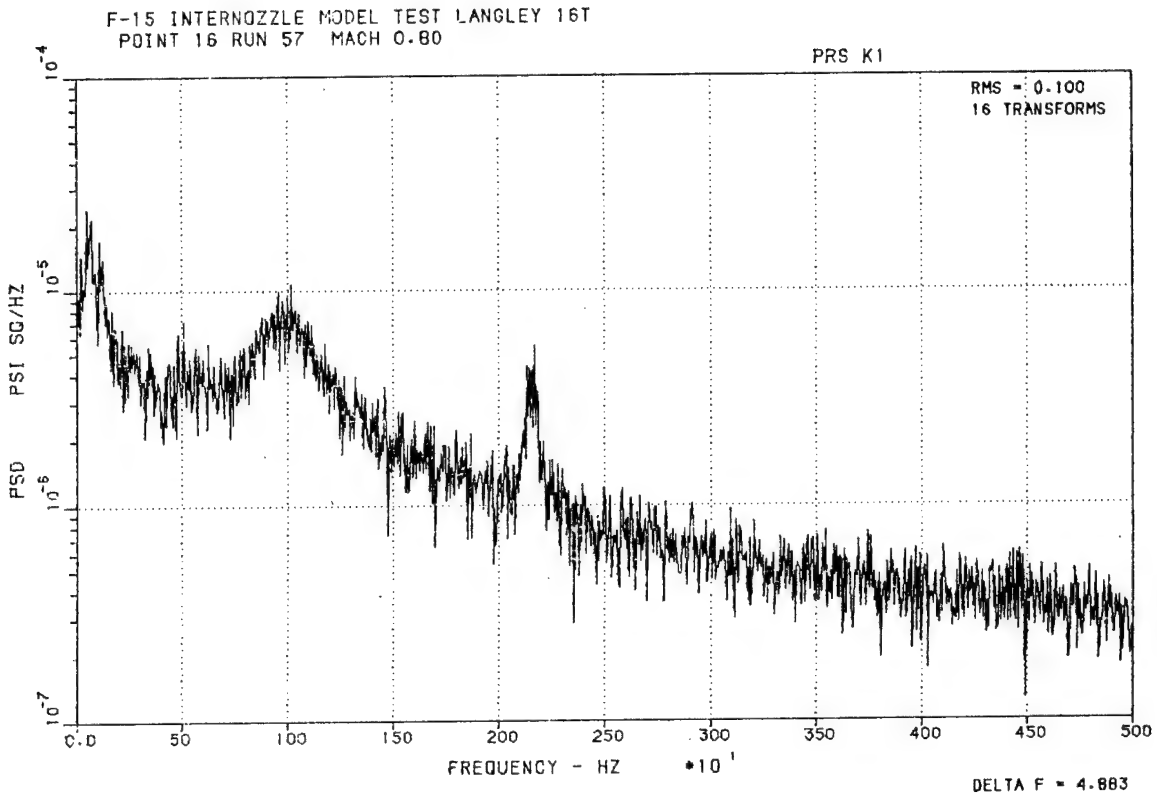

Figure 217. PSDF-Baseline Kulite 1 MACH 0.80 EPR 1.0 α 0.0

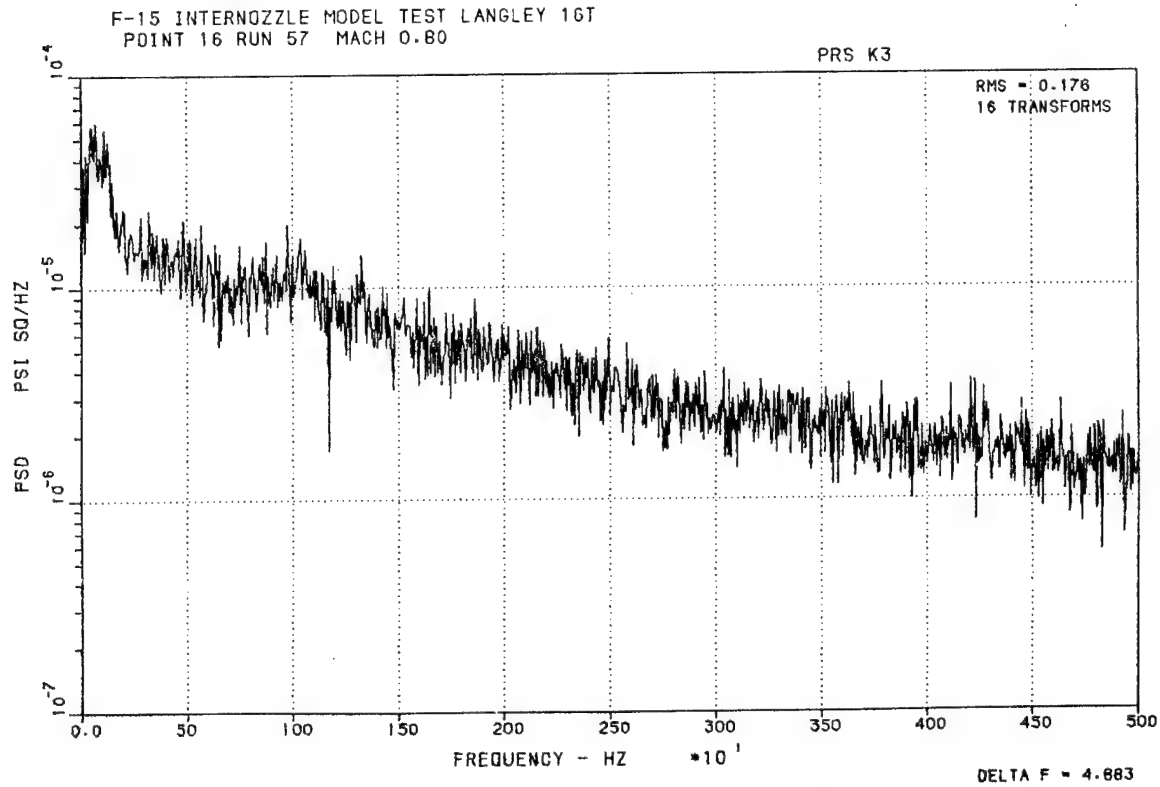

Figure 218. PSDF-Baseline Kulite 3 MACH 0.80 EPR 1.0 α 0.0

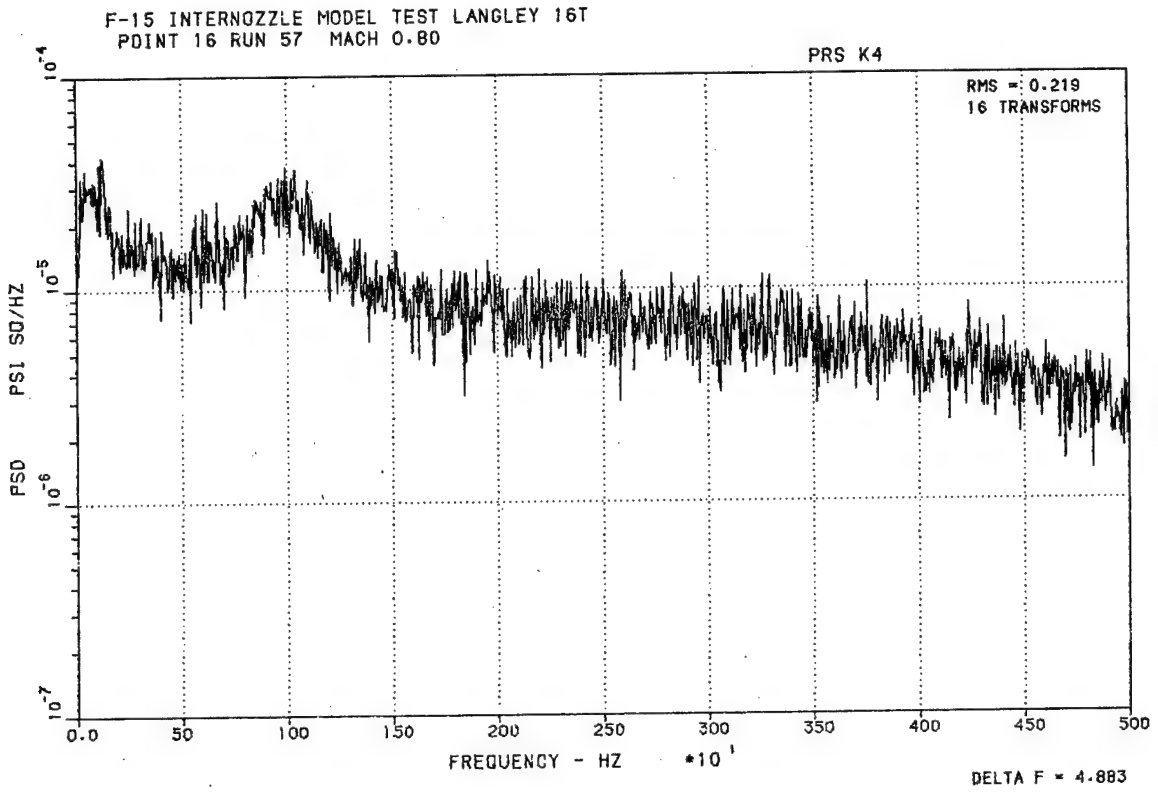

Figure 219. PSDF-Baseline Kulite 4 MACH 0.80 EPR 1.0 α 0.0

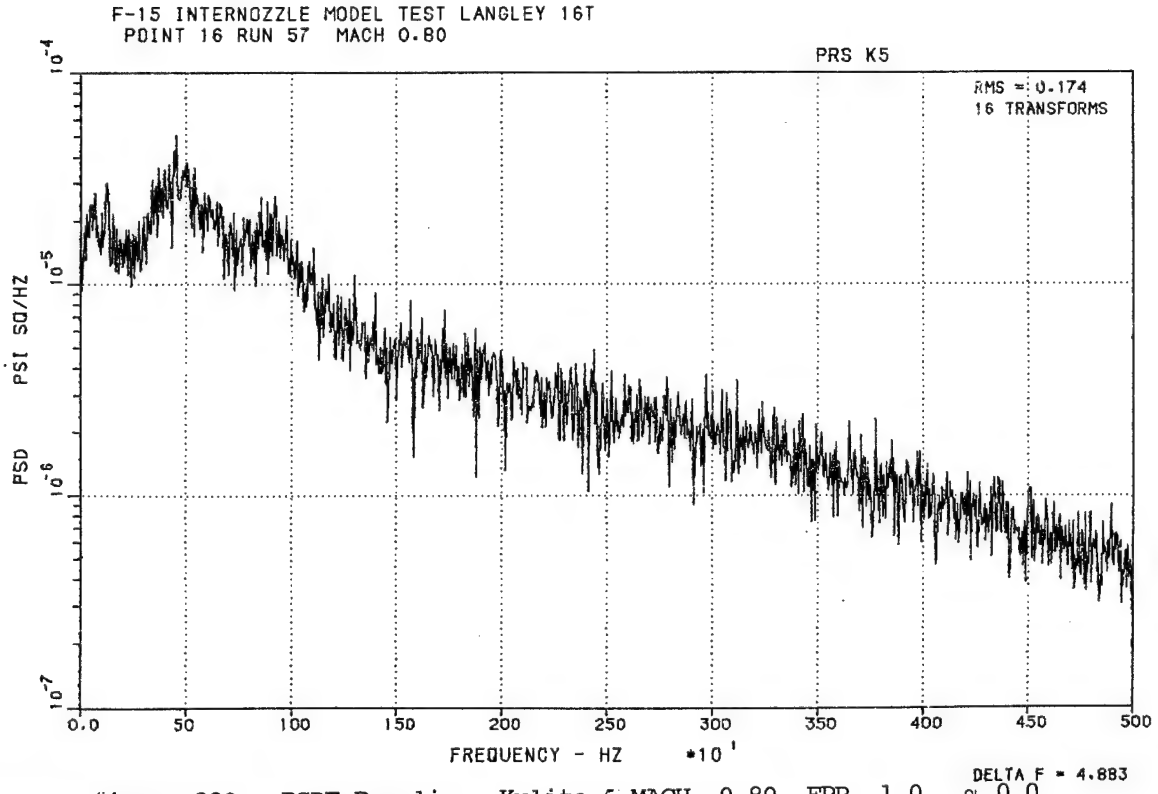

Figure 220. PSDF-Baseline Kulite 5 MACH 0.80 EPR 1.0 α 0.0

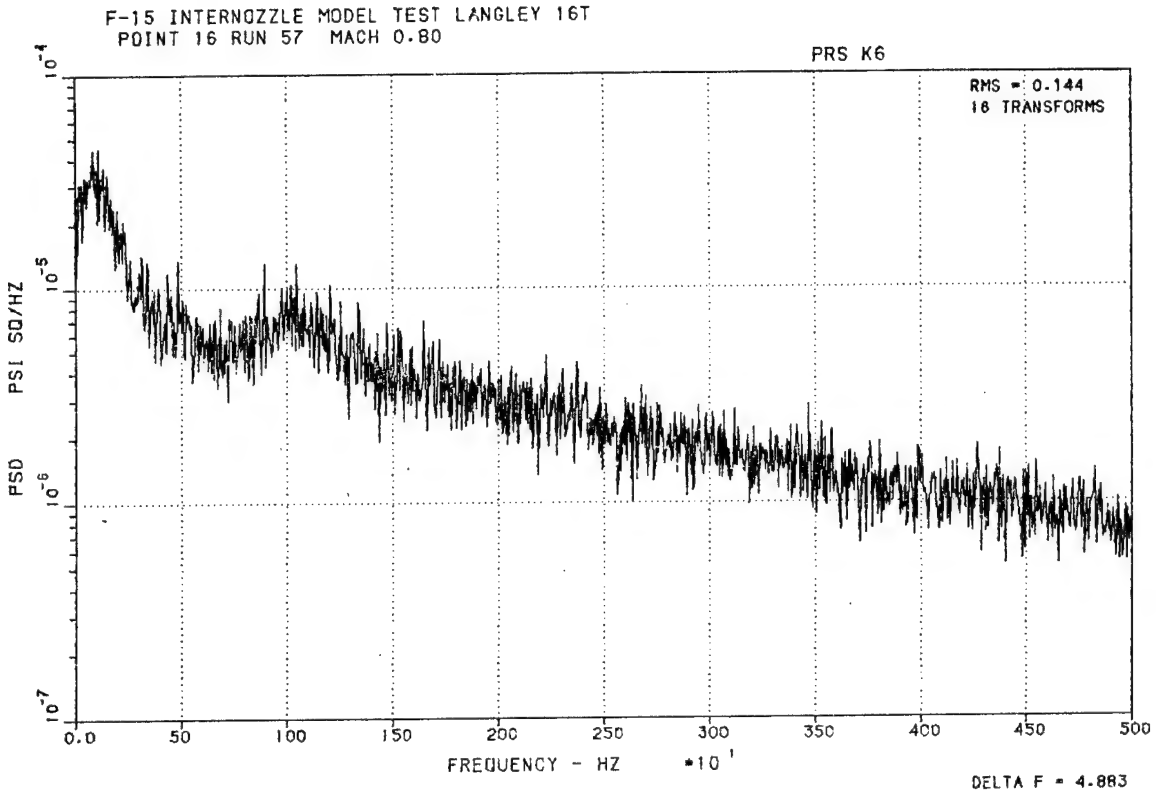

Figure 221. PSDF-Baseline Kulite 6 MACH 0.80 EPR 1.0 α 0.0

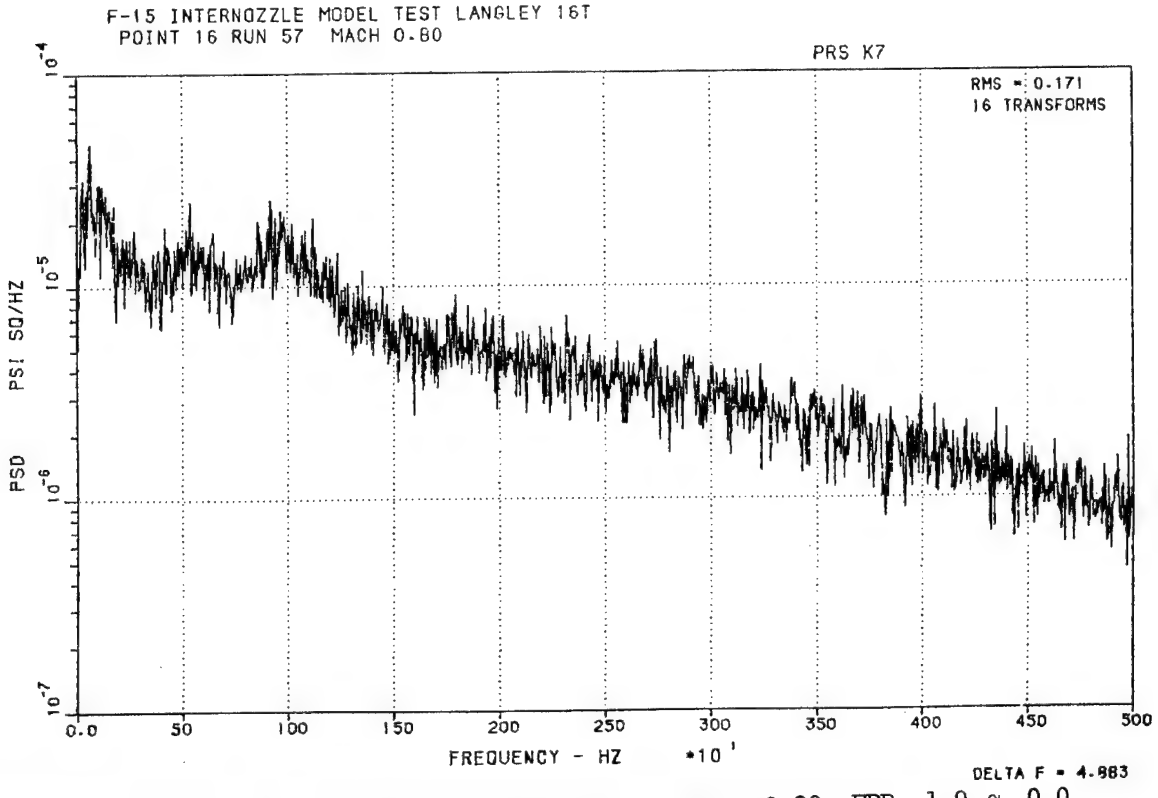

Figure 222. PSDF-Baseline Kulite 7 MACH 0.80 EPR 1.0 α 0.0

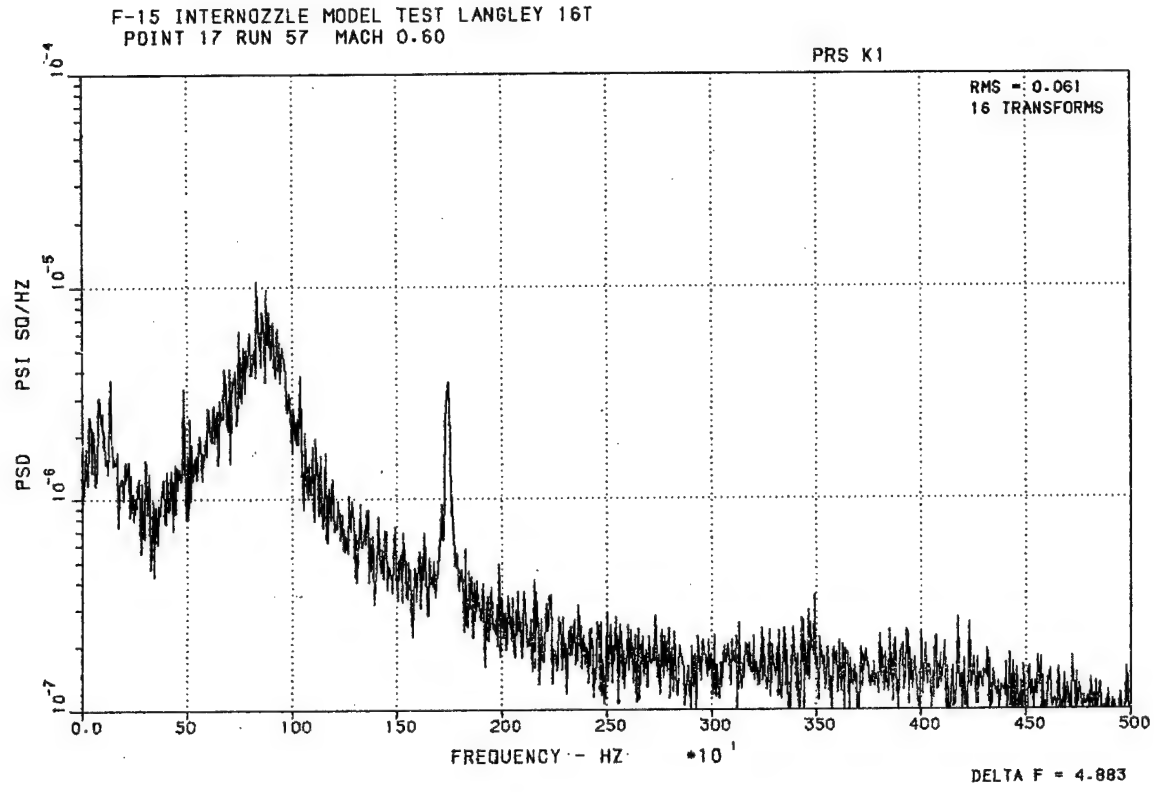

Figure 223. PSDF-Baseline Kulite 1 MACH 0.6 EPR 1.0 α 0.0

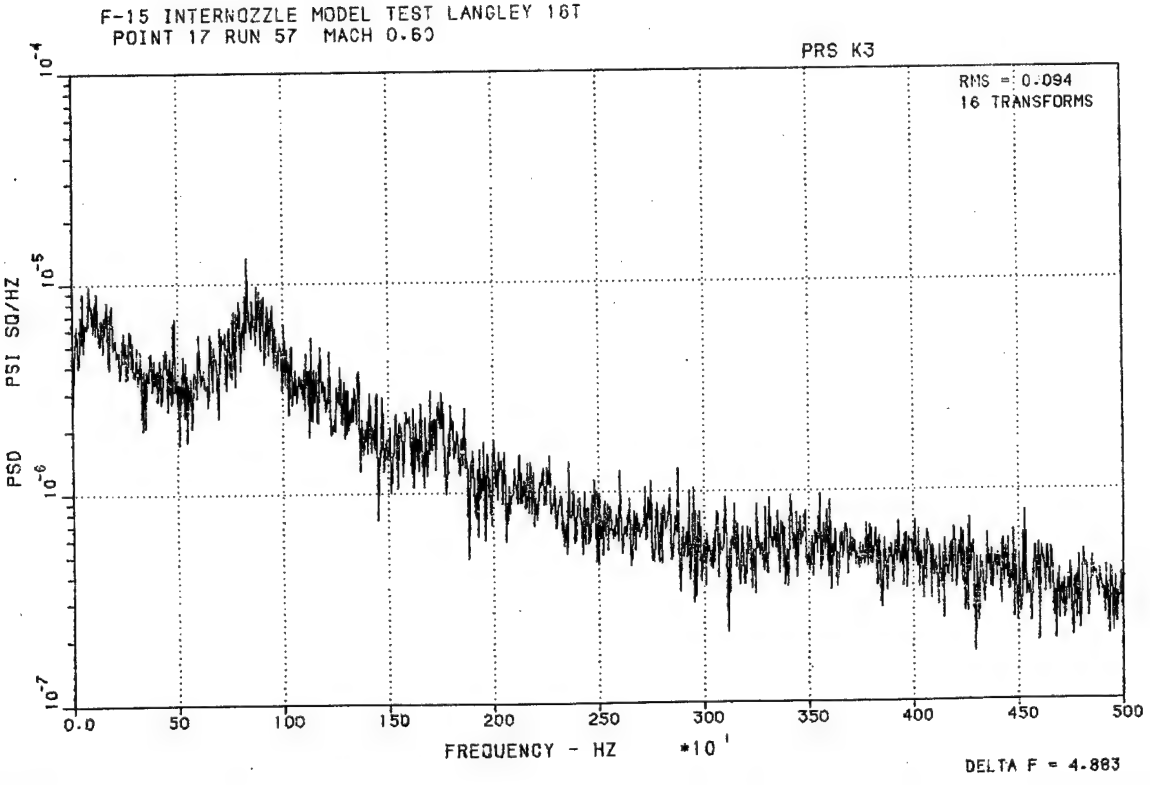

Figure 224. PSDF-Baseline Kulite 3 MACH 0.6 EPR 1.0 α 0.0

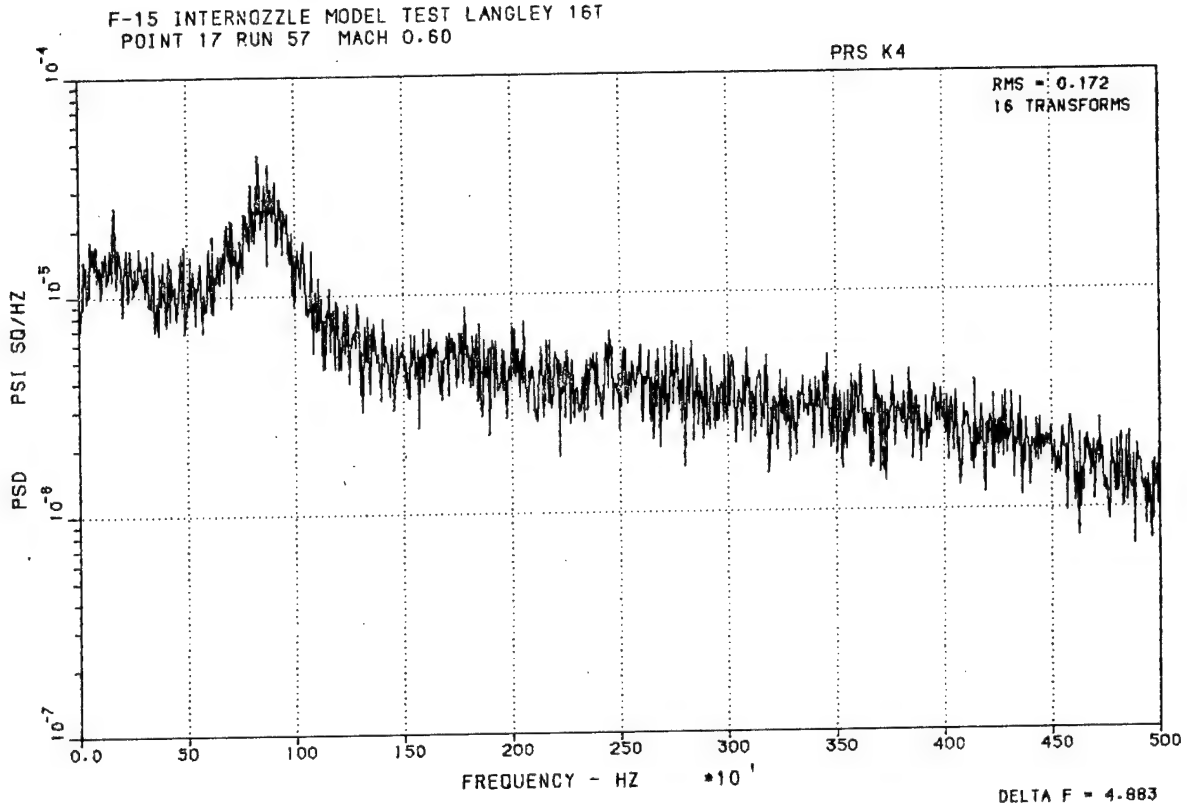

Figure 225. PSDF-BAseline Kulite 4 MACH 0.60 EPR 1.0 α 0.0

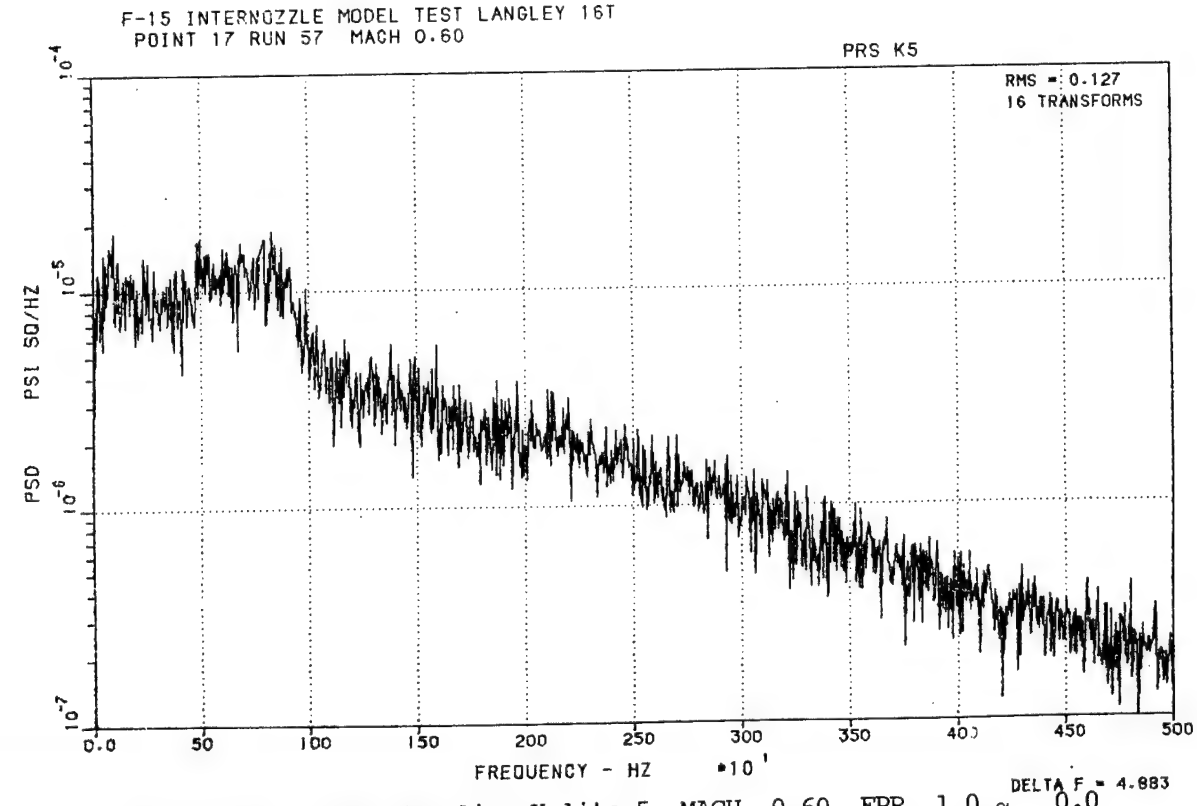

Figure 226. PSDF-Baseline Kulite 5 MACH 0.60 EPR 1.0 α 0.0

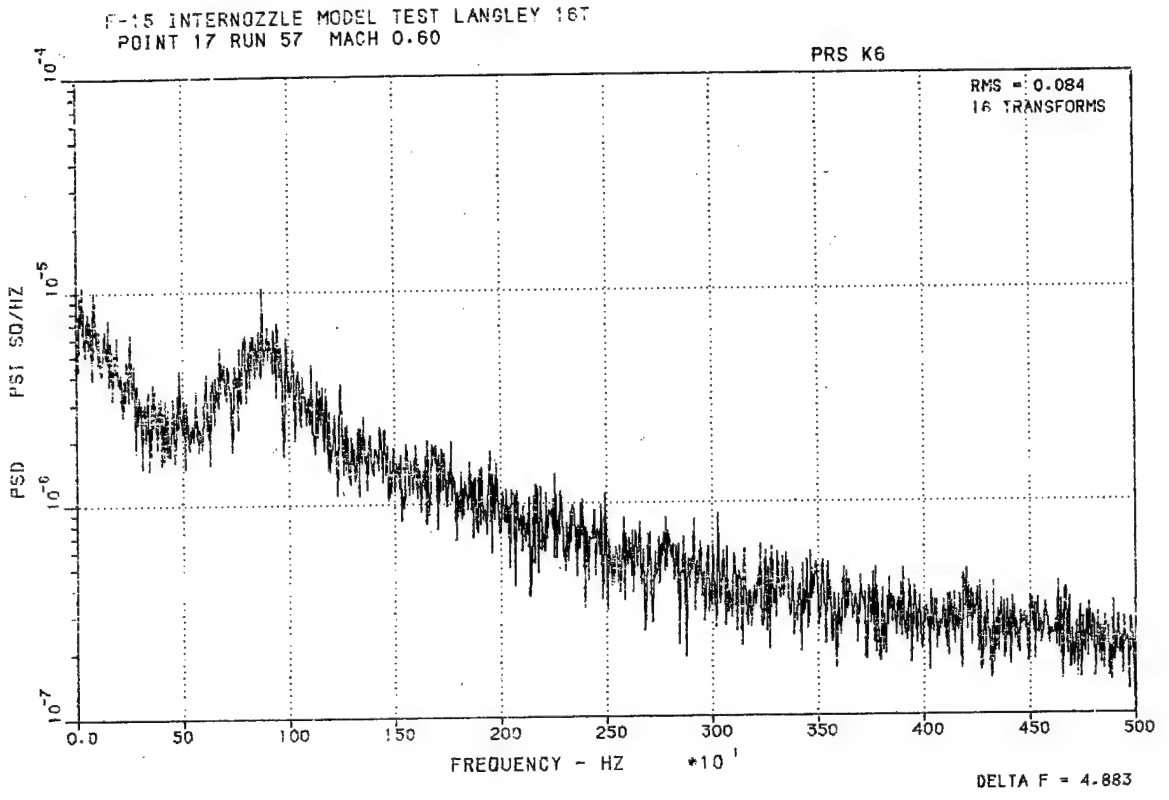

Figure 227. PSDF-Baseline Kulite 6 MACH 0.60 EPR 1.0 α 0.0

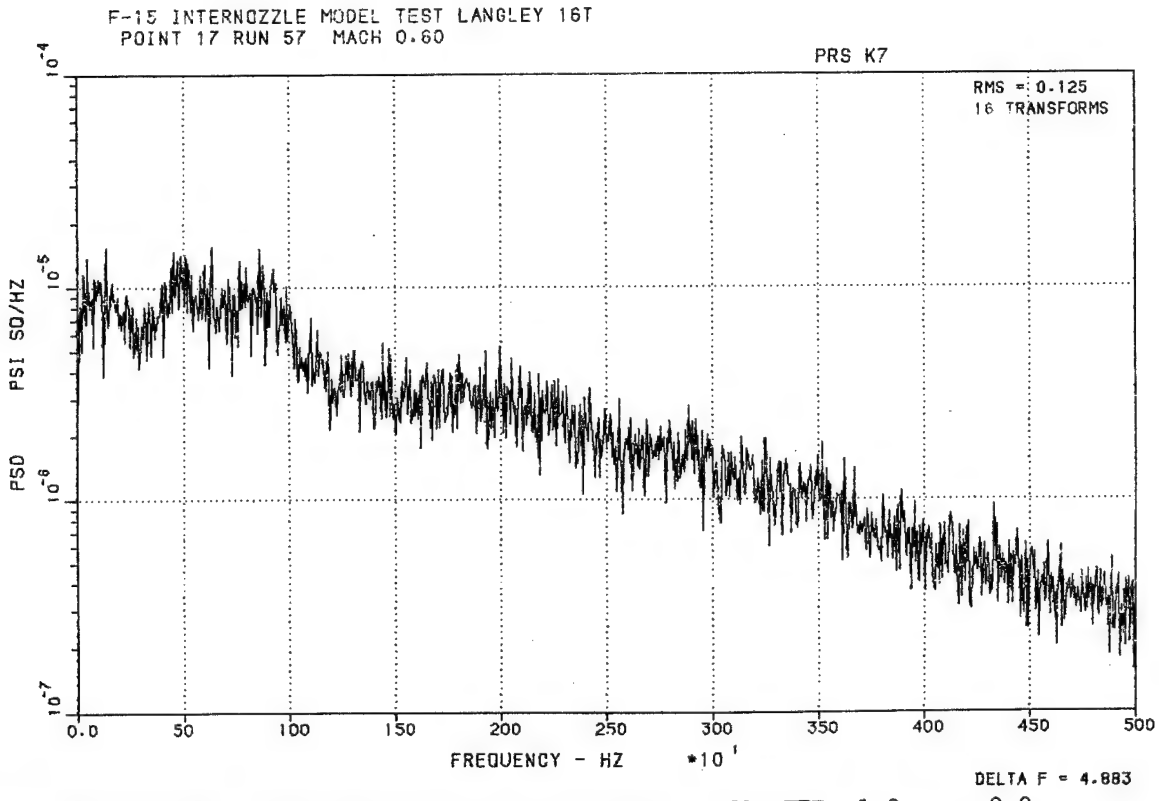

Figure 228. PSDF-Baseline Kulite 7 MACH 0.60 EPR 1.0 α 0.0

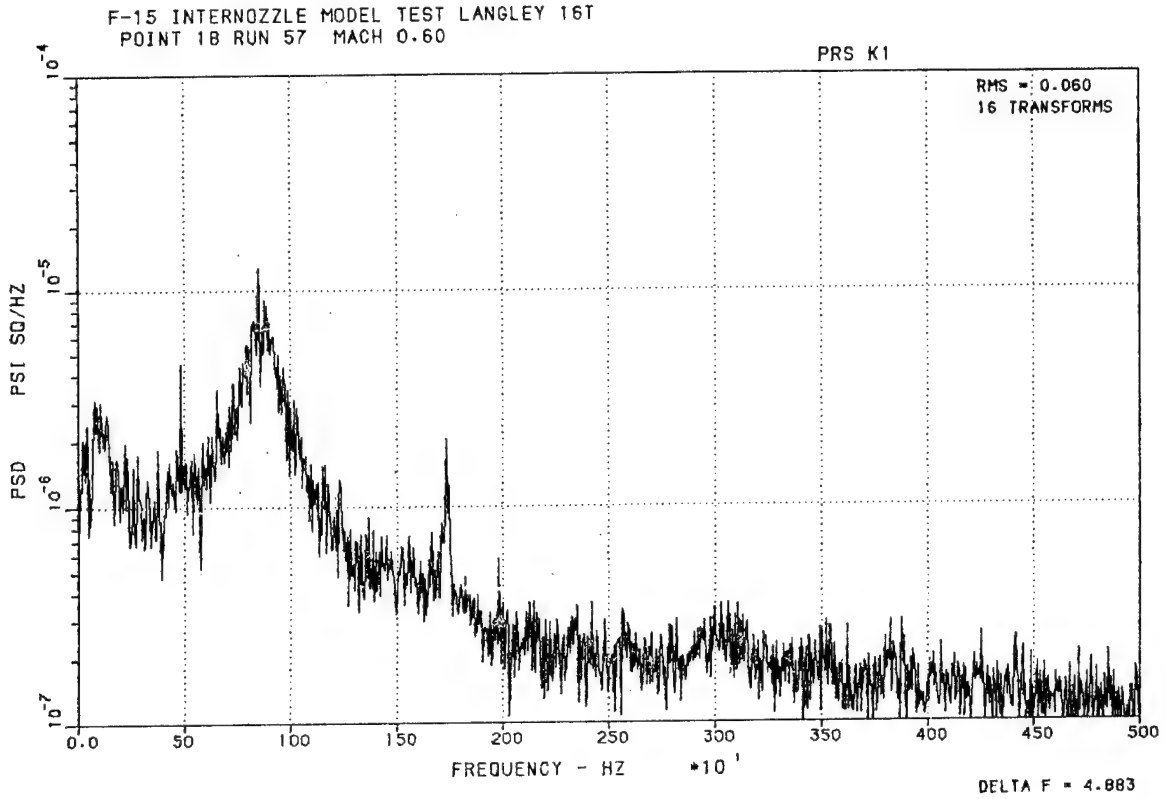

Figure 229. PSDF-BAseline Kulite 1 MACH 0.6 EPR 3.5 α 0.0

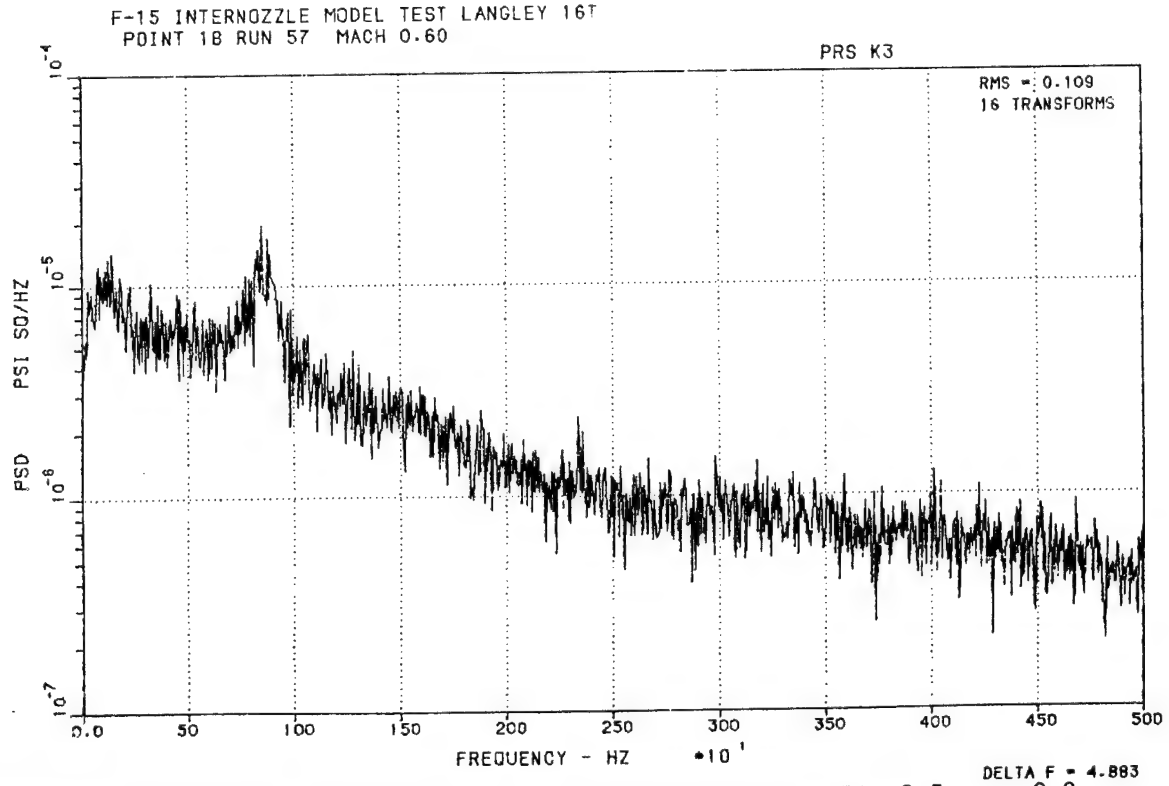

Figure 230. PSDF-Baseline Kulite 3 MACH 0.6 EPR 3.5 α 0.0

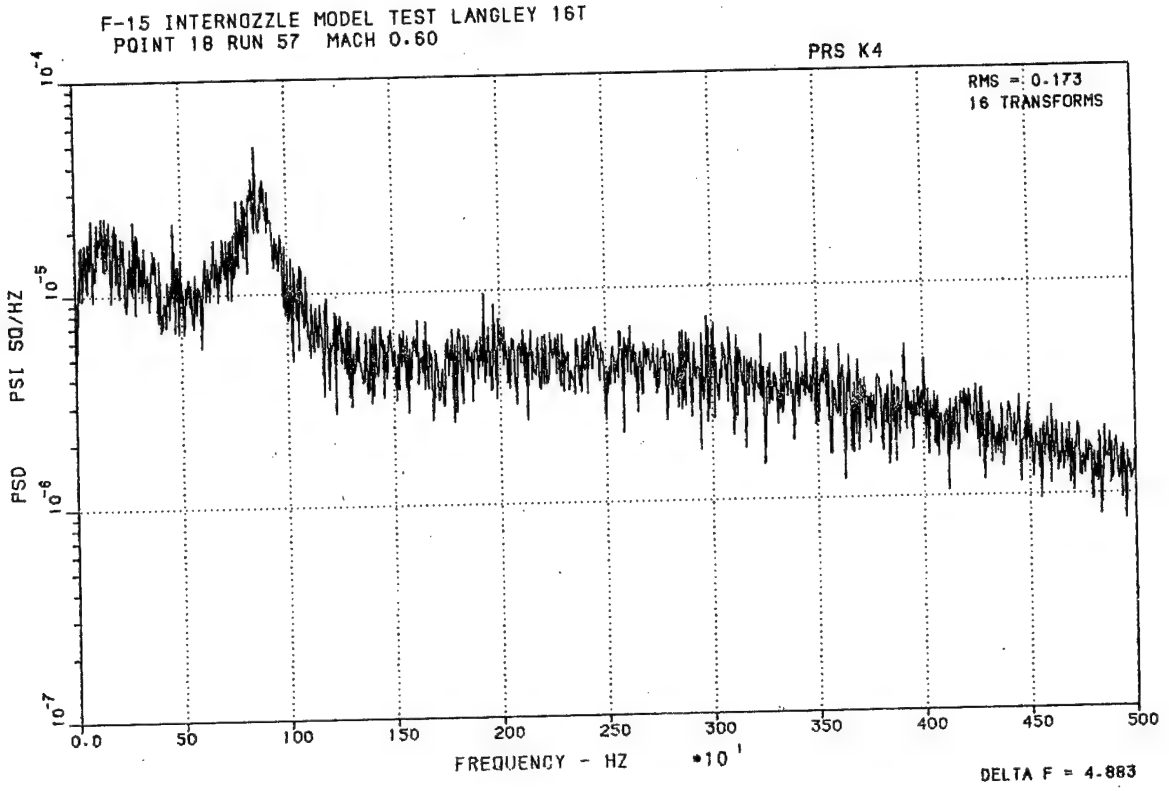

Figure 231. PSDF-Baseline Kulite 4 MACH 0.6 EPR 3.5 α 0.0

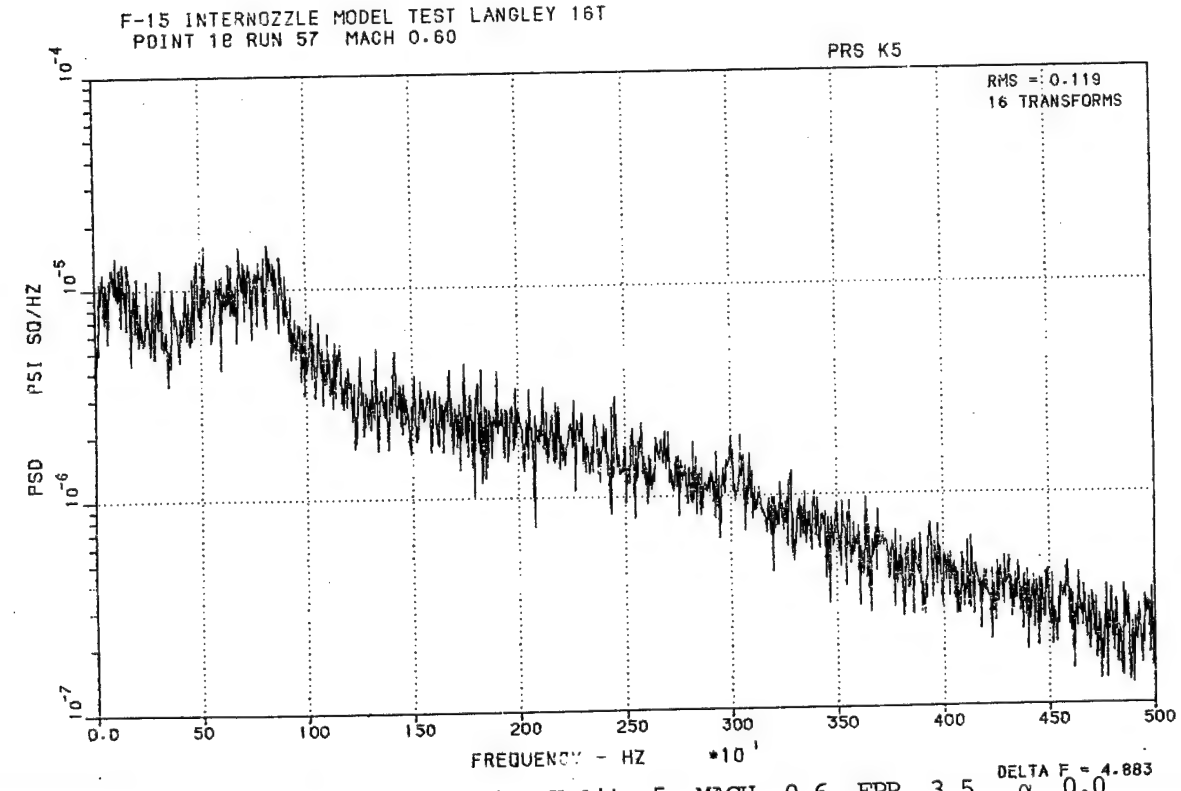

Figure 232. PSDF-Baseline Kulite 5 MACH 0.6 EPR 3.5 α 0.0

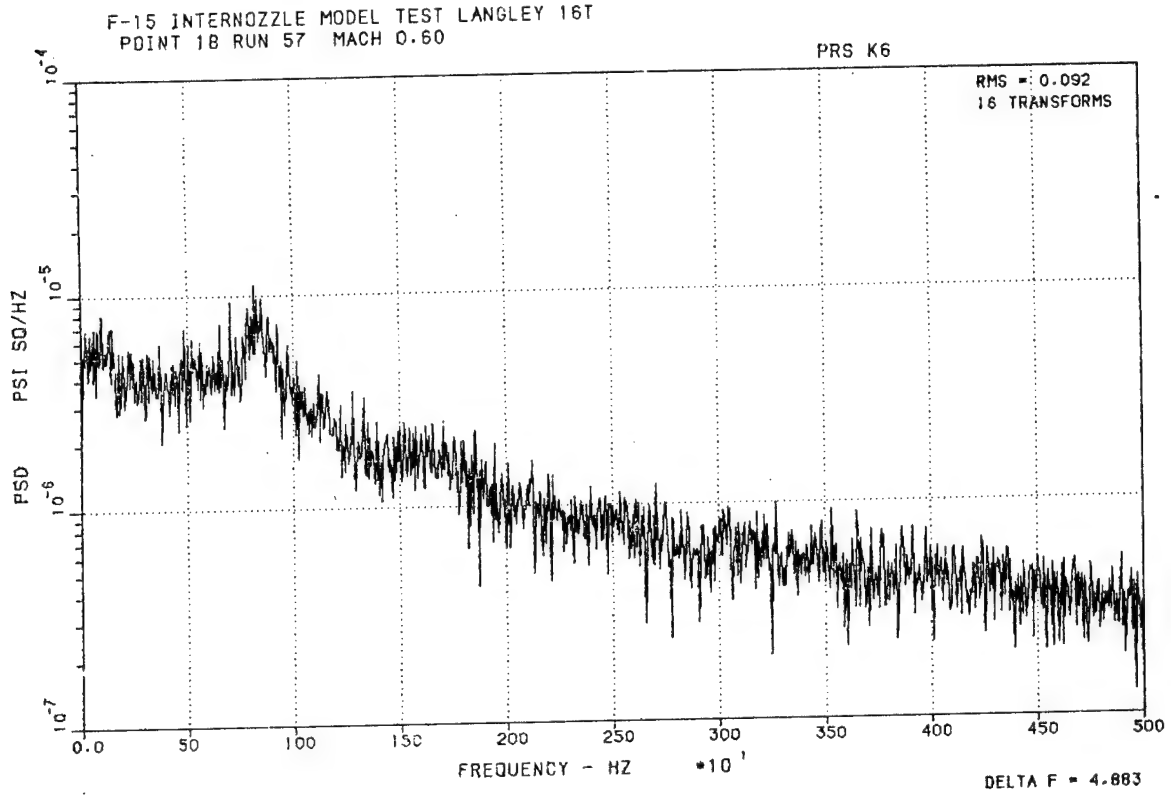

Figure 233. PSDF-Baseline Kulite 6 MACH 0.6 EPR 3.5 α 0.0

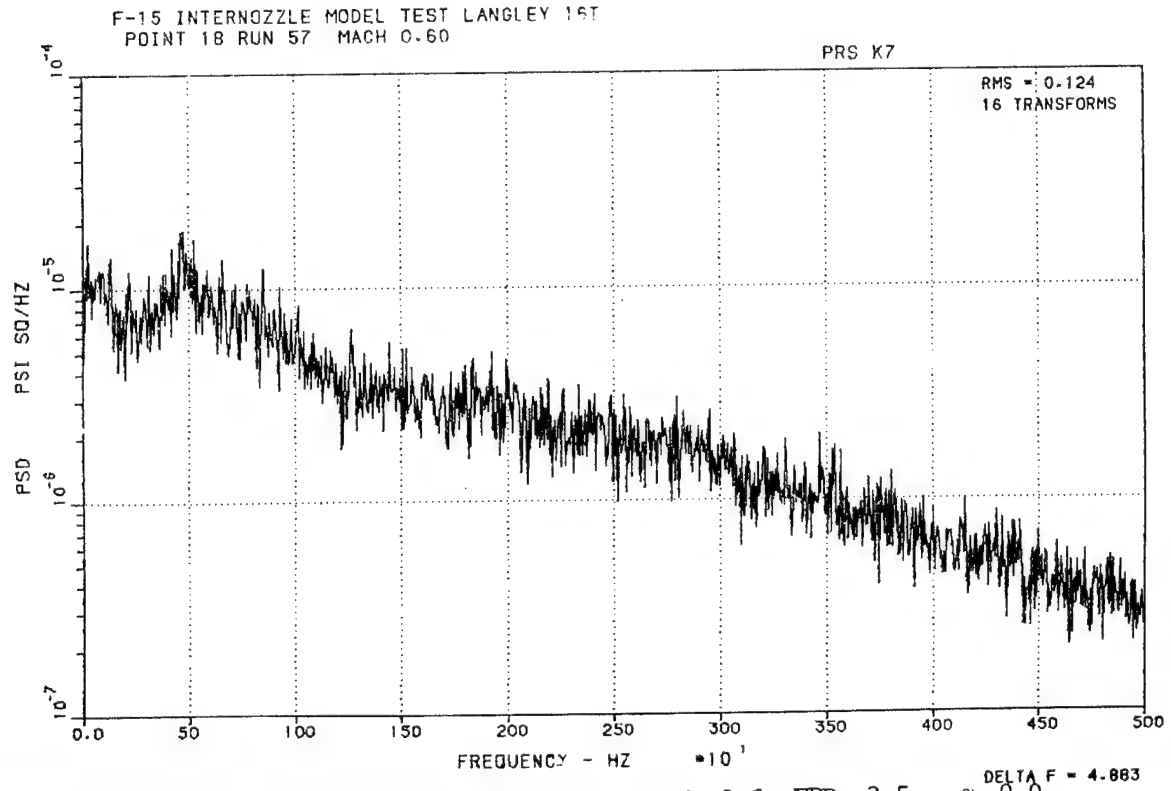

Figure 234. PSDF-Baseline Kulite 7 MACH 0.6 EPR 3.5 α 0.0

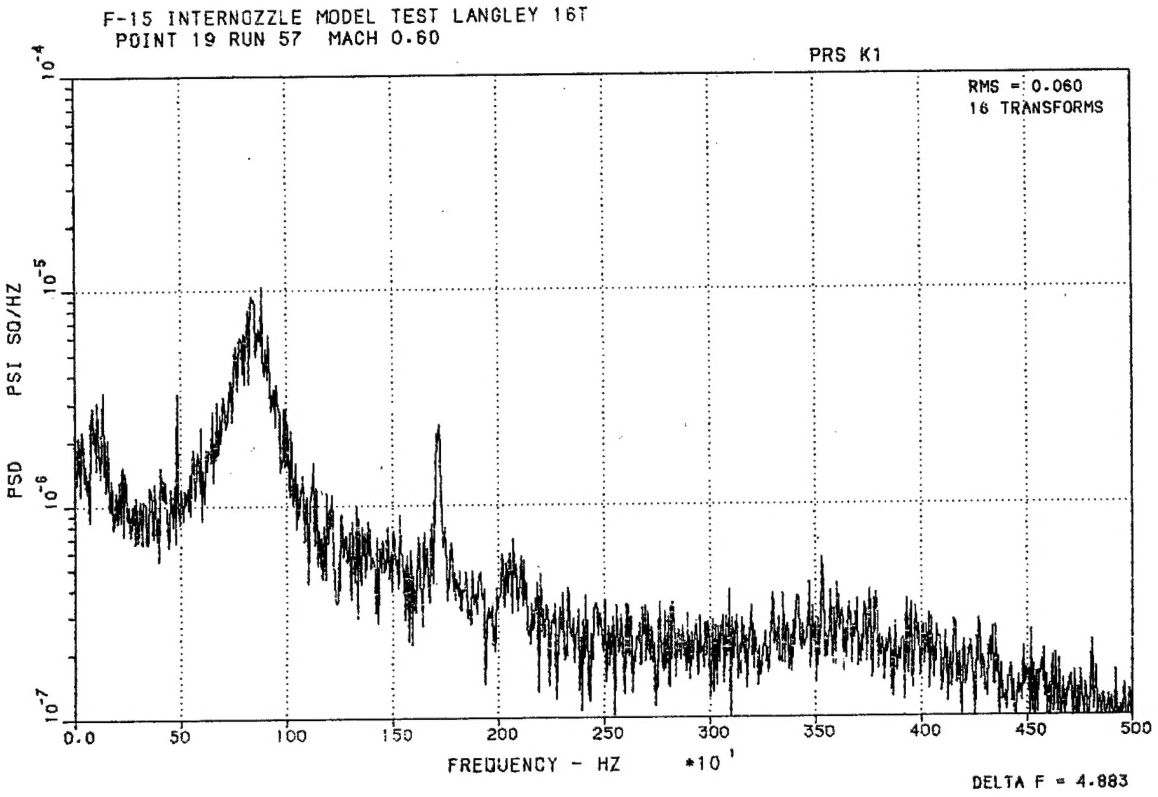

Figure 235. PSDF-Baseline Kulite 1 MACH 0.6 EPR 5.0 α 0.0

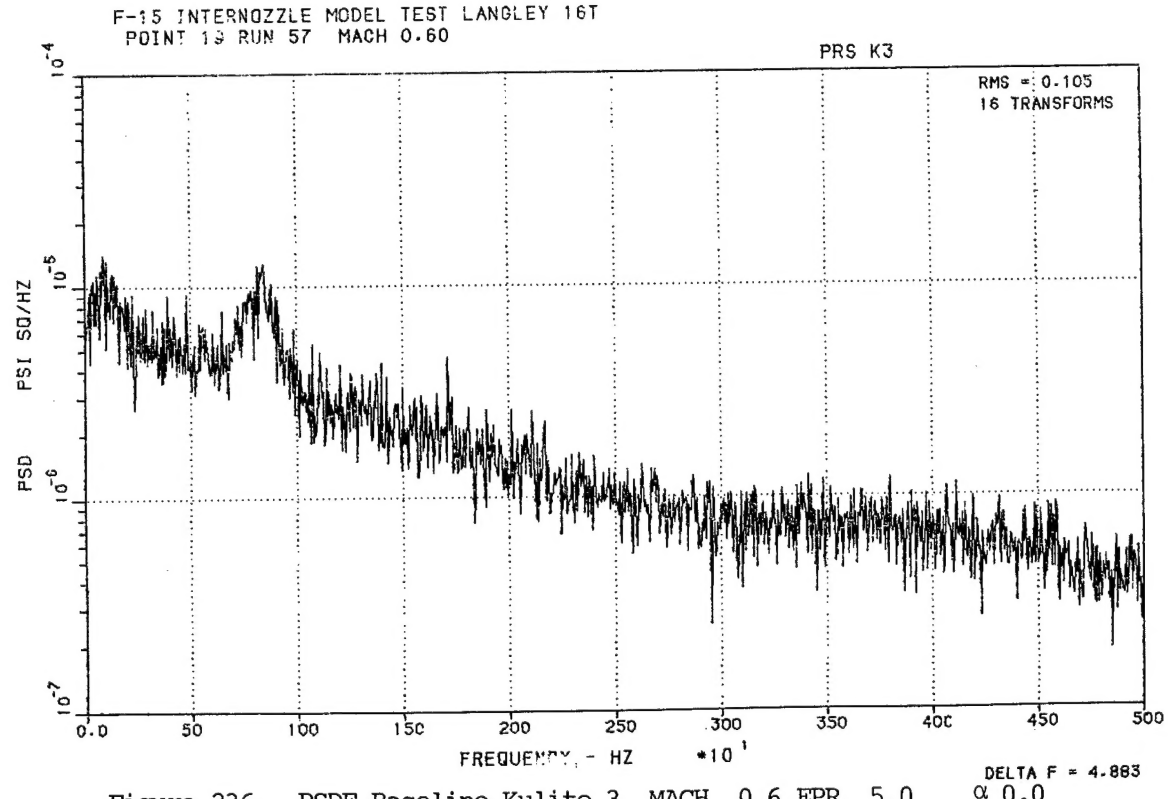

Figure 236. PSDF-Baseline Kulite 3 MACH 0.6 EPR 5.0 α 0.0

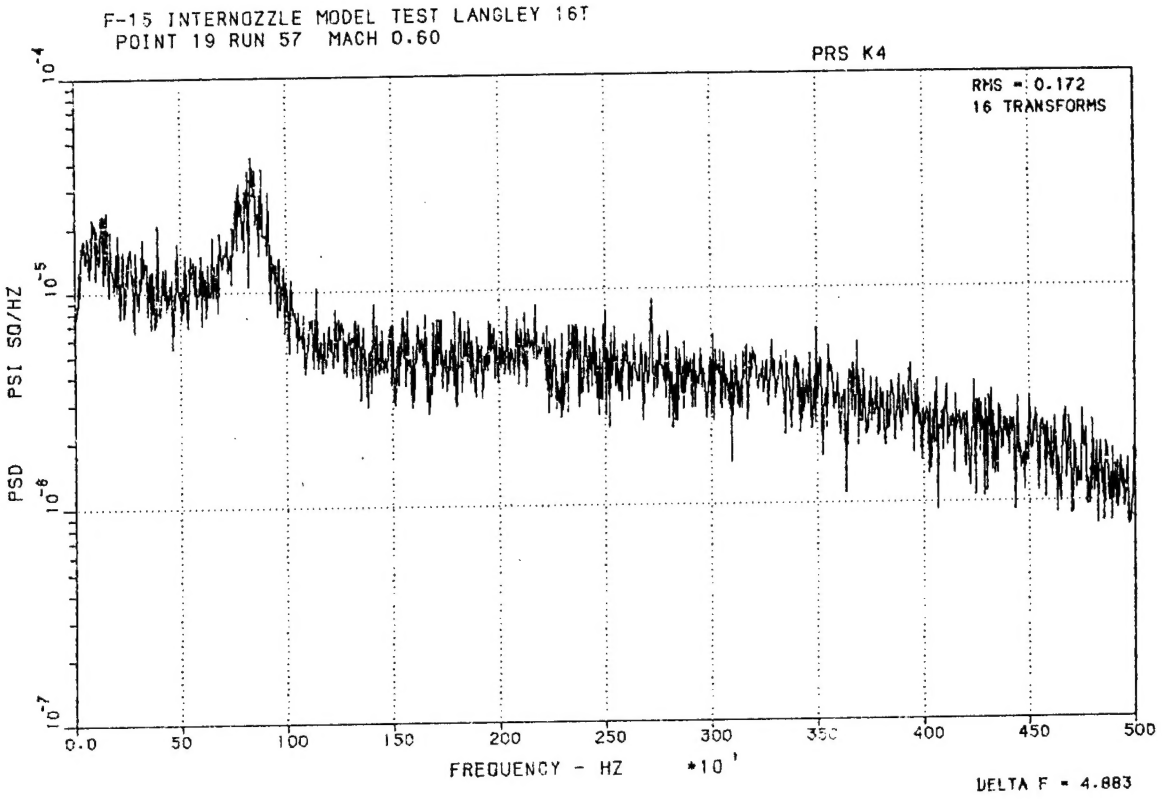

Figure 237. PSDF-Baseline Kulite 4 MACH 0.6 EPR 5.0 α 0.0

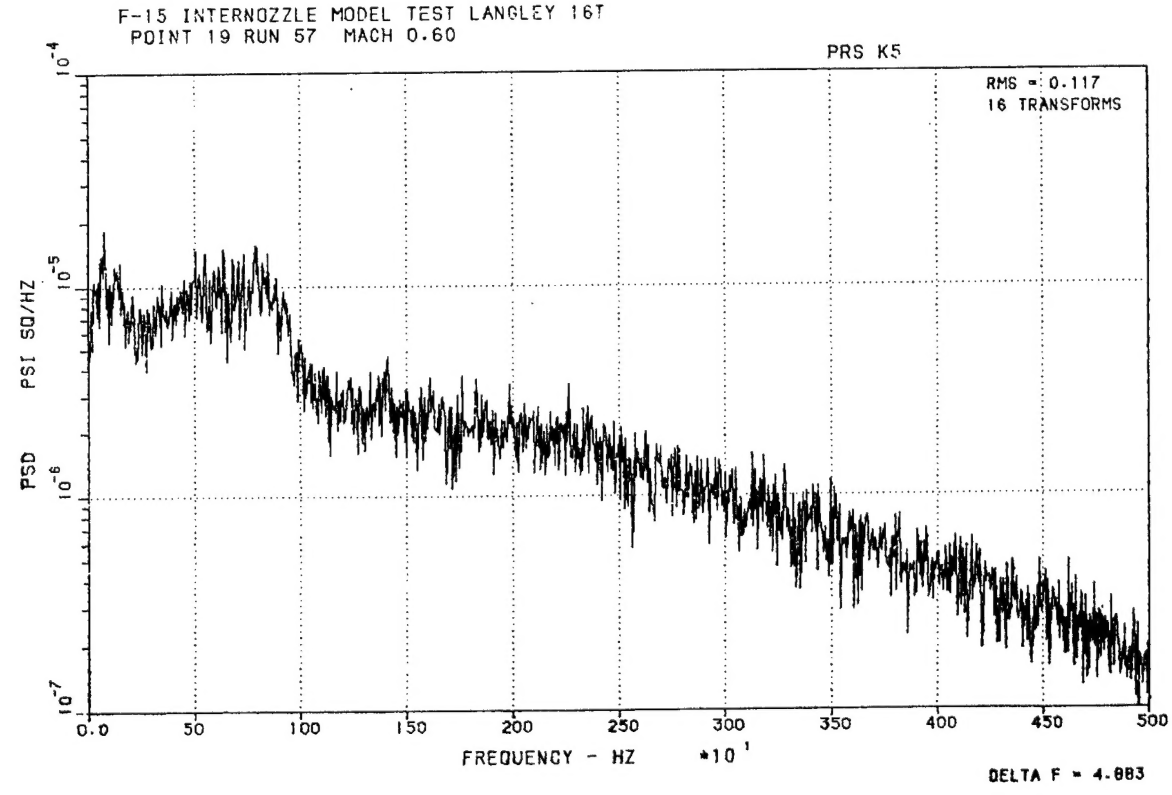

Figure 238. PSDF-Baseline Kulite 5 MACH 0.6 EPR 5.0 α 0.0

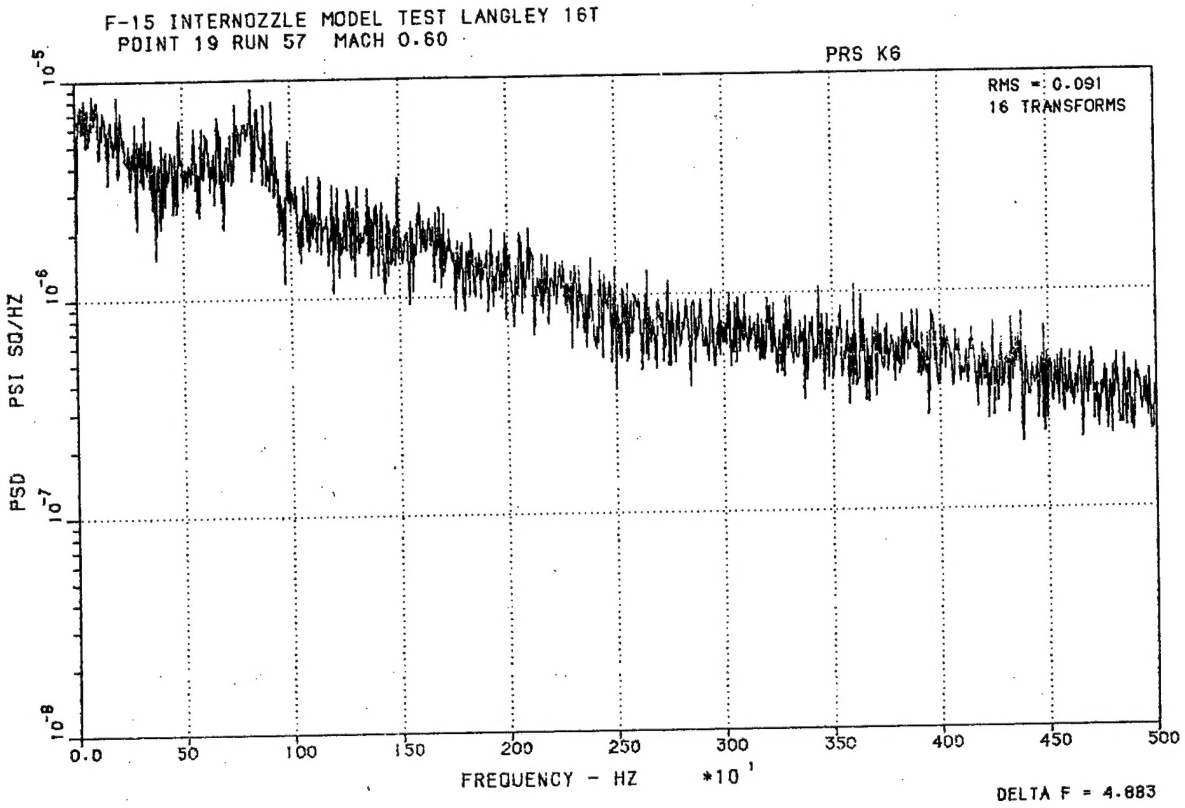

Figure 239. PSDF-Baseline Kulite 6 MACH 0.6 EPR 5.0 α 0.0

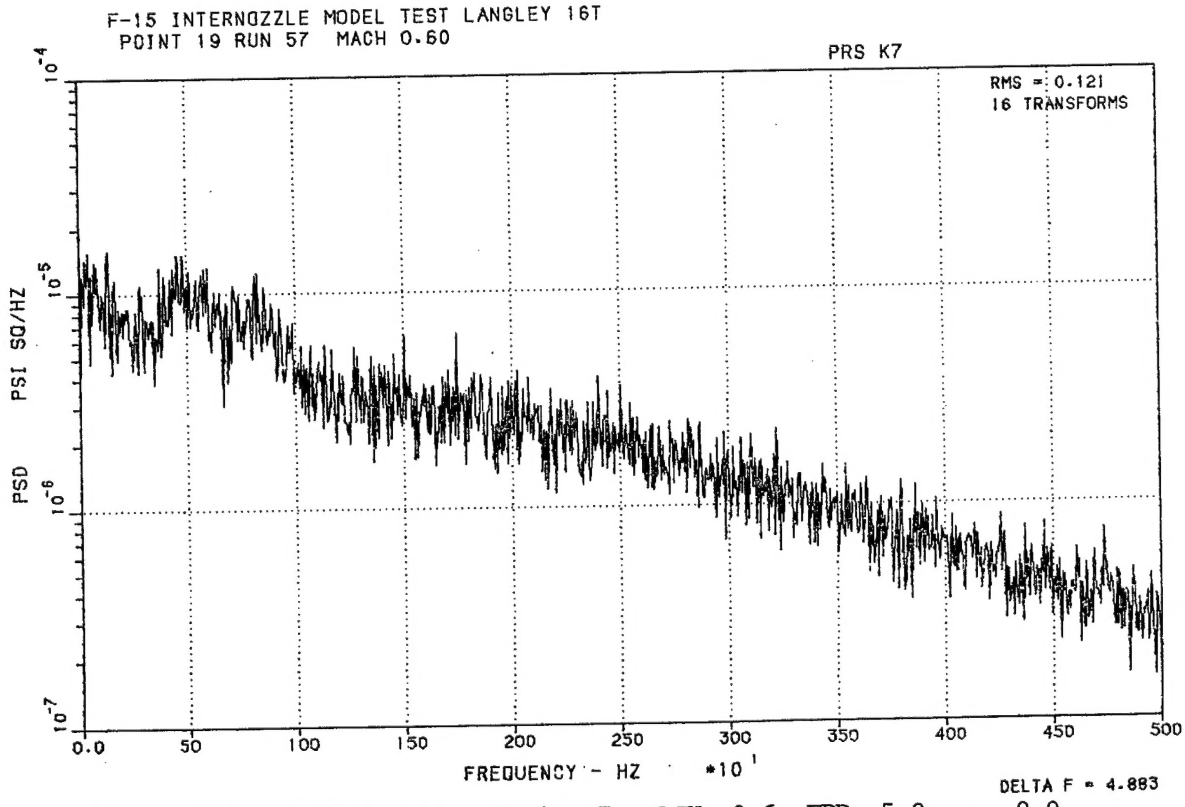

Figure 240. PSDF-Baseline Kulite 7 MACH 0.6 EPR 5.0 α 0.0

REFERENCES

1. R. G. Merkle, Statistical Measures, Probability Densities & Mathematical Models for Stochastic Measurements, Air Force Flight Dynamics Laboratory, AFFDL-TR-76-83, October 1976.

2. P. G. Bolds, Analysis of Unsteady Pressures from Missile Model Wind Tunnel Tests, Air Force Flight Dynamics Laboratory, AFFDL-TR-76-109, August 1976.

3. W. E. Triple II, Pressure Measurements on Twin Vertical Tails in Buffeting Flow, Volume I - General Description, McDonnell Aircraft Company, AFWAL-TR-82-3015.